A biomechanical evaluation of intramedullary nails during simulated fracture healing

Eveleigh, Rebecca

Award date:
1997

Awarding institution:
University of Bath

A BIOMECHANICAL EVALUATION OF INTRAMEDULLARY NAILS DURING SIMULATED FRACTURE HEALING

submitted by Rebecca Eveleigh
for the degree of Ph D
of the University of Bath
1997

R. J. Eveleigh

ProQuest LLC
789 East Eisenhower Parkway
P.O. Box 1346
Ann Arbor, MI 48106-1346

Bears keep me humble. They help me to keep the world in perspective and to understand where I fit on the spectrum of life. We need to preserve the wilderness and its monarchs for ourselves, and for the dreams of children. We should fight for these things as if our life depended on it, because it does.

W. Lynch, 1993

ABSTRACT

Intramedullary nailing is a widely used surgical method of internal fracture fixation used in long bones and despite the large number of nails used, complications and implant failures are still common. This may in part be due to the lack of mechanical evaluation prior to their clinical use. This study aimed to formulate a realistic protocol to provide a mechanical analysis of femoral intramedullary nails.

The protocol involved testing an intramedullary nail during a simulated healing process using a commercially available composite bone model. The nail and femur were strain gauged to allow the antero-posterior and medio-lateral bending moments and the torsional moment taken by each to be measured throughout the study. The nail/femur construct was loaded at each stage of the healing simulation under conditions experienced by the femur during single legged stance. The new test method allowed the load transfer between the implant and femur to be measured and the level of stress protection due to the implant after fracture healing was complete to be determined.

One reamed and one unreamed intramedullary nail were tested. The unreamed nail had a smaller diameter and was more flexible in both bending and torsion than the reamed nail. The results demonstrated that the flexibility of the nail influenced the proportion of the load supported by the femur during healing. The nails both took a high percentage of the load when the bone was fractured but this decreased as the fracture stiffness increased. The results were used to explain implant failures and slow healing reported in the literature.

This test method allowed the nail characteristics important to achieve adequate fracture fixation to be evaluated. It is essential that these mechanical characteristics should be assessed using a standardised test procedure prior to their clinical use.

ACKNOWLEDGMENTS

My thanks go to.....

Tony Miles for introducing me to the world of biomechanics, for his supervision and his great talent for finding the money that has kept me in Bath over the last few years!

Richard Weston for his technical brilliance and his patience in putting up with my changing ideas without complaint. Remember, your tools are never lost, they are just temporarily misplaced in the biomechanics lab! To Jim Askew for his strain gauging and all the other technicians whose paths I have crossed at one time or another.

Philip Procter for taking the time to read this document. Your comments and criticisms were all appreciated.

Michael Bishay and Mark Goodwin for the surgery they performed on the composite bones and Yiannis Karnezis, for his amazing ability to find interlocking screw holes without imaging.

All who were at Bath with me and who made the last few years such fun. Especially to Rhona, whom I missed greatly in my last year, to Jon and Tone for their infamous skip antics and to Fraser, so valiant in defeat both at tennis and pool!

To Jason for his patience and to Mum, Dad, Debbie and Nicole who have always encouraged me in whatever I have chosen to do.

The School of Mechanical Engineering and EPSRC for their financial assistance.

CONTENTS

LIST OF FIGURES

LIST OF TABLES

CHAPTER 1

INTRODUCTION

1.1 FRACTURE MANAGEMENT

Modern fracture management is becoming less conservative, and more frequently surgical intervention is the treatment of choice. This is due to the advent of better intra-operative visualisation, better surgical training, improved instrumentation and greater experience over recent years. Treating a fractured bone traditionally with a plaster cast is an inexpensive solution but can lead to a number of complications. These include limb shortening, malunion, where the bone heals abnormally, joint stiffness and muscle wastage. Today the surgeon has a number of available options that can help to reduce these complications. Surgical methods, such as plating, external and intramedullary fixation each have their place in fracture treatment although they are not trouble free themselves (figure 1.1). These devices provide the fractured bone with mechanical stability and allow rotational, compressive and bending forces to be transmitted across the fracture site while healing occurs. Thus, normal activity is possible preventing the problems of joint stiffness and muscle wastage caused by immobilisation. In addition the problems of malunion will be reduced as the implant helps to maintain the anatomic alignment of the bone.

Intramedullary nailing is a surgical method of internal fracture fixation used in long bones such as the femur, tibia and humerus. Within a population of 60 million such as the United Kingdom, approximately 660 000 bone fractures will occur per year. Twenty one percent, 138 600, of these are fractures of the thigh bone or femur (Procter, 1996). The development of specialised nails for the fixation of different regions of the femur means that over 50% of femoral fractures may now be treated using a nailing procedure.

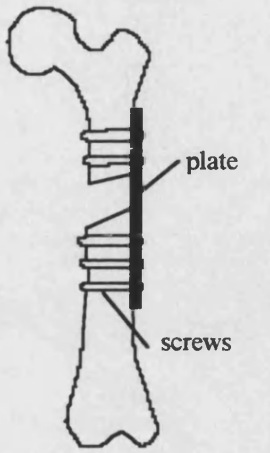

PLATING

PROS	CONS
• Internal device	• Open fracture site increases infection risk
• Compression of fracture fragments possible	• Bone absorbtion under plate
• Ease of use	• Blood supply disruption
• Inexpensive	
• No X-ray exposure required	

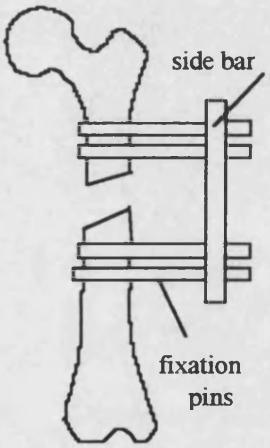

EXTERNAL FIXATION

PROS	CONS
• Less invasive	• Physically outside patient
• Easy to remove	• Risk of loosening
• Less risk of deep infection	• Risk of infection at skin/screw interface
• No X-ray exposure required	

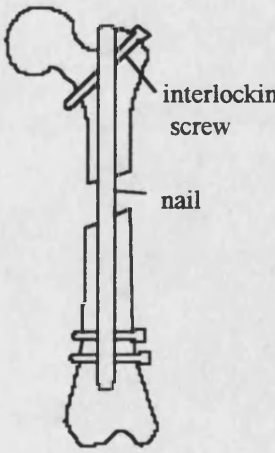

INTRAMEDULLARY NAILING

PROS	CONS
• Internal device	• Removal may be problematic
• Remote insertion reduces infection risk	• Reaming disrupts bone's blood supply
• Multiple fractures treated with one device	• Technically demanding
	• X-rays required for locking procedures

Figure 1-1 Surgical methods of fracture fixation

The nail is inserted through an incision typically 6-8cm in length. The incision is made at one end of the bone, remote from the fracture site, down the central medullary canal of the bone. It can be locked in position distally, at its lower end, and proximally, at its top end, with interlocking screws that pass through the bone cortices, the hard outer part of the bone, and holes in the nail (figure 1.2). The proximal screws are usually inserted with a guide while distally, to save time and because mechanical guides have been shown to be unreliable, surgeons prefer using a 'free hand' technique (Hall, 1987). This relies on the use of an image intensifier for correct positioning. When both the proximal and distal screws are employed, known as 'static locking', they provide resistance to compression of the fracture fragments and to rotational movement. One set of interlocking screws, either proximally or distally, may be removed after several weeks of static locking once initial healing has occurred. The first stages of healing involve a fibrous tissue filling the fracture gap before it calcifies and becomes bone. The removal of one set of screws is known as 'dynamisation', or a conversion to 'dynamic locking'. Dynamic locking maintains a degree of rotational stability while allowing axial compression which is thought to benefit fracture healing (Egger *et al.*, 1993).

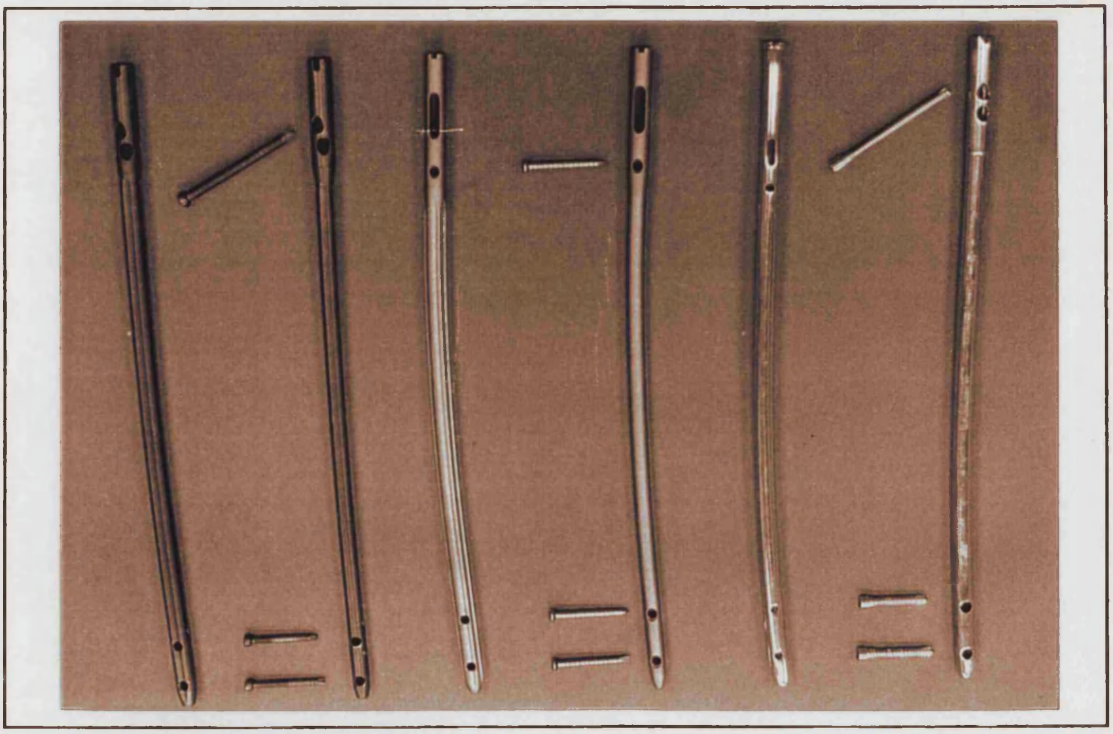

Figure 1-2 A selection of femoral intramedullary nails

1.2 THE DEVELOPMENT OF INTRAMEDULLARY NAILING

There are more than 50 different intramedullary nails available commercially and these can be divided into two main categories, reamed and unreamed. The unreamed nails are inserted directly in to the medullary canal of the bone or minimal reaming is carried out to remove obstructions from the canal before insertion. The reamed nails require more material to be removed from the medullary canal as they are usually greater in size.

1.2.1 Historical review

The first intramedullary nails, popularised by the German surgeon Küntscher in the 1940's, were unreamed nails. This was due to the fact that there were no flexible reamers available at this time. The nail was chosen to fit the canal size of the patient and therefore only small diameter nails could be used. This lead to the overloading and failure of some nails (Pennig, 1994). In 1950, the arrival of the flexible reamer allowed Küntscher to ream the medullary canal (Chao and Aro, 1994). This enabled larger diameter nails to be inserted giving even contact between the nail and bone. The nails he designed had a clover leaf cross section (figure 1.3) which allowed them to compress on insertion and then, due to their elasticity, spring open providing a good interference fit and therefore better fixation (Küntscher, 1958).

The demand for nails that would allow more complex and unstable fractures to be treated led to the manufacturers increasing the wall thickness of the nails. This increased their stiffness enabling greater loads to be transmitted through these devices. In 1968 Küntscher introduced a new concept that increased the indications for the use of intramedullary nails. Screws were positioned above and below the fracture, passing through the intramedullary nail, which prevented shortening and rotation in comminuted fractures, where the bone breaks in to more than two pieces (Bunker, 1989). The use of this 'detensor' nail, later renamed the interlocking nail, became more widespread with advances in image intensification that allowed the screws to be positioned more easily.

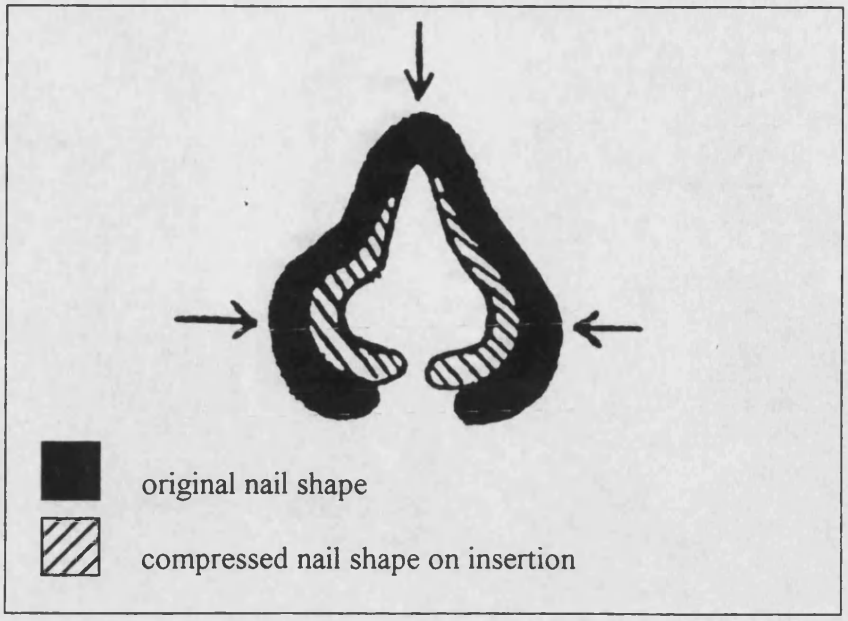

Figure 1-3 Küntscher's clover leaf nail - cross-section

From Küntscher, 1958

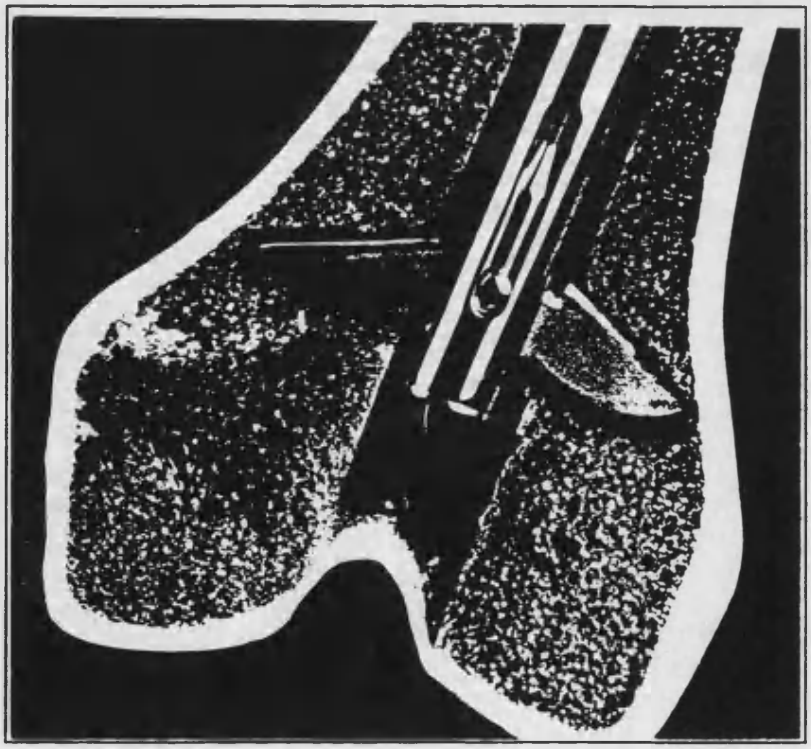

Figure 1-4 Deploying fins for distal fixation

From The Derby Nail catalogue, Thackray

Other methods of interlocking were also proposed, including the idea of distally deploying fins (figure 1.4). These fins were activated from the proximal end after nail insertion. They aimed to reduce the time taken to distally lock a conventional interlocking nail. Rotational and axial stability were achieved by the fins anchoring themselves in to the bone. However, there were often technical difficulties in the deployment of the fins and complications post-operatively, such as the protrusion of the fins through the distal femur suggesting a lack of stability (Blumberg *et al.*, 1990).

Cases of fatigue failure were experienced with the early interlocking nails. The number of failures were reduced using closed cross-section nails which had a greater amount of material around the interlocking screw holes (Bunker, 1989). The holes were also cold worked to reduce stress concentrations (Beals *et al.*, 1990). In addition, the closed section nail was also more torsionally rigid than the open sectioned clover leaf design (Tarr and Wiss, 1986). This reduced the amount by which the nail twisted on insertion making it easier to insert the interlocking screws because the holes would remain perpendicular to the horizontal (Browner and Cole, 1987).

At the end of the 1980's unreamed nails were introduced in the USA. They were thought to have a number of advantages over reamed nails. However, the benefits were not clinically proven before their widespread inception. The main arguments for their introduction were that unreamed nails minimised damage to the bone and reduced the risk of infection. Studies have since shown that disruption of the blood supply still occurs with unreamed nailing although it is significantly less than with reamed intramedullary nailing (Schemitsch, 1993). Solid unreamed nails have also been associated with a lower risk of infection than open section nails. Their smaller surface area reduces the probability of bacterial adhesion and they have no 'dead space' (Melcher *et al.*, 1994). A 'dead space' is a poorly vascularised area that defence mechanisms may have difficulty reaching, such as the centre of a hollow nail. However, there are problems with the unreamed nail. Their smaller diameter, to avoid reaming, makes them mechanically weak and more susceptible to bending and screw breakage than a reamed nail (Fairbank *et al.*, 1995). The relative benefits of reamed and unreamed nailing are still under investigation.

Probably of great significance to the argument is the discovery that the introduction of guide wires and reamers in to the medullary canal causes a rise in intramedullary pressure (Heim *et al.*, 1993). The pressure rise may lead to fat emboli, or clots, entering the blood stream which can at worst prove fatal (Stürmer, 1993). Again however, all is not clear cut. The introduction of an unreamed nail can lead to high pressures if the mode of insertion is incorrect. The intramedullary pressure rises associated with reaming can be reduced using sharp reamers and by introducing the reamers slowly (Müller *et al.*, 1993). The issue of whether to use reamed or unreamed nails is still very much under debate.

1.2.2 Recent innovations

The orthopaedic surgeon is exposed to the greatest level of radiation during distal locking of intramedullary nails. Inexperienced surgeons using the free-hand technique and image intensifier to locate the distal screw holes are particularly vulnerable. The fluoroscopic time for femoral nailing was found to be 2.6 times greater when distal interlocking was added (Sanders *et al.*, 1993). Although it is unlikely that the level of maximum exposure would be reached, the connection between low-dose radiation and malignancy is unknown and therefore exposure must be minimised.

The possibility of using ultrasound as an alternative to fluoroscopic monitoring during nail insertion has been investigated (Mahaisavariya and Laupattarakasem, 1993). The operating times for closed, unlocked nailing using both imaging procedures were comparable. The study recommended that the use of ultrasound to aid interlocking procedures required further investigation.

Several new devices have recently been reported in the literature that attempt to reduce exposure to radiation using alternatives to interlocking screws for distal fixation. Marchetti *et al.* (1993) introduced a new nail, the universal elastic bundle nail, that consists of five or six secondary nails which are stored together during nail insertion (figure 1.5). Once inserted the nails are activated to diverge distally and achieve fixation by embedding themselves in the cortical bone. The principle is similar to that used in intramedullary nails with distally diverging fins.

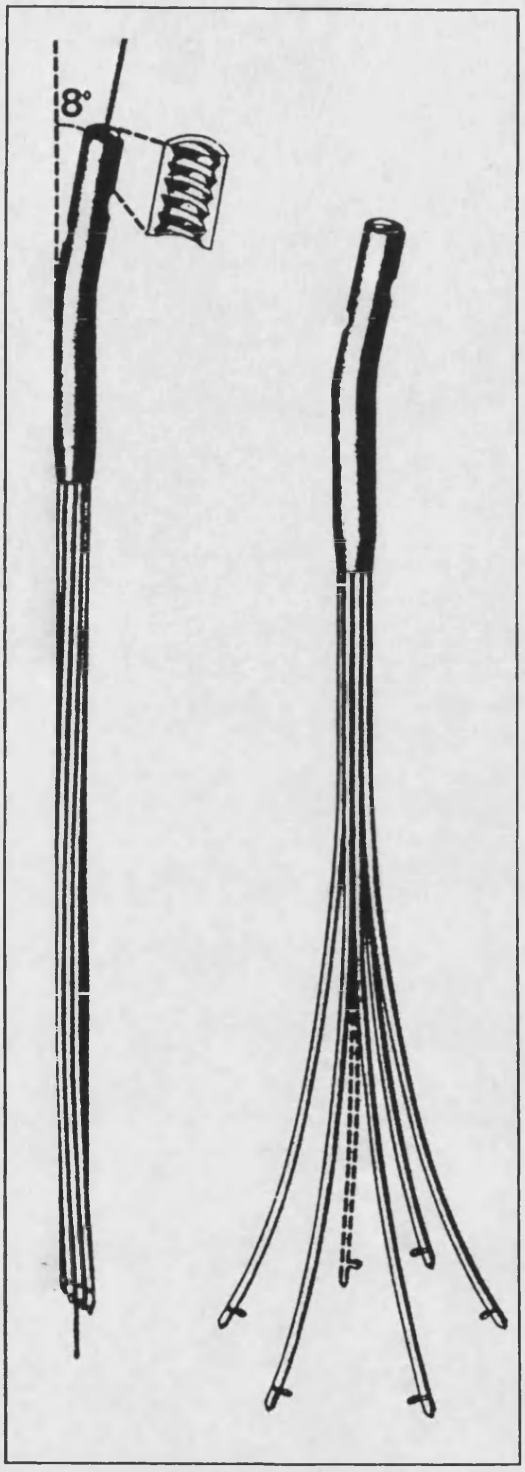

Figure 1-5 The Marchetti nail

From Marchetti *et al.*, 1994

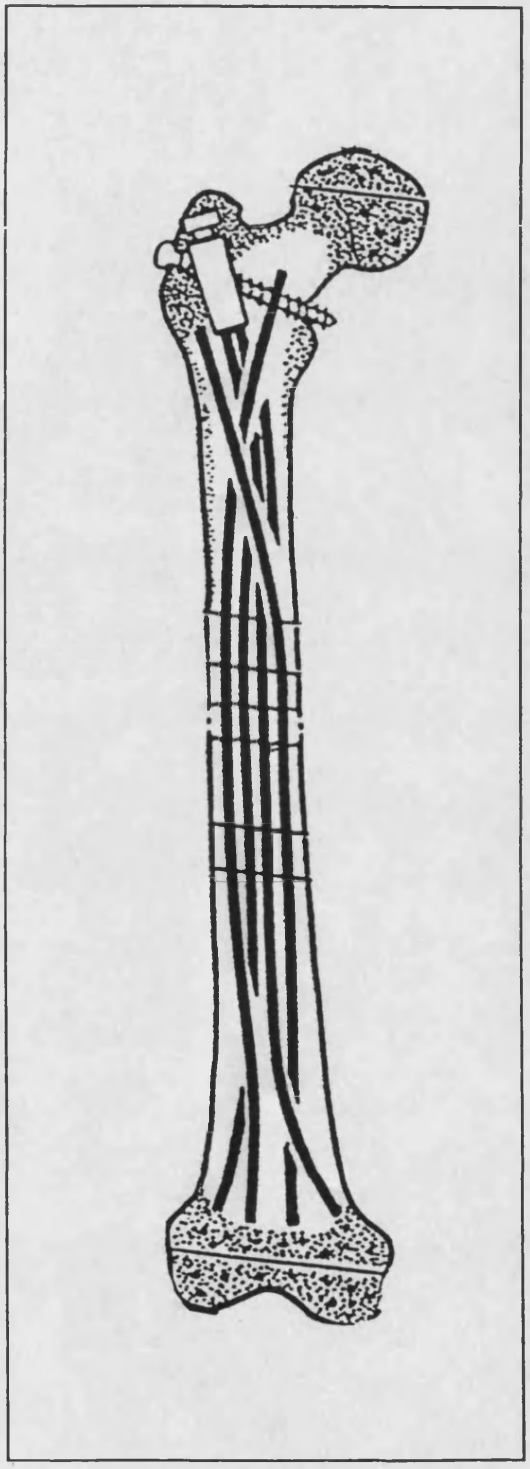

Figure 1-6 The LIFO device

(Locked Intramedullary Flexible Osteosynthesis)

From Caffinière *et al.*, 1994

The ability of the Marchetti nail to reduce operating and screening times is not disputed (Ali *et al.*, 1995), however, a high number of complications have been reported. A study by Hargreaves *et al.* (1995) documented a 63.5% complication rate in femoral nailings (44% in the tibia) apparent as rotational deformities, angulation, shortening and migration of the nail proximally.

A new system, the locked intramedullary flexible osteosynthesis technique (LIFO), was proposed by Caffinière *et al.* (1994). Two 4mm diameter pins, pre-bent prior to the operation, were inserted into the fractured bone. Distal fixation was achieved when the pin ends became embedded in the bone (figure 1.6). The proximal ends of the pins were located in a small locking block which also housed a proximal interlocking screw. It was recommended that one or two additional pins were also inserted to increase the stiffness of the device.

Simple biomechanical testing of the device showed significant shortening and angular distortion under small loads when compared to a conventional femoral interlocking nail. Despite these results a clinical trial was undertaken using the nail in unstable fractures. Angulation was seen in 38% of femoral fractures and some cases of pin migration occurred. These problems were always associated with technical error or where the bone was comminuted or osteoporotic.

Azer *et al.* (1991) designed a self guiding (SG) interlocking nail. The intramedullary nail is located by keying in on a transversely placed drill bit at the location of the most distal screw (figure 1.7). This eliminated the need to locate the fixation holes after nail insertion. The second distal screw was positioned with a guide that also keyed in on the drill bit. This design appears to solve the radiation exposure problem while retaining the rigidity of a standard locked intramedullary nail.

Coutts *et al.* (1994) proposed a novel idea for nail fixation. This involved injecting a bioresorbable cement down the intramedullary nail following insertion. Apart from solving the problem of distal targeting, it eradicated the need for removal of the locking screws to achieve dynamisation. The cement will gradually degrade allowing increased

loading of the bone. Other new ideas under investigation include the use of complete biodegradable implants which would eliminate the need for a second operation to remove the nail (Hofmann, 1992). In addition, the implant naturally transfers load to the bone as it is absorbed and loses its mechanical properties.

However at present, biodegradable implants have to be used in low load situations like in maxillofacial surgery. This is because they are mechanically 'weak' in comparison with more conventional stainless steel alternatives (table 1.1). A biodegradable nail used in a weight bearing bone such as the femur would inevitably lead to problems of shortening, angulation and failure. A further difficulty is the control of the degrading process. The implant must retain sufficient stiffness and strength over the time taken for the bone to heal.

	Self-reinforced biodegradable polylactic acid	Steel
Bending strength (MPa)	**250**	**400**
Young's modulus (GPa)	**10-15**	**200**

Table 1-1 Strength values for a biodegradable material and steel

From Raiha, 1992

One successful use of a biodegradable material has been to coat an intramedullary nail with an antibiotic-impregnated biodegradable layer (Lin *et al.*, 1994). The antibiotic coating was absorbed over a period of time in order to prevent infection and treat any that did occur. The avoidance of any infection is a primary concern in fracture management. It has been shown to be a predominant cause in the non-union of femoral shaft fractures (Curylo and Lindsey, 1994).

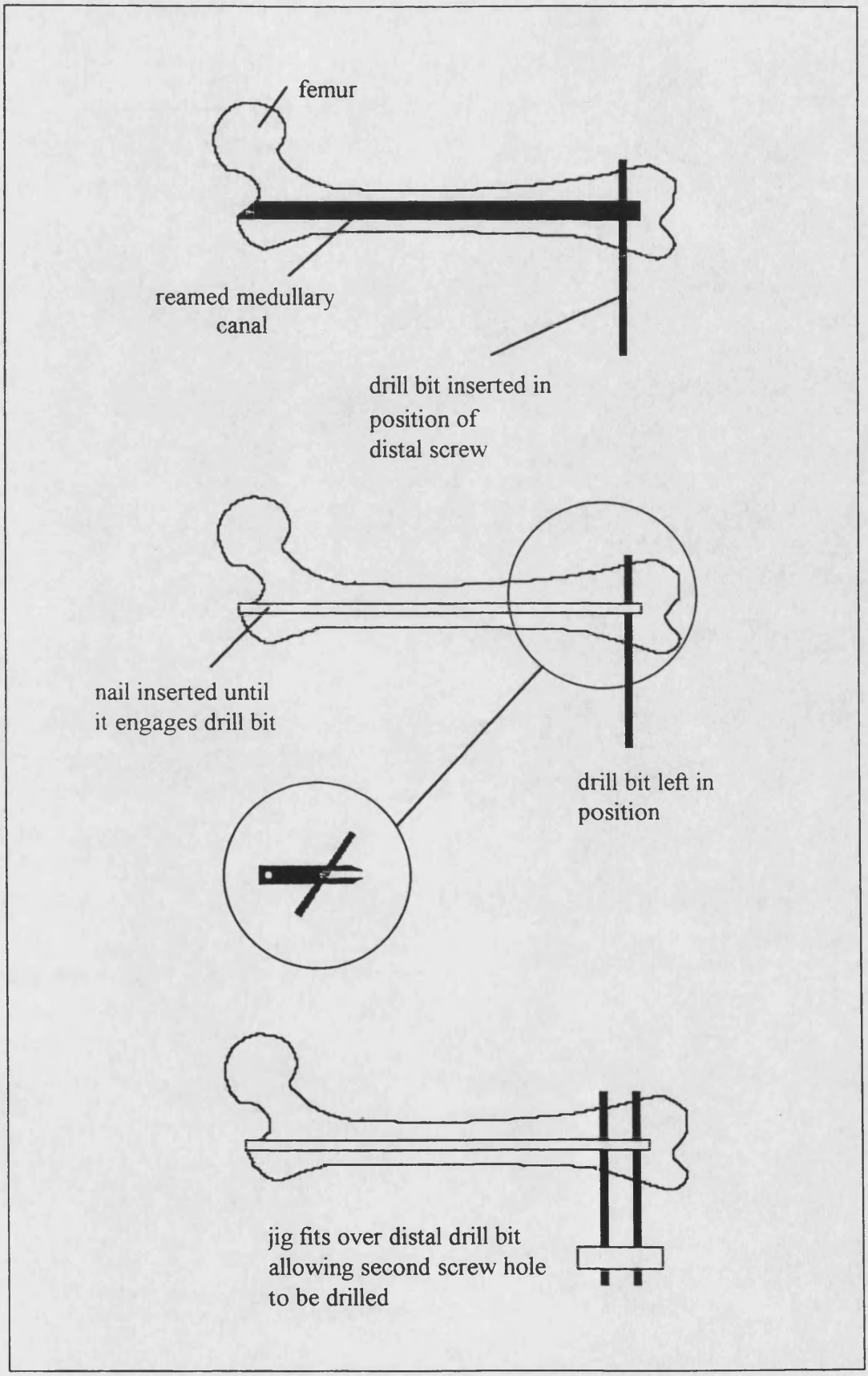

Figure 1-7 Distal targeting with the SG nail

1.3 CURRENT TEST PROCEDURES

Despite the multitude of nails available, complications and failures are still common. The literature documents relatively few cases of mechanical testing of orthopaedic implants and the rationale behind the methods used. Clinical testing most often takes the form of case studies rather than randomised prospective trials. A randomised prospective study involves comparing two implants by assigning a patient randomly to one device prior to treatment and subsequently reviewing the results. Mechanical testing often takes place alongside clinical testing rather than prior to it. Standardised test procedures are therefore required to try to reduce problems before an implant goes in to widespread use.

A search of international testing standards for the evaluation of orthopaedic implants produces few results if one considers the enormous number of devices commercially available (BSI, DIN, AFNOR, ASTM, ANSI and ISO). Two standards were found that related to intramedullary nails. BS3531 (1990) and the equivalent ISO 5837 (1980) specify the main dimensions of nails with a V-shaped and clover leaf cross section. Only the American Society for Testing and Materials, a voluntary organisation, documents a procedure for evaluating the mechanical properties of intramedullary nails. ASTM F383-73 descibes a practice for static bend and torsion testing of intramedullary rods to determine their bending strength, bending rigidity and torsional rigidity.

Due to the lack of standardised procedures, a large variety of tests have been used to determine the mechanical properties of intramedullary nails experimentally, *in vitro* (Eveleigh, 1995). The alternative methods make it difficult to compare different intramedullary nails and to show that results are consistent between centres of research. These studies have also concentrated on testing the nails in isolated loading modes, as in ASTM 383-73, which is not representative of the physiological situation.

A realistic test procedure should aim to replicate the loading conditions that the nail would be subjected to *in vivo*. A more reasonable comparison of the implants would be possible, and a better insight in to the failings of each. If implants were evaluated using such a standardised protocol it could be established whether a device was safe for clinical use. Pre-clinical mechanical testing might have reduced the complications seen with

devices such as the Marchetti nail (Hargreaves *et al.*, 1995) by limiting its indications for clinical use.

A standard testing procedure would prove beneficial to hospitals, surgeons and the patient as an implant would have to have undergone recognised testing before clinical use. The findings of such implant testing must be well documented to allow all interested parties access to the resulting information. Clinical studies can then be designed ethically (Einhorn *et al.*, 1997), and surgeons can make an educated decision when treating patients, leading to better fracture management as the indications and contraindications for a device would be known. In addition, standardised testing procedures will be of use to the implant manufacturers themselves as regulatory authorities are increasingly requiring pre-clinical data as a pre-requisite to the approval of orthopaedic devices.

1.4 PROJECT AIMS

It was hypothesised that testing intramedullary nails under conditions similar to those that it would be subjected to *in vivo*, would allow a greater insight in to the function of the nail compared with that which is obtained from isolated static testing. The resulting information would provide a basis for the realistic comparison of different nail types.

It was the aim of this study to review the current literature concentrating on the biomechanical and clinical testing of femoral intramedullary nails, the loads that a femoral implant is subjected to *in vivo*, and the fracture healing process. This information was to be used to 1) formulate a protocol for the realistic mechanical testing of intramedullary nails and 2) to demonstrate the mechanical test method with reference to a number of intramedullary nails in current use.

The results will lead to a greater knowledge of the nail performance and the characteristics important to achieve successful fracture fixation. These mechanical characteristics should be evaluated in a pre-clinical standardised test procedure.

Although only femoral nails were concentrated on in this study, the results are as equally relevant to tibial and humeral intramedullary nails as well. The general methodology used in the design of this test protocol may easily be adapted for any orthopaedic implant.

CHAPTER 2

LITERATURE REVIEW

2.1 ANATOMY

2.1.1 The hip joint

The hip is one of the largest and most stable joints in the body. Its stability comes from two highly conforming surfaces that form a ball and socket configuration; the head of the femur being the convex and the acetabulum of the pelvis the concave element of the joint (figure 2.1). Both the femoral head and the acetabulum are covered with a layer of cartilage that varies in thickness across each surface. Cartilage is thickest at the centre of the femoral head and at the upper part of the acetabulum. This is at the point where body weight is transmitted through the hip when standing upright. The two primary functions of cartilage are to 1) distribute load over a wide area thus preventing excessive stress concentrations and 2) allow the relative movement of the joint surfaces with the minimum of friction and wear.

Movement is facilitated by muscular action and the hip joint is surrounded by large, strong muscles for this purpose (figure 2.2). Muscles are attached to bone by tendon. The tendon transmits the tensile muscle forces to the bone thereby producing motion. Muscles are capable of producing large forces and are therefore very important when determining the loads acting on joints. Excessive movement of the hip is prevented by three ligaments that form the exterior of the joint capsule at the hip (Green and Silver, 1981). Ligaments link bone to bone across a joint. Ligaments and tendons do not have the ability to contract like muscle but are slightly extensible. However, if they are stretched beyond their elastic limit, they remain stretched. The original length can only be restored via surgery.

2.1.2 The femur

The femur is the longest bone in the body (figure 2.3). When standing upright, it is obliquely orientated, making an angle of about 11° with the vertical in the frontal plane (McLeish and Charnley, 1970), with the distal ends of the left and right femur almost touching at the knee. This aligns the lower extremities with the body's centre of gravity line, making it more stable.

Figure 2-1 The hip joint
From Nordin and Frankel, 1989

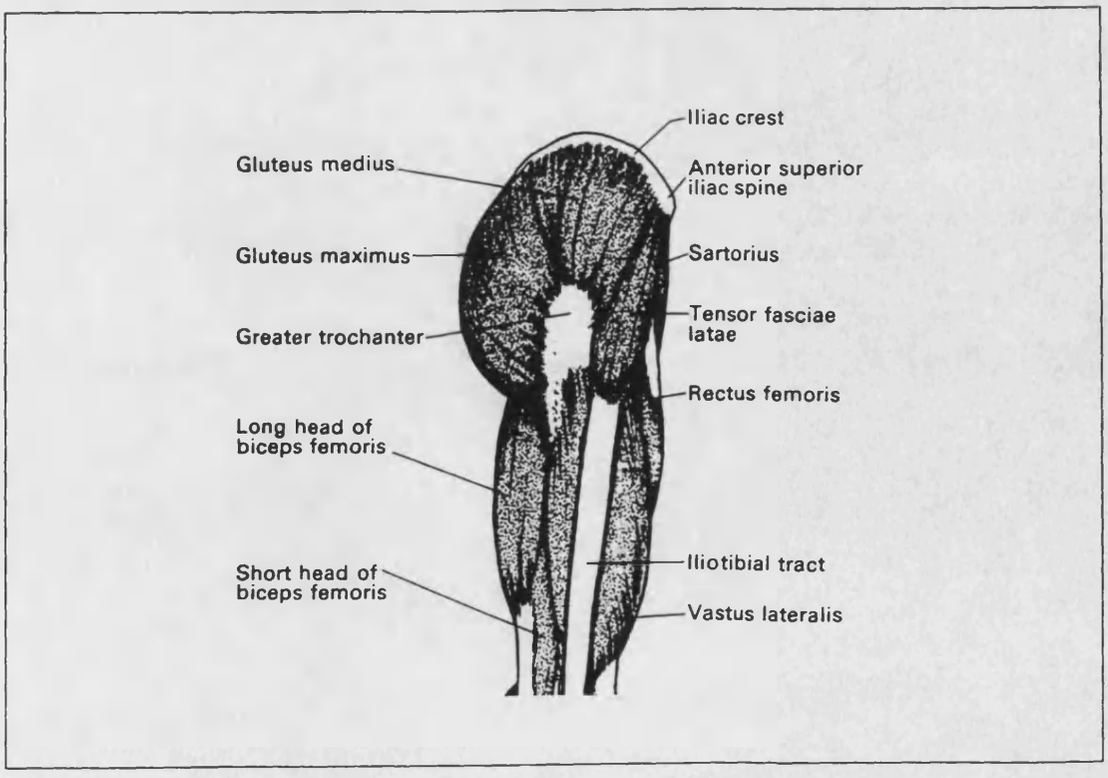

Figure 2-2 Muscles of the lower limb
From Green and Silver, 1981

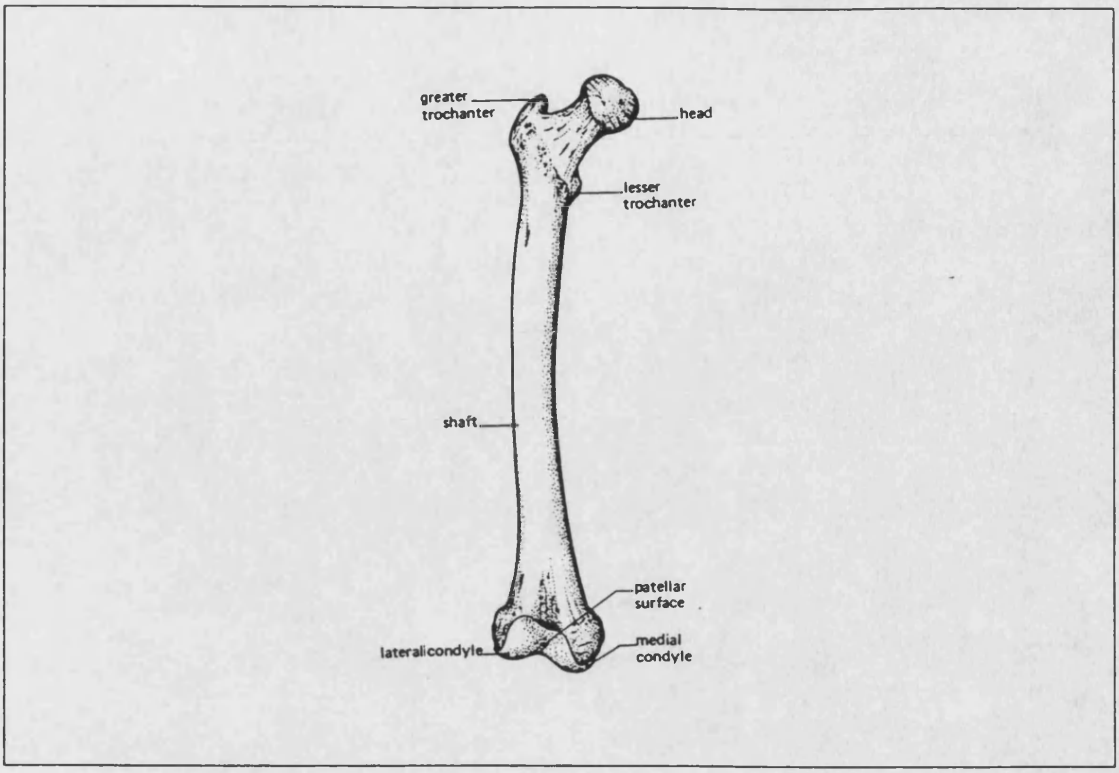

Figure 2-3 The femur (front view)
From Oxford concise medical dictionary

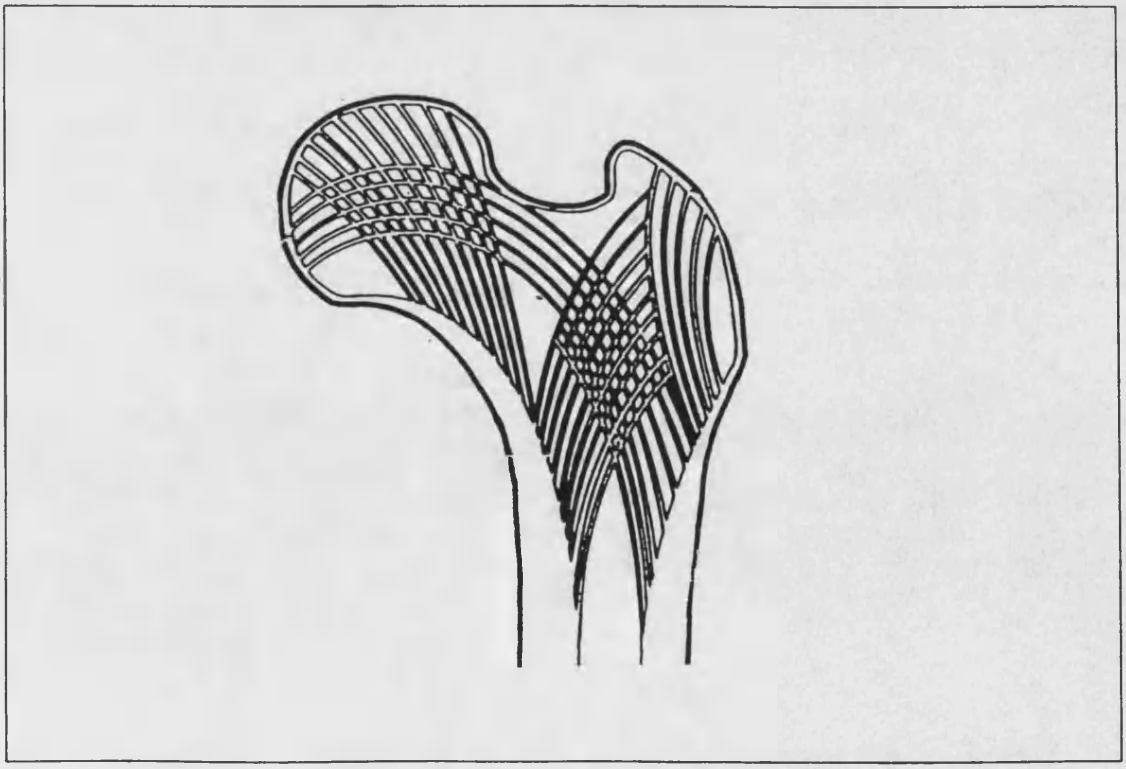

Figure 2-4 The trabeculae in the proximal femur. From Kyle, 1994

The femoral head articulates with the acetabulum to form the hip joint. The femoral head is approximately a half sphere and is connected to the bone shaft by the neck of the femur.

The greater trochanter is positioned at the upper part of the junction of the neck and shaft of the femur and is a large quadrangular projection. It provides anchorage for most of the muscles of the buttock or gluteal region of the hip (see figure 2.2). The lesser trochanter is situated at the lower posterior part of the juncture and is a conical protrusion. Again it acts as an insertion point for muscles. The junction between the neck and shaft is characterised by an oblique rough ridge on the anterior surface of the bone, known as the intertrochanteric line, that runs from the greater to the lesser trochanter. On the posterior surface, the greater and lesser trochanter are joined by another ridge known as the intertrochanteric crest.

The shaft or diaphysis of the femur is essentially a cylinder of compact or cortical bone with a large medullary canal at its centre. The cortical wall is thickest in the middle third of the shaft where the outer diameter of the bone is smallest. The narrowest point of the medullary canal is known as the isthmus. The cortical bone thins towards either extreme of the shaft and the medullary canal gradually fills with spongy cancellous bone. The femoral head and the femoral condyles consist mainly of spongy cancellous bone covered with a thin layer of cortical bone. Cancellous bone consists of thin bars of bone or trabeculae arranged in a lattice. The trabeculae in the proximal femur are thought to be positioned along the lines of greatest stress. In this way they can help to transmit this stress through the hip to the shaft of the femur (figure 2.4).

The posterior surface of the femoral shaft usually forms a rough ridge, the linea aspera, on to which several muscles are attached. The ridge itself is a result of the continual pull of the muscles on the posterior surface of the bone. The exterior of the bone, except the articular surfaces, is covered with a dense, highly vascular connective tissue known as periosteum while the marrow cavity of the bone is lined with a membrane, known as endosteum. Periosteum is a primary source of new bone in all species (McLean and Urist, 1961). Its internal layer builds up new tissue on top of the existing bone leading to circumferential growth (Hall, 1995). Longitudinal growth of bones occurs at the epiphyses, the growth plates which are found near the ends of long bones. These produce new bone cells.

The bone shaft widens at its distal extreme to form the femoral condyles. The condyles are two knuckles of bone that form the upper articulating surface of the knee. The medial condyle, that nearest the centre of the body, is the most prominent. Posteriorly, the condyles are separated by a deep gap, known as the intercondylar notch.

2.1.3 The abductor muscles

A group of muscles that have particular relevance in this study are the abductor muscles. This group consists of three individual muscles, the gluteus medius, gluteus minimus and tensor fasciae latae. Their function is to allow the leg to be moved away from the midline of the body known as abduction (see figure 2.2). During single legged stance they act to stabilise the hip allowing the body to remain balanced. All three muscles originate from the pelvis. The gluteus medius and minimus attach to the greater trochanter of the femur, whilst tensor fasciae latae inserts in to the iliotibial tract.

The iliotibial tract is a tendon that runs down the lateral side of the thigh parallel with the femur (figure 2.2). The tract is attached to the linea aspera and distally to the lateral condyle of the tibia. Tensor fasciae latae and the iliotibial tract not only act to stabilise the hip like the other abductors, they also help to distribute load in the femur. Ling *et al.* (1996) have compared the function of the fasciae latae and tract with that of the rigging on a sailing yacht (figure 2.5). Tension in the rigging holds the mast in compression. Due to body weight being transferred through the hip, which is offset from the femoral shaft, the femur is subjected to large bending forces (figure 2.6). Tensor fasciae latae and the iliotibial tract act like the rigging producing compression of the femur, the mast, which reduces bending of the shaft of the bone.

2.2 JOINT LOADING

2.2.1 Determining hip joint loads

Knowledge of the forces that act at a joint is important in understanding degenerative disorders such as osteoarthritis. Activities that cause high forces leading to joint wear can be avoided. It is also important to know the details of loading for the design of prostheses such

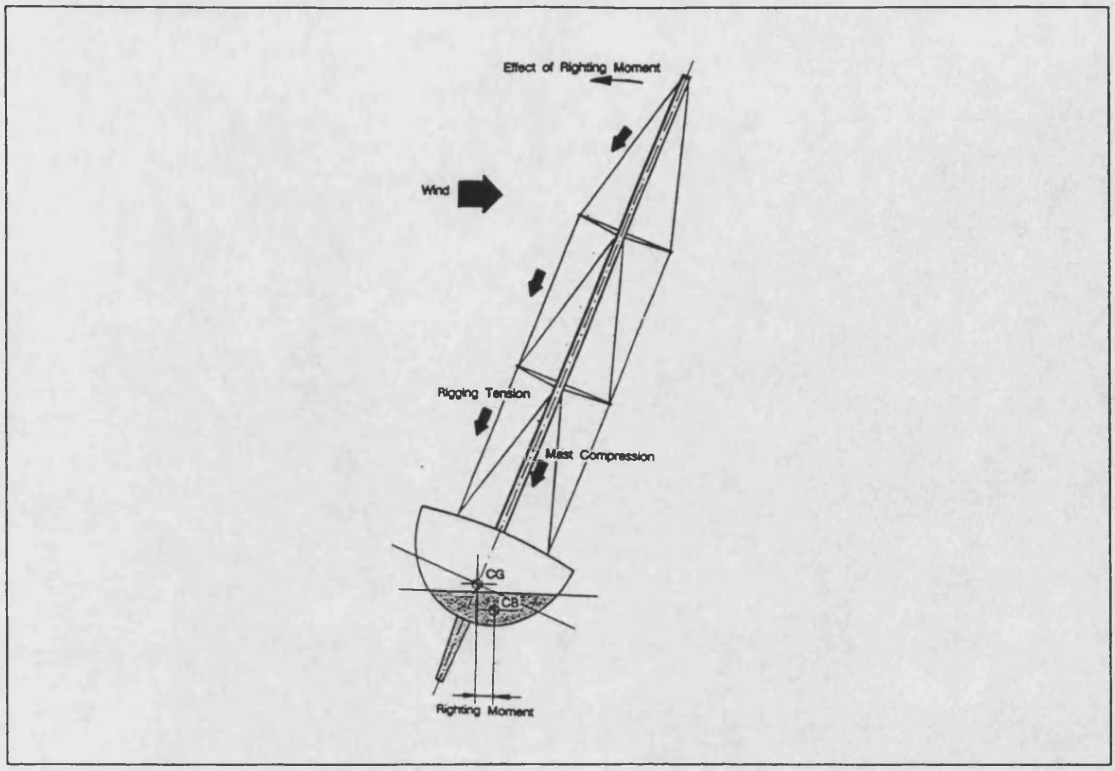

Figure 2-5 The mast of a sailing yacht is held in compression by the rigging, which is in tension. From Ling *et al.*, 1996

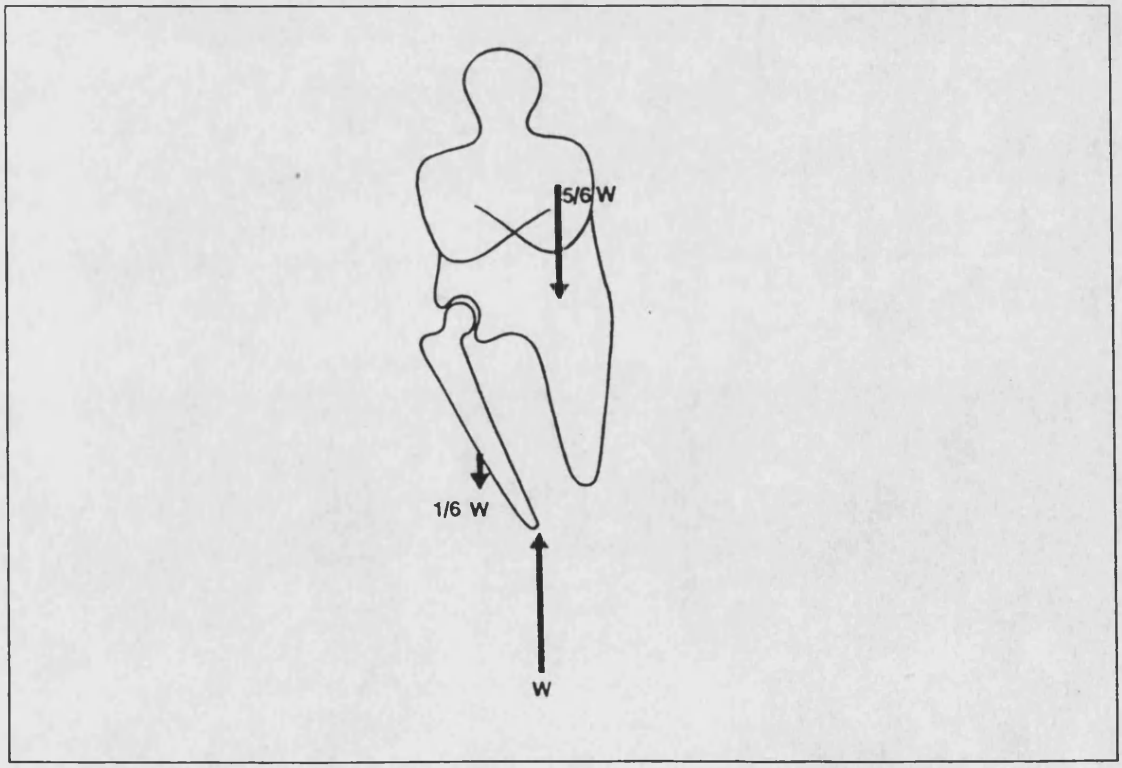

Figure 2-6 Large bending moments act on the femur due to the offset of body weight. From Nordin and Frankel, 1989

as joint replacements and fracture fixation devices to ensure they will not fail *in vivo*. There are two ways of determining joint forces. The first is to predict the force based on a model which is of the correct geometry and by resolving the components of body weight and the external forces that act on it. The second is to take direct measurements using instrumented devices.

Basic calculations can be performed to determine the joint reaction force acting on the hip during a single leg stance for example. The following assumptions are made.

- The pelvis is level during single legged stance. In reality, the pelvis must be tilted slightly in order to balance the body.
- The lower leg has a weight equal to one sixth body weight.
- The abductor muscles (gluteus medius, gluteus minimus and tensor fasciae latae) are the only muscles active during single legged stance. Muscle action can be recorded using electrodes which register their electrical activity (UCLA, 1953; Carlsöö, 1972; Crowninshield *et al.*, 1978). Figure 2.7 shows that at the point between 15% and 30% after heel strike, which is equivalent to single legged stance, the hip abductors are the only active muscles.
- The action of the abductor muscle forces can be resolved to one force acting at 30° to the vertical (Nordin and Frankel, 1989).

Using figure 2.8, where W=body weight, M=abductor muscle force and J=joint reaction force:

Moment equilibrium gives $$Mc - \frac{5}{6}W \times b = 0$$

From X-rays it can be determined that b=2.4c. Therefore

$$M = 2W$$

Resolving into horizontal (x) and vertical (y) components

$$M_x = M \sin 30° = W$$
$$M_y = M \cos 30° = 1.7W$$

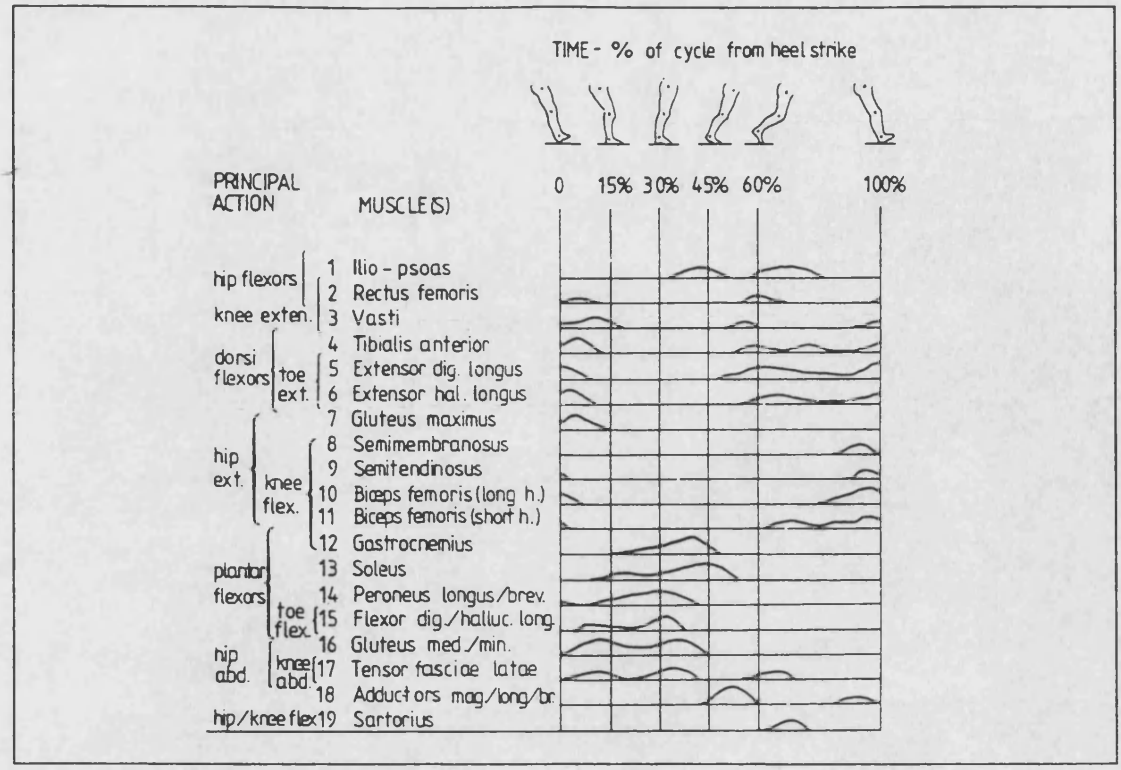

Figure 2-7 Phasic activity of the lower limb muscles
From UCLA, 1953

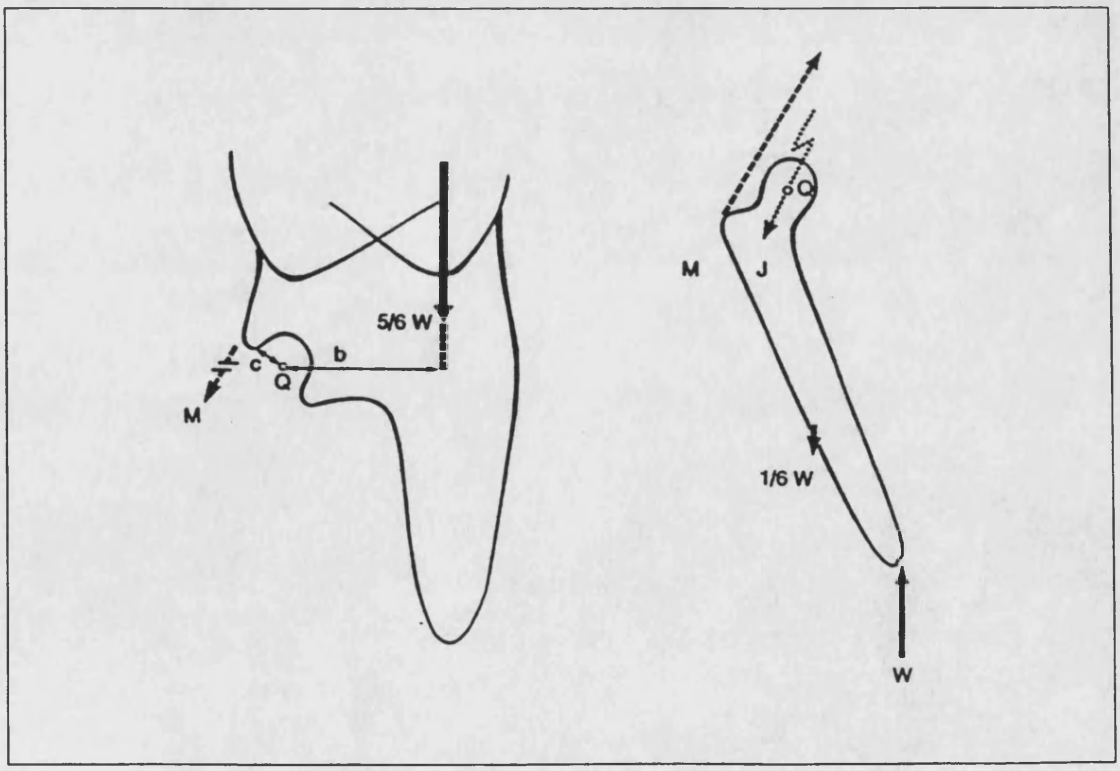

Figure 2-8 Free body diagrams of the lower limb
From Nordin and Frankel, 1989

Resolving horizontally (x) and vertically (y)

$$M_x - J_x = 0 \Rightarrow J_x = M_x = W$$

$$M_y - J_y - \frac{1}{6}W + W = 0 \Rightarrow J_y = 2.5W$$

This gives the resultant joint reaction force J=2.7W @ 22° to the vertical, nearly three times body weight.

Calculating joint forces at further stages of the walking cycle and during other activities, such as running, may not be as simple as this. A large number of muscles are required to produce such motion, and therefore due to the unknown magnitude of the muscle forces, make the equations indeterminate.

Paul (1966-67) carried out more detailed calculations of the hip joint force. Test subjects had markers placed on their ankle, knee and hip joints and were photographed with cine cameras whilst walking. Ground reaction forces and moments were recorded from a force plate which the subjects walked across. The test subjects also wore electrodes to monitor which groups of muscles were active during walking. The information was used to calculate the forces acting at each joint by considering the mass and acceleration of each segment of the leg (lower and upper). But again, due to the number of active muscles, major assumptions had to be made to avoid indeterminate equations, notably the neglect of the internal and external rotators.

The results of Paul's study showed that the joint reaction force varies during walking and has a two peak characteristic (figure 2.9). The first peak corresponds to the impact after heel strike. The second peak is a result of the subject accelerating towards toe off at the end of the step. The maximum joint reaction force calculated was approximately four times body weight occurring before toe off. The force was found to act at an angle of 12.5° with the hip-knee axis in the medio-lateral (ML) plane, and -7° with the hip-knee axis in the antero-posterior (AP) plane (figure 2.10). Single legged stance occurs after heel strike, with the joint reaction force between two and three times body weight, angled nearer 21° and 12° in each plane respectively (figure 2.10)

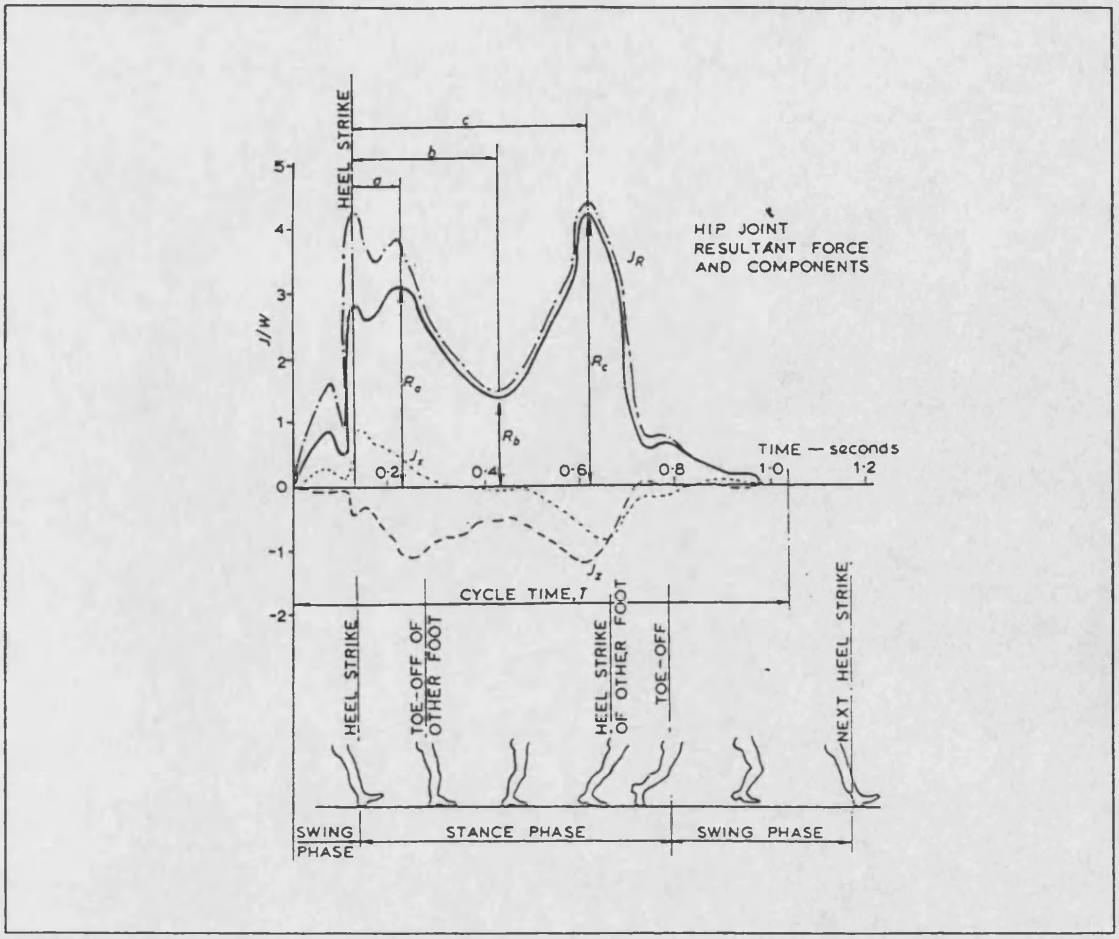

Figure 2-9 The variation of hip joint reaction force, J_R, with time. The peaks occur at a) 7% and c) 47% of the cycle from heel strike. From Paul, 1966-67

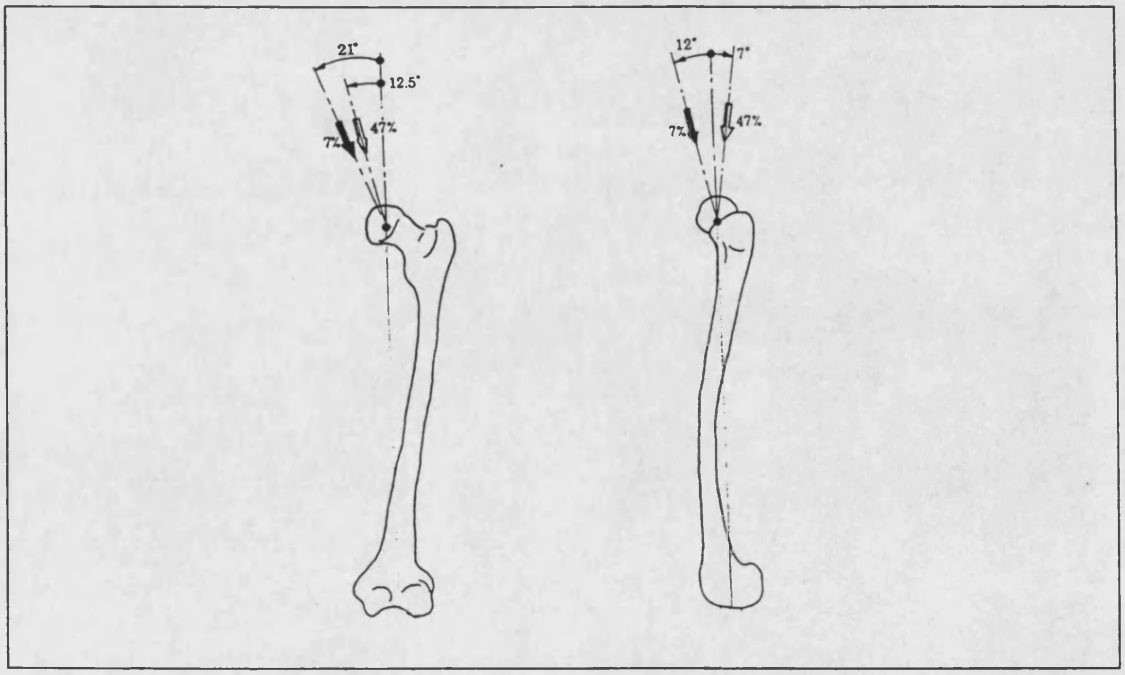

Figure 2-10 Directions of the hip joint reaction force relative to the femur at 7% and 47% of the cycle from heel strike. From Paul, 1976

Direct measurement of joint forces *in vivo* eliminates the problem of unknown muscle forces and can provide detailed joint force information during complex movements. However, due to the difficulty and ethicacy of implanting instrumented devices for this purpose, few studies have been carried out.

The first direct measurement of hip joint force was achieved by Rydell in 1966. He implanted a strain gauged prosthesis in two patients to measure the load acting on the head of the femur. Six months post operatively, the wires from the device were exposed through the skin and readings were taken while each patient walked. Measurements were also taken with the patients standing on one leg. The results during walking showed the characteristic two peaks. The maximum joint force was approximately 2.5 times body weight. This was lower than Paul's predicted value of four times body weight and was thought to be due to the assumptions he made. Rydell also measured hip joint force during running. The maximum value increases up to four times body weight and the two peaks merge in to one.

English and Kilvington (1979), Davy *et al.* (1988), Bergmann *et al.* (1993) and Brand *et al.* (1994) have also conducted studies using instrumented femoral prostheses to calculate joint forces. These studies used telemetric devices that transmit the transducer signals from the implant to an external receiver. Generally, values for the magnitude and direction of the maximum joint reaction force agreed. Differences between the studies were attributed to the speed of walking and the condition of the patient at the time of the tests. Data from each of these studies on the joint reaction force during single legged stance is given in table 2.1.

	Joint reaction force (x body weight)	**Load angle ML plane**	**Load angle AP plane**
Rydell, 1966	2.3, 2.8	40°, 33°	7°, 10°
English and Kilvington, 1979	3.59		
Davy et al., 1988	2.1	32°	15°
Bergmann et al., 1993	2.7	23°	15°
Brand et al., 1994	2.5-3.0		

Table 2-1 Joint force magnitudes and directions during single legged stance

The load component acting in the ML plane will produce bending of the femoral shaft while the AP load component will produce twisting (figure 2.11). Torsion of the femoral shaft is often ignored during testing. Several authors have commented on the magnitude of the torsional moment. Davy *et al.* (1988) reported a maximum torsional moment around their stem of 22Nm. Bergmann *et al.* (1993) commented on the torsional moment round the stem of their implant. The torsional moment at the single legged stance point of gait was roughly 13Nm. This value was found to increase with walking speed and reached a maximum value of 40.3Nm when the patient stumbled. The torsional moment is considerable and should not be neglected.

2.2.2 Hip joint simulators

Hip joint simulators have been designed to reproduce forces that the hip is subjected to allowing for the realistic evaluation of hip joint and femoral prostheses. As with the standards for testing intramedullary nails (chapter 1.3), the British Standard 'Recommendations for simulators for evaluation of hip joint prostheses' is inadequate (BS7251: part 7, 1990≡ISO/TR 9325, 1989). A general arrangement of the apparatus that should be used is given along with the description 'the femoral component should be mounted in an orientation that resembles the anatomical configuration'. There are no details of the angle at which the prosthesis should be mounted and the apparatus does not include the effects of muscle pull. Hence, numerous configurations of hip joint simulator have been used.

The majority of simulators, as with hip joint force analysis, examine loading during single legged stance because there is general agreement about the muscles and forces in this position. However, even with this knowledge there are huge variations in the configurations used. Table 2.2 gives a summary of the hip simulators used by a number of authors during simulation of a single legged stance. Several authors failed to document and justify details of the rig used making interpretation of the results more difficult.

Most authors realised that simulating muscle forces is important to achieve realistic strains in the proximal femur. However, the most common configuration used included only the abductor muscle force. This does change the strain environment (Hazlewood, 1996) when compared with the application of just a joint reaction force. However, the authors that

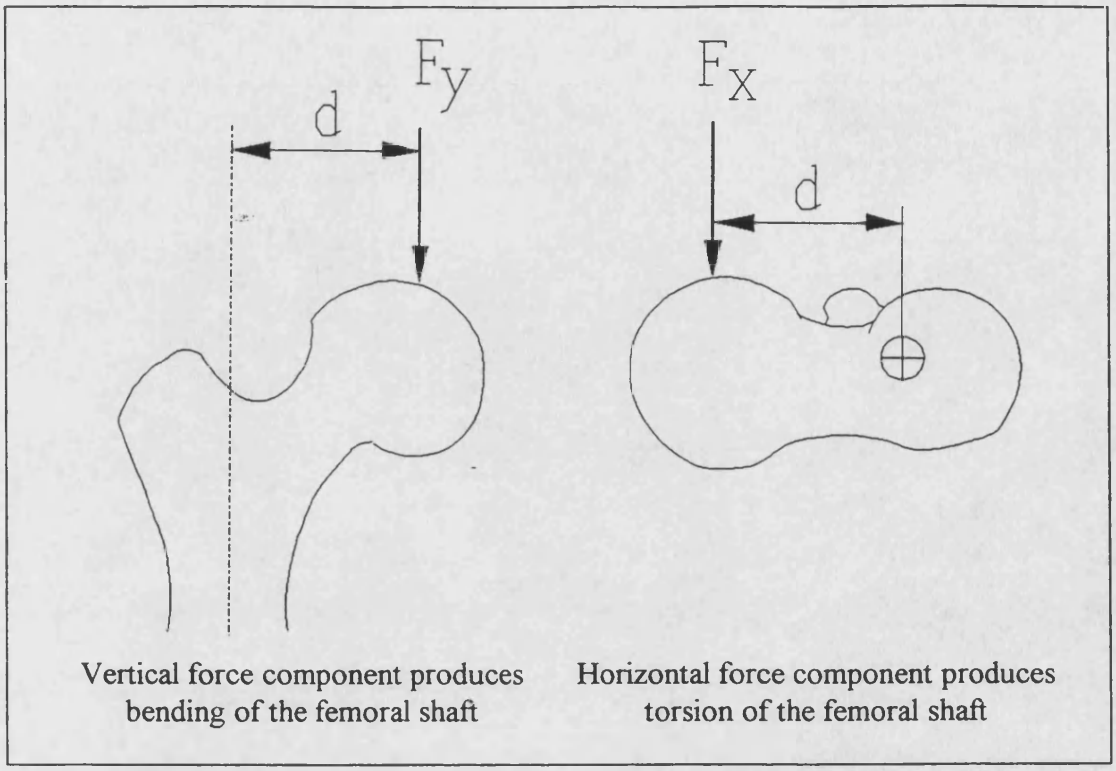

Figure 2-11 The joint reaction force produces bending and torsion of the femoral shaft.

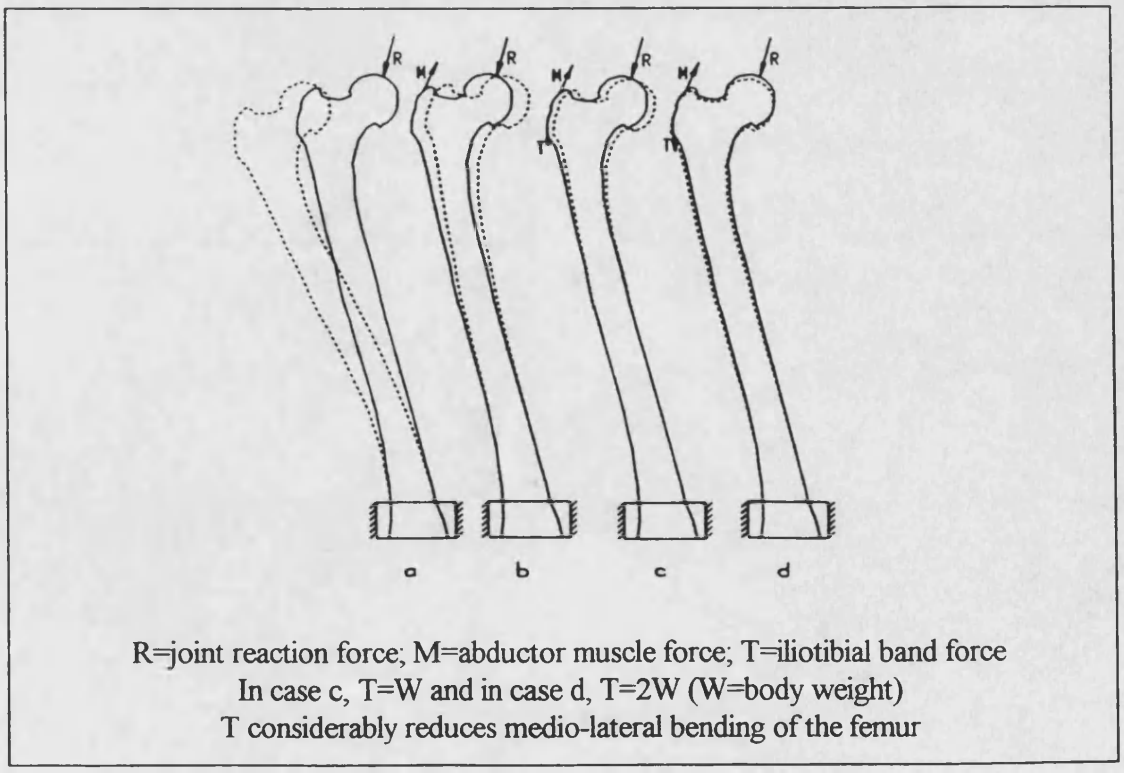

Figure 2-12 Deflections of the femur as a result of joint loading From an F.E. study by Rohlmann *et al.*, 1982

Study	Femoral shaft angle	Joint reaction force, R	Abductor muscle force, M	Tensor fasciae latae and iliotibial band, T
Callaghan, '92	12°	Offset load of 1500N applied vertically	15° ?	x
Cristofolini, '96	11°	Vertical	x	x
Engh, '92	12°	Offset load (445N) applied vertically to give R=1335N @ 21°	M=701N @ 15°	x
Field, '89	condyles horizontal	Load applied thro' hemi-pelvis gives R=1440N max. at 16°	M=800N @ 30°	x
Finlay, '89	11.3°	572N (=5/6W) thro' condyles. Femoral head in cup at 45°	20°±4°	x
Finlay, '91	11°	600N (=5/6W) thro' condyles. Femoral head in cup at 45°	M=594N @ 22° This was the force required to keep the pelvis level	T=396N @ 10° This was the force required to keep the pelvis level
Fischer, '92	20°	2.5W vertically. Shaft angle ensures resultant acts in correct direction	x	x
Hazlewood, '96	10°	2000N	M=702N @ 28°	x
Lengsfield, '96	-	R=2624N @ 21° ML and 13° AP Varied in both planes	M=2036N Varied between -10° and 35° AP	T=611N parallel to femoral axis
Merchant, '65	'neutral'	267N centrally through pelvis	Gluteus medius=334N, minimus=289N	T=133N All muscles had anatomic insertion points
Oh, '78	5-20° adduction	R=2683N max vertically	x	x
Rohlmann, '82	Anatomical	W=755N applied offset to give R=1980N	M=1375N	T=W and 2W
Schmotzer, '92	vertical	W applied offset @ 7°	30°	x

Table 2-2 Loading configurations used to simulate single legged stance
N.B. Unless otherwise stated, all force directions refer to the angle made by the force with the vertical in the medio-lateral plane

simulated tensor fasciae latae and the iliotibial band concluded that meaningful strain data was only obtainable with the inclusion of these effects (Finlay *et al.*, 1991). It reduced unrealistic bending of the femoral shaft (figure 2.12).

Two groups also commented on the importance of torsion acting round the femoral stem (Engh *et al.*, 1992; Fischer *et al.*, 1992) but then failed to include this in their single legged stance model. However, both groups went on to test implants during simulated stair climbing which, because of the flexion of the femur, includes an out of plane force creating a torsional moment around the femoral shaft. Lengsfield *et al.* (1996), were the only group to include an AP component of load during single legged stance in their finite element study. They found that the strain energy density (strain energy/bone volume) was particularly sensitive to the introduction of the iliotibial tract force and an out of plane component of joint reaction force. In fact, the strain energy density had a minimum value when 1) the iliotibial force was approximately 50% of the abductor muscle force and 2) when the joint reaction force was angled at 13° to the vertical directed posteriorly. It can not be coincident that the iliotibial band is believed to exert a force of one times body weight, and the abductor force, two times body weight on the femur (Rohlmann *et al.*, 1982; Gerlach and Lierse, 1990). The joint reaction force has also been found to act posteriorly at roughly 15° to the vertical in the AP plane during single legged stance (table 2.1). The body has evolved to reduce excessively large strains itself.

2.3 BONE FRACTURE AND HEALING

2.3.1 Fracture classification

A surgeon must recognise the pattern and assess the stability of a three dimensional fracture from a two dimensional X-ray and chose the most appropriate treatment for the patient. A stable fracture, one in which the bone is in equilibrium and not easily moved after reduction, requires minimalist treatment. An unstable fracture needs more rigid support to allow healing without complications. The implant must maintain the anatomic alignment of the bone and perhaps carry all of the load while initial healing occurs. A number of classification systems have been designed to help with making this decision. Fracture classification is also useful when documenting clinical studies. When quoted in the literature it enables the reader to

recognise a fracture pattern without the need to include multiple X-rays. It also allows the outcome of various studies using different devices for fracture treatment to be compared.

Bone is a viscoelastic material and its mechanical properties vary with the rate of loading. Bone loaded at higher rates, provided it is within a physiological range, has a higher stiffness and can withstand a greater load to failure than that loaded at lower rates. High loading rates produce comminuted fractures because the large amount of energy stored by the bone is released suddenly. Bone that fractures under low rates of loading is able to dissipate the stored energy through a single crack with no comminution. Bone fractures can be grouped as low, high and very high energy fractures according to the fracture pattern. High energy fractures can be sustained during car accidents while very high energy fractures are often the result of gun shot wounds.

The AO system of fracture classification groups fractures according to their location and geometry (Appendix A). Each bone is numbered, the femur being bone 32. Fractures of the shaft of long bones are divided in to three types: type A-simple fractures, characterised by a single cortical disruption of at least 90% of the bones' circumference; type B-wedge fractures where there is always some contact between the main fragments and where the length and alignment of the bone are usually restored; and type C-complex fractures in which there is no contact between bone fragments. Each of these fracture types can be subdivided again in to three groups 1,2 and 3. Group 1 deals with spiral fractures, the result of torsional loading; groups 2 and 3 describe those that are the result of other loading configrations. As an example, a fracture of the femur shown in figure 2.13 is classified as type 32-B1. It is a multifragmentary wedge fracture having a spiral pattern inducating that it was the result of torsional loading. There are further subdivisions but it is unecessary to explore these in this report.

Fractures are also termed 'closed' or 'open'. An open or compound fracture is one where the bone ends have pierced the skin. These types of fracture are particularly vulnerable to infection (Lin *et al.*, 1994). Open fractures are graded using the Gustilo and Anderson scoring system (Helfet *et al.*, 1994). A grade I classification indicates a wound of less than 1cm, and a grade IIIc wound is one associated with injury to an artery which requires repair.

2.3.2 Fracture healing

Bone is one of the most dynamic and metabolically active tissues of the body and has an excellent capacity for self repair. Fracture healing begins with the clotting of blood in and around the fracture gap after injury (McLean and Urist, 1961). Within 24 hours, organisation of the blood clot begins leading to the production of fibrin, a fibrous mesh which seals the damaged blood vessels. Within a few days the fibrin is replaced by granulation tissue, a vascular connective tissue that covers the healing surfaces of the wound.

Histogenic cells, used in the formation of new tissue, are supplied to the fractured bone ends from the torn periosteum, endosteum and bone marrow. These cells develop into fibrous connective tissue and cartilage with the help of lymphocytes, a variety of white blood cell usually involved in immunisation. These cartilaginous tissues are a temporary filling before the formation of new bone. The tissue deposition around the bone ends is known as a callus.

Bony tissue now unites across the fracture gap. Initially, an external callus consisting of an inner layer of osteoblasts, bone forming cells, and an outer layer of fibroblasts develops from the periosteum on either side of the fracture towards the centre of the fracture gap. Fibroblasts are responsible for the production of the precursors of collagen and elastic fibres. Collagen is a constituent of bone and accounts for approximately 25-30% of its dry weight. The osteoblastic layer grows outwards depositing new bone upon the surface of the fibrocartilaginous callus, forming an external arch of bone. The new bone then grows centripetally inwards replacing the cartilaginous tissue. Finally the external callus is remodelled, eventually disappearing, leaving no evidence of the initial fracture.

Healing characterised by abundant external callus is known as secondary bone healing but bone healing can also occur without callus formation, known as primary bone healing (figure 2.14). In this case cells bridge the fracture gap directly leading to the gradual disappearance of the fracture line radiographically. Primary union is not the bone's natural healing process but a natural bone turnover which occurs all the time in the skeleton (McKibbin, 1978).

The stiffness of a healing bone returns before its strength. The bony callus, distributed at a distance from the neutral axis of the bone, increases the second moment of area and hence the

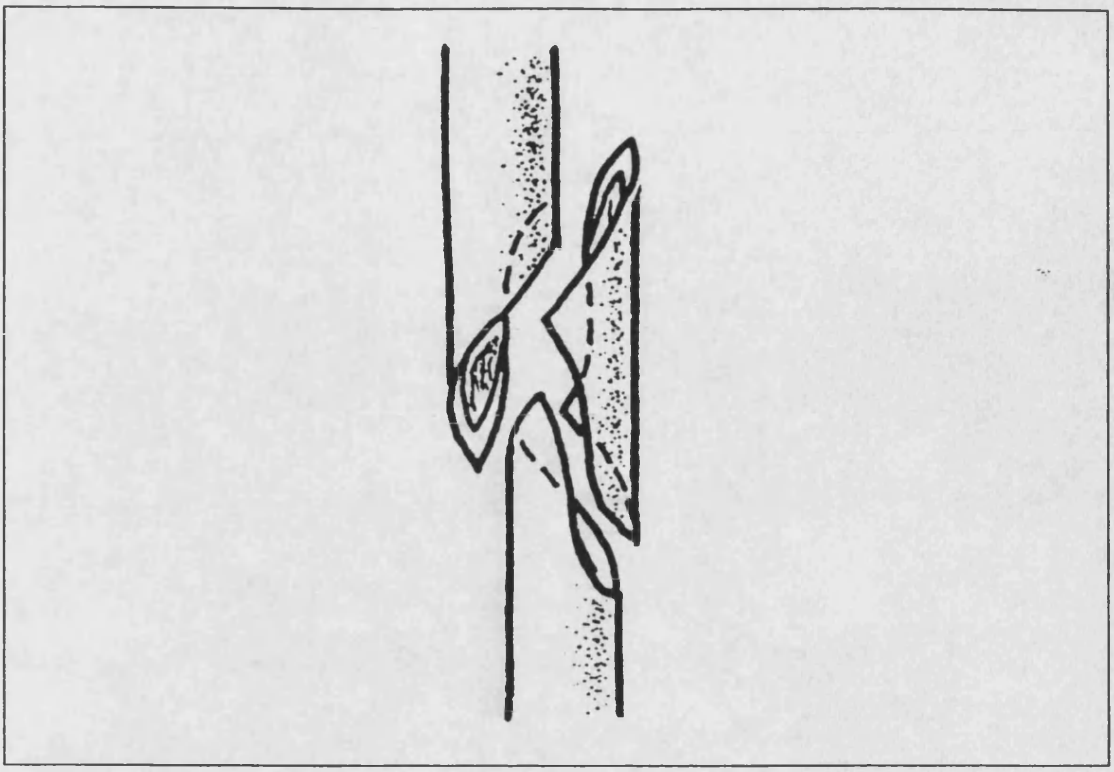

Figure 2-13 A femoral fracture 32 B-1 according to the AO fracture classification

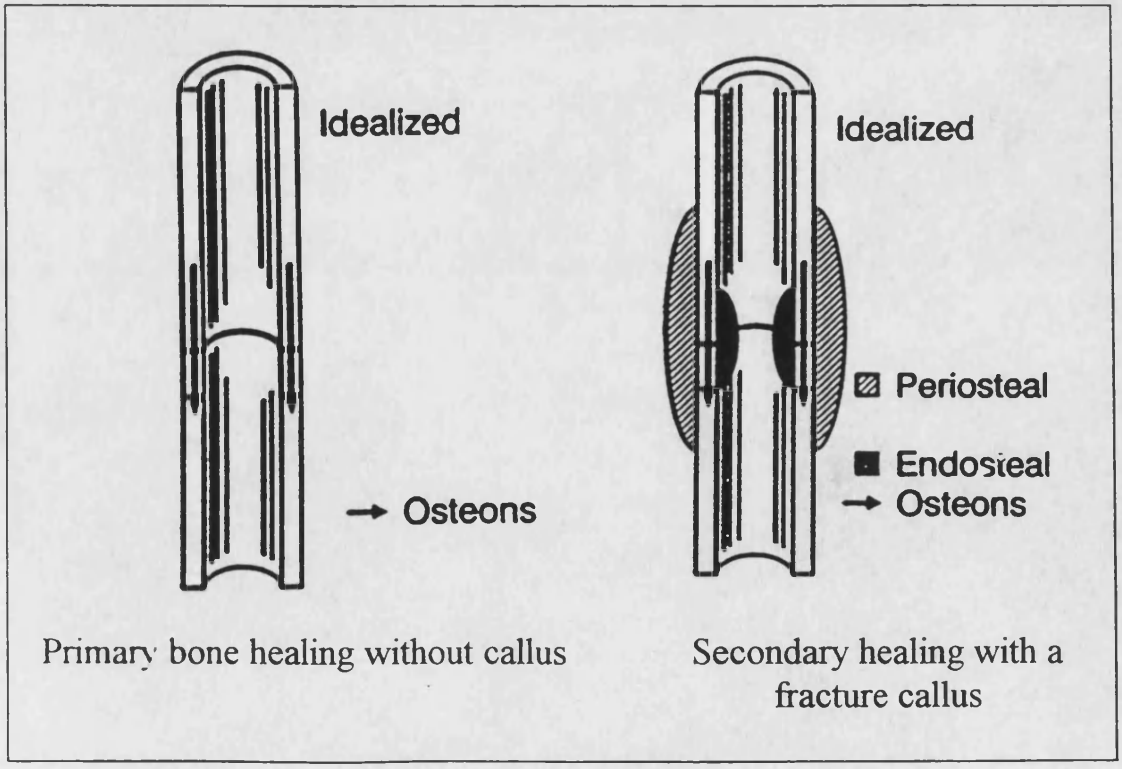

Figure 2-14 Primary and secondary bone healing patterns
From Aro and Chao, 1993

stiffness of the bone. The stiffness of the bone is reduced when the callus is remodelled because the excess material is removed. The strength of the bone, or its ability to resist load, returns later in the healing process after the return of stiffness (Black, 1988). A study by White *et al.* (1977) surmised that there were four stages of fracture repair relating to the strength and stiffness of the healing bone. Fractured rabbit tibiae were harvested at intervals post operatively and tested in torsion until failure. Figure 2.15 shows the torque-displacement curves of each 'stage of healing'. As the healing time increases, the amount of energy that the fracture can absorb before failure increases, as does the peak load to failure. Therefore, although the bone is able to support physiological loads early during the healing process because its stiffness has returned, it should not be overloaded until its strength returns to avoid refracture.

2.3.3 Mechanical environment for fracture healing

In 1979 Perren hypothesised that the rate of fracture healing, the change in matter from granulation tissue to bone, was influenced by the interfragmentary strain at the fracture site. The interfragmentary strain is the strain experienced by the tissue between the bone ends. Different tissues will form depending on the strain present. For example, granulation tissue can withstand strains up to 100% so forms initially in the fracture gap. This increases the rigidity, thereby reducing the possible motion, allowing other tissues to form that are less resilient to higher strains. Cartilage can tolerate strains of about 10% and bone approximately 2%.

Implants can be used to influence the strain environment and hence the healing process. Plaster casting a fractured limb allows a great deal of movement at the fracture site resulting in abundant callus, secondary bone healing. Rigid plate fixation, which immobilises the fracture interface results in very little callus with bone union achieved by primary healing (Terjesen and Svenningsen, 1988). Today, devices that promote secondary bone healing are considered desirable because primary healing is slow and lacks stiffness because of the absence of a fracture callus (McKibbin, 1978).

Wu *et al.* (1984) looked at the effects of external fixator stiffness on fracture healing in an animal model. The fixator stiffness was varied using six trans-fixation pins in one case, the stiffest device, and four in the other, the least stiff device. At 30 days post-

operatively the 4 pin fractures showed no torque resistance compared to the 6 pin cases, which had some resistance but fractured through the original osteotomy site. At 120 days, there was found to be no difference in the torque resistance between the two groups although a greater amount of callus was found in the less rigid system. However, callus with the 4 pin configuration was not 'mature'.

A similar study by Goodship *et al.* (1993) showed different results. Fixator frame stiffness was altered by moving the fixator bar further from the leg. A greater distance between bar and leg produces a less rigid device allowing more interfragmentary strain. At 6 weeks, the bones fixed with the less rigid device showed more advanced healing radiographically, a rapid rise in fracture stiffness (figure 2.16) and a greater bone mineral content. The stiffer group showed incomplete callus bridging and persistence of the fracture gap.

The difference in the results of these two studies emphasizes the uniqueness of each case. It is possible that the two extra pins of the stiffer device in Wu's study may have affected the healing process, for example by changing the blood supply to the fracture. This may have influenced the outcome. Goodship's study kept all other factors constant. It is agreed that greater interfragmentary strain, as a result of weight bearing on less rigid implants, does produce greater amounts of bone callus which is probably beneficial to the healing process.

Kershaw *et al.* (1993) took this idea one stage further. If axial movement at the fracture site was desirable, what effect would an imposed axial strain have on healing? Patients with tibial fractures were treated using external fixators. Half the group had a pneumatic actuator attached to the fixator which exerted a 1mm axial movement on the frame and was used at 0.5Hz for 20 minutes from one week post-operatively. This was continued until the patients were weight bearing. The fractures treated with this imposed micromovement achieved clinical healing in significantly less time than the control group (23 cf. 29 weeks). The authors concluded that micromovement in the first days after fracture might have produced the difference. This is a time when patients are normally very inactive and not even weight bearing.

stage 1- bone has low stiffness, failing through the original fracture site
stage 2- bone has high stiffness but fails through the original fracture site
stage 3- bone's stiffness increases slightly-fails partially through original fracture site
stage 4- bone's stiffness does not increase but failure is not associated with original fracture site

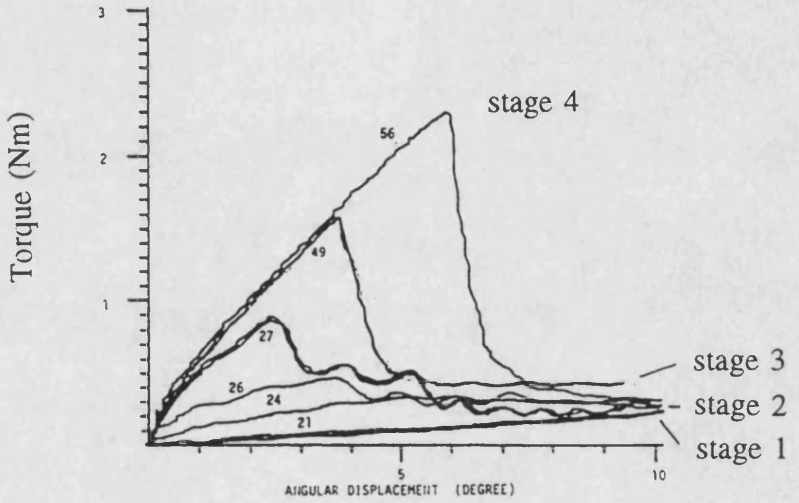

Figure 2-15 The four biomechanical stages of fracture repair. The numbers on the chart refer to the days of healing. From White *et al.*, 1977

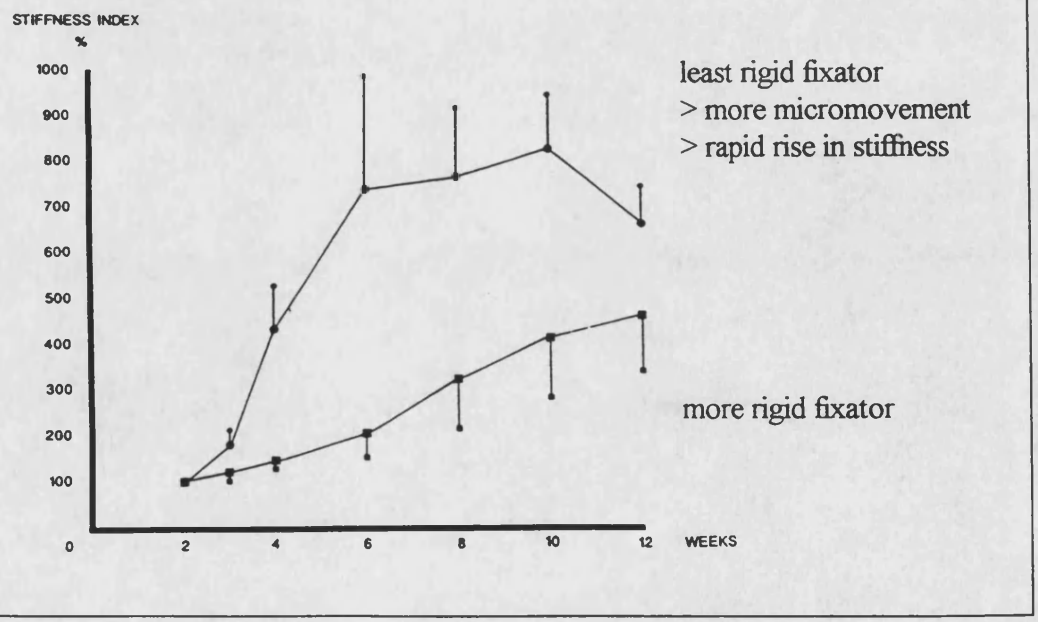

Figure 2-16 The increasing stiffness of two fractures with time treated using external fixators having different rigidities. From Goodship *et al.*, 1993

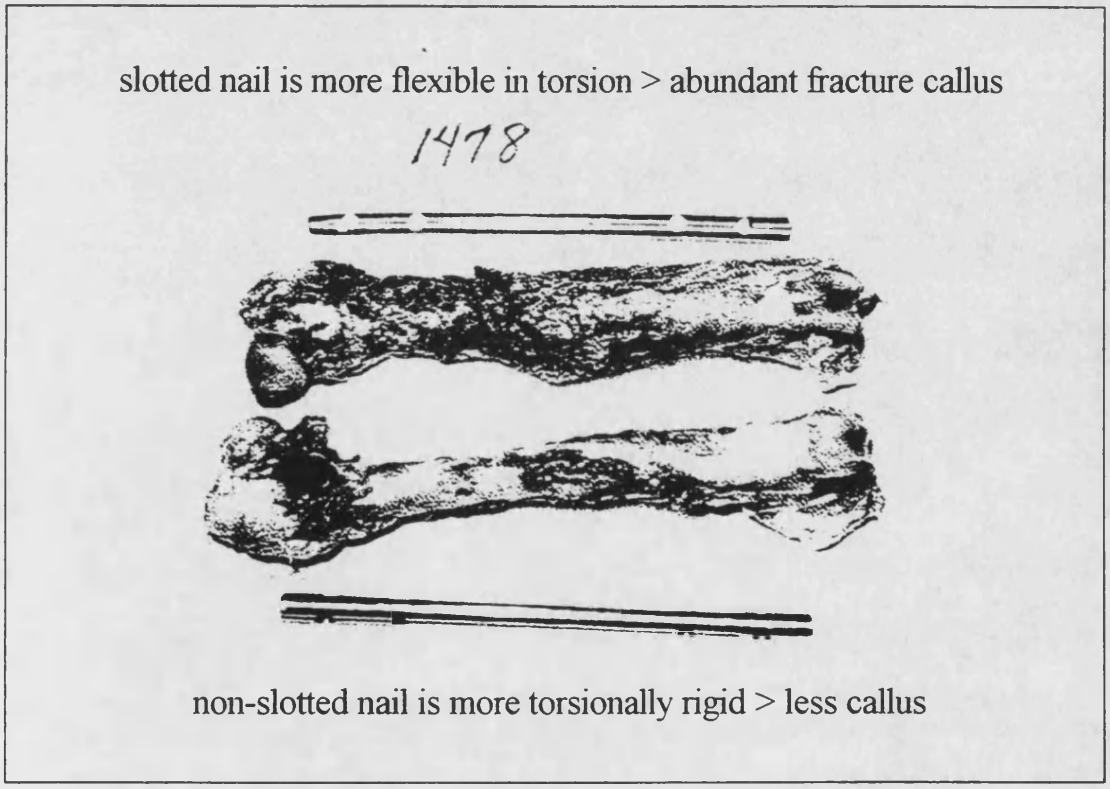

Figure 2-17 Two femora treated with intramedullary rods with different torsional stiffnesses. From Woodard *et al.*, 1988

A change in the axial loading of a fracture can be induced part way through the healing process. With an external fixator this can be achieved by allowing the fixation bar to telescope and an intramedullary nail can be dynamised by removing one set of locking screws. Egger *et al.* (1993) found that dynamising a fracture did not lead to greater callus formation. The fracture gap closed, due to the lack in axial stability, and a greater degree of the gap was filled with bone when compared to the undynamised group at six weeks. Aro and Chao (1993) also found no proliferation of callus on dynamisation. However in unstable fractures with delayed dynamisation, bone callus showed early signs of remodeling compared with the undynamised group. It is now clinically accepted that dynamisation does not accelerate bone union (Brumback *et al.*, 1988b). Most implants allow enough movement at the fracture site without dynamisation for satisfactory bone union. However, dynamisation is useful in promoting healing where a non-union is evident (Court-Brown, 1991).

These studies all document the effects of axial loading or axial strain on fracture healing. Relatively few studies have been found in the literature which deal with other loading conditions. Woodard *et al.* (1988) used two intramedullary rods in an animal study which had identical axial and bending stiffnesses but very different torsional stiffnesses. One nail was slotted and the other non-slotted. The slotted nail group showed 'exuberant callus' but was associated with some non-unions (figure 2.17). There were no differences in the mechanical properties of the two groups at any time. This is contrary to the results of Grundnes and Reikerås (1993) who found no difference in callus formation between two groups treated with nails, one with and one without rotational stability. They found that the fractures treated with rotationally stable implants had an ultimate bending strength three times greater than the unstable group.

There are few studies of this type, making it difficult to draw a conclusion on the effects of rotational instability on fracture healing. Different animal models were used and the rotational stiffnesses of the implants in the latter study were not quoted. Clearly more research on loading regimes is required if we are to determine the optimum mechanical environment for fracture healing.

2.3.4 Non-invasive monitoring of fracture healing

Fracture healing has been traditionally assessed by the physician using X-rays and by manually sensing the stability of the fracture. This is achieved by applying a bending moment across the fracture site and judging the patient discomfort and the visible angular deformation of the fracture (Matthews *et al.*, 1974). *In vitro* testing of a fractured forearm model by 90 orthopaedic surgeons with differing levels of experience, showed that the bending moment applied by each was remarkably consistent. The surgeons were also able to sense an angular deformation of 2.3 degrees at the fracture site. If the fracture bent to a greater degree the surgeon ceased to apply the bending moment to avoid refracture and agreed that union was not adequate.

This traditional method is used to estimate the stiffness of the healing fracture to judge whether union has occured. However, it often results in a limb being immobilised for longer than necessary. A fractured bone may be functional before it is declared 'healed' clinically using this method. The removal of a plaster cast or implant at an earlier stage might prove beneficial to the patient. Different ways of monitoring fracture healing have been investigated to try to accurately assess the mechanical integrity of a healing bone.

Richardson *et al.* (1994) calculated the bending stiffness of tibial fractures by measuring the angular deflection of the fracture under a given load (figure 2.18). The first group of patients were assessed clinically to determine whether the fixator should be removed. In group 2, the fixators were only removed after the fracture stiffness had reached 15Nm/degree. The change in stiffness with time is shown in figure 2.19. The authors found that there were no cases of refracture in group 2 patients, but that 7% of the group 1 patients experienced refracture. All cases of refracture occured in cases where the fixator was removed at a stiffness below 15Nm/degree. It was also noted that the patients in group 2 achieved full weight bearing in a shorter length of time compared to the group 1 patients (21.7 weeks compared to 24 weeks median). It was concluded that a stiffness of 15Nm/degree was a suitable indicator of union in tibial fractures.

A similar study by Shah *et al.* (1995) used this method to look at twenty cases where union was not seen radiographically at 20 weeks. Over the following weeks a definite increase in

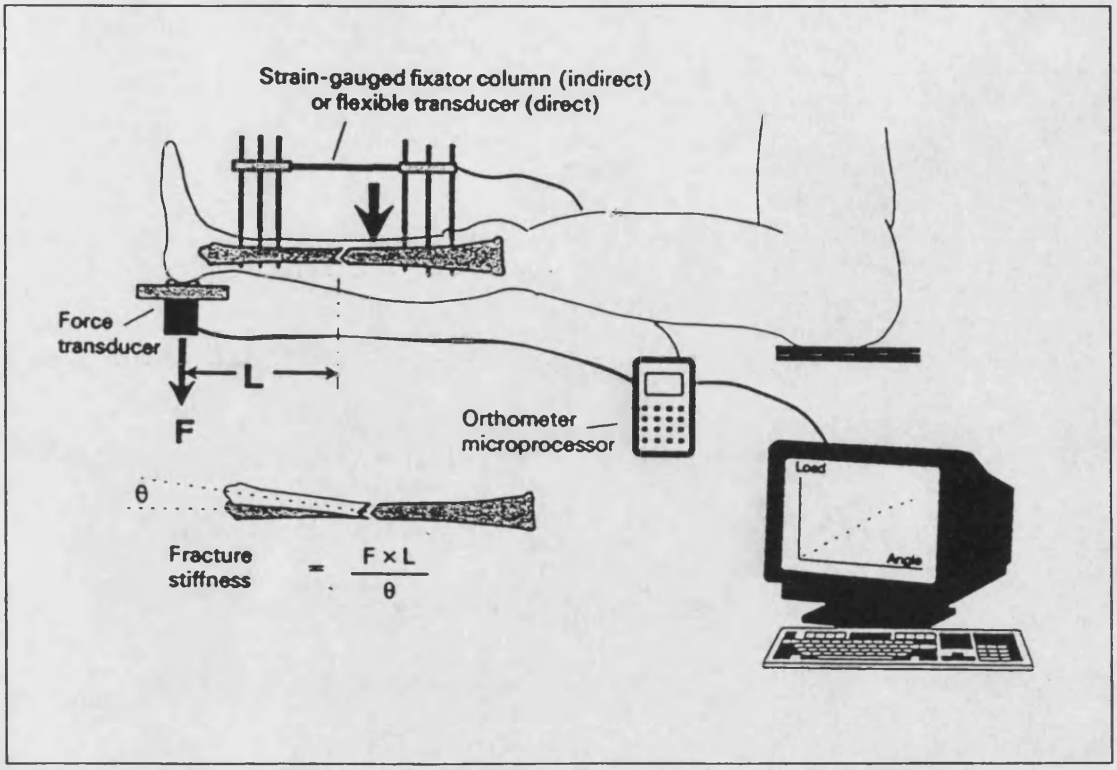

Figure 2-18 Measurement of fracture stiffness
From Richardson *et al.*, 1994

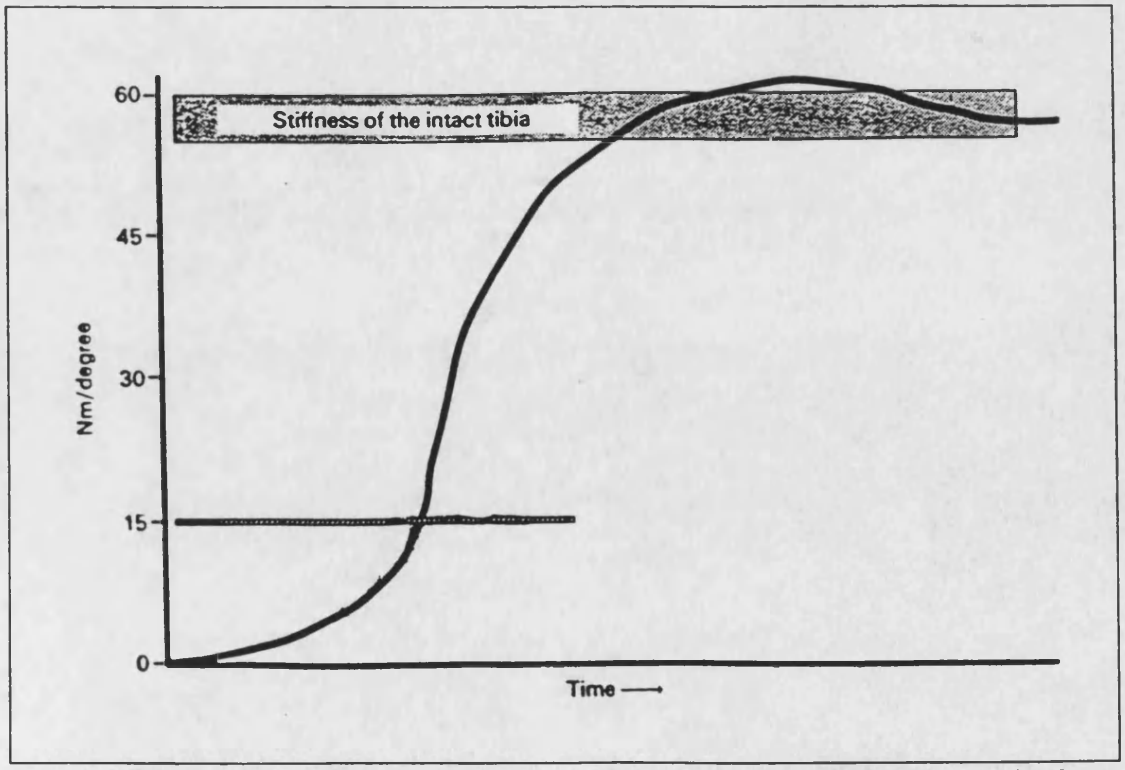

Figure 2-19 Fracture stiffness increasing with healing time. 15Nm/degree indicates tibial fracture union. From Richardson *et al.*, 1994

stiffness was seen with time. However, most of the fractures were stiffer than Richardson's 15Nm/degree at the outset of the study. The consistent increase in stiffness prevented surgical interference from the clinicians who were worried about non-union from the X-ray evidence.

Strain gauges applied to a humeral external fixator (Kristiansen and Borgwardt, 1992) were used to monitor the decrease in deflection, and hence an increase in fracture stiffness, during healing. The authors stated that the deformations reached a 'plateau of 50%' at 2-4 weeks after fixation in 6 out of 7 cases. Removal of the fixators at this stage was found to be safe.

Resonance analysis has frequently been investigated as a tool for measuring fracture healing. A hammer is used to excite the bone and an accelerometer used to pick up the response. From this test, information on the resonant frequencies of the bone can be found. Some studies have examined the shift, change in amplitude and change in phase of resonant frequencies seen with healing (Lewis, 1975; Nikiforidis *et al.*, 1990). Others aimed to relate the mechanical properties of the healing fracture with the resonant frequencies using *in vitro* healing bone models (Cornelissen *et al.*, 1982 & 1983; Laura *et al.*, 1990; Lowet *et al.*, 1993).

The models were often simplifed to a rod having a central section of a different material to simulate a fracture. The central material can be changed to vary the Young's modulus of the section as occurs with a healing fracture. Using the Bernouilli-Euler equation for the resonant frequency, f, of a beam, its mechanical properties can be determined.

$$f = const \bullet \sqrt{\frac{EI}{mL^3}}$$

where E=Young's modulus, I=second moment of area, m=mass and L=length of the beam. All studies recorded encouraging results with the stiffness properties predicted from the natural frequencies closely matching the actual stiffnesses.

In vivo studies using resonance analysis have concentrated more on comparing the resonant frequencies of the fractured and intact bones, assuming they should have the same response. Christensen *et al.* (1984) found clinical healing had occured when the fractured bone had a

resonance of approximately 80% of the normal side. This method does not determine early union but might be more reliable than using conventional X-rays to assess healing. Tower *et al.* (1993) correlated the ratio of the resonant frequencies of the fractured and intact bones with clinical healing indicators. There was significant correlation between the two even in cases where an unlocked, unreamed tibial nail was in place. Unfortunately this correlation was not evident in cases with locked, unreamed nails and reamed nails.

The problem evident with all these studies is their limitations. They all concentrate on the tibia because it is accessable rather than surrounded by musculature and other soft tissue such as the femur. The fractures tested have not been treated using internal fixation devices as this would affect the results (Tower *et al.*, 1993). Analysis of the tibia is also facilitated as it is an extremity and not constrained in the way the femur is.

Ultrasound has been used to monitor fracture healing. High frequency sound waves (>20,000Hz) are directed on to the body through a transmitter. At a boundary between two tissues, some waves are reflected and others continue. The reflected waves are picked up by a transducer. It is able to determine the depth of an interface by examining the time it takes the wave to be returned. The amplitude of the echo is dependant on the composition and structure of the reflector and is used to determine a brightness factor. This information allows an electronic image to be created (Fish, 1990). Used simply in this manner on fractured bones, ultrasound imaging was able to predict union before it was radiographically evident (Ricciardi *et al.*, 1993; Moed *et al.*, 1995).

Ultrasound travels with a constant velocity through a medium. It can be measured by recording the time it takes an ultrasonic wave to travel between a pulse generator and a transducer which are a known distance apart. Table 2.3 lists the velocities for several types of biological tissue.

Lowet and Van der Perre (1996) investigated the change in ultrasound velocity in a bar with defects to simulate a fracture. By examining the path of the wave and the effects of surrounding materials they were able to accurately predict the velocities. However their assumptions might make clinical use less successful: 1) the tissue between the transducers and

bone had to have a constant thickness and 2) the ultrasound velocity must be constant in the surrounding tissue over the measurement area. These assumptions might be applicable to the tibia but not for many other bones of the body. In addition the exact wave path had to be known. With a simple fracture this would be predictable but much more difficult in a wedge or complex fracture (AO types B and C) where the ultrasound wave is likely to be deflected by a defect.

Medium	Velocity (m/s)
Air	330
Water (20°C)	1480
Blood	1570
Fat	1460
Muscle	1580
Bone	3500
Soft tissue (mean)	1540

Table 2-3 Ultrasound velocities in biological tissues
From Fish, 1990

Measuring the ultrasound velocity is clearly problematic so ultrasound is being used in other ways to measure fracture healing. As an ultrasonic wave passes through a medium it will lose intensity due to absorption, scatter, reflection and refraction. The loss of intensity can be calculated as an attenuation coefficient and is tissue dependant. *In vitro* and clinical work is being used to assess this as a method of determining fracture healing (Cunningham, 1997).

Markel and Chao (1993) investigated other non-invasive techniques for monitoring fracture healing. Quantitative computed tomography (QCT) can be used to measure bone density and single-photon absorptiometry (SPA) and dual-energy X-ray absorptiometry (DEXA) to measure bone mineral content. These parameters will both be influenced by the stiffness of the healing fracture. In tests on osteotomised canine tibia, all three methods of fracture assessment were found to correlate strongly with the structural properties of bone. DEXA showed lower correlations than either QCT or SPA. The authors believed that this lower correlation was due to the low resolution of the DEXA scanners but that with an increased resolution this method of monitoring might be the most useful. This is due to the comparatively faster scanning time and lower radiation emission of DEXA. These are important if repeated measurements are required.

The non-invasive monitoring of fracture healing without the use of X-rays has great potential and is clearly possible using a number of methods. If union, delayed union and non union can be anticipated at an early stage with these methods then treatment can be adapted accordingly. The exact mechanical integrity of a fracture may also be diagnosed enabling the early removal of a fixation device.

2.4 BIOMECHANICAL STUDIES OF INTRAMEDULLARY NAILS

2.4.1 Introduction

Biomechanical studies of intramedullary nails tend to concentrate on comparing the large number of nails available. As an introduction to a review of these studies, a description of the most commonly used nails is necessary. A general summary of their geometry, dimensions and form of interlocking is given in table 2.4. Some features are worth a further mention.

The slotted nails are sometimes liable to 'twist' during insertion. Attempts have been made to reduce 'twisting' in the AO Universal nail. At the proximal end of the nail, the edges form mating parts in the form of a keystone configuration (figure 2.20). This prevents the nail from opening out around the slot and reduces rotation during insertion. The Grosse-Kempf nail is slotted distally but has a closed section proximally to prevent these problems.

The majority of nails provide holes at their proximal and distal extremes for interlocking screws to prevent shortening and rotation of the fracture fragments in unstable fractures. Distally, most nails allow for the possibility of transverse interlocking with two screw holes. The Brooker-Wills and Derby nails differ. Distal fixation is achieved by deploying fins from the proximal end of the nail, through distal slots, into the bone cortices after nail insertion is complete. The aim of these devices was to reduce the surgeons' exposure to radiation during implantation (Sanders *et al.*, 1993). The Derby nail also differs from most other nails in its method of proximal fixation. Instead of interlocking screws, four distally facing pins are attached to a collar that can be threaded over the outside of the intramedullary nail head. The pins can then be locked into the greater trochanter of the femur.

Conversion to dynamic locking, or 'dynamisation', achieved by removing one set of locking screws, may be carried out in cases of delayed union. This will increase loading of the fracture site which is thought to stimulate healing. The AO Universal nail has two proximal fixation holes, the most proximal hole being oval rather than circular in shape. The nail can be dynamised by removing the lower proximal screw to allow limited axial compression, the length of the oval hole, while maintaining rotational stability.

Implant	Distributor	Cross section	Wall thickness	Proximal interlocking	Distal interlocking
ACE AIM system (Ti)	DePuy	solid with rectangular slot		45° 6.5mm screw	2 transverse $\phi \geq 13$mm, 6.5mm else 4.5mm screw
AO Universal	Synthes	open clover leaf	1.2mm	two 4.4mm transverse screws	two 4.4mm transverse screws
Brooker-Wills	Biomet	open clover leaf		oblique screw	fins
Derby	Thackray	closed circular		trochanteric pins	fins
Enders	Howmedica	solid circular	ϕ=4/4.5mm	x	x
Grosse-Kempf	Howmedica	slot distally	1.5mm	50° 6.35mm screw	two 6mm transverse screws
Huckstep (Ti)	Aesculap	solid rounded square		4mm screws at 15mm intervals along entire nail length	
Klemm-Schellmann	Biomet	slotted		30° screw	transverse screws
Küntscher		open clover leaf		x	x
Küntscher interlocking		open clover leaf		transverse screw	transverse screw
Russell-Taylor	Smith & Nephew	closed clover leaf	$\phi \geq 12$mm, 1.2mm else 1mm	45° 6.4mm screw	two 6.4mm transverse screws
URFN (Ti) {unreamed femoral nail}	Synthes	$\phi \geq 12$mm solid fluted else solid circular		two 4.9mm transverse screws	two 4.9mm transverse screws

Table 2-4 Characteristics of common intramedullary nails
N.B. (Ti) indicates the implant is titanium or titanium alloy. Interlocking screw angles are with reference to the vertical in the medio-lateral plane.

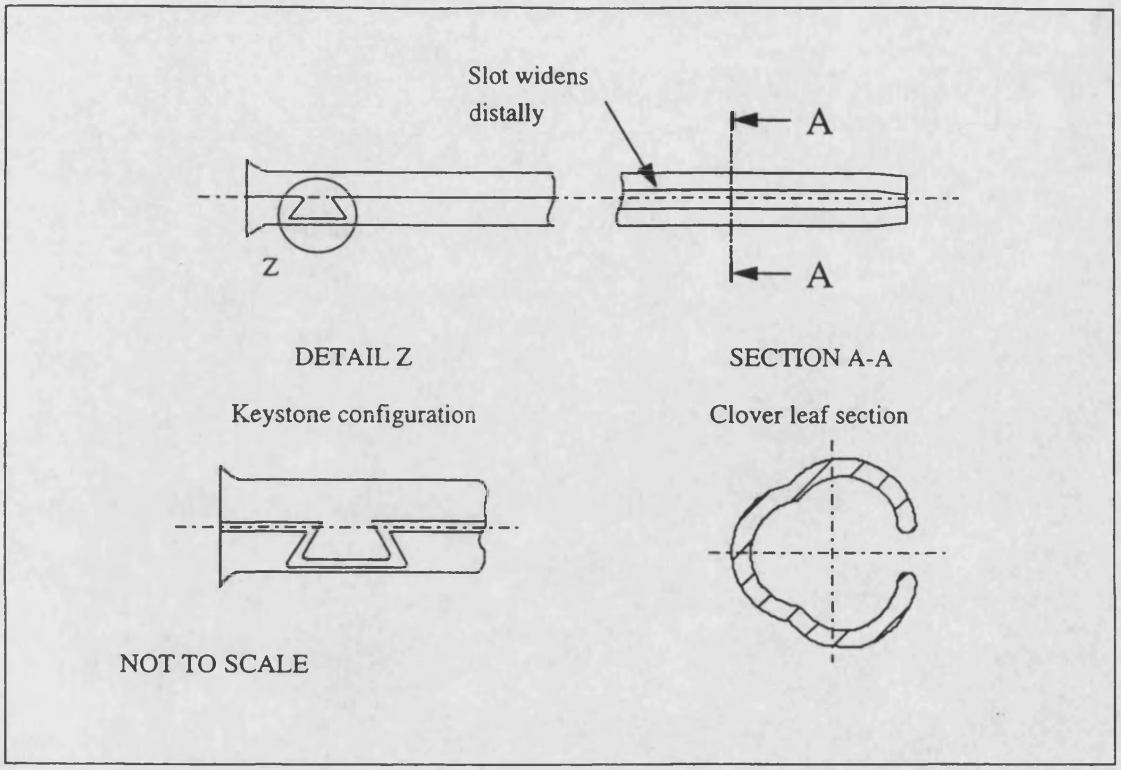

Figure 2-20 The AO Universal nail proximal keystone configuration

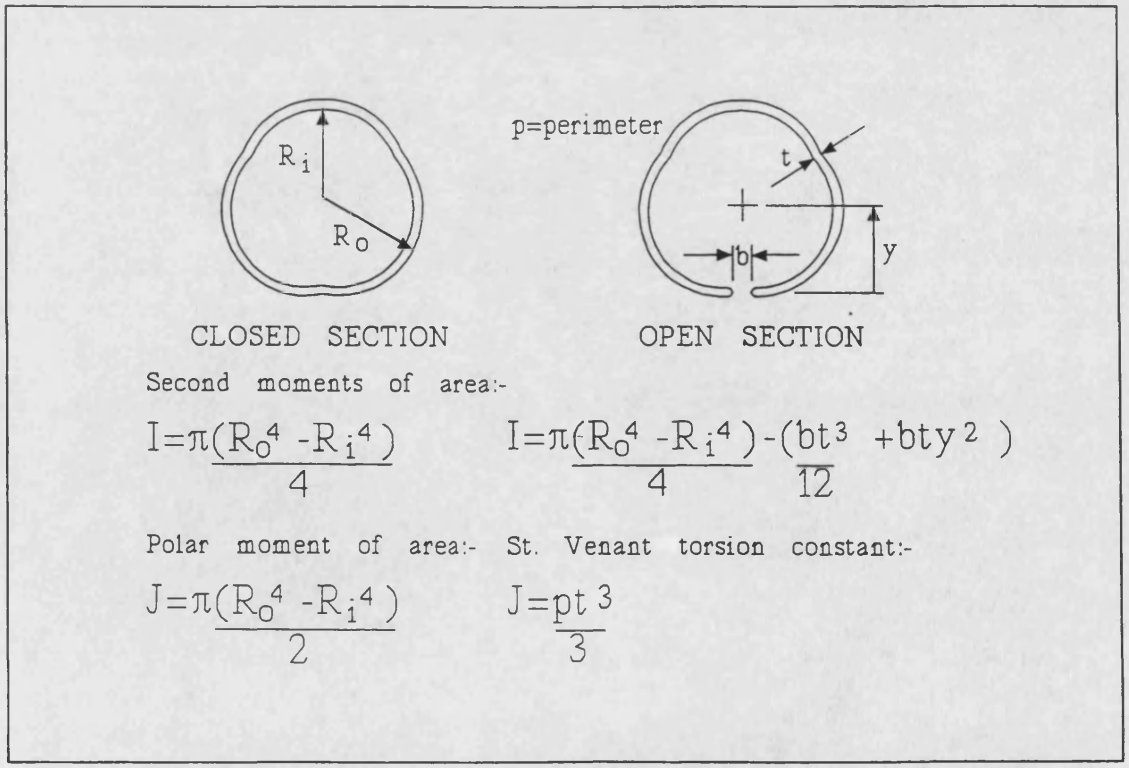

Figure 2-21 Theory of second moments of area for an open and closed circular section

2.4.2 Isolated nail studies

The intramedullary nail is responsible for stabilising a fracture and sharing load while the fracture heals. It is important to determine the mechanical characteristics of these devices in order that they can be designed to withstand failure. Several studies have compared the mechanical characteristics of different nails. Guichet *et al.* (1992) characterised various intramedullary nails including the Grosse-Kempf, Russell-Taylor and AO Universal nails. The bending properties were determined in four point bending in both the antero-posterior and lateral planes. Two tests were completed in each plane; the first test included the proximal interlocking screw holes within the outer reaction points but these holes were excluded from the second test. The torsional properties were determined using a 100mm superior section of each nail. Finally the ultimate torsional strengths of the inferior sections of the nails were found.

The Russell-Taylor nail was found to be the stiffest nail overall while the AO Universal nail was the least stiff of the nails. It was found that the bending stiffnesses of the Russell-Taylor and Grosse and Kempf nail increased when the proximal screw holes were included within the nails working length. This was explained as an effect of the increased nail diameter and wall thickness around the trochanteric screw holes of the two nails leading to a greater second moment of area (I) and hence greater bending stiffness. The maximum bending stiffnesses occurred in the antero-posterior plane. In torsion, all but the AO Universal nail had comparable stiffnesses. This is due to the slot that runs along the entire length of the open sectioned AO Universal nail which reduces the St Venant torsion constant (J) considerably and hence its torsional stiffness. The effect of the distal slot of the partially slotted Grosse-Kempf nail was not visible in the results due to the torsional tests being completed using the solid proximal portion of the nail.

Beals *et al.* (1988), Russell *et al.* (1991) and Miles *et al.*(1994) all conducted tests to determine the stiffness of a slotted AO Universal nail and a non-slotted Russell-Taylor nail in bending and torsion. A comparison of bending results is given in table 2.5. The AO Universal nail was stiffer in Russell's study because a 13mm nail was tested, rather than the 12mm as in other studies. However, the 13mm Russell-Taylor nail is not stiffer than the 12mm designs. This is because the 13mm nail has a wall thickness of only 1mm

compared to the 1.2mm thickness of the 12mm nail. All three studies demonstrated that the Russell-Taylor nail was approximately thirty times more torsionally rigid than the AO Universal nail.

The studies all conclude that the nails have a similar bending stiffness because their second moments of area (I) are similar, but that the polar second moment of area (J) for a closed circular section, or non-slotted nail, is far greater than that of an open circular section, or slotted nail (figure 2.21). Hence a closed section nail will be more rigid in torsion.

Study	Bending stiffness (Nm^2)		Nail diameter (mm)
	AO Universal nail	Russell-Taylor nail	
Beals et *al.* (1988)	55.85	70.72	12
Miles et *al.* (1994)	59.35	79.12	12
Russell et *al.* (1991)	73.7	77.05	13

Table 2-5 Comparison of intramedullary nail bending study results

2.4.3 Implanted nail studies

2.4.3.1 Femoral bone models

Once inserted, the nail and bone form a new mechanical construct. The construct acts differently to the nail alone due to proximal and distal fixation and friction, which occurs as a result of the interference between the nail and the wall of the medullary canal. Obtaining fresh disease free cadaveric bones, with similar properties and shape, in which to implant prostheses for testing is difficult and expensive. For this reason, synthetic materials have been developed for use in the mechanical testing of orthopaedic devices.

A composite femur model that offers the physical properties of real bone, is manufactured by Pacific Research Laboratories Inc. (Vashon Island, WA, USA) and is available in Europe from Sawbones Europe AB (Malmö, Sweden). The model consists of a glass reinforced epoxy exterior and a polyurethane interior, representing cortical and cancellous bone respectively, and is available in three sizes. A comparison of these materials with bone is given in table 2.6.

Several studies have compared the geometry of the composite femur with data from the human femur (Bianco *et al.*, 1989; Cristofolini *et al.*, 1996). They conclude that dimensional variations between composite specimens is small and that they are similar in shape and size to human femora although they have a reduced anterior-posterior bow and lack any linea aspera (table2.7). X-rays of the composites revealed them to have a medullary canal and isthmus of 'normal' dimensions.

	HUMAN*		COMPOSITE †	
	cortical	**cancellous**	**glass fibre epoxy**	**polyurethane foam**
Tensile modulus (GPa)	11.4-19.1	0.2-5.0	18.6	0.06-0.4
Tensile strength (MPa)	107-146	3-20	171.8	3.44-10.3
Compressive modulus (GPa)	15.1-19.7	0.1-3.0	not given	0.1-0.4
Compressive strength (MPa)	156-212	1.5-50	not given	4.83-13.8
Shear modulus (GPa)	3.3 ‡	-	4.12-5.50	not given

Table 2-6 Comparison of human and composite bone properties
*** From Tencer and Johnson, 1994, † From manufacturer, ‡ From Reilly and Burstein, 1975**

The mechanical properties of whole femoral models have also been examined. A study by Beals (1987) compared one composite femur with an embalmed human femur in compression and three point bending and found stiffnesses between the two to be similar. However, when tests were completed on several composite bones, although they showed good consistency in size (Szivek *et al.*, 1990), the torsional deformation response between the four bones tested varied by up to 48%.

A second generation femur was produced and a subsequent study by Szivek and Gealer (1991) showed a smaller variation in properties. More recently, bending tests on four composite femora and one embalmed femur found a very low variability (s=0.6%) in the force-displacement curves (McNamara *et al.*, 1994). In the most thorough study to date (Cristofolini *et al.*, 1996), four composite, four dried-rehydrated and four fresh-frozen femora were compared under axial, torsional and bending loading in both the antero-posterior and medio-lateral planes. In axial loading and in both bending planes there was found to be a significant difference between the stiffnesses of the composite femora tested. Only in torsion

	Composite	Dryed cadaveric				Fresh-frozen cadaveric			
		#73	#74	#80	#82	#172	#173	#174	#175
Side	left	left	left	right	right	left	left	left	right
Length	425 ± 0.5	421 ± 0.5	427 ± 0.5	422 ± 0.5	446 ± 0.5	424 ± 0.5	402 ± 0.5	449 ± 0.5	427 ± 0.5
Outer ant-post diam.	26.96 ± 0.27	28.03 ± 0.75	29.90 ± 0.61	28.51 ± 1.1	29.49 ± 1.3	24.63 ± 0.93	27.47 ± 0.31	34.83 ± 1.3	32.70 ± 1.1
Outer med-lat diam.	27.01 ± 0.37	27.62 ± 0.62	30.17 ± 1.6	27.10 ± 0.66	30.63 ± 0.25	26.70 ± 2.1	28.92 ± 0.36	30.83 ± 0.54	27.68 ± 1.6
Endosteal ant-post diam.	15.1 ± 0.18	17.4 ± 2.2	15.3 ± 0.72	17.1 ± 1.0	14.4 ± 3.1	13.2 ± 1.7	12.4 ± 1.8	13.6 ± 2.2	12.4 ± 1.4
Endosteal med-lat diam.	13.8 ± 0.38	17.5 ± 2.8	13.1 ± 3.2	16.4 ± 1.3	13.1 ± 3.7	15.4 ± 2.1	13.0 ± 2.3	14.1 ± 2.8	13.6 ± 2.6
Radius of curvature	3200 ± 250	1670 ± 250	1400 ± 250	1140 ± 250	2520 ± 0.5	1470 ± 250	1930 ± 250	1480 ± 250	1100 ± 250
Singh index	—	5	5	2	4	5	4 to 5	6	6

The Singh Index (SI) is a measure of the density of the trabecular bone in the proximal femur. An SI of 6 describes normal healthy bone whereas with an SI=1, the bone is very osteoporotic (Singh *et al.*, 1970). The diameter values are the average of the mid-diaphysis measurement and those at ±50mm from this point.

Table 2-7 A comparison of composite and human femur dimensions. From Cristofolini *et al.*, 1996

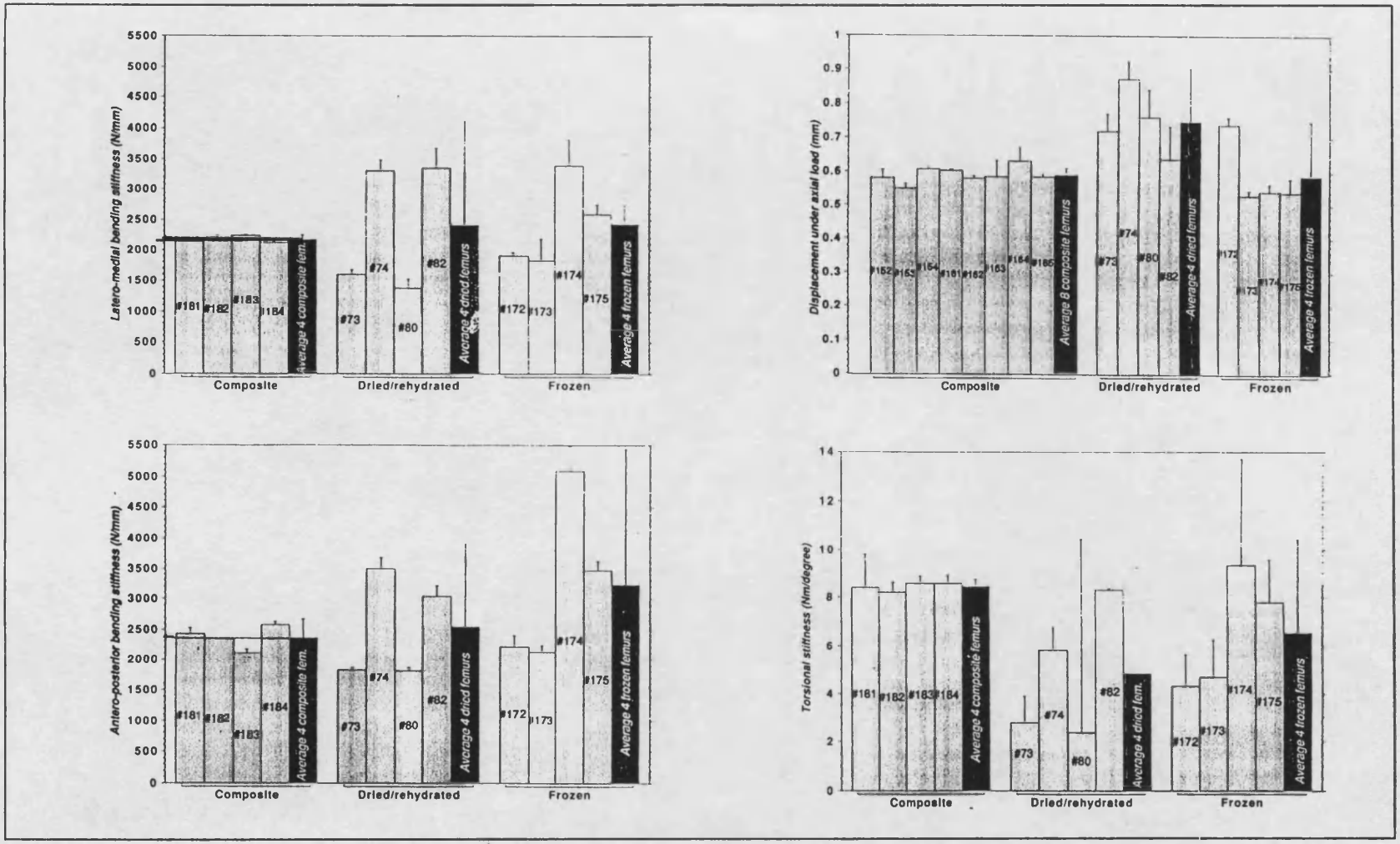

Figure 2-22 A comparison of the deflection of composite and human femora subject to axial, bending and torsional loads. From Cristofolini *et al.*, 1996

was there no significant difference in the stiffness of the four composite femora. However, when compared with the two human groups, the variance of the composite bones was twenty times less axially and in antero-posterior bending and up to 200 times lower in torsion and medio-lateral bending. In all cases, values for the stiffness of the composite femora were found to fall well within the range of the human specimens (figure 2.22).

Strain measurement is an important technique in analysing the effects of a prosthesis on its host. Again, due to the variability in cadaveric material, several studies have been conducted on composite bones to determine their suitability for strain measurement. Otani *et al.* (1993) compared composite and fresh-frozen femora in a study investigating the effect of femoral components of different moduli on the proximal strain distribution. The authors concluded that under axial loading, longitudinal strains in the composite and cadaveric femora showed good agreement. But circumferentially under axial loads and in both directions as a result of torsional loading, strain measurement in the composite femur was unreliable. Tensile readings were obtained followed by compressive readings in the same location. This was thought to be the result of the glass fibres in the model being orientated at 45° to the circumferential direction so that the gauges picked up only a small strain. However, although the strains measured from the cadaveric bones were more predictable i.e. the same gauges gave tensile and compressive readings before and after implantation, the standard deviation of the readings were often greater than with the composite bones.

A study by Cristofolini *et al.* (1996) compared the proximal longitudinal strain readings in two composite femora and 3 dried-rehydrated cadaveric specimens under an axial load. It was concluded that the composite femora gave highly consistent strain values well within the range obtained from the human specimens because of their uniform geometry. Some local abnormalities were observed as a particularly high strain in the proximal-medial region of the composite femora. This was thought to be due to the glass fibre layout in the area which they recommended that the manufacturers improve. Like real bone, the composite bones were found to exhibit viscoelastic behaviour. The authors suggested that 4 minutes after load application would be sufficient to by-pass time dependent effects during strain measurement.

These studies show the Sawbone composite femur to have the shape, size and overall stiffness properties that a human femur would have, with a far lower variability in these properties when compared with cadaveric material. When using the models in strain measurement studies, care should be taken to avoid viscoelastic effects. All strain results should be viewed subjectively while considering the fibre make up of the models.

2.4.3.2 In vitro studies

Kyle *et al.* (1985) tested several intramedullary nail systems once they had been inserted into fractured cadaveric femora. Amongst those tested were an unlocked AO Universal nail, a Grosse-Kempf interlocked nail and Enders nails. Enders nails are cylindrical solid nails available with a diameter of 4 or 4.5mm. Several nails are inserted, from a small distal incision, up the medullary canal for fixation of fractures. The canal does not require reaming and the nails are generally not locked in position. The bending stability of the locked Grosse-Kempf nail, in three point bending, was found to be slightly greater than the AO Universal nail, with the Enders nails having very little resistance to bending loads. This is due to the material being distributed close to the bending neutral axis, and hence having a very small second moment of area and therefore bending stiffness. In torsion, the AO Universal nail was the least stable of the nails tested because it was unlocked, while the interlocked system was by far the most torsionally stable of the devices. A spring-back test was carried out to determine the ability of each device to return to its' original position once it had been rotated through 50 degrees. The AO Universal nail had a spring-back of below 40%, while the Enders nails had a 92% spring-back. The Grosse-Kempf interlocking nail with an open slot and clover-leaf section maintained a 100% spring-back rate.

A second set of tests were completed by Kyle et *al.* (1985) using the statically locked Grosse-Kempf nail in cadaveric femora with increasing degrees of mid-shaft defect. The torsional stability of the construct and the degree of spring-back after 10 degrees of rotation was examined. The results can be explained by considering the working length of the nail (figure 2.23), which is the portion of the nail that lies between the points of fixation proximally and distally (Browner and Cole, 1987; Bunker, 1989). This might be at the site of an interlocking screw or where the nail is in contact with the medullary canal wall and is fixed due to the interfacial friction. For a constant mode of fixation, as

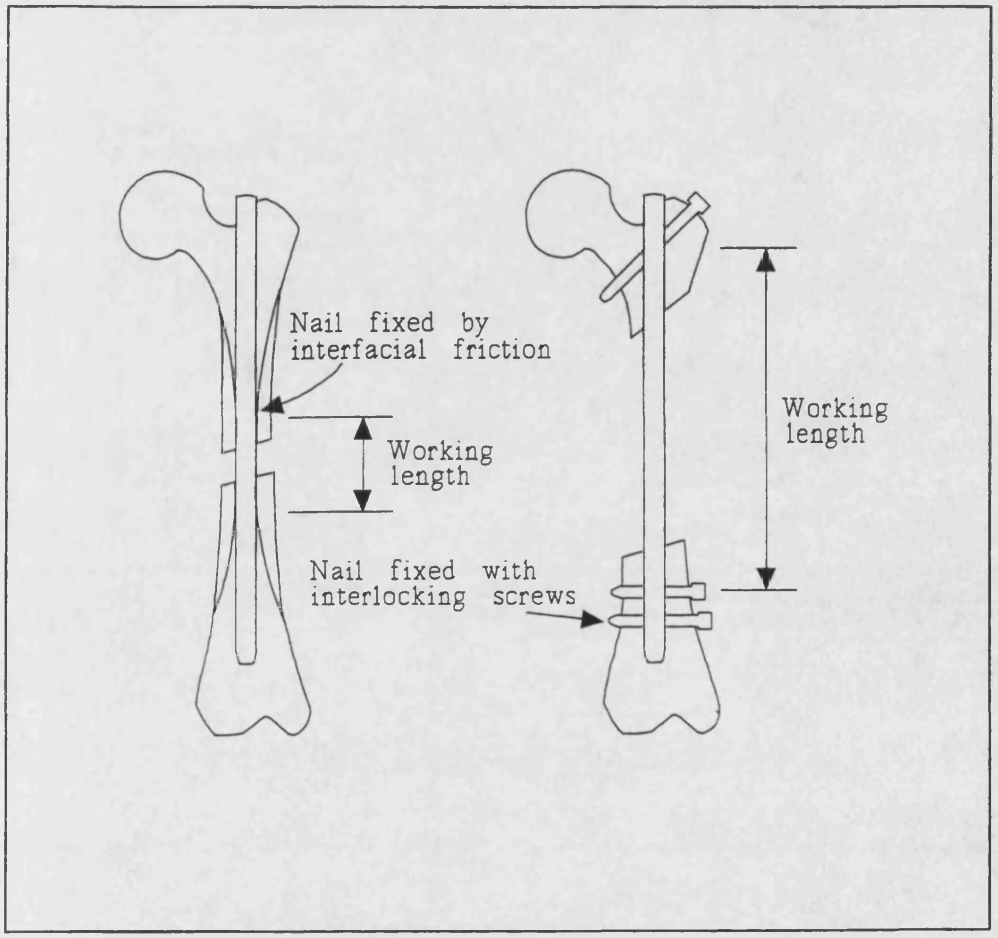

Figure 2-23 The working length of an intramedullary nail

the segmental defect increased in size, the working length of the nail increased. The torsional rigidity of the construct decreased as there was less bone to nail contact along the bone shaft and hence reduced friction to resist the rotation. For the same reason, the percentage spring-back increases. The torsional rigidity of the nail and bone construct is therefore inversely proportional to the working length of the nail (Russell, 1991). It was also noted that an interlocking system must be used to resist compressive loads if a great deal of comminution is present.

Alho *et al.* (1992) conducted a study to examine the differences between two slotted nails and a non-slotted nail, both locked, in torsion. The nails were inserted into cadaveric femora with mid-shaft fractures. The femora fitted with the non-slotted nails had a stiffness value that was 40% of an intact control femur and the slotted nail constructs had a stiffness that was 6-8% that of the control bone. The non-slotted nail constructs were able to withstand a maximum moment that was three times greater than that which the non-slotted nail constructs could resist.

Lynch and Davidson (1989) investigated the motion at the bone fracture interface with a slotted and non-slotted nail. The two diameter nail types were each inserted into a cadaveric femur that had been transversely sectioned mid-shaft. Both nails were locked proximally and distally. A direct load was applied to the femoral head of the cadavers and the relative displacement of the two bone halves at the fracture site was measured due to bending and rotation. It was found that there was no difference in the bending displacement between the two nail types but that the rotational displacement between bone halves in the cadaver fixed with a slotted nail, was significantly greater than with the non-slotted nail. These results are consistent with the fact that in bending there is little difference between the stiffnesses of slotted and non-slotted nails, but a considerable difference in torsion.

More complex fractures require further investigation as the performance of the intramedullary nail is tested to the maximum. Comminuted fractures have been found to correlate with the incidence of interlocking nail failure in the tibia (Deehan et *al.*, 1993), while very distal fractures remain hard to fix as the fracture may not always lie between

the interlocking screws. The subtrochanteric region of the femur is subjected to high bending moments, stresses and compression, and a fracture in this region requires fixing with an implant able to withstand these loads.

Johnson *et al.* (1986) compared the performance of four intramedullary fracture fixation devices implanted into cadaveric femora with mid-shaft and subtrochanteric comminuted fractures. The Grosse-Kempf and Klemm-Schellman nails, the Brooker-Wills nail which employs fins for distal fixation, and Enders nails were investigated. The results showed that the three interlocking nail systems behaved similarly in torsion while the Enders nails had a lower stiffness, with the nails tending to slip in the canal on release of the load. There were only slight differences between the two fracture models in torsion. In bending, the stiffnesses of the interlocking nails were significantly higher than that of the Enders nails. The femora with mid-shaft defects were found to have lower stiffness values than those with subtrochanteric fractures. During axial loading, the interlocking nails with distal locking bolts failed at the highest loads.

The Klemm-Schellman nail has a proximal bolt angled at 150° to the vertical compared with the Grosse-Kempf's 130° bolt. The more oblique angle of the Klemm-Schellman nail is believed to have resulted in its slightly lower load to axial failure value, as there was less bone to anchor the bolt in at this angle. The Brooker-Wills and the Enders nails both permitted load bearing to a maximum value, below that of the standard locking nails, followed by sliding of the device in the femur. It was concluded that in comminuted fractures, nails proximally and distally locked with bolts were superior to the other devices tested. It was suggested that the fractures nailed with the Brooker-Wills and Enders devices should be protected from excessive weight-bearing, which might result in shortening.

Tencer *et al.* (1984) looked at the fixation of subtrochanteric femoral fractures with seven different types of intramedullary and plate implant. The intramedullary devices included Enders nails and three different slotted interlocking nails. The devices were implanted into cadaveric femora with simulated subtrochanteric fractures both with and without bony contact between the fracture ends. In bending it was found that the Enders

nails were considerably less stiff than the other fixation devices tested. The other intramedullary implants of similar diameter had comparable bending stiffnesses. Without bony contact, the bending stiffness of all the implants was reduced, but not significantly. All four devices had similar torsional stiffnesses and these were slightly reduced without bony contact. In the combined loading mode the femora were tested without bony contact to ensure that the load was transmitted through the implant and not the fracture ends. The Enders nails slipped at a load of 600N due to the lack of any form of interlocking fixation. The distal end of the Brooker-Wills nail slipped at a load of 1000N due to poor distal fixation using small fins. The two interlocking nails withstood a considerably greater load before failure. The authors concluded that based on their results, the interlocking intramedullary nail could be used for unstable subtrochanteric fractures.

In two studies, Bankston *et al.* (1986, 1992) calculated the torsional rigidity and compressive strength of several nail types. These included the Küntscher nail, an unlocked nail, an unlocked AO Universal nail, the Küntscher interlocking nail and the Brooker-Wills nail. The nails were inserted into cadaveric femora with a transverse fracture created distal to the isthmus before torsional testing. In the compression study, a 30mm section of bone was removed distal to the isthmus to eliminate any contact between the bone ends during loading. The study concluded that the Küntscher nail and the unlocked AO Universal nail did not provide significant resistance to compression or torsion for use in oblique or comminuted fractures where its lack of distal and proximal fixation might lead to limb shortening. The Brooker-Wills nail provided a satisfactory degree of rotational stiffness to be used in distal fractures but proximal fixation is necessary to avoid limb shortening in comminuted fractures. The Küntscher interlocking nail was found to be the most rigid of the nails tested and, due to the proximal and distal interlocking screws, gave adequate rigidity for use in fractures liable to shortening.

Covey *et al.* (1990) compared slotted and non-slotted nails in cadaveric femora with fractures created distal to the isthmus. Torsional and axial testing was completed with a 30mm section of bone being removed before axial testing to avoid load transmission through the fractured bone ends. In torsion, the non-slotted nail was significantly stiffer

than the slotted nail. In compression there was a significant difference in the amount of load that each nail could sustain before failure. The authors explained that the slotted nail was more able to share load with the bone than the non-slotted nail because of the geometry of its interlocking screws. The slotted nail had an interlocking screw head-thread diameter ratio greater than the non-slotted nail which improved its resistance to failure by increasing cortical bone contact and enabling a greater cortical penetration by the screw head. The lower angle of the proximal interlocking screw was also thought to resist slightly greater compressive loads in the slotted nail-130° compared to 135° in the non-slotted nail. At this lower angle, there is more bone in which the screw can be anchored.

Papagiannopoulos *et al.* (1985) and Pratt *et al.* (1987) compared the performance of the Derby nail with other commercially available nails inserted into transversely fractured cadaveric femora. The studies concluded that the Derby nail, with its closed cross-section, had a greater strength in torsion than the Kuntscher and Zickel nails tested. This would be due to the fact that the Kuntscher nail has a longitudinal slot and is not fixed proximally or distally, and the Zickel nail, with its solid, square cross-sectional shape, is a 'short' nail with no distal fixation. This gives both nail types a low resistance to torsion. In three point bending, the Derby nail was again found to be stronger and stiffer than the other two nail types.

2.4.4 The effects of interlocking

It is general practice to lock an intramedullary nail using both distal interlocking screws and at least one proximal screw, although it has been shown that this is not always necessary to achieve adequate fixation.

McDermott *et al.* (1987) conducted a study into the locking nail principle using a single device placed initially into the intramedullary canal of a fractured cadaveric femur without interlocking, secondly with interlocking screws and finally the device was attached to the lateral aspect of the femur and locked in position, as if a plate. It was found that in bending, the locked and unlocked intramedullary nails behaved similarly but in torsion the locked nail was able to resist greater torsional loads than the unlocked nail and the plate-like device. Less physical distortion was seen with the intramedullary nail

devices. In compression the locking nail and the plate-like device had a similar response. It was noted that the load transferred to the bone was greatest in the interlocking screws that were most distant from the fracture site. The screws closest to the osteotomy carried little load.

Kyle *et al.* (1985) examined the effect of using varying combinations of interlocking screws on the torsional rigidity of a cadaveric femur with a mid-shaft fracture. The authors found that the nails without any interlocking and those fixed with just one oblique proximal screw had a very low torsional rigidity. The fractures fixed with the proximal screw and either one of the distal screws had comparable rigidities and were four times more rigid than the construct that was not locked. The construct fixed with all three screws had the highest rigidity, four and a half times greater than that without any interlocking fixation. The same pattern was seen in the ability of the nails to spring-back to their original position after a standard rotational displacement. The nail locked with all three screws had the greatest ability to spring-back.

Hajek *et al.* (1993) implanted Klemm-Schellman nails into the distal third of cadaveric femora. The nails were either locked with both the distal screws or with just the most proximal of the two screws. Torsional testing revealed that the constructs fixed distally with one interlocking screw had the same rotational stiffness as those fixed with two screws. There was not a significant difference in the load to failure between the two groups when axially loaded, but the mode of failure was significantly different. In the constructs fixed with one screw, it was the screw that failed whereas the nail failed in the constructs fixed with both distal screws. The authors conclude that with a slotted nail system, one distal screw will provide adequate distal fixation for femoral shaft fractures.

The strength of proximal interlocking screws was investigated by Kinast *et al.* (1987) in the treatment of subtrochanteric and diaphyseal fractures. Intramedullary nails locked with either a proximal oblique screw or a transverse screw were inserted into the proximal fragment of an osteotomised cadaveric femur. Distally the nails were embedded in bone cement and the femur was loaded in compression through the femoral head with an abductor force acting at the greater trochanter. The transverse screw could

maintain a greater maximum load before yielding than the oblique screw in both fracture types although it was noted that with a subtrochanteric fracture, both screws would be submitted to loads which could lead to screw breakage during single-legged stance. The greater strength of the transverse screw in situ was thought to be due to the screw's smaller diameter allowing for a smaller diameter clearance hole in the nail, and hence improving the strength of the nail construct altogether.

2.4.5 Nail performance during healing

During the healing process, the nail behaves as a load sharing device. Initially, the majority of the load must be supported by the nail, but as the fracture heals and gains a greater mechanical stability, the load will be shared by the bone. A finite element study (Hoeltzel *et al.*, 1985) investigated the load carrying capacity of a fractured femur. It showed that even when the femur was unfractured the nail supported a fraction of the applied bending moment; between 10% and 30% depending on the size of nail. When a mid shaft transverse fracture was modelled the nail supported almost the entire bending moment in the region of the fracture. The greater the diameter of the nail, and hence the greater contact between bone and nail, the larger the fraction of the total moment was supported by the nail.

The ME Müller Institute in Switzerland strain gauged an intramedullary nail to determine the loads acting on the implant *in vivo* and during healing (Schneider *et al.*, 1990; Michel *et al.*, 1991). Readings from the telemetric device, implanted in to a 73kg male, enabled the 3 loads and 3 moments acting on the nail to be calculated. Figure 2.24 shows the loads measured during single legged stance. It must be noted that the patient would have been unable to stand on the injured leg early during the healing process so readings were taken during the latter stages only. The torsional moment and the forces show a constant or declining load taken with time but the bending moments in the medio-lateral and antero-posterior planes show an increasing trend. No explanation for this increase is given. The following results were emphasised. The loads generated in the nail were higher than those expected, including a significant torsional moment. The loads on the nail were still significant after fracture consolidation, up to 40%, and might cause increased loading of the bone after implant removal.

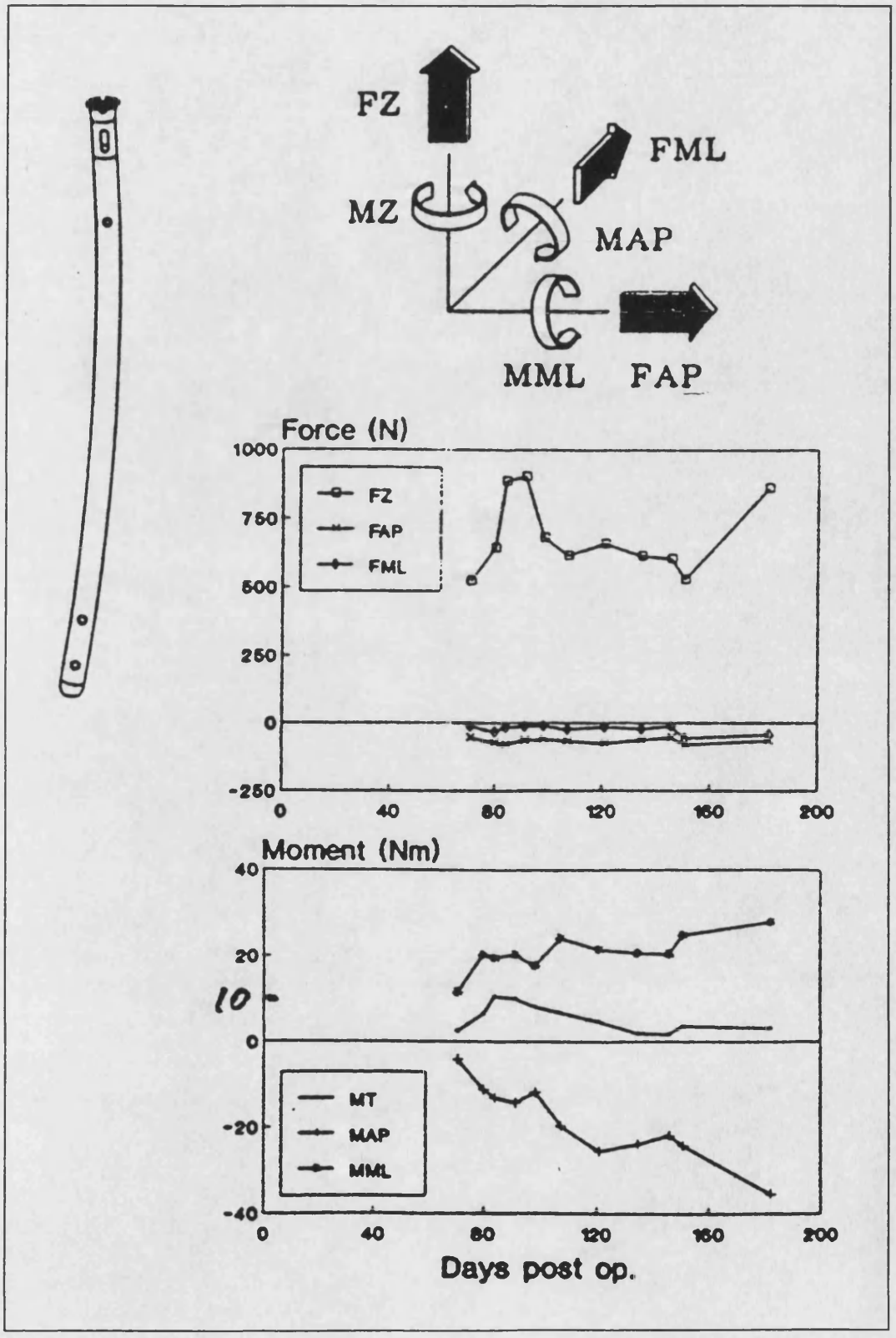

Figure 2-24 Loads measured from an instrumented femoral intramedullary nail during single legged stance (N.B. MT=MZ). From Schneider *et al.*, 1990

2.4.6 Surgical Technique

The performance of an intramedullary nail *in vivo* is highly dependant upon the way it is inserted. A poorly performed operation may leave the fracture inadequately fixed which might lead to problems postoperatively. Several authors have attempted to highlight the effect that surgical variables, such as the reamed canal diameter and the size and position of the nail entry hole, may have on the stability of the healing construct.

Johnson *et al.* (1987) and Tencer *et al.* (1988) carried out biomechanical studies of factors associated with nailing technique that might lead to fracture instability and shattering of the femur. Using five different intramedullary nails and mid-shaft fractured cadaveric femora, the authors investigated 1) the force required to insert each nail, 2) the results of changing the reamed diameter of the canal, 3) the effect of entry hole location on the nailing outcome and 4) the hoop stresses associated with these tests at the fracture site. The results showed that the most flexible nail of those tested produced the lowest resistance force on nail insertion. The greatest resistance was generated by a stiff nail that had an anterior-posterior curvature very close to that of the femur used during the tests. This would have lead to a high degree of interfacial friction between the nail and the bone and hence the high resistance to insertion. This nail also produced high hoop stresses at the fracture site that might lead to shattering of the femur. It was found that reaming of the medullary canal only 0.5mm larger than the nominal size of the nail lead to a very low pushout force in the distal fracture component which might result in a loss of rotational control. It must be noted that the tests were carried out without distal fixation of the nails, and so relied only on frictional interference between the nail and bone for fixation. Placement of the starting hole 6mm or more anterior to the axis of the medullary canal produced high hoop stresses at the level of the fracture which was consistent with cracking of the femur.

Miller *et al.* (1993) investigated the effect of entry hole size and location on the strength of the proximal femur. It was found that there was reduced stiffness and load to failure when the nail entry hole was positioned anterior to the ideal. This suggested that the anterior portion of the femoral neck was a more important load-carrying medium than the posterior portion under the given loading regime. It was noted that the location of

the hole was more important than the size of the hole when concerned with maintaining the strength of the proximal femur.

Both these studies emphasize that the reamed diameter of the medullary canal and the position of the entry hole for nail insertion, were important factors if adequate fixation was to be achieved and to avoid high levels of stress which might lead to further bone fracture.

2.5 CLINICAL STUDIES OF INTRAMEDULLARY NAILING

2.5.1 Clinical outcome of intramedullary nailing

Clinically, interlocking intramedullary nailing has been successfully used in the treatment of femoral shaft fractures, with many trauma surgeons regarding it as the treatment of choice in such cases. McLeod (1991) documented numerous studies in a survey of intramedullary nailing procedures all of which reported excellent results when compared to outcomes using other implants such as plates.

Clinical results recommend the following for the successful treatment of femoral shaft fractures.

1. During closed intramedullary nailing the nail is inserted at a distance from the fracture site. Opening closed fractures, to assist with alignment of the fragments, should be avoided at all costs. This has been found to lead to a high incidence of infection and non-union (Curylo and Lindsey, 1994).
2. Fractures treated with interlocking nails should be statically locked, especially comminuted fractures. Surgeons should look for reasons why they should not statically lock (Brumback *et al.*, 1988a).
3. Static locking in a standard reamed nail using only one distal locking screw has been found to provide adequate distal fixation of fractures of the femoral shaft (Hajek *et al.*, 1993). All of the fractures healed without incidence and the implants did not fail. However, in a study of unreamed tibial nailing (Kneifel and Buckley, 1996), failure of the distal screw was seen in 59.1% of cases where only one distal locking screw was used. This compared

with a failure rate of only 5% when two screws were used. Failure occured in the heavier individuals, when the patients increased weight bearing and where there was a large medullary canal.

Only a few studies have compared the clinical outcome of fractures treated using different nails *in vivo*. Lowden *et al.* (1989) treated 24 fractures with the AO nail. Only ten of the fractures were statically locked initially, and none of these were dynamised. Union occured in all fractures. One comminuted fracture which had been locked using two distal screws, without proximal locking, led to limb shortening of 1cm.

A comparison of the Brooker-Wills (slotted with distal fins) and Russell-Taylor (non-slotted with screw fixation) nails showed that, although the biomechanical properties of the nails differed, these did not affect the clinical outcome (Blumberg *et al.*, 1990). However, the Russell-Taylor nail was associated with fewer technical difficulties, a shorter operative time and less blood loss. Alho *et al.* (1992) compared a non-slotted and slotted nail in a randomised study of 46 femoral shaft fractures, 24 fixed with slotted nails. In the series, there were only 3 complications that were considered to result from the type of nail used, and all of these occured in the non-slotted nail group. The stiffer non-slotted nails produced splintering of the distal bone fragment. However these patients were susceptible to splintering because they were elderly and had osteoporotic bone. Overall, no differences were found in the healing results between the slotted and non-slotted groups.

Clinical results using unreamed femoral intramedullary nails have been good although relatively few reports have been published. Long term clinical studies may not yet be available because of the short length of time since the nails were introduced. Kröpfl *et al.* (1995) reported eighty one femoral shaft fractures, 53% were comminuted, treated with the AIM titanium nail from the ACE Medical Company. The nails were inserted without reaming. A 9mm nail was used in all but 13 cases where the medullary canal was considered too wide and a 10mm nail used. In every case the nail was statically locked. No infections occured and all fractures went on to uneventful union in an average of 3.8 months. Krettek *et al.* (1996) published their results of 133 femoral shaft fractures treated with the AO unreamed femoral nail over 3 years. They achieved good results with a shorter time to healing than was

experienced with the AO Universal nail. However, a comparison of the two nails was not undertaken in a prospective randomised study.

The indications for intramedullary nailing of the femur have increased considerably with the introduction of 'second generation', or reconstruction, locking nails (figure 2.25). These nails allow a screw to be inserted up in to the femoral head allowing the simultaneous fixation of femoral shaft and femoral neck fractures. They are often used in subtrochanteric fractures, in the most proximal region of the femoral shaft. Subtrochanteric fractures are difficult to treat because of the large stresses transmitted through this region. Compressive forces of up to 8.3MPa may occur along the medial cortex of the femur making it the most highly stressed area of the skeleton. The Russell-Taylor reconstruction nail has an expanded proximal diameter over its upper 8cm (15mm c.f. 13mm in the standard nail). This makes it more rigid and capable of withstanding greater loads than the standard nail.

This decision of whether to treat a subtrochanteric fracture with a standard nail or reconstruction nail is left to the judgement of the individual surgeon at present. Patients with comminuted subtrochanteric fractures, including comminution of the intertrochanteric region of the femur, have been treated with the reconstruction nail (Smith *et al.*, 1991). No complications were seen and healing occured in an average of 10.5 weeks. But low subtrochanteric fractures, with the lesser trochanter intact, have also been successfully treated with a standard interlocking nail (Ryder *et al.*, 1993; Kyle, 1994). Further work on the stability of subtrochanteric fractures treated with both standard and reconstruction nails needs to be completed.

The question of if and when an implant should be removed is still debated. The manufacturer's view is that the implant should be removed once its 'service as an aid to healing has been accomplished' (Russell *et al.*, 1996) and 'when the fracture has completely healed: a condition which is determined from radiographs and clinical experience' (Ordway, 1991). Removal of nails in the elderly is contraindicated due to the trauma involved in a second operation.

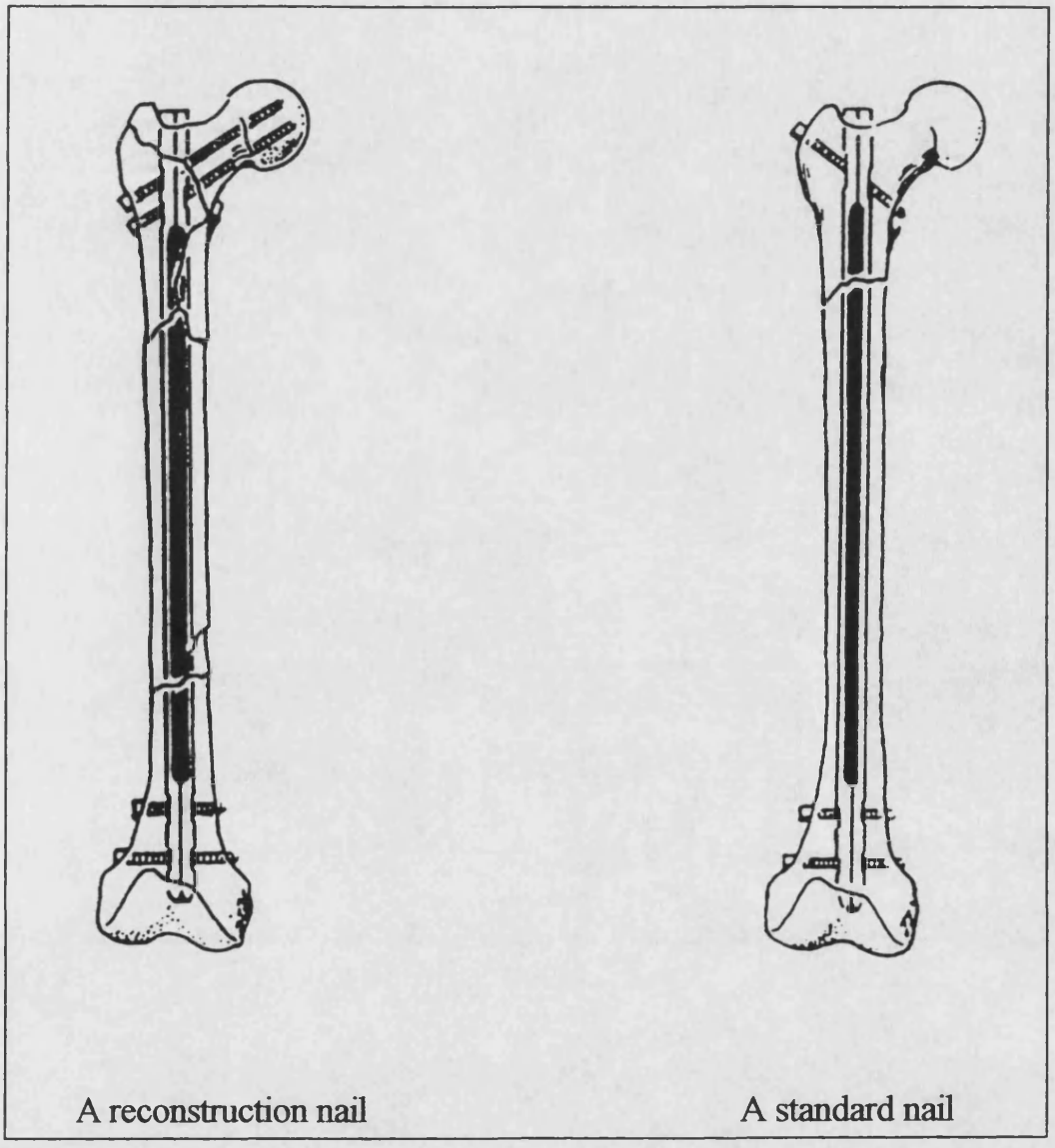

Figure 2-25 A second generation or reconstruction femoral intramedullary nail with the proximal interlocking screws passing up in to the femoral head, and a standard nail. From Kyle, 1994

A study by Kapp *et al.* (1994) evaluated 17 patients where the nail had been left in following union (times ranging from 18 months to five years). When compared to the opposite limb in each case, the implanted femora showed a decrease in bone mineral density. This may be due to stress shielding by the implant. In addition, although the implanted limb was fully functional, there was a decrease in muscle strength. Traisnel *et al.* (1990) removed twelve stainless steel (AISI 316) intramedullary nails after a period of eight years *in vivo*. The implants were corroded and when tested, the plasma and blood of the patients were found to contain high concentrations of nickel and chromium. There are not thought to be any chronic conditions associated with this but the localised effect has not been investigated thoroughly. Zimmerman and Klasen (1983) also reported four cases where the intramedullary nail failed after fracture consolidation. Difficulty was experienced in removing the broken nail, particularly the distal portion.

On the above evidence, intramedullary nails should be removed in all but the elderly. Unfortunately nail removal is not always a straight forward procedure. In the first instance, removal might not occur in the hospital where the original procedure took place. Different nails have different proximal connections for removal and hospitals will probably not keep the instrumentation for all. There is a need for the standardisation of nail connections. Secondly, the proximal interior of most intramedullary nails is threaded. This allows an extraction rod to be attached which is then used to remove the nail. Over the period of time that the nail is *in vivo* however, the extraction thread is likely to be filled with new bone which must be excised prior to any removal attempt. The AIM titanium nail (ACE Medical Company) and AO unreamed femoral nail have an end cap which screws in to the proximal thread, preventing such problems. Difficulties have also been reported when removing a fluted intramedullary nail (Star *et al.*, 1989). In six cases the fluted nail broke before complete removal. The nail always fractured in areas of stress concentrations, for example where the nail's cross section changed from the smooth to fluted design. The failures were considered to be a result of the nail's geometry: difficulties with the removal of a Küntscher nail were uncommon.

2.5.2 Clinical complications

Complications may occur as a result of the nailing procedure. Clinical testing might not actually highlight the difficulties with a design as most reports are anecdotal and based on

experience with one implant. Randomised prospective trials using several implants for the treatment of a particular fracture are necessary for the scientific analysis of implant performance. However, they are difficult to set up and costly.

Cases of limb shortening, angular rotation and migration have been documented for the Marchetti nail and LIFO (locked intramedullary flexible osteosyntheis) device (section 1.2.2). A study by Ebraheim and Paley (1993) also reported distal migration with the Brooker Wills nail in 11% of femoral fractures that they treated. These complications are a result of the instability of the implant. The use of these devices could have been contraindicated in unstable fractures by pre-clinically testing the implants using simliarly unstable fracture patterns.

Malunion may not be due to the inadequacy of a device but due to clinical and intra-operative complications. Bråten *et al.* (1993) measured the degree of torsional deformity in 110 patients treated by intramedullary nailing for femoral fractures. They found that 21 patients had a deformity of 15° or more and that 8 of these had complaints associated with this deformity. They reported that the incidence of deformity was similar in statically and dynamically locked nails. It was concluded that torsional deformities were often established during the operation.

Christie and Court-Brown (1988) and Simonian *et al.* (1994) both reported cases of femoral neck fracture during closed intramedullary nailing. This may have been due to anterior placement of the nail entry point leading to high hoop stresses resulting in fracture of the femoral neck (Johnson *et al.*, 1987; Miller *et al.*, 1993). Christie and Court-Brown (1988) stress the need for correct insertion clinically while Simonian *et al.* (1994) concluded that neck fracture may not be entirely due to an improper starting position. They emphasized the need to thoroughly image the femoral neck before fixation to check for fractures. An unnoticed fracture might become apparent during nailing and lead to complications.

Haddad *et al.* (1996) reported their findings on a series of twenty nine tibial shaft fractures treated with the AO unreamed nail. They reported that the fractures were slow to unite, on average taking 22 weeks to reach clinical union (range 13-43 weeks). This problem has been

indicated in several other studies including two randomised prospective trials. In both tibial (Anglen and Blue, 1995; Blachut *et al.*, 1997) and femoral fractures (Giannoudis et al., 1997; Tornetta and Tiburzi, 1997) treated with unreamed nails, the authors reported slower union in the fractures treated with unreamed nails compared with reamed nails. The fractures treated with unreamed nails often required secondary operative intervention. The studies concluded that there were no major advantages to using unreamed nails and that they should not be used routinely.

A reason for the slow union with unreamed nails is not suggested. It may be a result of some mechanical factor i.e. they are too small and flexible. Pre-clinical standardised testing may have highlighted this problem. However, it could also be due to a biological factor. It has been suggested that the 'bone graft' produced during reaming is osteogenic (Keating, 1996), and that the lack of reaming products with use of the unreamed nail may lead to slow union. However, all solutions are speculative at this stage.

2.5.3 Implant failures

It has been reported that the incidence of technical complications with intramedullary nails may not have been fully documented (Benirschke *et al.*, 1993). The incidence of nail failure has been reported by Wu and Shih (1992) in a series of 274 femoral nailings over approximately 2.4 years. Thirteen nails broke, all in the region of the initial bone fracture, 10 of which were statically locked. The distal third of the intramedullary nail, in the proximity of the first interlocking hole, was identified as being the most at risk with stress concentration effects around the hole, nicking of the nail during drilling of the fixation holes, and weight bearing all thought to contribute to failure. The authors recommended using a nail of greater size, improving drilling techniques and allowing only partial weight bearing until fracture consolidation to reduce the risks.

Benirschke *et al.* (1993) reported the failures of the AO Universal nail that they experienced in a total of 267 patients. Only one nail failed, becoming bent during a secondary incident involving the patient concerned. Several problems were experienced with distal locking including missing the locking holes (n=3) and breaking the interlocking screws (n=3). Meislin *et al.* (1993) reported one case of nail failure. The fracture was a two part subtrochanteric fracture and was fixed using a Grosse-Kempf standard locking nail. The authors admit using

an undersized nail, an incorrect reaming diameter and insertion point. Incorrect placement of the nail lead to angulation of the proximal bone fragment but nevertheless, the fracture went on to unite. However, six months post-operatively, the nail had fractured just proximal to the original fracture site. This was thought to be due to increased loading of the nail as a result of the bone's angulation.

Franklin *et al.* (1988) presented 51 cases of femoral nail failure that they experienced over 25 years. A variety of different nails had been used for treatment of the fractures. About half of the fractures occured where they was a delayed or non-union, the rest when the fractures had healed. The authors concluded that an unstable fracture pattern was a predisposing factor to nail breakage. As with the non-unions, there would have been considerable stress placed on the nails. In addition, the diameter of the nails was found to strongly correlate with the incidence of failure: small nails fractured the most frequently at the site of the original fracture. Other nail failures occured through the distal screw holes and at the junction of the open and closed cross sections in slotted nail designs. In early designs the proximal and distal sections of the nail, having different cross-sections, were manufactured separately and then welded together. These are both areas of high stress concentrations. The implants failing due to stress concentrations (AO Universal and Grosse-Kempf) have been altered since the study.

A unique case of failure was reported in an Enders nail (Naidu *et al.*, 1996). The implant had fractured at the site of a mechanical stamp detailing the nail type. Failure was initiated by the increased stress intensity caused by the stamping. Crack propagation advanced initially due to fatigue and in the final stages was assisted by corrosion. The nail had been *in vivo* for seven years.

There have been many reports of implant failure in unreamed tibial nails (Whittle *et al.*, 1992, 1995; Hutson *et al.*, 1995). The incidence of nail failure has been reported to be as high as 6% (Whittle *et al.*, 1992). Two of these failures occurred in ununited fractures at the site of the fracture after eight and fifteen months post-operatively. The small diameter nails (8 and 9mm) would have been subjected to considerable cyclic loading. However, the majority of failures associated with unreamed tibial nails are due to locking screw breakages. Failure rates of 12.3% have been documented (Whittle *et*

al., 1995). However, unlike nail breakages, locking screw failures may not cause adverse clinical effects. They can often be left in situ and the fracture will go on to unite.

There are far fewer reports of failure in unreamed femoral nails. This may be because the femoral nails used have a larger diameter than the tibial nails and are less susceptible to failure or because reports have yet to be published. Krettek *et al.* (1996) reported one nail failure and two broken screws in 133 fractures treated with the AO unreamed femoral nail. The nail failed in a patient where early weight bearing was encouraged. The broken nail was removed and replaced with another unreamed nail. It went on to heal uneventfully.

2.6 SUMMARY

Biomechanical studies of intramedullary nails have calculated the relative mechanical properties of the large number of intramedullary nails available. Most work has concentrated on testing the nails in bending and torsion, in isolation or once they have been inserted in to cadaveric or composite bones. These loading modes are not representative of the physiological situation. New work should look at characterising the nails when subjected to combined bending, torsional and axial loads, to give a clearer indication of the nail differences *in vivo*. Comparison of studies to date is difficult because of the large number of methods used. A realistic standard is required to which all new devices could be tested.

Although clinical studies report nail failures it must be remembered that these are in the minority and that intramedullary nailing is the 'gold standard' when stabilising fractures of the femoral shaft. Clinical studies do not always highlight the problems associated with a particular device unless prospective randomised trials are carried out. Questions still arise on how to treat particular fractures such as those in the subtrochanteric region of the femur. Realistic testing might enable the relative stability of different devices used in the treatment of these fractures to be determined.

The difficulties associated with implant removal and the timing of extraction often mean that the nail is left in situ after fracture union. However, problems are experienced when leaving a nail in place long term such as stress shielding, loss of muscle strength and implant failure. In addition, new non-invasive methods of assessing fracture healing may encourage the early removal of devices which could prove beneficial to the patient.

A review of joint loading studies has shown that the hip joint reaction force can be as high as three times body weight during level walking. This is not a purely vertical force but has direction in both the frontal and sagittal planes. This leads to bending in both the antero-posterior and lateral planes and torsion of the femoral shaft. The realistic reproduction of femoral forces cannot be achieved with out the inclusion of muscle forces. During single legged stance the abductor muscles act to stabilise the hip and the iliotibial tract reduces the degree of medio-lateral bending.

A mechanical test for intramedullary nails should simulate the *in vivo* forces acting on the device in order to ascertain the true function of the nail. In this way, the nail's suitablity to treat different types of fractures could be determined. Such testing might reduce the number of complications seen *in vivo* due to incomplete mechanical testing and allow for the optimum management of a fracture.

CHAPTER 3

MATERIALS

3.1 INTRAMEDULLARY NAILS

Six femoral intramedullary nails were used in this study. Figure 3.1 shows a cross-section through the centre of each nail. Table 2.1 gives a general summary of each nail type. A more complete description of their form and geometry is given in the following list. All the nails involved in the study were 380mm in length. This was the correct length for the Sawbone adolescent composite femur model which was used in this study. Four of the nails used had a diameter of 12mm. This was appropriate for the 13mm medullary canal diameter of the adolescent femur. In addition two small diameter unreamed nails were tested with a diameter of 10mm. The fact that these nails have a smaller diameter than the medullary canal of the composite femur is not thought to be significant. Regardless of the canal size, Kröpfl *et al.* (1995) treated all their patients with 9 and 10mm unreamed nails. Krettek *et al.* (1996) found that 30% of the nails they used in 133 femoral fractures had a diameter of 10mm; 61% were 9mm nails.

- The Russell-Taylor nail (RT)

  The Russell-Taylor nail (Smith and Nephew Richard's) is a stainless steel nail with a closed clover leaf cross section (figures 3.1e and 3.2). It can be locked distally using 2 transverse screws and proximally with one cortical bone screw which is positioned obliquely at 45° to the vertical, passing from the greater trochanter downwards (antegrade fixation). The design of the nail, allowing it to be used in either the left or right femur, means that the nail can also be fixed retrograde, with the proximal locking screw passing up in to the femoral head. This might be useful in ipsilateral fractures of the femoral shaft and neck. The 12mm diameter nail used in this study has a wall thickness of 1.2mm. The Russell-Taylor nail has a 2300mm antero-posterior radius of curvature.

- The AO/ASIF Universal nail (AO)

  The AO Universal nail (Synthes) is another stainless steel nail with a cloverleaf cross section (figure 3.1f). However, the AO nail has a slot along the length of its anterior surface. At its proximal end, the nail has a keystone slot (figure 2.20). This prevents the nail from opening up around the slot and reduces twisting during insertion. The nail can be locked distally and proximally with two transverse screws. The most proximal screw hole is elongated. If the nail is fixed proximally using one screw through this oval hole, it allows a greater degree of compression at the fracture site. The nail has a wall thickness of 1.2mm and a 1500mm radius of curvature in the antero-posterior plane. The 12mm diameter nail was used in this study.

- The ACE nail

  The AIM system of the ACE Medical Company uses a titanium nail made from an alloy containing aluminium and vanadium, Ti-6AL-4V. It has a rectangular slot along its posterior surface (figure 3.1a,b) but its proximal and distal extremes have a closed circular section. It can be fixed distally with two interlocking screws and, like the Russell-Taylor nail, can be fixed either antegrade or retrograde proximally. The proximal locking screws are located at ±45° to the vertical. The nail has a 4000mm radius of curvature in the antero-posterior plane. The 10mm and 12mm diameter ACE nails were tested.

- The AO unreamed nail

  The unreamed femoral nail (URFN, Synthes) is another titanium based nail containing aluminium and niobium, Ti-6AL-7Nb. It can be fixed using the same locking system as the AO Universal nail with transverse screws both proximally and distally. The 10mm diameter nail has a solid circular cross section. The 12mm nail has a solid cross section but is fluted, having 6 longitudinal grooves equidistant around its circumference (figure 3.1c,d). Both the 10mm and 12mm diameter nails were tested. Both nails have a 1500mm antero-posterior radius of curvature.

3.2 COMPOSITE FEMORAL MODELS

Composite bone models are available commercially from Sawbones Europe AB, Sweden (figure 3.2). Sawbones sell three sizes of composite femora (lengths 480, 420 and 260mm). The medium sized femora (part no. 3103) were used as bone models in this study. The femur has a length of 420mm and has a medullary canal diameter of 13mm. The external diameter of the diaphysis, mid-shaft, is 27.2mm. The radius of curvature of the composite femur is 3200±250mm (Cristofolini *et al.*, 1996). A comparison of these dimensions with those of human bones is given in table 2.7. When compared with the load-deflection characteristics of eight human femora, of roughly the same dimensions, the composite models were found to be more consistent and fell within the range of the human bones. This makes them ideal for standardised testing of orthopaedic implants.

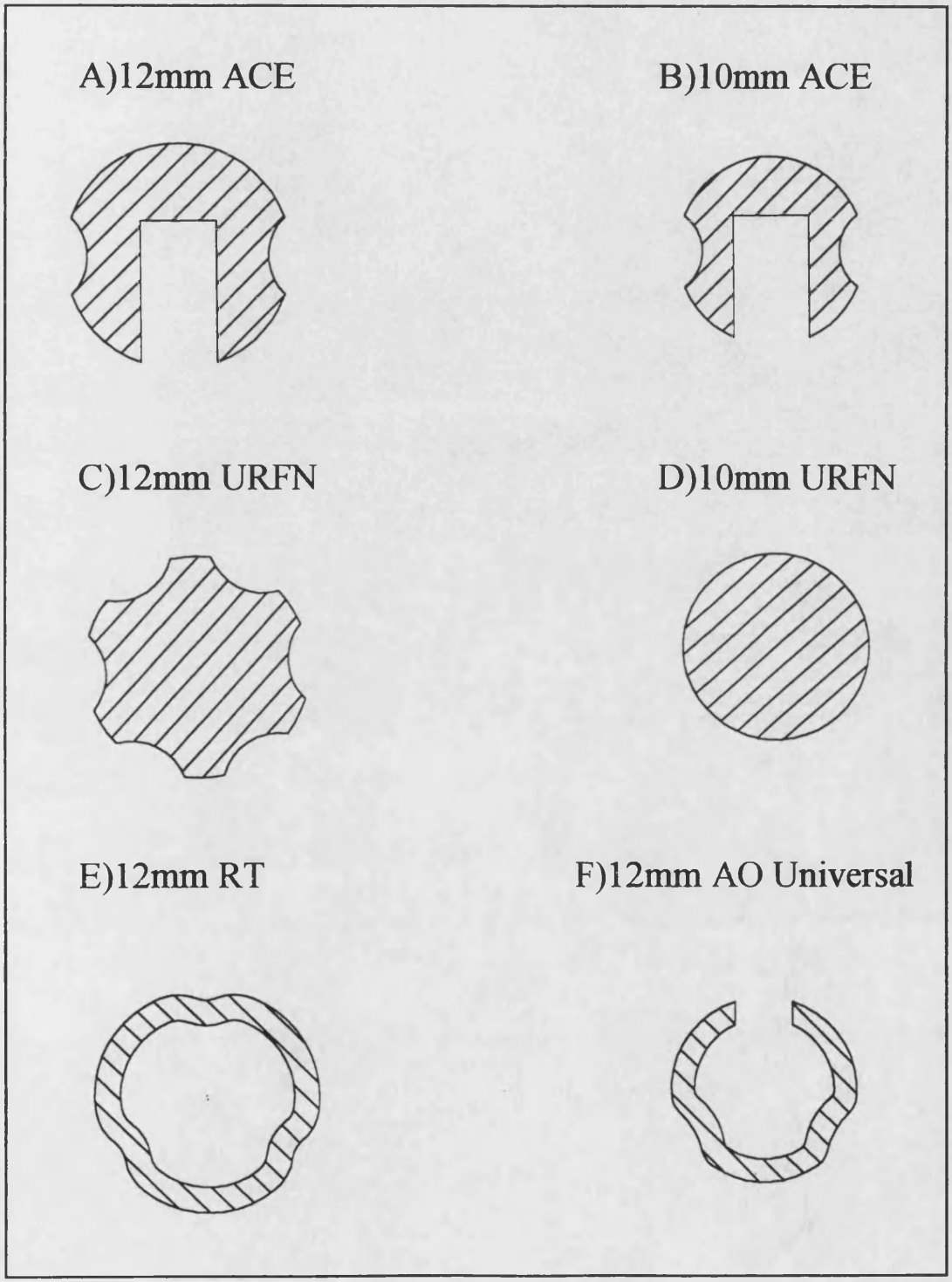

Figure 3-1 Femoral intramedullary nail mid-shaft cross-sections

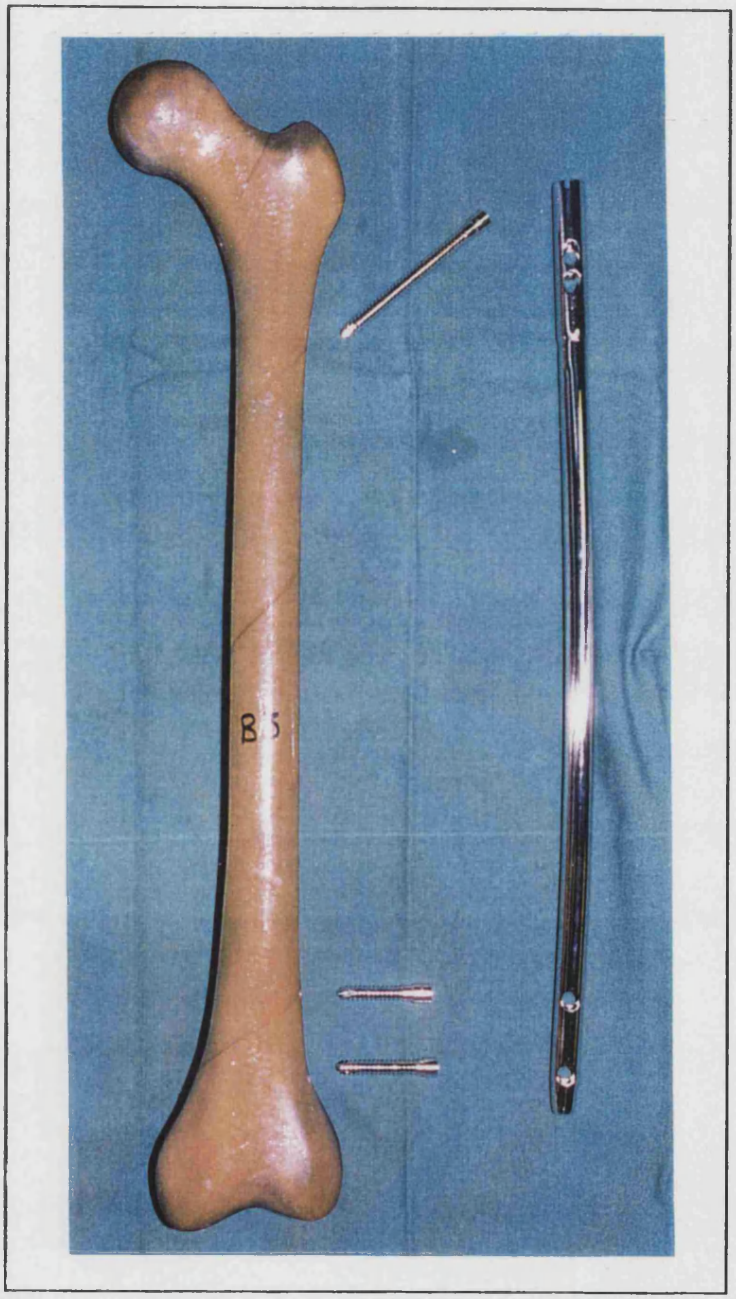

Figure 3-2 The RT nail and Sawbone composite femur

CHAPTER 4

CHARACTERISATION IN ISOLATED LOADING MODES

4.1 INTRODUCTION

The intramedullary nails were tested in pure bending and torsion in order to determine their mechanical characteristics. Isolated testing of the AO Universal nail, the Russell-Taylor nail and the composite femur had already been completed in antero-posterior bending and in torsion in an earlier study (Miles *et al.*, 1994). These results will be presented with those of the other nails later in this chapter for comparison. The mechanics of the remaining four nails were determined according to the following protocol.

4.2 METHOD

In bending, the nails were loaded in two planes; the antero-posterior plane with loading increasing the nail curvature, and in the medio-lateral plane. These bending modes are representative of those experienced by the femur *in vivo*. A four point bend rig (figure 4.1) was placed in an Instron testing machine (Series no. 4303). The nails were pre-loaded to 100N to stabilise them in the correct plane. A further 200N was applied. This is equivalent to an applied bending moment of approximately 10Nm. This is within the range recorded by Schneider *et al.* (1990) from an instrumented femoral intramedullary nail. A stroke rate of 2.54mm/min was used according to Russell *et al.* (1991). The load-deflection characteristics of each nail were recorded. Three tests were completed on all nails in each plane of bending. In addition the AO Universal nail, Russell-Taylor nail and the composite femur were characterised in medio-lateral bending as they had not been tested in this mode during the previous study.

Torsional testing was completed using a specially adapted torsion rig. Figure 4.2 shows the rig set up. During testing, one end of the specimen was held rigidly and a torque was applied by adding weights to a hanger at the end of a moment arm. Torsional moments

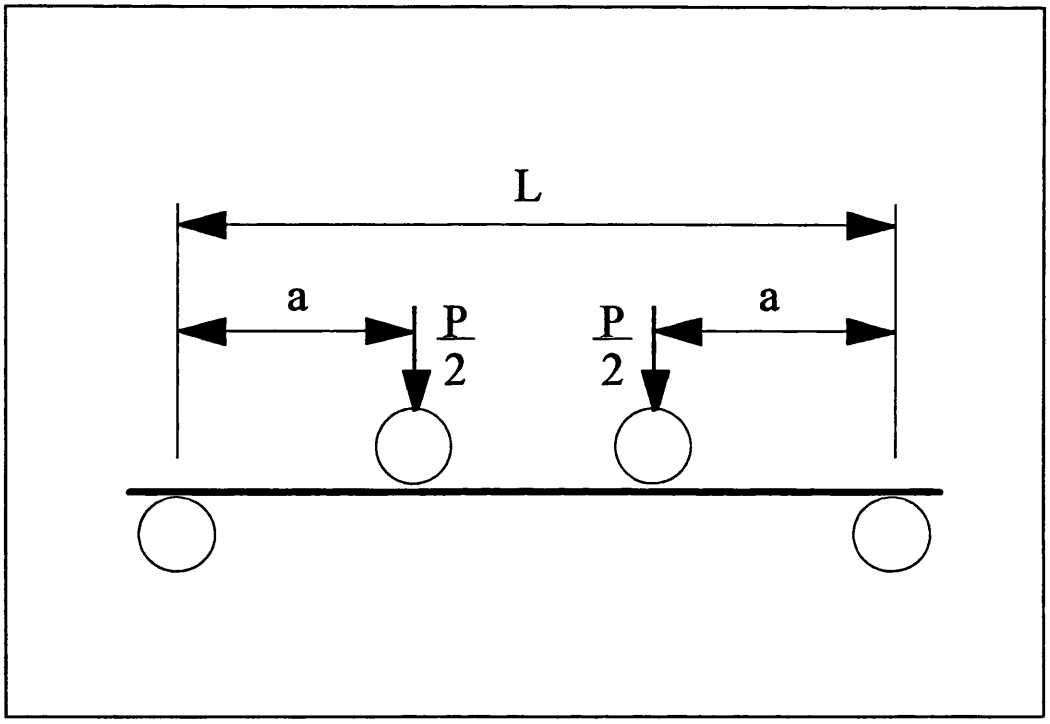

Figure 4-1 Four point bending rig. The load, P, was applied by the Instron to the two top rollers

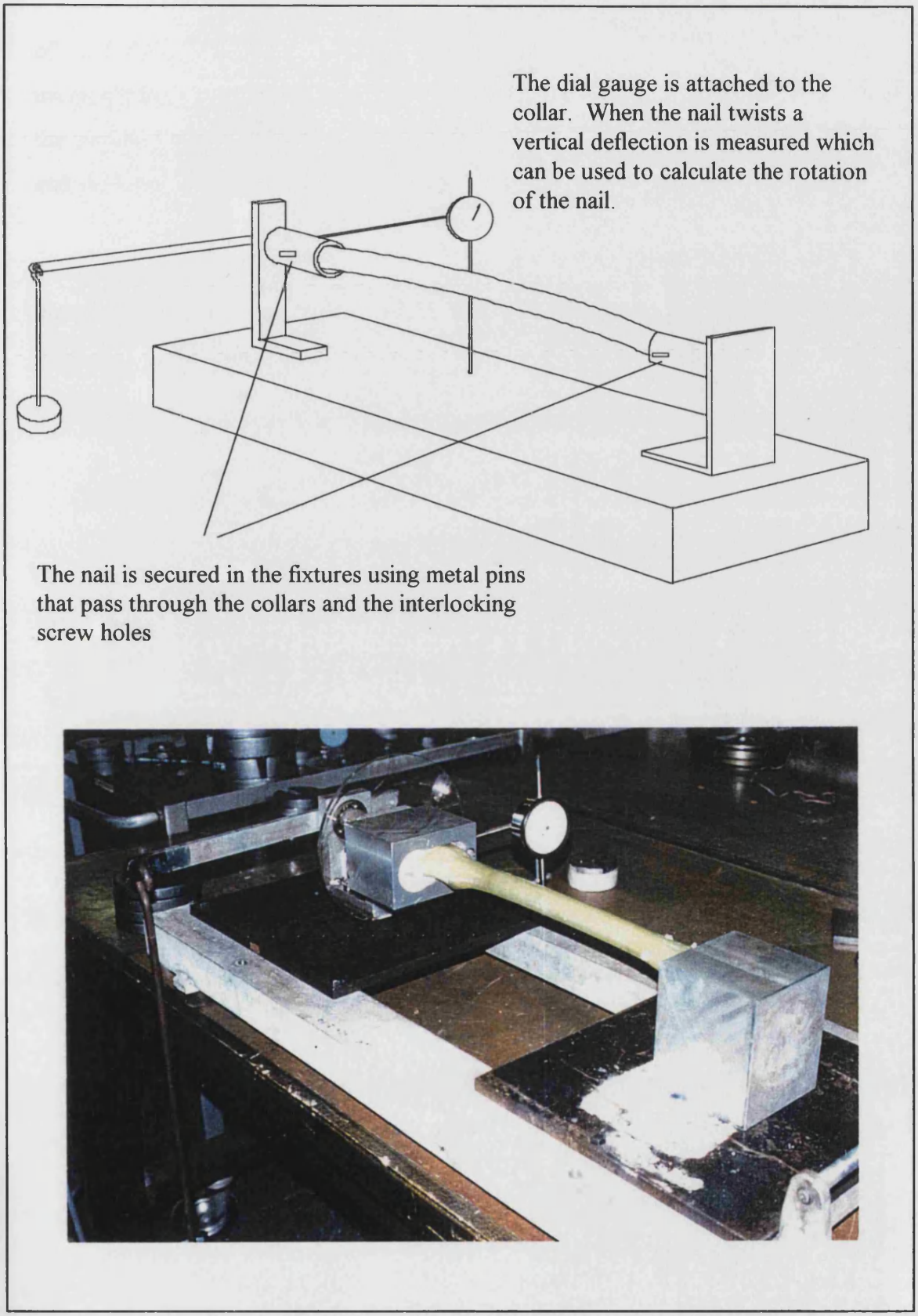

Figure 4-2 The torsion rig used to test the nails and Sawbone femur model

of up to 7Nm were applied. Again, this value is in the range recorded from a femoral intramedullary nail *in vivo* (Schneider *et al.*, 1990). A dial gauge was used to measure the angular deflection of the test piece. Three tests were completed on each of the nails and the load-deflection characteristics were recorded.

Two other methods were used to find the rigidities of the intramedullary nails. Firstly, the second and polar moments of area of each nail were calculated theoretically. The following assumptions were made about the nail's geometry based on information available from the manufacturer's literature.

- The Russell-Taylor nail (figure 4.3a)

  It was assumed that the nail had a hollow circular section with an outer radius, R_o=6mm and inner radius, R_i=4.8mm. The second moments of area in the antero-posterior plane, I_x, the medio-lateral plane, I_y, and the polar moments of area, J, were found with respect to the centroid of the circles using the following equations:

$$I_x = I_y = \frac{\pi}{4}\left(R_o^4 - R_i^4\right)$$

$$J = \frac{\pi}{2}\left(R_o^4 - R_i^4\right)$$

- The AO/ASIF Universal nail (figure 4.3b)

  Like the Russell-Taylor nail the AO nail was assumed to have a hollow circular section. However, the name of the nail was found to be misleading because the 12mm AO Universal nail was found to fit inside an 11mm diameter circle and not one of 12mm as its name would suggest. The theoretical calculations were based on the assumption that the nail's cross section consisted of three areas; a circle with R_o=5.5mm; an inner region with R_i=4.3mm and a rectangular region representing the slot with length b=3mm and thickness, t=1.2mm. The centroid of this composite area was determined and the moments of area found with respect to this origin using the parallel-axis theorem, where d is the distance between the axis of each area and the centroidal axis (Gere and Timoshenko, 1989).

$$I_x = \left(\frac{\pi}{4}R_o^4 + \pi R_o^2 \cdot d_1^2\right) - \left(\frac{\pi}{4}R_i^4 + \pi R_i^2 \cdot d_2^2\right) - \left(\frac{bt^3}{12} + bt \cdot d_3^2\right)$$

$$I_y = \frac{\pi}{4}R_o^4 - \frac{\pi}{4}R_i^4 - \frac{tb^3}{12}$$

The AO Universal nail is slotted and therefore has an open cross-section. Using the theory of thin strips and open sections (Rees, 1990), the St. Venant Torsion constant, equivalent to the polar moment of area, was calculated assuming the section to have a perimeter, p=35mm ($p=2\pi R_o$-b).

$$J = \frac{pt^3}{3}$$

- The ACE nail (figure 4.3c)

  The ACE nails were assumed to consist of two regions, an outer circle and a rectangular slot. The centroid of this area was determined and the parallel-axis theorem used to calculate the second moments of area with respect to this origin. The 12mm nail has a radius, R=6mm, and a slot with a width b=3.95mm and height h=7.98mm. The 10mm nail has R=5mm, with the same width of slot but height, h=6.98mm.

$$I_x = \left(\frac{\pi}{4}R^4 + \pi R^2 \cdot d_1^2\right) - \left(\frac{bh^3}{12} + bh \cdot d_2^2\right)$$

$$I_y = \frac{\pi}{4}R^4 - \frac{hb^3}{12}$$

The ACE nails have an open section. However, because the wall thickness of the nail is not constant, an average value was estimated in order to calculate J. The nails have a perimeter of p=33.75mm and 27.47mm, and an average wall thickness, t=3mm and 2mm for the 12mm and 10mm nails respectively. The St. Venant torsion equation gives:

$$J = \frac{pt^3}{3}$$

- The AO unreamed femoral nail

  The 10mm URFN has a solid circular section, R=5mm and so the moments of area can be easily calculated.

$$I_x = I_y = \frac{\pi}{4} R^4$$

$$J = \frac{\pi}{2} R^4$$

  The 12mm URFN has a solid section with 6 longitudinal grooves around its circumference. As the nail is symmetrical about both its x and y axes, the moments of area for a quarter of the nail were calculated and multiplied by four to find the values for the whole (figure 4.4). The following equations were used to give an approximate value of the area properties of the nail using R_o=6mm and R_g=1.5mm. Although not strictly true, it was assumed that I_x=I_y.

$$I = \frac{\pi R_o^{\,4}}{16} - \left(\frac{\pi R_g^{\,4}}{16} + A \cdot d_1^{\,2} \right) - \left(\frac{\pi R_g^{\,4}}{8} + 2A \cdot d_2^{\,2} \right)$$

$$J = \frac{\pi R_o^{\,4}}{8} - \left(\frac{\pi R_g^{\,4}}{8} + A \cdot d_1^{\,2} \right) - \left(\frac{\pi R_g^{\,4}}{4} + 2A \cdot d_2^{\,2} \right)$$

Once values of I and J had been calculated theoretically for each nail, the rigidity (EI or GJ) was found by multiplication with the appropriate elastic modulus.

As a final method of determining rigidity, each nail was measured using Vernier calipers and radius curves. These measurements were used to plot the nail cross-sections on Autocad, which can be used to calculate the area properties of a complex region. Using the SOLMASSP command, the nail's second moments of area were determined by the Autocad software. The area properties of the nails along with the elastic moduli of each material were used to calculate the rigidity.

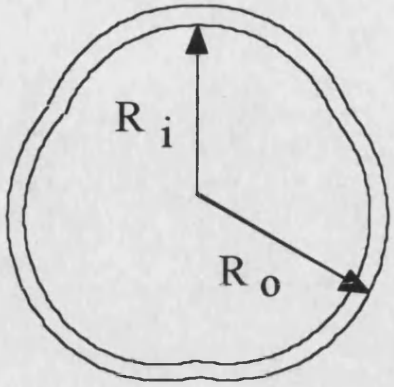

A) The Russell-Taylor nail

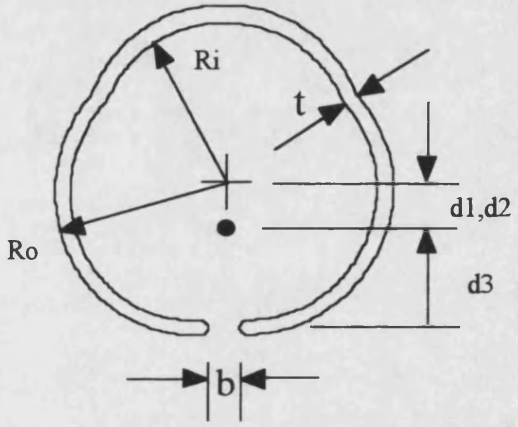

● centroid

B) The AO/ASIF Universal nail

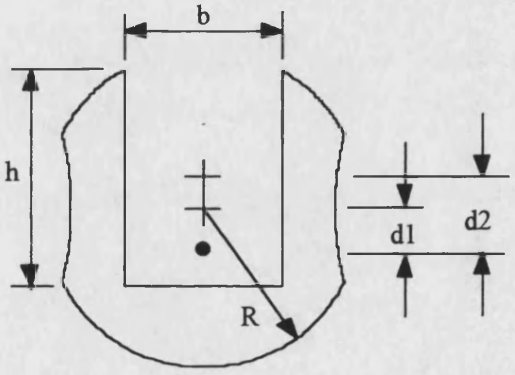

● centroid

C) The ACE nails

Figure 4-3 Notation for the calculation of nail second and polar moments of area

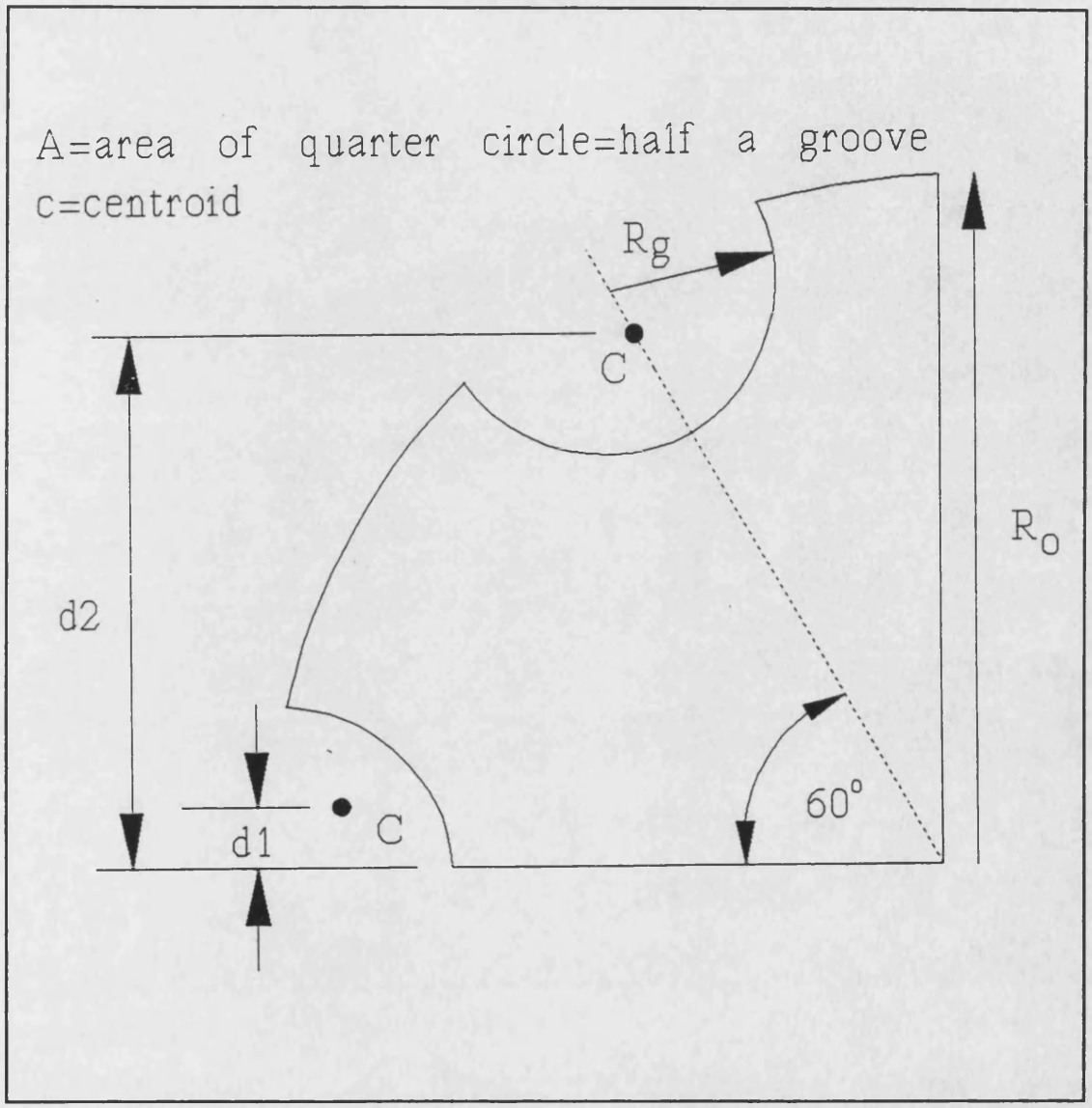

Figure 4-4 Calculating the moments of area for the fluted 12mm URFN. The diagram shows one quarter of the nail which is symmetrical about its x and y axes.

4.3 RESULTS AND DISCUSSION

4.3.1 Bending Tests

Figures 4.5 and 4.6 show the load-deflection curves of the first test on all six nails in antero-posterior and medio-lateral bending respectively. A linear regression was performed on each data set and the gradient of this line was found. The correlation coefficient, R^2, was greater than 0.997 in each case. The average gradient (P/δ) of the three tests was found and the four point bending equation for a simple beam was used to calculate the bending rigidity of each nail (see figure 4.1 for symbols).

$$EI = \frac{P}{\delta} \cdot \frac{a}{24}\left(3L^2 - 4a^2\right)$$

The nail rigidities were found by multiplying the theoretical and Autocad produced moments of area with the appropriate modulus of elasticity; E=200GPa for the stainless steel nails and E=110GPa for those made from titanium alloys. The experimental, theoretical and Autocad rigidities are presented graphically in figures 4.7 and 4.8. The area properties of the nails are given in Appendix B.

In figure 4.5, the 12mm ACE nail appears stiffer in antero-posterior bending than the 12mm RT nail - it requires a greater load to give the same deflection . However, when the final rigidities are calculated (figure 4.7), the Russell-Taylor nail is more rigid than the ACE nail. This is because the Russell-Taylor nail was tested in an earlier study (Miles *et al.*, 1994) with a four point bending rig having a greater distance between rollers, distance a. When this is taken in to consideration in the four point bending equation, the Russell-Taylor nail is the more rigid of the two.

A two tailed Student's t-test was used to compare the experimental rigidities of the nails. This test is suitable for use with small samples. In all comparisons, the null hypothesis was assumed to be that there was no significant difference between the rigidities of the nails. If the probability, p, value was less than the conventional level of 5% ($p<0.05$), then the null hypothesis was assumed to be untrue.

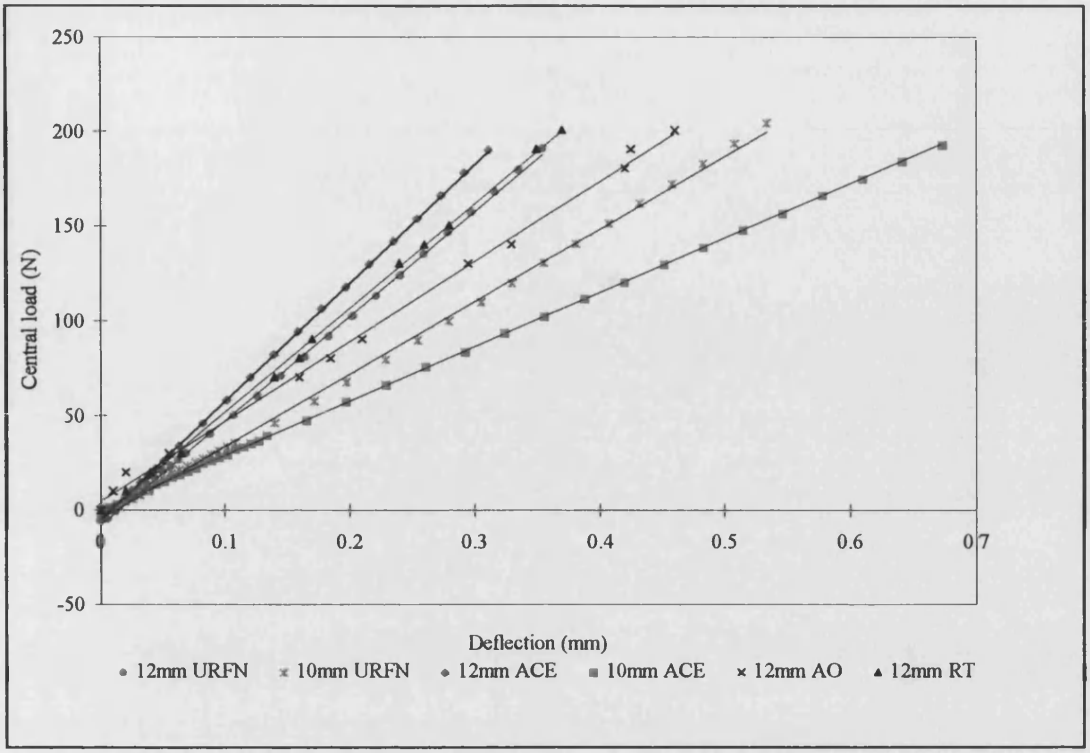

Figure 4-5 Load-deflection curves for bending in the antero-posterior direction

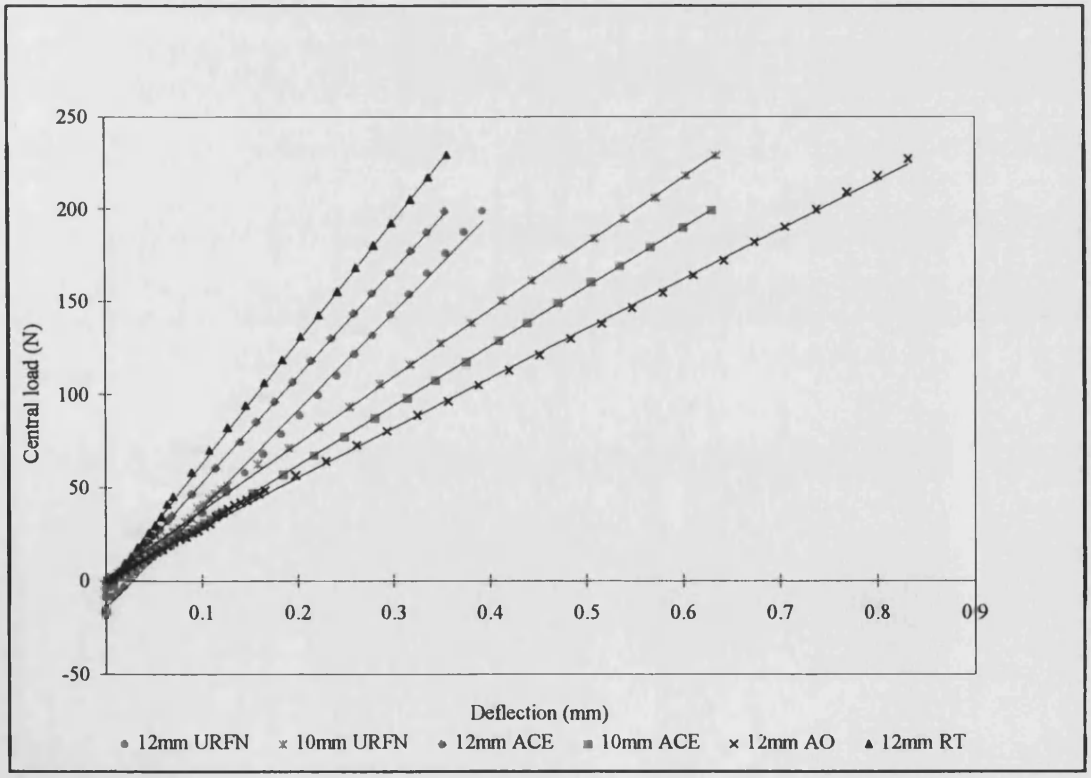

Figure 4-6 Load-deflection curves for bending in the medio-lateral direction

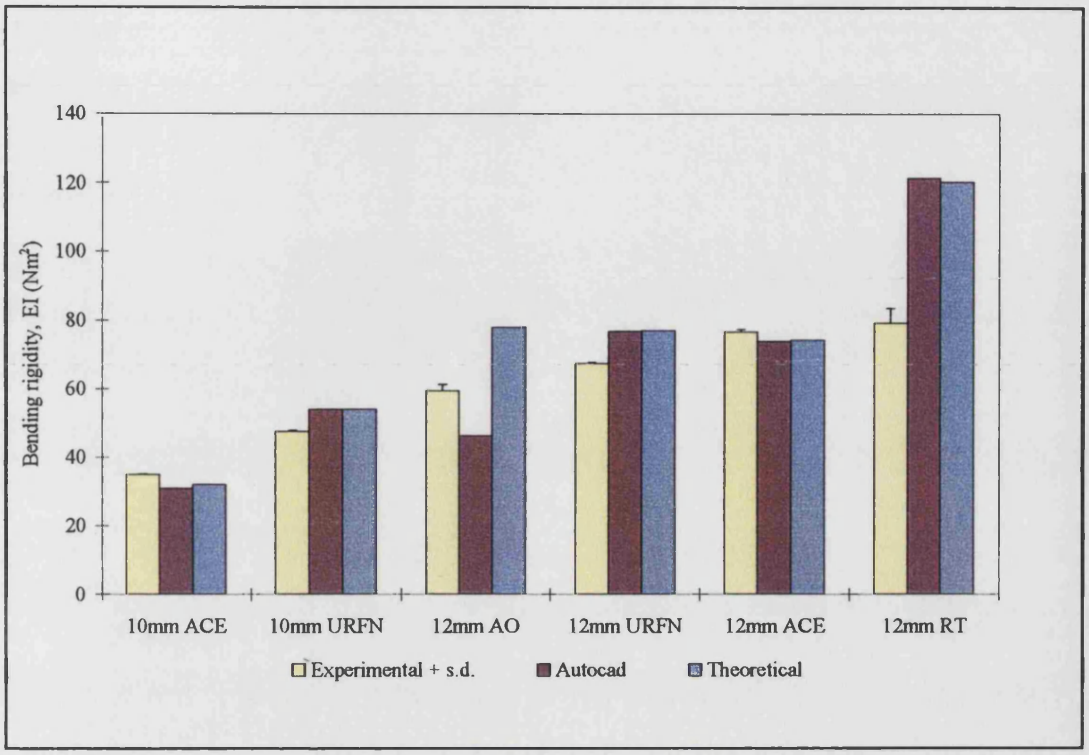

Figure 4-7 Antero-posterior bending rigidities

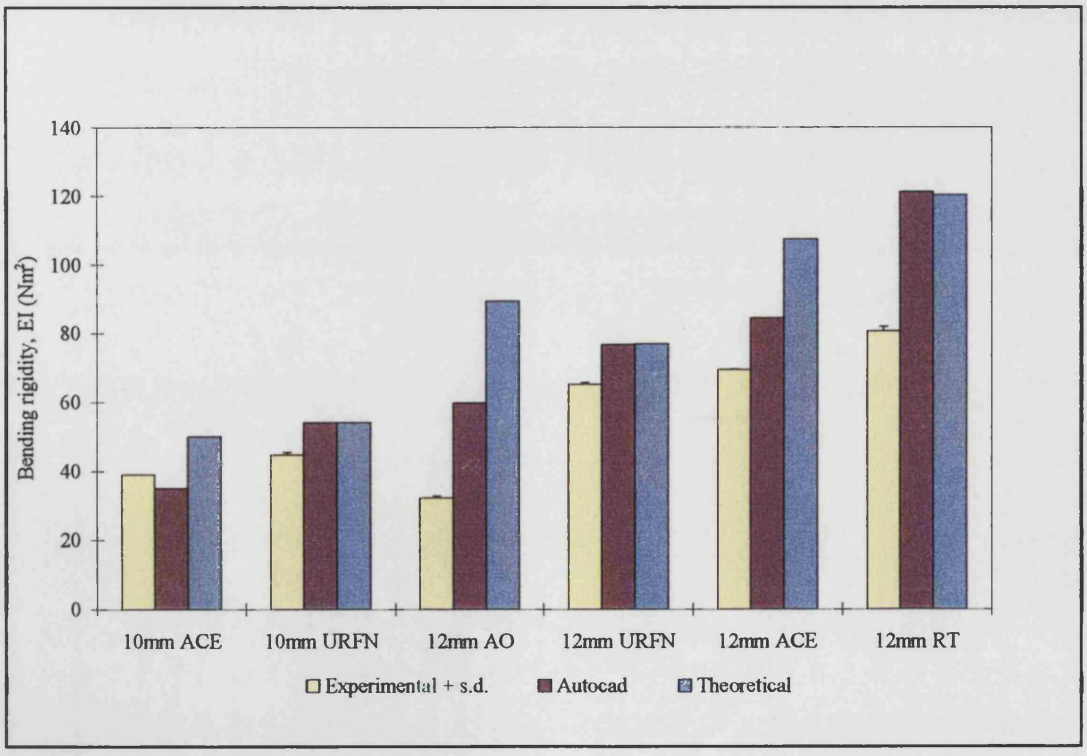

Figure 4-8 Medio-lateral bending rigidities

In both planes, the Russell-Taylor nail has the greatest rigidity of all the nails tested. This is due to its closed cross section and because it is stainless steel. However, in the antero-posterior plane its rigidity is not significantly different from the 12mm ACE nail ($p=0.41$). The most frequently quoted advantages of titanium over stainless steel are that it has half the elasticity of stainless steel which is closer to that of bone. It also has a greater strength (table 4.1), and biocompatibility but it is more expensive and particularly sensitive to notching. Therefore, the ACE nail might be used instead of the Russell-Taylor nail because it has the same stiffness but a better strength. However, the strength properties of the nails were not investigated in this study because only one nail of each type was acquired.

Material	Modulus of Elasticity E (GPa)	Shear modulus of elasticity G (GPa)	Yield stress σ_y (MPa)
Stainless steel	200	80	280-700
Pure titanium	110	40	400
Titanium alloys	100-120	39-44	760-900

Table 4-1 Mechanical properties of stainless steel, titanium and its alloys.

From Gere and Timoshenko, 1989

Although in both bending planes the nails were all found to have significantly different rigidities ($p<0.05$), the values are all of the same order and follow the same trend (most to least rigid). The exception to this trend is the AO Universal nail in medio-lateral bending. The 12mm AO Universal nail was found to be significantly less rigid than either the 10mm URFN or 10mm ACE nails ($p=4.1\times10^{-5}$ and $p=0.0017$ respectively). The 10mm nails are both made from titanium alloys. This may be significant in the clinical selection of a nail, with the titanium nails being advantageous over the stainless steel AO Universal nail because of both their smaller diameter and greater rigidity.

In general, the nails' rigidities were significantly different in medio-lateral bending than in antero-posterior bending ($p<0.05$). The most significant difference is seen with the AO Universal nail which is almost twice as rigid in the antero-posterior direction compared

to the medio-lateral ($p=8.5x10^{-4}$). Bending in the medio-lateral direction allows the slot of the nail to compress more easily which will reduce the rigidity.

The large number of different test protocols used to study intramedullary nails makes a comparison of the results difficult. These tests show the Russell-Taylor nail to be 1.3 times more rigid in antero-posterior bending than the AO Universal nail ($RT=79.1Nm^2$, $AO=59.4Nm^2$). The same ratio of rigidities is found by Beals *et al.* (1988: see table 2.5). Guichet *et al.* (1992) tested 11mm Russell-Taylor and AO Universal nails. Although the nails tested were of a smaller diameter, the rigidities given are of the same order as those presented here ($RT=79\text{-}105Nm^2$, $AO=27\text{-}54Nm^2$). It is generally agreed that nails, of the same material and comparable size, have similar bending rigidities. Differences in the cross sectional geometry have little effect in bending.

Figures 4.7 and 4.8 show that the theoretical rigidities are greater than those calculated experimentally and using Autocad. This is due to the simplification of the nail geometry for these calculations. As an example, the Russell-Taylor nail was assumed to have a hollow circular cross section when, in reality, it has a clover leaf shaped section.

The Autocad estimations of the nail rigidities are a better approximation of the experimental values than the theoretical. This is because the moments of area were based on measurements taken from each of the nails. Differences between the experimental and Autocad values will be due to errors in the human measurements and difficulty in reproducing the exact geometry without scale drawings. The Autocad calculations are also based on the assumption that the mid-shaft cross-section will be constant along the length of the nail. This is not the case, with all the nails having different proximal and distal sections to accommodate the interlocking screws.

The composite femora were found to have a rigidity an order greater than that of the nails. In antero-posterior bending the average rigidity was $201.3 \pm 2.3Nm^2$ and in medio-lateral bending, $174.9 \pm 2.3Nm^2$. Using the Student's t test, the rigidity of the femur was found to be significantly different in each plane ($p<0.05$). The non-

homogeneity in the rigidity of the femur is a result of the composite nature of the glass reinforced epoxy and the varying wall thickness of the epoxy exterior.

The results obtained in this study were compared with those from two other studies. In all three studies the four point bending rigs used were of the same dimensions. Table 4.2 gives the average slope of the load-deflection curves in each study, where the deflection is measured at the mid point.

	Mean bending stiffness (N/mm)	
	A-P	M-L
Present study	1657.2±19.0	1439.4±18.9
McNamara *et al.* (1994)	-	2174*
Cristofolini *et al.* (1996)	2400	2150

*The paper gives the stiffness as 2.174kNm^{-1}. This value clearly has the incorrect units.

Table 4-2 Comparison of composite femora bending stiffnesses

The bending rigidity of the femur in this study is lower than those tested in the other studies. Although the McNamara study does not state which size of bone was used, because of the good agreement with the Cristofolini study, it was also assumed to be a medium sized femur. Therefore, the difference is unlikely to be due to the use of a different sized femur or the rig, because they were identical. It is possible that both studies used a first generation femur with different properties to those produced at a later date. However, the results of this study were repeatable with low standard deviations and still within the range found for human femora by Cristofolini *et al.* (1996) in figure 2.22.

4.3.2 Torsion tests

Figure 4.9 shows the load-deflection curve of the first torsional test on each nail. A linear regression was performed on each set of data and the gradient of this line was found. The correlation coefficient, R^2, was greater than 0.996 in each case. The average gradient, (T/θ), of the three tests was found and the following equation was used to calculate the torsional rigidity, where L is the working length of the device tested.

$$GJ = \frac{T}{\theta} \cdot L$$

Autocad does not generate a value for the polar moment of area of a two dimensional region. However, in cases where the nail had a closed cross section, the polar moment of area could be calculated using the I_x and I_y values generated by Autocad.

$$J = I_x + I_y$$

The theoretical and Autocad rigidities were calculated assuming G=80GPa for stainless steel and G=40GPa for the titanium alloys. Figure 4.10 presents the three nail rigidities as a bar chart. Values for the nail polar moments of area and torsional rigidities are presented in Appendix B.

A two tailed Student's t-test was used to compare the experimental rigidities of the nails. A value of $p<0.05$ was assumed to show a significant difference between values as in bending.

The Russell-Taylor nail has a significantly greater torsional rigidity than the other nails tested ($p<0.05$). This is due to its closed cross-section making it particularly rigid in torsion. The open sectioned nails, the AO Universal and ACE nails, have a rigidity an order less than the Russell-Taylor. The solid unreamed nails have an intermediate rigidity. There is no significant difference between the 10mm and 12mm URFN ($p=0.11$). This is due to the grooves in the 12mm nail reducing its polar moment of area and hence its rigidity.

As with bending, the fact that the 10mm URFN is more torsionally rigid than some of its larger diameter competitors might be useful in nail selection. It may be more desirable due to its smaller size and its greater strength compared to the 12mm AO Universal stainless steel nail.

Russell *et al.* (1991) and Beals *et al.* (1988) both conducted torsional tests on the AO Universal and Russell-Taylor nails. Both studies state that they found the Russell-Taylor

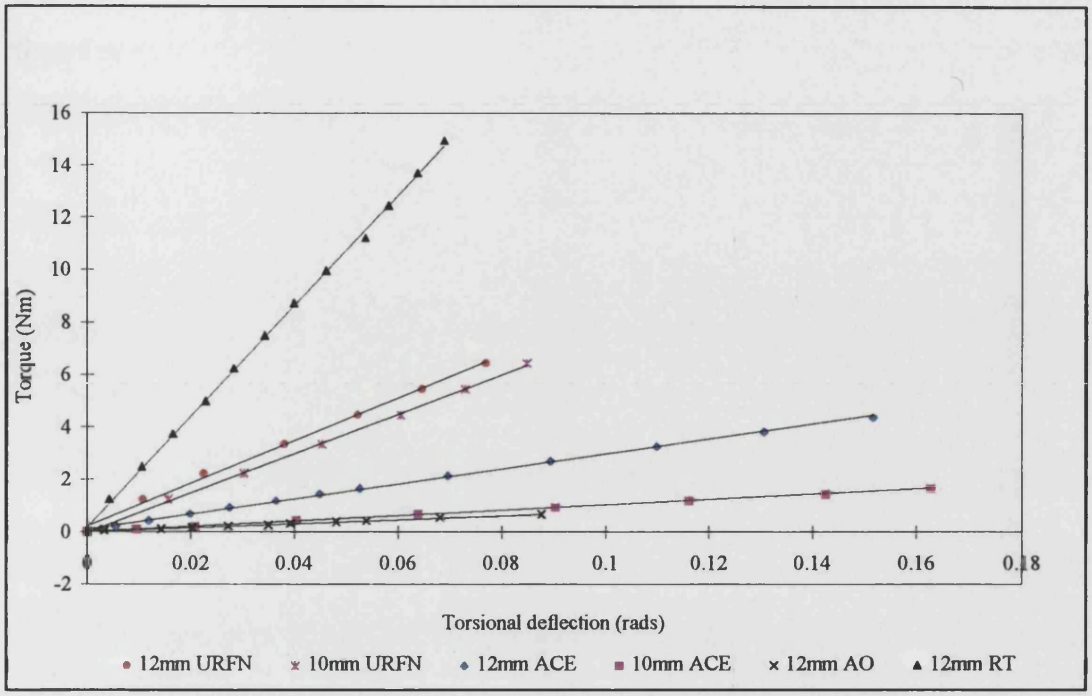

Figure 4-9 Load-deflection curves in torsion

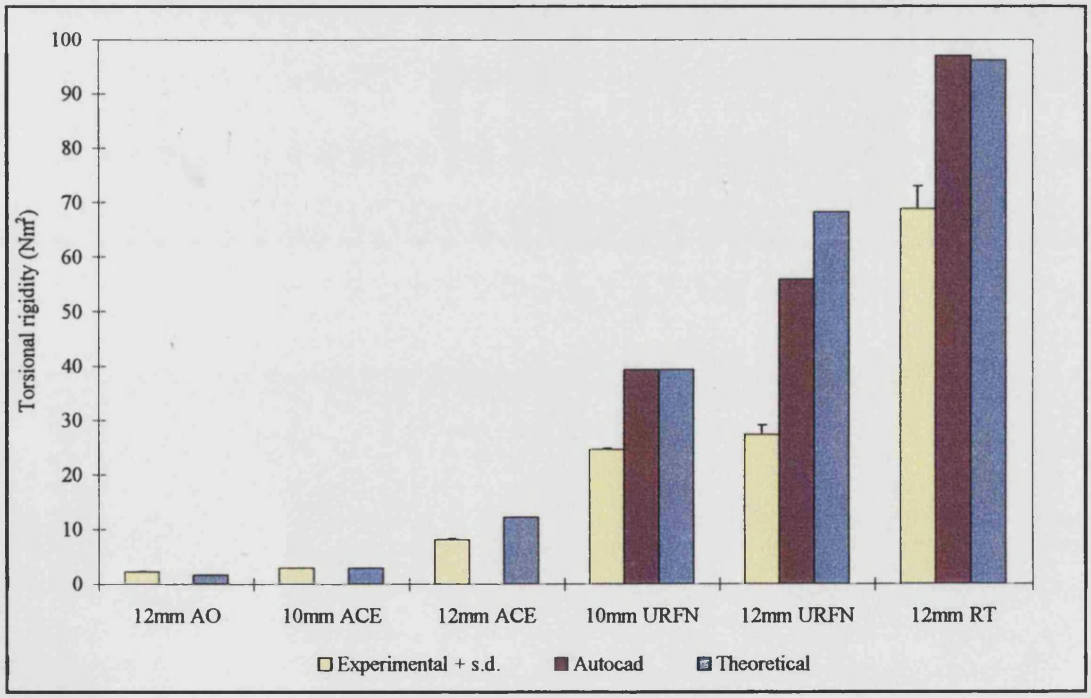

Figure 4-10 Torsional rigidities

nail to be thirty times more rigid than the AO Universal nail. This agrees with the values found in this study (RT=68.8Nm^2, AO=2.2Nm^2). In addition Guichet *et al.* (1992) also found the torsional stiffness of the AO nail to be 2Nm^2.

As with bending, the theoretical values are larger than those found experimentally because of the assumptions made. There are still differences between the rigidities calculated with Autocad and the experimental values. This will be due to errors in the estimated nail geometry, and due to the assumptions made by Autocad for the calculations.

The average torsional stiffness of the composite femur was found to be 211.1 ± 12.9Nm^2 (9.8Nm/deg), an order greater than the Russell-Taylor nail. Szivek *et al.*, (1990) also tested a composite femur and found its torsional stiffness to be 4.4Nm/deg. The Szivek paper does not detail the size of femur tested so this may account for the difference. The torsional rigidity of the composite femur was calculated theoretically using

$$J = \frac{\pi}{32} D^4$$

where D=27.2mm and is the mid-shaft outside diameter of the femur. Sawbones quote a shear modulus of elasticity for the composite bone of 4.12-5.50GPa. This gives a torsional rigidity of 221.4-295.6Nm^2. The value found in this study, 211.1Nm^2, is very close to this range.

4.3.3 Nail deflections

Using the nail rigidities found in this study (Appendix C), the deflections of each of the nails under 'worst case' loading conditions were found. *In vivo* loads were obtained from Schneider's work on an instrumented intramedullary nail (1990). The worst case loads were recorded during single legged stance on the injured limb. The maximum bending moments were 35Nm in antero-posterior bending, 30Nm in medio-lateral bending and 10Nm in torsion. The bending moments were recorded from 80 days post-operatively and so may have been greater earlier in the healing process. However the AP and ML bending moments showed an increasing trend with time. Table 4.3 shows the nail deflections under these bending moments.

	AP bending deflection, mm (load=35Nm)	ML bending deflection, mm (load=30Nm)	Torsional deflection, degrees (load=10Nm)
Russell-Taylor	2.0	1.5	2.7
12mm URFN	2.0	1.8	7.0
10mm URFN	2.9	2.6	7.6
12mm ACE	1.8	1.7	20.0
10mm ACE	3.9	3.0	55.6
AO Universal	3.1	3.5	76.9

Table 4-3 Nail deflections under worst case loads for level walking

These are the maximum deflections under worst case loading conditions for level walking. The bending deflections will be inhibited by the medullary shaft, however these deflections are large and result in severe cyclic loading of the nail. Implants subjected to a prolonged period of excessive weight bearing, as in delayed and non-unions, may be particularly susceptible to fatigue failure (Hutson *et al.*, 1995; Whittle *et al.*, 1995). Angulation of a healing bone may also result from large bending deflections.

The torsional deflections produced in the ACE and AO Universal nails as a result of only 10Nm are excessive. However, torsional moments of up to 40Nm have been recorded during stair climbing (Bergmann *et al.*, 1993). These rotations will be limited to some extent by the interlocking screws after initial fracture consolidation, helping to prevent malrotations. The flexibility of these nails makes distal locking more difficult as the nails twist on insertion. Lowden *et al.* (1989) experienced difficulty in 'introducing the distal locking screws on a number of occasions' with the AO Universal nail. Their technique improved with time.

4.4 SUMMARY

Tests were carried out in torsion, medio-lateral and antero-posterior bending on six intramedullary nails and a composite femur. These modes of loading are comparable with those experienced by the femur *in vivo*.

In bending, the Russell-Taylor nail is the most rigid while the AO Universal nail is the least rigid of the 12mm nails because of the longitudinal slot along its length. The AO Universal nail is also significantly less rigid than either of the 10mm titanium nails in medio-lateral bending.

In torsion, the Russell-Taylor nail was the most rigid nail due to its closed cross sectional area. The URFNs had an intermediate rigidity due to their solid sections, while the ACE and AO Universal nails were the least rigid. The AO Universal nail was, again, found to be less rigid than the smaller diameter titanium nails. This might influence the choice of nail clinically, with a more rigid small diameter titanium nail with potentially greater strength, being preferable over the 12mm stainless steel nail.

Where it was possible to compare the results with the work of other authors, there was found to be good agreement between rigidity values. The rigidities calculated using Autocad were a better approximation of the experimental results than the theoretical values.

The composite femur had a bending and torsional rigidity an order of magnitude greater than the intramedullary nails. When the antero-posterior and medio-lateral rigidities were compared they were found to be significantly different, proving the femur to be non-homogeneous due to its composite make-up. The bending stiffness of the femur was found to differ when compared with other studies. However, the results were repeatable and still within the range of human bone stiffness. The experimental torsional stiffness agreed well with theoretical calculations of its rigidity.

The worst case deflections of each of the nails during level walking were calculated. The magnitude of the bending deflections could result in fatigue failure of intramedullary nails subjected to prolonged loading as seen in cases of delayed and non-unions. The large torsional deflections seen with the ACE and AO Universal nails would be inhibited by the interlocking screws. However, such large rotations during nail insertion make distal screw targeting difficult. The size of the deflections calculated could lead to fracture malunions.

CHAPTER 5

HEALING STUDY IN ISOLATED LOADING MODES

5.1 INTRODUCTION

The isolated testing of intramedullary nails allows a comparison of several devices but does not provide much information directly relevant to the clinical situation. *In vivo* the nail is part of a construct, of which it is a component along with the fractured bone. The next part of the study involved the investigation of the bone/nail construct during a simulated fracture healing process. Loading of the construct was still conducted in isolated bending and torsion in order to first determine the feasibility of the simulated healing process.

5.2 METHODS

After the initial characterisation of the individual components, each nail was inserted into a composite Sawbone. The composite femur was reamed to a diameter of 13mm for the 12mm Russell-Taylor and the AO Universal nails, 1mm greater than the nail diameter as is standard for reamed nails. The femora implanted with the AO unreamed femoral nails were reamed to the exact diameter of the nails i.e. 12mm and 10mm for the two sizes respectively. Although in practice these nails would be inserted without reaming, it would have been impossible to do so using the composite bones. The ACE nails would be inserted without reaming in practice. However in this case they were inserted as if they were reamed nails, the femur being reamed to a diameter 1mm greater than the appropriate nail size. The nails were all locked distally using two transverse locking screws. Proximally the nails were locked as follows:

- AO Universal nail - two transverse proximal locking screws
- Russell-Taylor nail - one antegrade oblique screw
- ACE Medical Company nails - one antegrade oblique screw
- AO URFN's - one transverse locking screw

A) Fully healed construct, healing=100%

B) Fractured or non-healed construct, healing=0%

C) Healing construct

Figure 5-1 The simulated healing process

Once the nails had been inserted in to the bones and locked, the nail/femur construct was assumed to be fully healed (figure 5.1a). The constructs were tested in torsion and antero-posterior bending according to the methodology documented in chapter 4 for the isolated testing of the nails. The stiffness of this construct was assumed to be the same as a fully healed bone with the nail still in situ.

The nails were then carefully removed and a 30mm section cut from the femur mid-shaft to simulate a transverse fracture of the diaphysis. This could be classified as a type 32-C fracture, complex with no contact between bone fragments, according to the AO classification system. The nails and interlocking screws were reinserted and the nail/femur constructs assumed to have the stiffness of a recently fractured bone after fixation with a nail before any healing has occurred (figure 5.1b). The construct was again tested in torsion and antero-posterior bending.

The bone healing process was simulated by applying layers of glass fibre cloth (width=100mm, length=85mm) with an epoxy resin across the 'fracture' site, like callus formation in real bone (figure 5.1c). After each layer was applied, the healing nail/femur construct was tested in torsion and antero-posterior bending. *In vivo*, the stiffness of the bone increases beyond its original magnitude due to the distribution of callus around the fracture site. However, a fracture is usually diagnosed as having healed before reaching this point. Therefore the layering process was stopped when the construct reached its original rigidity as this was thought to the region of most interest. The data obtained from these tests was used to plot a healing curve for each of the nail/femur constructs.

5.3 RESULTS AND DISCUSSION

After the application of each layer the 'percentage healing' and percentage of the total load carried by the nail were calculated in order to plot a healing curve. The 'percentage healing' of the femur is a measure of the increasing stiffness of the fractured composite bone and was calculated as follows:

$$\%\ healing = \frac{current\ construct\ rigidity - rigidity_{0\%}}{rigidity_{100\%} - rigidity_{0\%}}$$

The percentage of the total torque taken by the nail was calculated as follows starting from the standard equation for torsion of a simple cylinder.

$$\frac{T}{J} = \frac{G\theta}{L}$$

where T=applied torque, J=polar moment of area, G=shear modulus of elasticity, θ=angle of twist and L=length of the cylinder. This equation can be applied to both the nail and the construct as a whole. Then, assuming the working length and rotation of the nail and construct are the same and equating gives:

$$\frac{GJ_{nail}}{T_{nail}} = \frac{GJ_{construct}}{T_{construct}}$$

Rearranging to find the torque carried by the nail.

$$T_{nail} = T_{construct} \cdot \frac{GJ_{nail}}{GJ_{construct}}$$

However, the rigidity of the nail (GJ_{nail}) does not account for the effects of the interlocking screws and friction between the nail and inside bone wall. So the percentage torque carried by the nail was eventually calculated using the rigidity of the construct when healing was zero instead of the rigidity of the nail alone.

$$\%Torque, T_{nail} = T_{construct} \cdot \frac{GJ_{construct=0\%}}{GJ_{construct}} \cdot 100$$

The femur was assumed to take the remaining torque not carried by the intramedullary nail.

$$\%Torque, T_{femur} = 100\% - \%T_{nail}$$

In the same way, the load carried by the nail and femur during bending was calculated.

$$\%Load, P_{nail} = P_{construct} \cdot \frac{EI_{construct=0\%}}{EI_{construct}} \cdot 100$$

$$\%Load, P_{femur} = 100\% - \%P_{nail}$$

where P=load, E=modulus of elasticity and I=second moment of area.

5.3.1 Bending tests

The rigidity of the nails alone and as a fully healed and non-healed construct are given in table 5.1. It can be seen that in the majority of cases, the non-healed rigidity is just greater than that of the nail alone. This is due to the effects of the interlocking screws and friction between the nail and inside bone wall. When fully healed, the bone/nail constructs have a rigidity greater than that of the femur alone. It was expected that the rigidity of the fully healed construct should be roughly equal to the sum of the individual nail and femur rigidities. This is true for the Russell-Taylor and AO unreamed models but the remaining constructs have a much lower rigidity. This could be put down entirely to the reaming process which removes the central polyurethane foam from the composite femur, thus reducing the composite bones' rigidity. The 'fit' of the nail within the femur, dependent on the radius of curvature, would also play a role in determining the fully healed rigidity.

	Nail only (Nm^2)	**Non-healed (Nm^2)**	**Fully healed (Nm^2)**
12mm AO Universal	59	53	217
12mm RT	79	94	274
10mm AO URFN	48	98	342
12mm AO URFN	67	113	342
10mm ACE	35	30	212
12mm ACE	77	77	211

Table 5-1 Summary of the average bending rigidities of the nail and bone/nail constructs N.B. The average femoral bending rigidity=201Nm^2. All standard deviations were no more than 5%

The healing curves showing the load taken up by the femur are plotted in figure 5.2a. Figure 5.2b shows the inverse graph, the decrease in load taken by the nails.

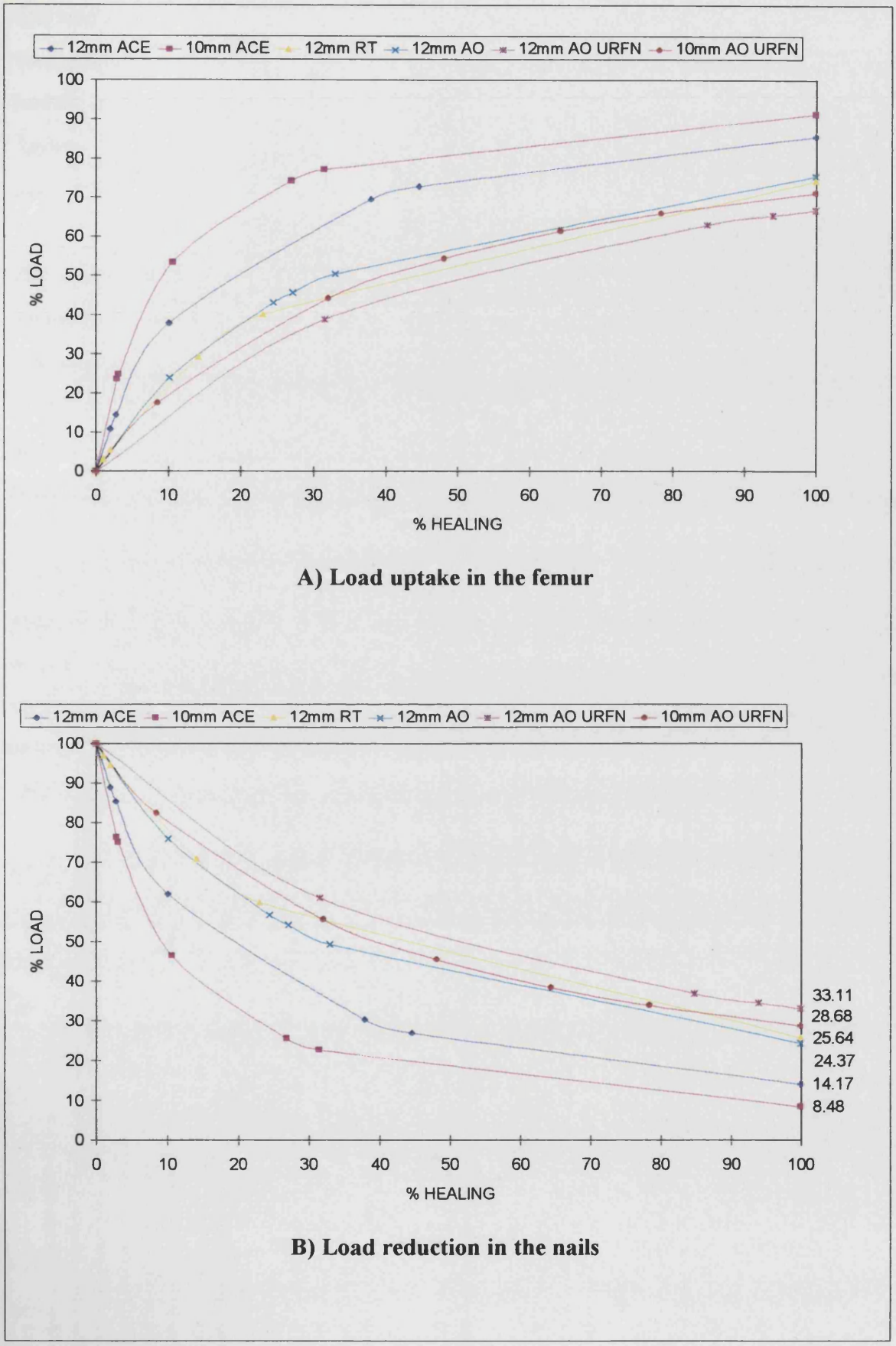

A) Load uptake in the femur

B) Load reduction in the nails

Figure 5-2 The bending healing curves

The rate of load uptake in the femur as the fracture stiffness increases is proportional to the rigidity of the nail in situ. A less rigid nail supports a smaller proportion of the load leading to a rapid load uptake by the bone. In figure 5.2a the AO Universal and Russell-Taylor nails, the reamed nails, produce a similar load uptake in the femur because they have similar bending rigidities.

The 10mm ACE nail produces the most rapid load uptake in the femur as it has the lowest bending rigidity. However, the 12mm ACE nail produces a similar load uptake characteristic which is suprising as it has the second highest bending rigidity of the nails tested. It is thought that this is a result of the fact that the nail has a much larger antero-posterior radius of curvature than the other nails and one similar to that of the composite bone models (ACE=4000mm, RT=2300mm, AO nails=1500mm, composite femur=3200mm). It is possible that the ACE nail could be inserted into the reamed medullary canal without mid shaft contact between the nail and the inside bone wall. This would reduce its rigidity compared to those nails having a smaller curvature which would undoubtedly make contact with the bone wall (figure 5.3). An indicator of the small amount of contact between the 12mm ACE nail and bone wall can be seen from the non-healed rigidity of the bone/nail construct (table 5.1). The non-healed construct is only 0.6Nm^2 more rigid than the nail in isolation.

Although both the 10mm and 12mm AO unreamed nails are less rigid than the Russell-Taylor nail in isolation, they both produce a more gradual load uptake in the femur. The characteristic is similar to that seen with both the reamed nails. This is probably because the medullary canal was reamed to the same dimensions as the nails ensuring greater nail/bone contact. The unreamed nails were noticeably more difficult to insert. This effect can also be seen in the rigidity of the constructs at the non-healed stage (table 5.1). The rigidities at 0% are about double that of the nails alone and are comparable with the rigidity of the Russell-Taylor construct.

The nail rigidities and their influence on load uptake in the healing bone may affect the biological process of fracture healing. Increased loading of a fractured bone, permitted by a more flexible implant, may lead to accelerated callus formation and hence fracture healing (Goodship *et al.*, 1993). However, the least rigid device is not always the best.

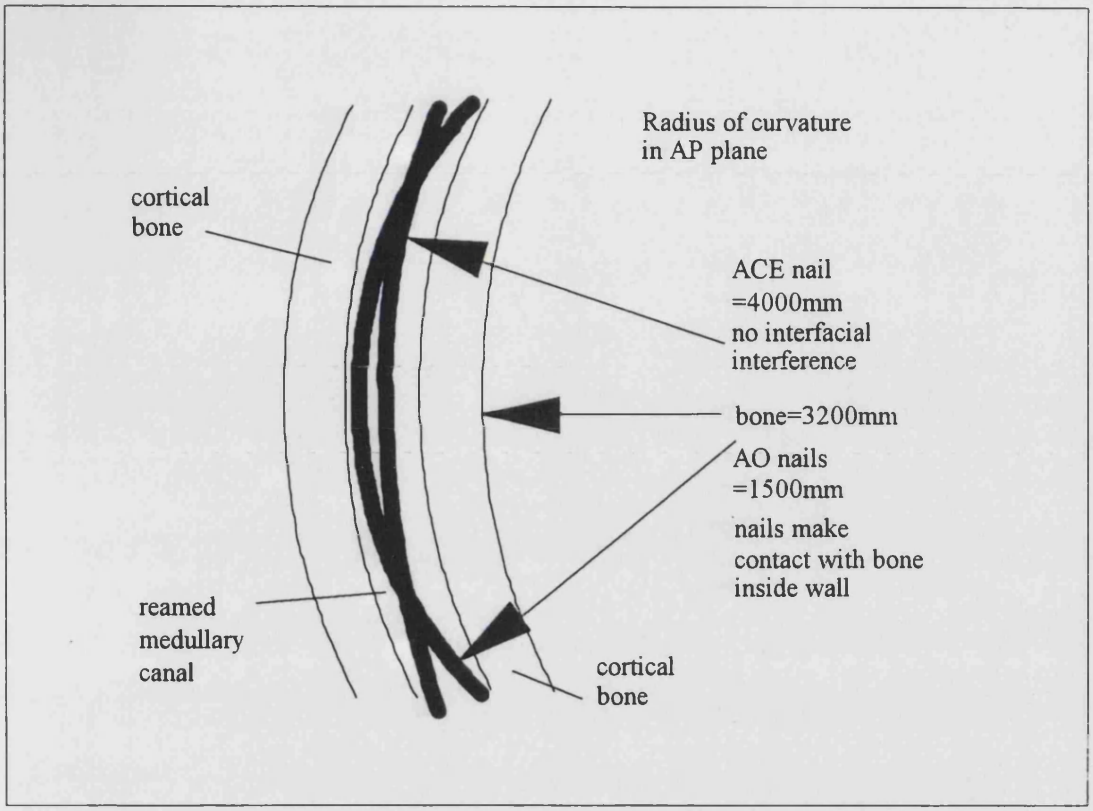

Figure 5-3 Radius of curvature of the composite femur compared to the nails

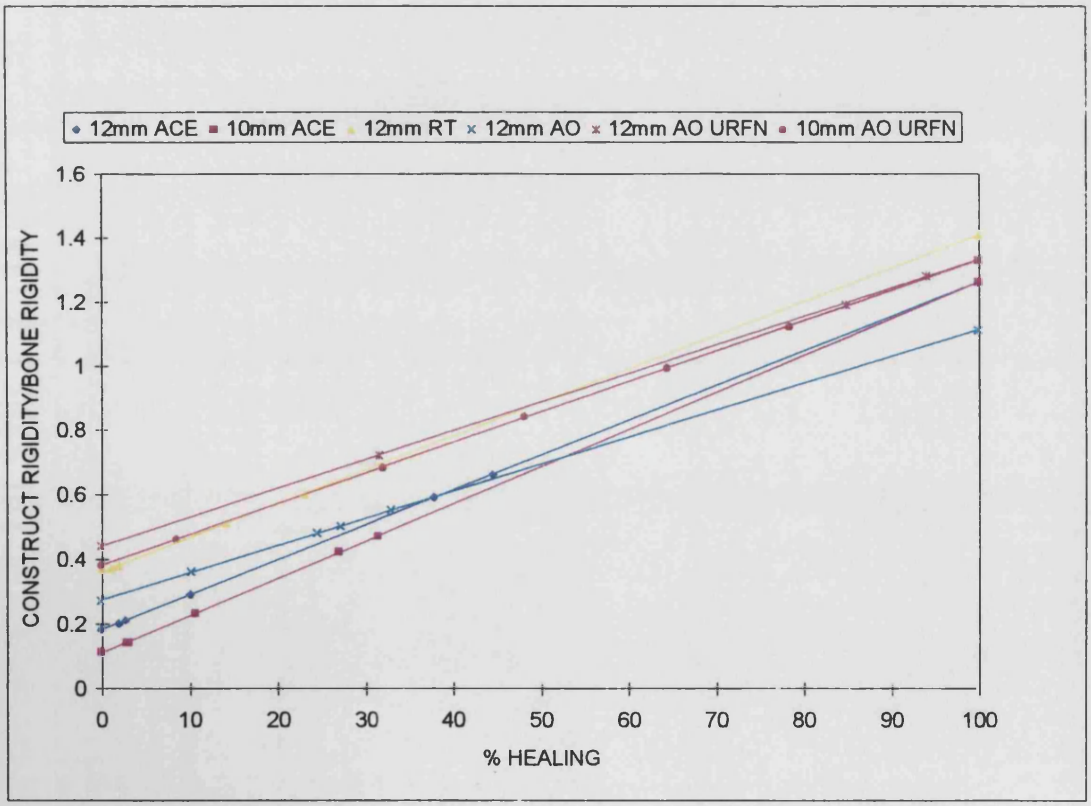

Figure 5-4 Relative bending rigidities

A particularly severe fracture, for example where there is bone loss, will require a greater degree of support to allow uneventful fracture healing without malunion. Increased loading, and hence interfragmentary strain, before initial fracture healing has occurred might prevent initial tissue formation, leading to delayed and possibly non-union (Perren, 1979).

Figure 5.2b, showing the decrease in load taken by the nails, reveals that even when the femur has reached its original stiffness the nails still carry a proportion of the total load. The ACE nails carry the smallest load because they have the lowest rigidity after insertion. The reamed nails, Russell-Taylor and AO Universal support approximately 25% of the total load when the fractured bone has reached its original stiffness. The unreamed AO nails carry the greatest load at the fully healed stage, up to 33% with the 12mm nail. This is due to their high rigidity as a result of friction between the nail and bone.

The clinical failure of implants after fracture union is evidence that the nails still carry a significant proportion of the total load. Zimmerman and Klasen (1983), Perren and Beaupre (1984) and Franklin *et al.* (1988) all reported nail failures after fracture union. The nails failed due to fatigue with breakages occurring at stress risers: 1) at a change in the nail cross-sectional geometry and 2) across the interlocking screw holes. Some of the nails reported in these studies have since been modified to reduce the incidence of nail breakage.

The degree of load carried by the nail when the fracture has 'healed' has implications for the procedure of implant removal. When the nail is removed the load previously carried by the implant will be transferred to the bone. If the bone has not regained sufficient strength, sudden overloading may lead to refracture. Obviously this problem will be more severe in those nails carrying the greatest proportion of the load - the AO unreamed nails.

Figure 5.4 shows the relative rigidities of the constructs as healing occurs. The Russell-Taylor construct is the most rigid construct at the fully healed stage although the

unreamed nails come close. Although the AO Universal nail produces the same load uptake in the femur as the Russell-Taylor nail it is a far less rigid construct overall. It is comparable with the ACE nail constructs but has the smallest rigidity at the fully healed stage.

5.3.2 Torsion tests

The torsional rigidity of the nails alone and as a fully healed and non-healed construct are given in table 5.2. A comparison of the experimental and theoretically calculated torsional rigidity of the Russell-Taylor construct during healing is given in Appendix D. There was good agreement between the two values.

	Nail only (Nm^2)	Non-healed (Nm^2)	Fully healed (Nm^2)
12mm AO Universal	2	6	229
12mm RT	69	81	350
10mm AO URFN	25	36	237
12mm AO URFN	27	35	240
10mm ACE	3	3	212
12mm ACE	8	10	220

Table 5-2 Summary of the average torsional rigidities of the nail and bone/nail constructs N.B. The average femoral torsional rigidity=211Nm^2. All standard deviations were no more than 5%

The non-healed construct rigidities are always greater than that of the nails alone. This is due to the interlocking screws and friction between the nails and the inside bone wall. The greatest change in rigidity is seen after insertion of the AO Universal nail. The rigidity increases by three between the nail in isolation and the non-healed construct. This is probably because the nail is the most flexible in torsion allowing it to deflect on insertion when it meets the bone wall. Hence, a large proportion of the nail could be in contact with the bone increasing friction and hence the rigidity of the construct. The fully healed constructs have a rigidity that is approximately the sum of the nail and bone rigidities. This is as expected.

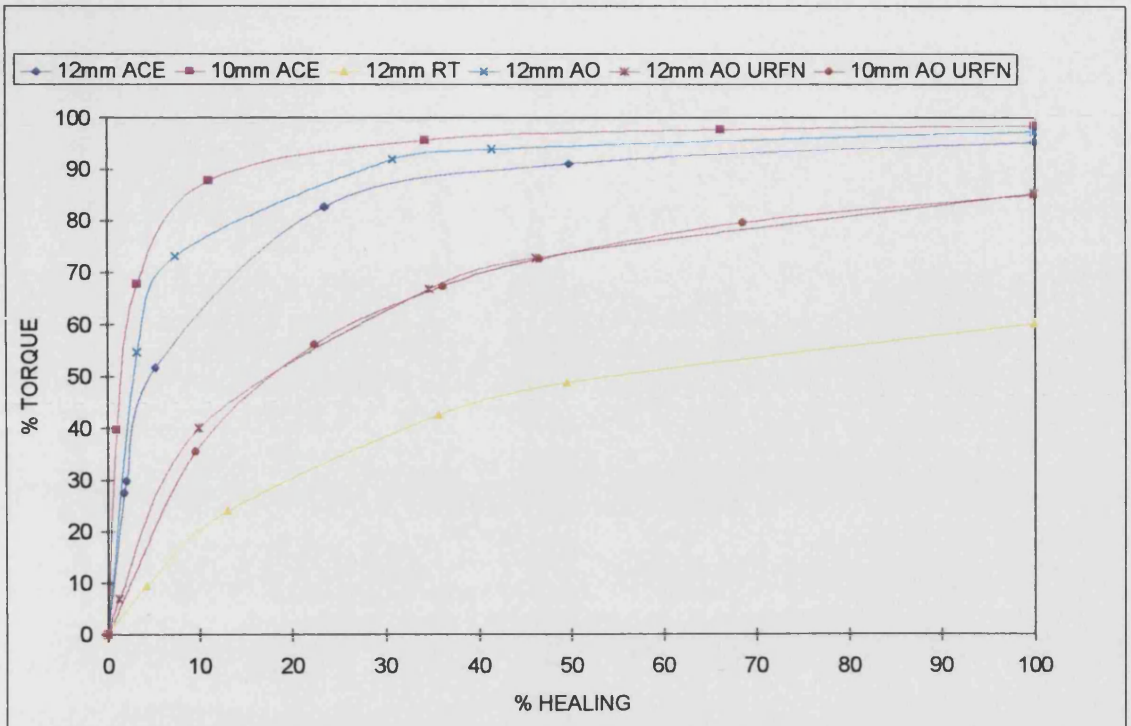

A) Load uptake in the femur

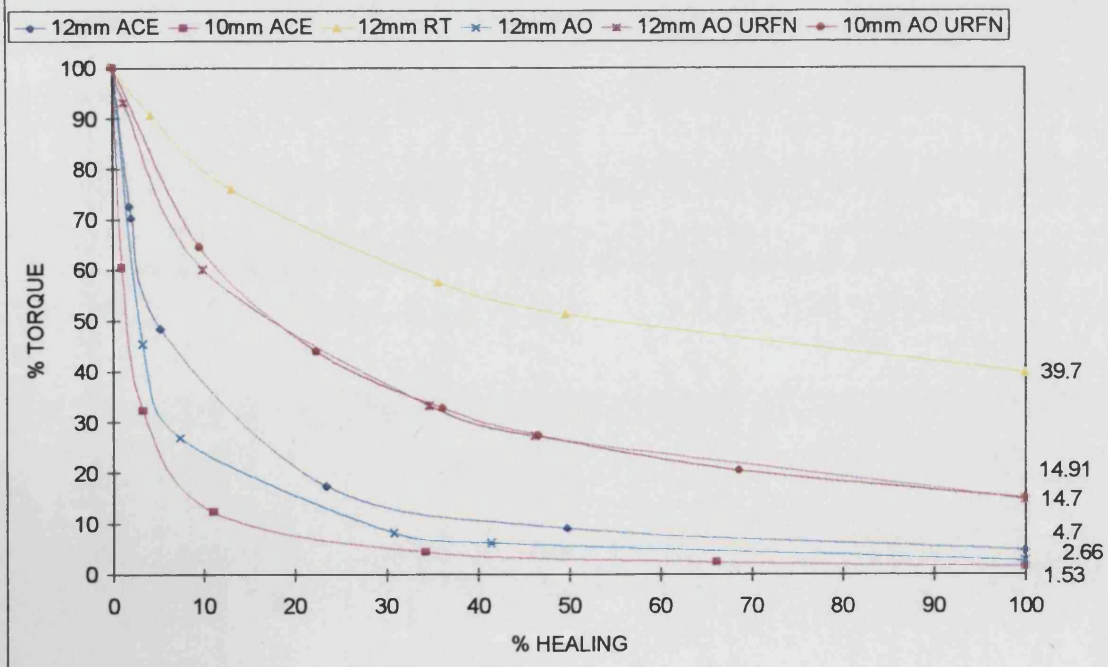

B) Load reduction in the nails

Figure 5-5 The torsional healing curves

Figure 5.5a shows the load uptake in the femur during healing. The Russell-Taylor nail produces the most gradual load uptake as it is by far the most rigid nail in torsion. The rate of load uptake then increases as the nail rigidities decrease. The only anomaly to this pattern is between the AO Universal and 10mm ACE nail, although their rigidities are very similar (2.22Nm^2 cf. 2.93Nm^2 respectively). The increased rigidity of the AO Universal nail after insertion, due to interfacial friction, has produced a more gradual load uptake than the 10mm ACE nail.

As with bending, the rapid load uptake by the femur with the least rigid nails may encourage fracture healing. The more gradual transfer of load to the femur with the Russell-Taylor nail may be appropriate for use in a less stable fracture requiring support for longer during the initial stages of fracture healing.

Figure 5.5b shows the reduction in load carried by the nail as 'healing' progresses. It can be seen that even when the fractured bone reaches its original stiffness, the nails still contribute significantly to the load carrying of the construct. The percentage of the total load supported by the nail is proportional to its rigidity. The Russell-Taylor nail still carries up to 40% of the total load at the fully healed stage. The less rigid nails, the AO Universal nail and the ACE nails, carry only a small fraction at this stage - no more than 5%. As with bending, the total load carried by the nail at the fully healed stage may be significant when considering implant removal.

Figure 5.6 shows the relative torsional rigidities of the constructs tested. The Russell-Taylor construct is considerably more rigid than any of the others. Although the AO unreamed femoral nails are significantly more rigid than the ACE and AO Universal nails in isolation, as constructs they have similar rigidities. The difference between the constructs is reduced as the fracture stiffness increases.

5.4 SUMMARY

Once inserted in to a femur the nails became part of a construct. When the femur was unfractured the construct had a rigidity roughly equal to the sum of the individual nail

and bone rigidities. When fractured, the construct generally had a rigidity greater than that of the nail alone. This was due to the contribution of the femur, the interlocking screws, and friction between the nail and bone wall where they came in to contact. When the experimental rigidity of the Russell-Taylor construct during healing was compared with values calculated theoretically, there was found to be good agreement. The AO unreamed nails were found to be considerably more rigid as a construct compared to in isolation. This was because the medullary canal was reamed to the exact diameter of the nails producing bone/nail contact along the length of the shaft. In reality these nails would be inserted without reaming.

During the simulated healing process in both bending and torsion, the rate at which the bone began to share the total load was found to be dependent on the rigidity of the nail. The most rigid nails gave a gradual load uptake whilst those having the lowest rigidity produced a rapid uptake of load in the femur. When fully healed, the nails still contributed significantly to load sharing. In torsion, the Russell-Taylor nail still carried 40% of the total load at this stage whilst the less rigid ACE and AO Universal nails only carried up to 5% of the load. The load carried by all six nails at 100% healing in bending ranged between 33% and 8.5% (12mm AO URFN and 10mm ACE respectively). The range was smaller than in torsion as the rigidities in isolated bending were less diverse.

Clinically a less rigid nail, which gives a rapid load transfer to the bone, might be used in a more stable fracture where the increased loading might lead to accelerated bone healing. However, in cases of fracture instability, a more rigid nail might be used. The gradual load transfer would provide stability during initial tissue formation thus reducing the possibilities of delayed union.

In bending the relative stiffness of the constructs is similar, the Russell-Taylor being the most and the AO Universal the least rigid structure when the fracture is fully healed. In torsion the Russell-Taylor construct is the most rigid. The remaining constructs have a similar rigidity with little difference between them when healing=100%.

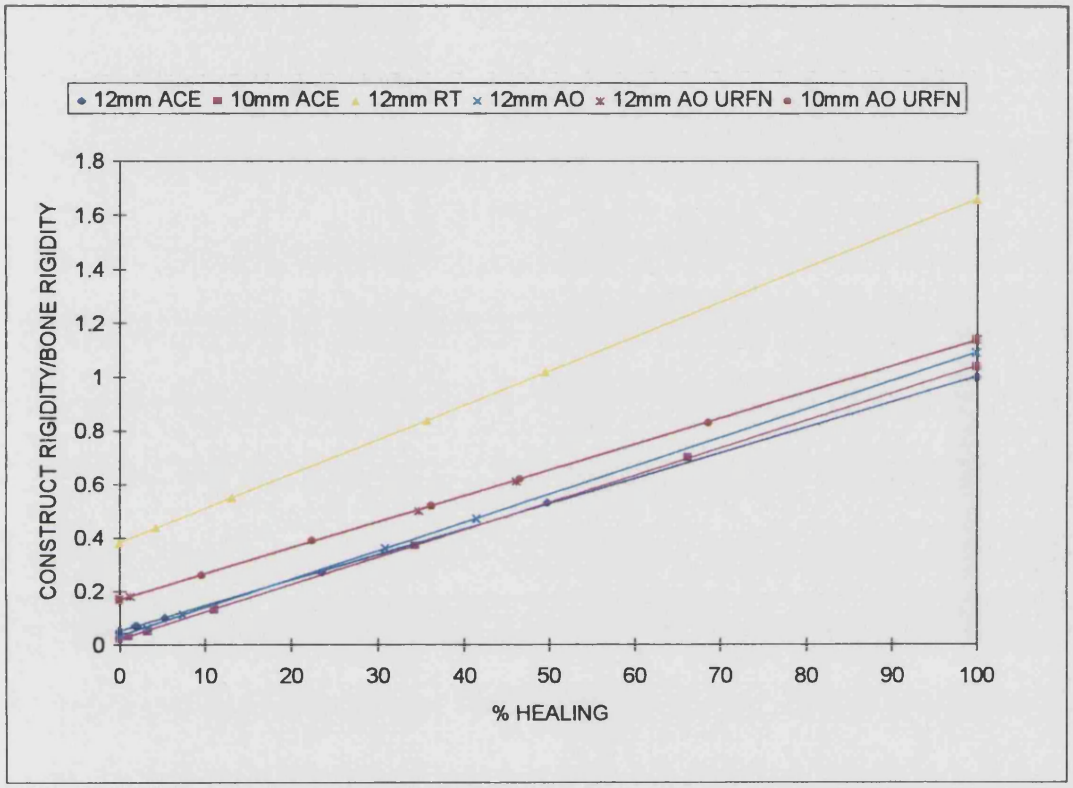

Figure 5-6 Relative torsional rigidities

CHAPTER 6

COMBINED LOADING STUDY

6.1 INTRODUCTION

The fracture healing simulation proved successful and provided a useful insight in to the load supporting role of the intramedullary nail as the stiffness of the healing bone was increased. However, the study was still carried out in isolated bending and torsion only. The next phase of the project involved designing a rig that would combine the loads experienced by the femur *in vivo*.

6.2 METHOD

6.2.1 Rig design

The forces the femur is subjected to *in vivo* vary continuously. Even within a simple walking cycle the joint force and muscle forces that are exerted on the femur change significantly in magnitude and direction. Figure 6.1 shows a three dimensional plot of the resultant hip joint force measured from a telemeterised hip prosthesis. The data was collected from a patient walking with crutches. The length of the lines indicate the magnitude of the force which can clearly be seen to travel over the surface of the femoral head. Therefore the forces acting on the femur at one instant were considered for simplification when designing the combined loading rig.

It was decided that the forces during single legged stance would be modeled. The whole body weight is transferred through the hip in this posture. In addition the body instantaneously passes through this loading state during gait. Single legged stance occurs just after heel strike when the hip joint reaction force reaches its first peak magnitude (Paul, 1966-67: see figure 2.9). There are a large number of studies published that have simulated the femoral forces at this stage providing a considerable amount of information on joint reaction forces and muscle actions (section 2.2). In contrast, there

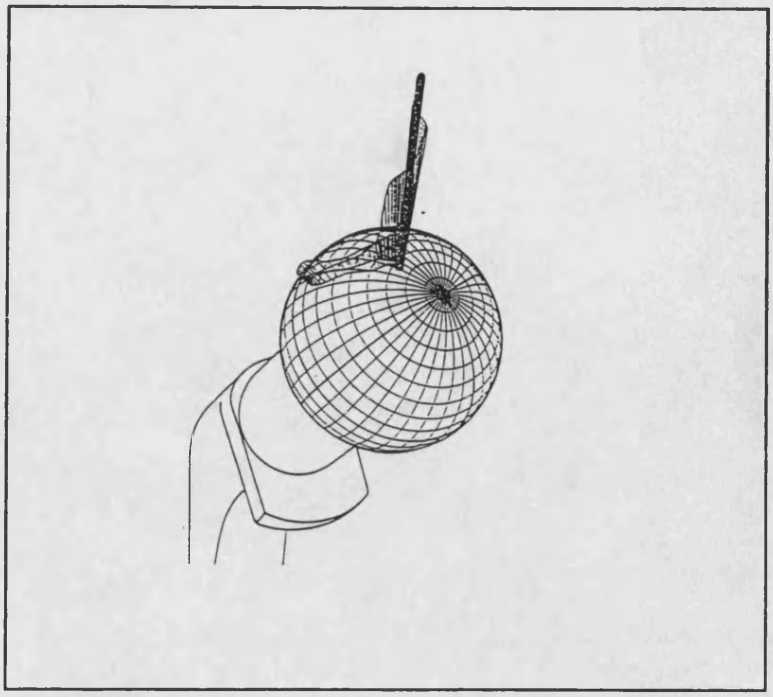

Figure 6-1 The changing magnitude and direction of the resultant hip joint force.

From Davy *et al.*, 1988

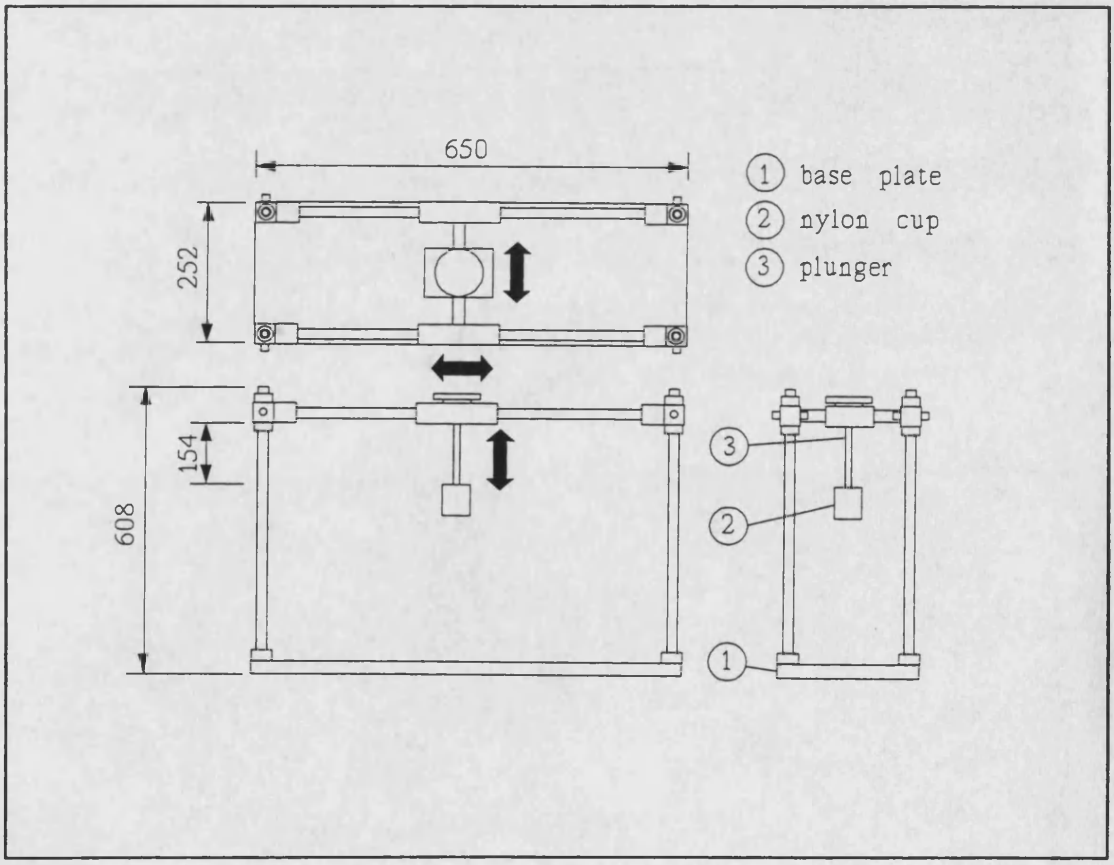

Figure 6-2 A schemetic diagram of the combined loading rig (dimensions in mm)

was little data in the literature describing the forces acting on the femur at any other phase.

The rig designed to load the femur in single legged stance consisted of an external frame on which a plunger was mounted on a sliding support plate (figure 6.2). The plunger, which had a nylon acetabular cup distally to interface with the femoral head, was movable and could be secured in any position required within the boundaries of the frame. The frame was placed in an Instron testing machine (Series no. 4303) with the plunger under the machine crosshead which was used to apply the joint reaction force. A ball bearing was placed between the crosshead and plunger to prevent unwanted shear and bending forces being transmitted.

In the first instance the femoral condyles were set distally in a shallow aluminium tray using Wood's metal, a low melting point alloy. The femoral shaft axis was angled at 11° to the vertical in the medio-lateral plane. This is the anatomic orientation of the femur during stance. The femur was then positioned in the frame with its femoral head in the nylon cup and secured with clamps to the frame base plate (figure 6.3). The joint reaction force was applied vertically through the nylon cup.

The rig was later modified to include the direction of the joint reaction force. Paul (1976) calculated that the joint reaction force acted at 21° to the hip knee axis in the medio-lateral plane and at 12° in the antero-posterior plane at heel strike (see figure 2.10). As single legged stance occurs just after heel strike, these force angles were incorporated in to the design. The aluminium tray containing the femur was orientated at the above angles using angled blocks. The femur was then positioned in the frame with the femoral head in the nylon cup and the Instron was used to apply a vertical force to the femoral head (figure 6.4). This produced the required orientation of the joint reaction force. A joint reaction force of 2.7W was applied to the femoral head through the nylon cup via the Instron crosshead in both cases.

The simulation of forces exerted by both the abductors and iliotibial band have been shown to be important in order to create realistic femoral strains during single legged

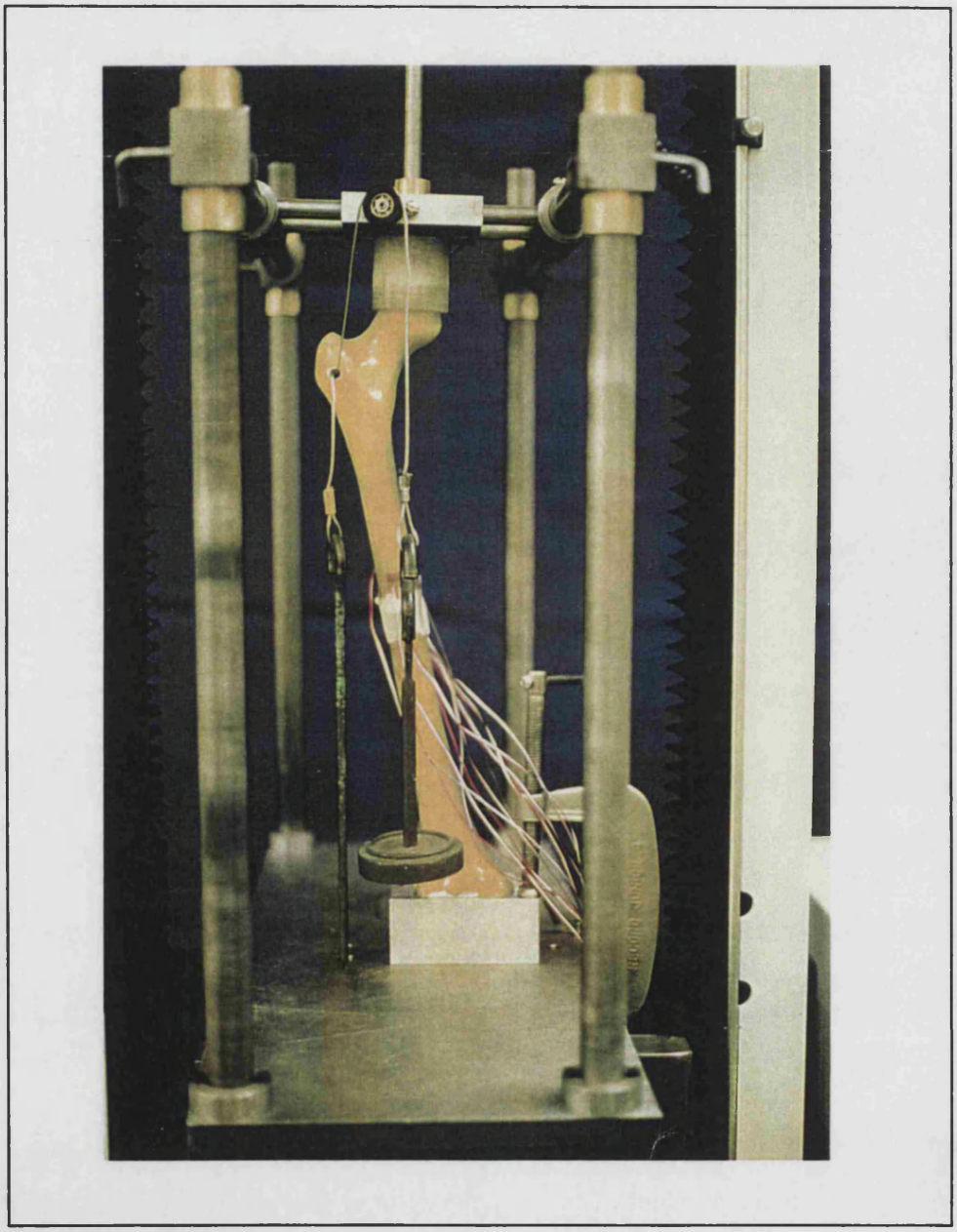

Figure 6-3 Photograph of a femur in the combined loading rig with the joint reaction force applied vertically

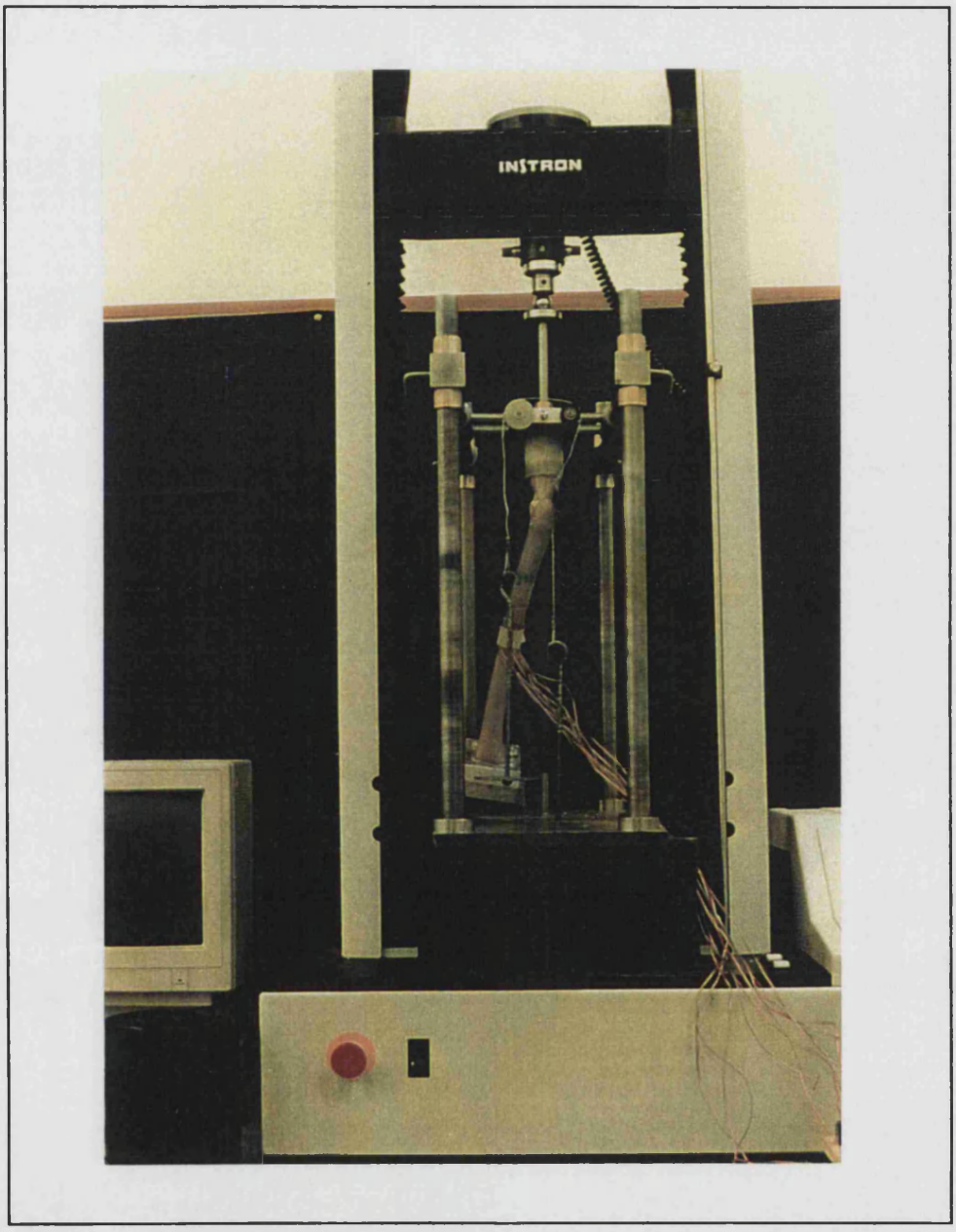

Figure 6-4 Photograph of a femur in the combined loading rig with the joint reaction force applied at 21° in the medio-lateral plane and 12° in the antero-posterior plane

stance (Hazlewood, 1996; Finlay *et al.*, 1991). The abductors act to stabilise the hip during single legged stance. They originate from the ilium on the pelvis and insert on to the greater trochanter of the femur. The abductor muscles modeled in this set-up were the gluteus medius and minimus, the resultant of which acts with a force of 2W at 20° to the vertical in the frontal plane. This force was applied using dead weights and a cable and pulley system which passed through a pre-drilled hole in the greater trochanter. The iliotibial band is not a muscle but tendon, a connective tissue which connects muscle to bone. It is bi-articular connecting the pelvis with the tibia, and is not directly attached to the femur itself. However, it has a considerable effect on the femur, acting like a tension band and reducing bending stresses in the medio-lateral plane (O'Connor, 1992). The tensioning force of the iliotibial band was also applied using a cable and dead weights. The distal end of the cable was attached to the base plate, and at the correct angle, passed upwards and through the greater trochanter. The tension in the band has been found to act parallel with the bone shaft in the frontal plane and with a force of one times body weight, W, during single legged stance (McLeish and Charnley, 1970; Gerlach and Lierse, 1990).

6.2.2 Femoral strain measurement

Strain gauges were placed on the shaft of a composite femur in order to determine four loading modes; bending in the antero-posterior and medio-lateral planes, compression and torsion (figure 6.5). These loading modes were thought to be the most significant during loading of the femur, as shown by the large magnitude of these forces measured by Schneider *et al.* (1990) *in vivo*. The strain gauges were applied at a distance of 167mm below the tip of the greater trochanter, 39% of the total length of the femur. This position was chosen to allow a mid-shaft fracture to be created without interfering with the strain gauge locations. The 45° rosette gauges on the anterior and posterior surfaces were the Measurements Group (UK Ltd.) type CEA 06 125UR 350. The axial gauges on the medial and lateral surfaces were type CEA 06 250UN 350 from the same supplier. The gauges were wired in to Wheatstone bridge circuits according to figure 6.6. This enabled the unwanted effects from other loads to be minimised. For example, the output from a circuit measuring compression would give twice the compressive strain but cancel out the effects of anterior posterior bending, if bending occured about the neutral axis, as both gauges will be subjected to equal and opposite bending strains.

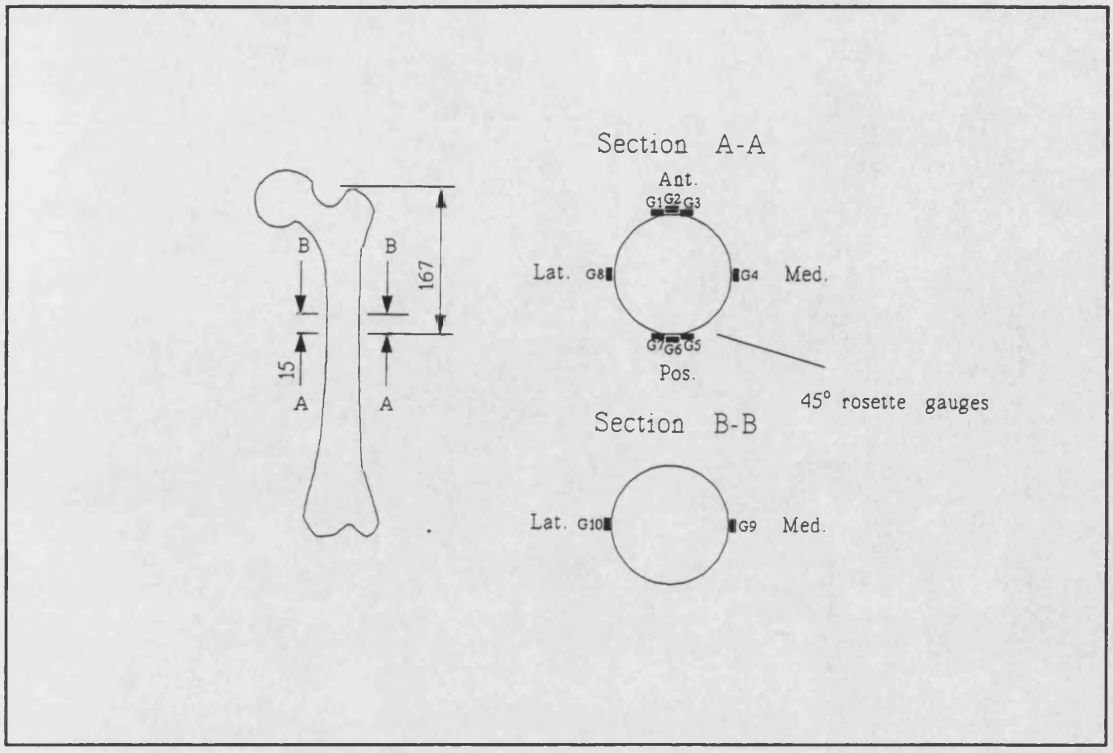

Figure 6-5 Arrangement of the strain gauges on the anterior, posterior, medial and lateral surfaces of the femur

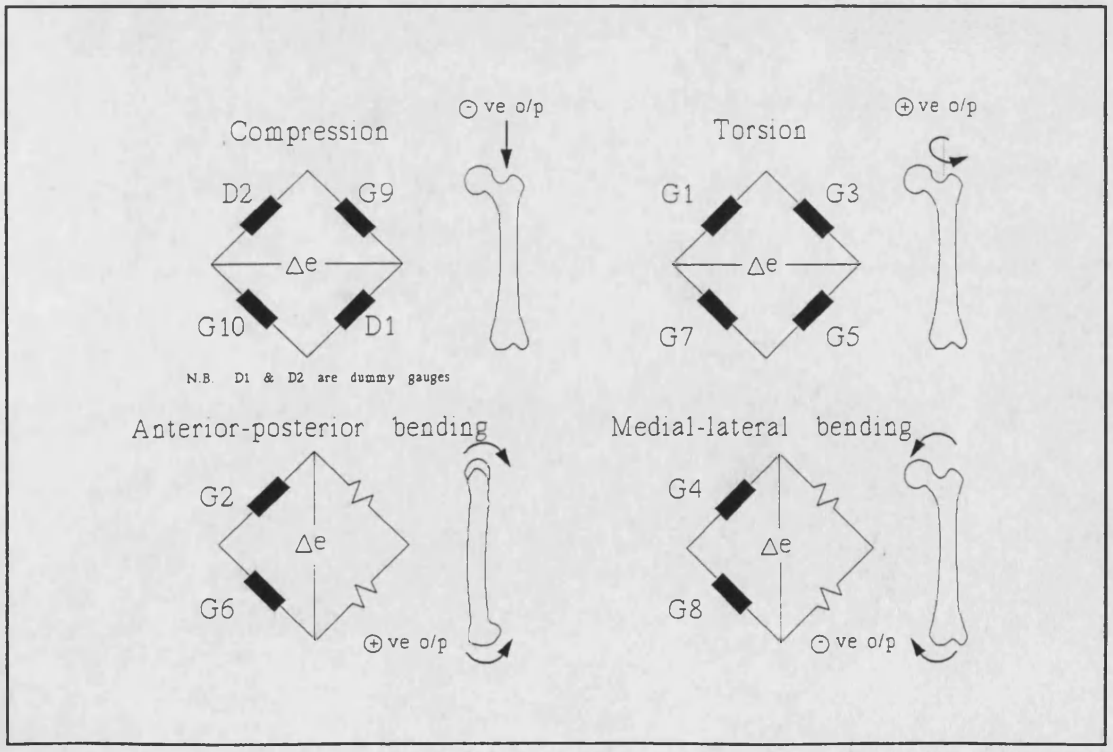

Figure 6-6 Wheatstone bridge circuits for the strain gauges. Δe=output

Strain readings were taken from the bridge circuits using a data acquisition system (ADU with card MM740, module with strain and resistance measurement capacity, Mowlem Microsystems).

6.2.3 The test method

The following protocol was used in all tests on the composite femur and enabled stiffness and strain data to be generated. The tests were carried out with scaled down loads (body weight, W=10kg).

1. The strain gauges were zeroed.
2. The muscle loads were applied; abductors=200N (2W), iliotibial=100N (W).
3. The femur was loaded to a maximum of 270N (2.7W) at 2.54mm/min.
4. Six strain readings were taken at one second intervals at this maximum load.
5. The femur was unloaded and the muscle loads removed.

Six tests, as above, were completed at four minute intervals. The four minute break allowed for stress relaxation due to the time-dependent behaviour of the composite bone as recommended by Cristofolini *et al.* (1996). This produced six load-deflection readings where the load was that applied by the crosshead and the deflection was the extension of the crosshead in the vertical direction. Thirty six strain readings were recorded in total. The mean and standard deviations of each quantity were determined.

6.2.4 Whole femur tests

The test procedure was evaluated for reproducibility. This involved:

1. Testing a whole femur in accordance with the above method.
2. Removing the femur entirely from the rig and its distal fixtures.
3. Remounting the femur distally.
4. Repeating steps 1-3 six times.

This enabled the error incurred during set-up to be established.

In order to determine the effects that the muscles and the correct orientation of the joint reaction force had on femoral loading it was decided to test the femur under five different loading configurations.

1. The femur alone with vertical joint reaction force (VF ONLY)
2. The femur plus the iliotibial force with vertical joint reaction force (ITB VF)

3. The femur plus the abductor force with vertical joint reaction force (ABD VF)
4. The femur with both the iliotibial and abductor forces with vertical joint reaction force (FULL MUSCLES VF)
5. The femur with both the iliotibial and abductor forces with the joint reaction force acting at 21° to the hip knee axis in the medio-lateral plane and at 12° in the antero-posterior plane i.e. full single legged stance (FULL SLS)

In each case, the femur was tested according to the stated protocol.

A further two composite femora were strain gauged as described in section 6.2.2. These two composite bones were analysed during the full single legged stance set-up, with strain and load-deflection characteristics recorded for each. This allowed the properties of three bones to be compared and inter-bone variability to be examined.

Finally, the strain gauged bones were calibrated in isolated loading modes in order to relate the recorded strain with the moments applied. This was completed using the isolated bending and torsion rigs described in chapter 4.

6.3 RESULTS AND DISCUSSION

6.3.1 Test set-up error

The load-deflection data for each test on bone 1 during full SLS was plotted and a linear regression used to determine the slope between 50N and the maximum load. Some settling of the bone was seen prior to 50N being reached. The correlation coefficient was greater than 0.996 in each case. The average stiffness and standard deviation for each run was determined and the results of the six tests are plotted in figure 6.7. The average stiffness of the six tests is 1163.9±41.0N/mm, a coefficient of variance (CoV) of 3.5%. This shows very good stiffness reproducibility in the set-up procedure.

The average strains and standard deviations for the six runs are shown in figure 6.8. No compressive strains were recorded due to damage to one of the gauges. The greatest

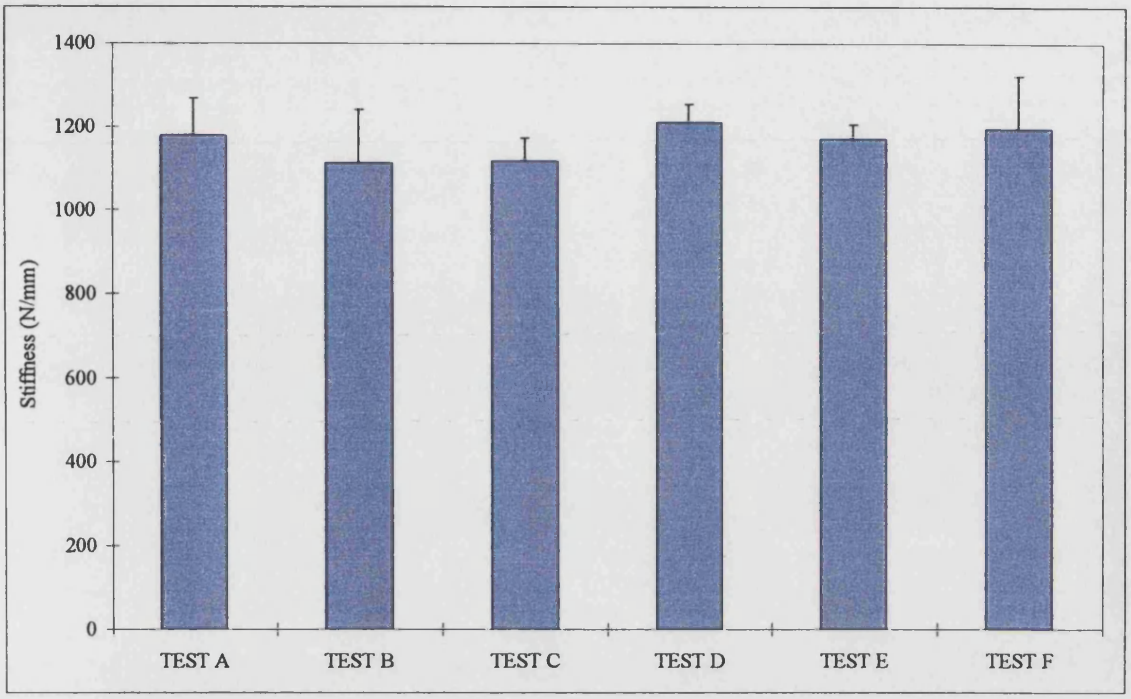

Figure 6-7 Stiffness variability (±standard deviations) with set-up in full SLS using bone 1

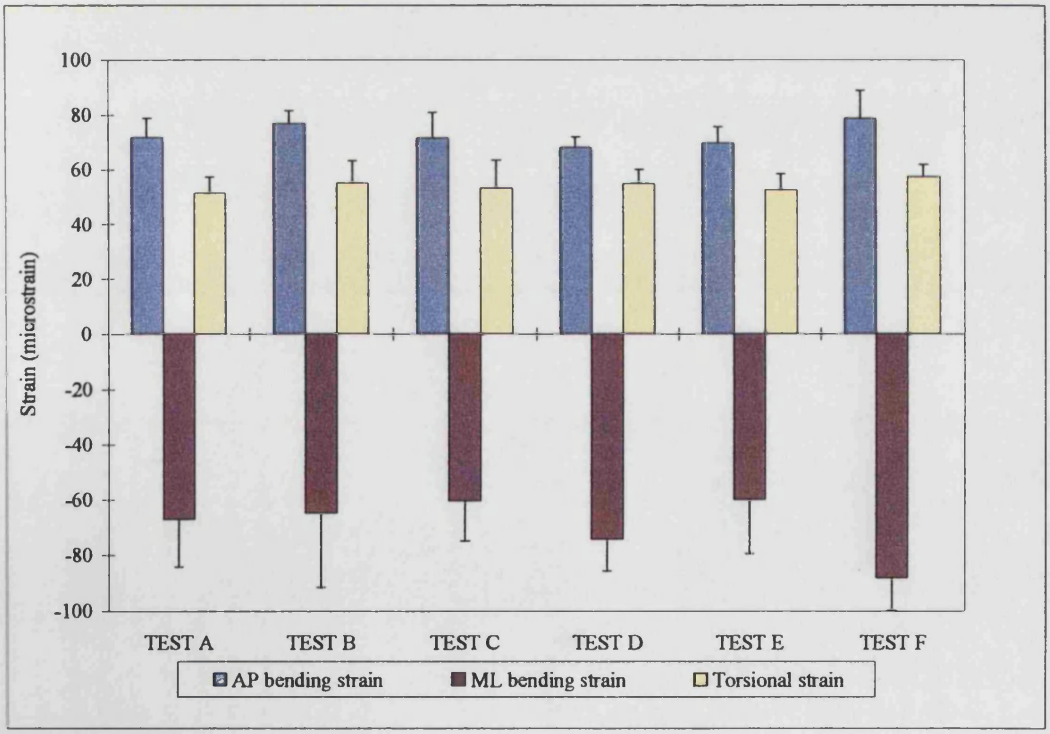

Figure 6-8 Strain variability (±standard deviations) with set-up in full SLS using bone 1

variance occurs in the medio-lateral strain, both in each test and between set-up procedures (CoV=15.3%). However, the results were all of the same order. The reproducibility between the AP bending and torsional strains is very good with little variance (CoV=5.8% and 3.9% respectively). These results show the set-up procedure gives reproducible stiffness and strain measurements.

6.3.2 Comparison of loading configurations

For each different loading configuration six load-deflection curves were plotted. A linear regression was used to determine the slope of each between 50N and the maximum load and the average stiffness was calculated. The correlation coefficients were greater than 0.993 for all configurations but for the abductor only set-up (ABD VF: R^2=0.953). The stiffness and standard deviation for each configuration is shown in figure 6.9.

The configuration with just the iliotibial force is the least stiff (518.4±4.8N/mm). This was expected as the resultant downward acting force of the tract acts to increase the bone deflection. The loading configuration found to be the most stiff was that with both muscle forces represented but where the joint reaction force was applied vertically (1317.7±54.3N/mm). The angled joint reaction force produces a less stiff construct.

The equivalent strains experienced by the femoral shaft for each loading configuration are shown in figure 6.10. The most significant changes in strain are those in the medio-lateral direction. With the iliotibial force acting alone, medio-lateral bending has the lowest value (-67.1με). The greatest value is seen when only the abductors are modeled (-785.1με). These results tend to support the argument that a force representing the 'tension band effect' of the iliotibial band is essential to reduce unnatural bending of the femur during *in vitro* tests. The full SLS model with the angled joint reaction force also reduces medio-lateral bending when compared with the full model where the joint reaction force is applied vertically (-93.5 με cf. -165.8με). This is because the angled force component in the frontal plane opposes deflection in the medio-lateral plane.

Antero-posterior bending strains are greatest when the angled joint reaction force is used which acts to increase the AP curvature of the femur. The full SLS model also increases torsion of the femoral shaft. However, although the AP force component acts

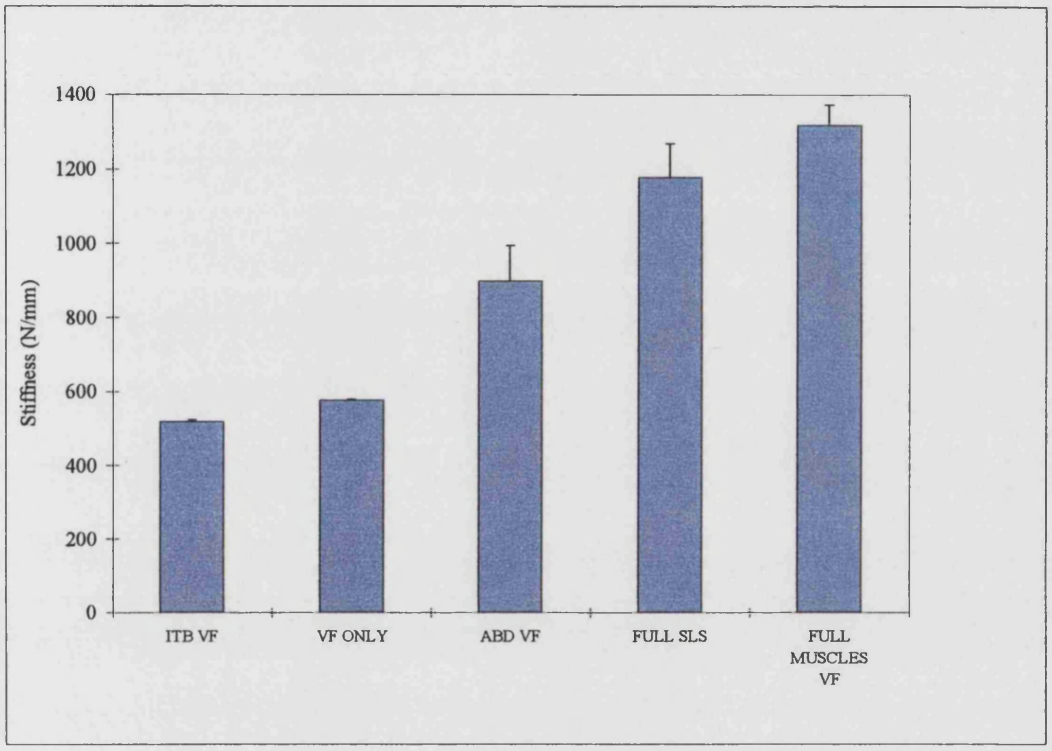

Figure 6-9 A comparison of the loading configuration stiffnesses (±standard deviations)

ITB VF- iliotibial band only with joint reaction force applied vertically; **VF ONLY**- vertical joint reaction force only-no muscles; **ABD VF**- abductor muscles only with joint reaction force applied vertically; **FULL MUSCLES VF**- both the iliotibial and abductors with a vertical joint reaction force; **FULL SLS**- both the iliotibial and abductors with the joint reaction force angled at 21° in the ML plane and 12° in the AP plane

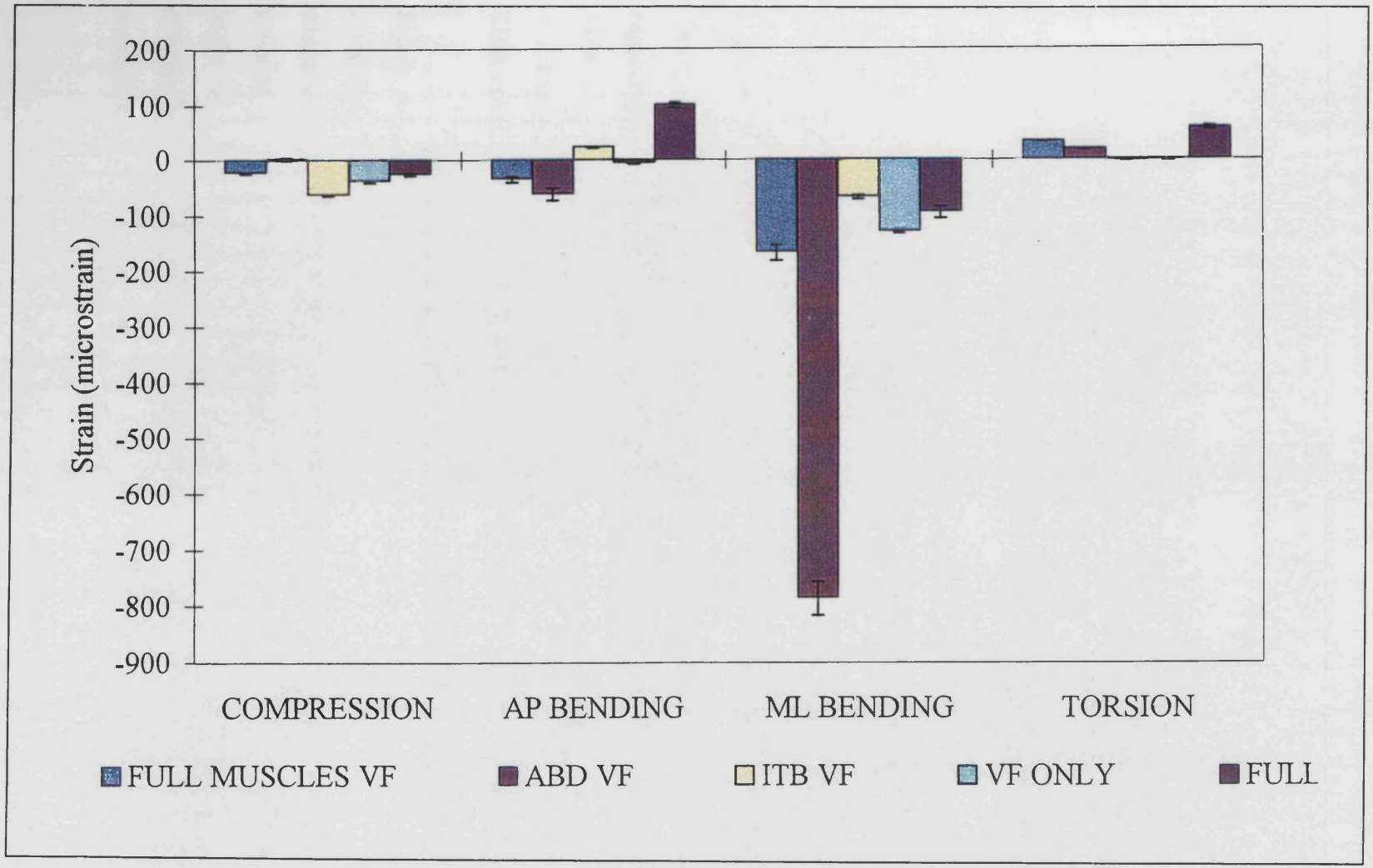

Figure 6-10 A comparison of the loading configuration strains (±standard deviations)

posteriorly and should cause a clockwise rotation of the shaft, a positive anti-clockwise strain is seen. This is thought to be because a cup is used to apply the joint reaction force instead of a point load. However torsion occurs in both directions *in vivo* and the magnitude measured is consistent with the work of Brown *et al.* (1982) and Schneider *et al.* (1990) who both recorded a significant degree of torsion acting on the femoral shaft using instrumented trauma devices. Torsion is often neglected in loading models. When compared with the magnitude of the other quantities the compressive strain is relatively small. It also appears erratic and probably falls within the 'noise band' of the data acquisition system. The neutral axis of bending is not coincident with the bone axis and so there will be a component of bending visible in the strain reading. This would also affect the results.

These tests support the use of the full muscle model to produce realistic strains during further testing.

6.3.3 Composite bone variability

The load-deflection curves for bone 2 and 3 in full SLS were plotted and a linear regression used to find the best fit slope through the points. The average slopes were 1144.7N/mm and 1115.1N/mm respectively. Figure 6.11 compares the stiffness of bones 1, 2 and 3. The stiffness repeatability between bones is good with an average value of 1146.1±31.8N/mm. The coefficient of variance is only 2.8%.

Figure 6.12 shows the femoral strains measured for each bone in full SLS. No compressive strain readings were taken from bone 1 due to a damaged gauge. The strains recorded are not as consistent between bones as the stiffness. However the variance in the strains in each bone were quite small. This suggests that the difference might be due to the local fibre make up of each bone rather than due to actual differences. Cristofolini *et al.* (1996) mentioned fibre variation as a cause of strain fluctuations in their work using composite femora.

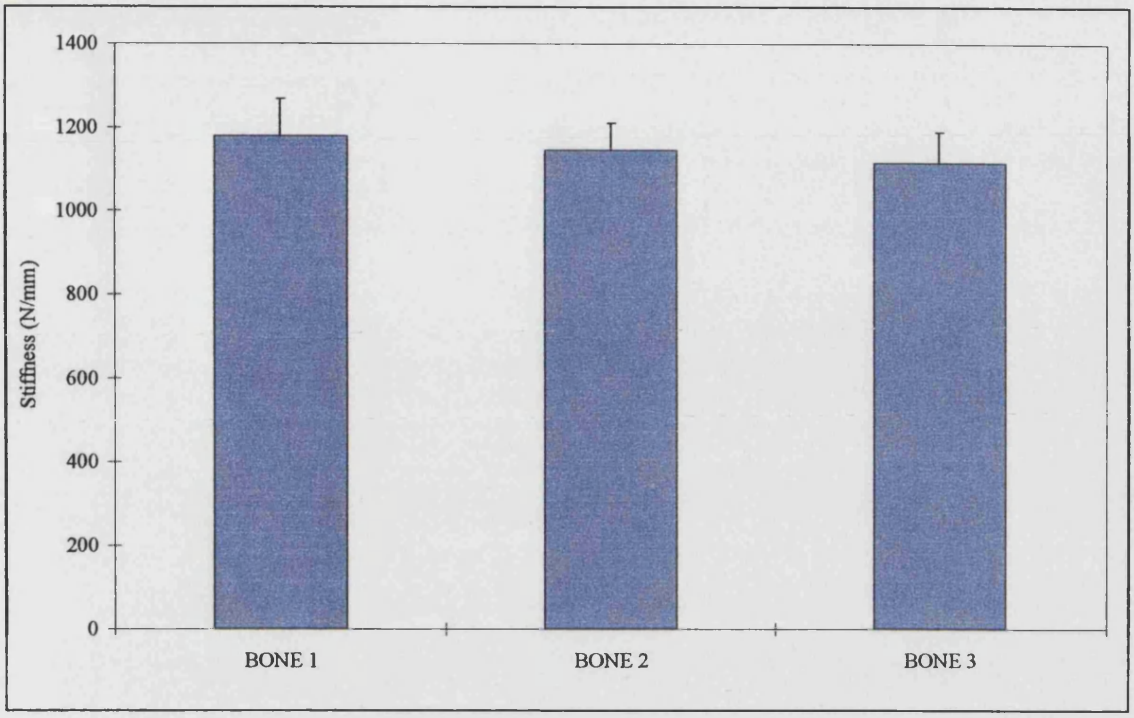

Figure 6-11 A comparison of the stiffness of bones 1, 2 and 3 in full SLS (±standard deviations)

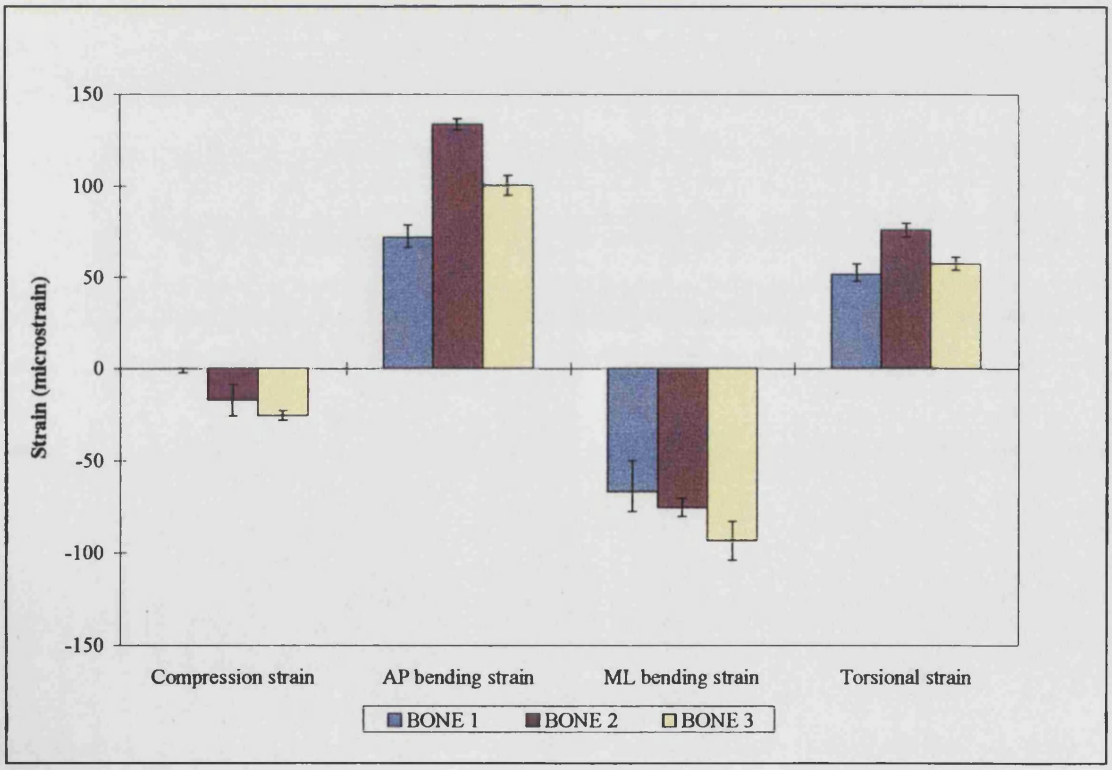

Figure 6-12 A comparison of the strains measured in bones 1, 2 and 3 in full SLS (±standard deviations)

6.3.4 Calibration of strains with applied moments

Table 6.1 shows the resulting strains measured in each bone when the given moment was applied using the isolated testing rigs described in chapter 4. Poor results were obtained when trying to calibrate the compressive strains with an applied load. The antero-posterior curvature of the femur made applying an isolated vertical load very difficult. For this reason and because the compressive strains recorded were so small, the compression results are not presented.

The calibration data was used to determine the moments that the femoral shaft was subjected to during the single legged stance tests with full muscles. The strains measured in the tests and the moments calculated from this data are given in table 6.2.

These moments are very small but this is due to the maximum load applied being only 270N (2.7W). This equates to a body weight of only 10kg. However, assuming that strain increases linearly with the application of load, we can scale up the results by a factor of 6.5 to represent a more realistic body weight (65kg). These results are given in table 6.3. Table 6.3 also includes the results of two studies that measured the loads acting on instrumented devices *in vivo*.

	Torsion	AP bending	ML bending
BONE 1 Moment (Nm)	7.26	11.08	11.08
Strain (με)	238.2±0.4	452.9±2.0	471.9±9.2
BONE 2 Moment (Nm)	6.79	11.08	11.08
Strain (με)	256.7±3.7	515.1±9.2	505.2±6.0
BONE 3 Moment (Nm)	7.08	11.08	11.08
Strain (με)	254.9±3.0	504.8±4.7	490.8±11.5

Table 6-1 Calibration data

The results of Schneider *et al.* (1990) were taken from an instrumented femoral intramedullary nail implanted in to a 73kg man. The results are taken from a chart which shows the peak load measured during single stance of the patient. Measurements were

taken from 80-200 days post operatively, hence the range of values given in table 6.3 (see figure 2.24). The study of Brown *et al.* (1982) shows the peak output from an instrumented hip nail during the unassisted walking of one patient (figure 6.13). In addition a study by Bergmann *et al.* (1993) used a telemeterised hip prostheses to measure forces with time during gait. The measurements used in the table were recorded at 30 months post operatively.

	Torsion	AP bending	ML bending
BONE 1 Moment (Nm)	1.6	1.8	-1.6
Strain (με)	51.3±5.8	71.7±7.0	-67.2±17.1
BONE 2 Moment (Nm)	2.0	2.9	-1.7
Strain (με)	75.9±3.7	133.5±3.2	-75.5±4.9
BONE 3 Moment (Nm)	1.6	2.2	-2.1
Strain (με)	57.4±3.5	100.2±5.3	-93.5±10.5

Table 6-2 Moments acting on the femoral shaft when load=270N (W=10kg) during full SLS

Despite the diversity between the studies there is remarkably good similarity in the results. They are generally of the same order. The agreement in the magnitude of the torsional moments acting on the shaft of the femur is particularly good and emphasizes the fact that this is a considerable force and should not be neglected.

6.4 SUMMARY

A loading rig was designed that simulated the forces acting on the femur during single legged stance. This included the effects of both the abductor muscles and the iliotibial band. Including both these forces was found to significantly affect the stiffness and strains in the femoral shaft. There was some variability between the stiffnesses and strains measured in the three bones. However, it must not be forgotten that this variability is probably considerably less than that found in cadaveric material (see section 2.2.2). Repeatability was found to be good between tests, with variance being greatest in the medio-lateral bending measurements. The gauge measurements were used to

determine the moments acting on the femur. These were compared with *in vivo* data from instrumented implants and there was found to be good agreement between results.

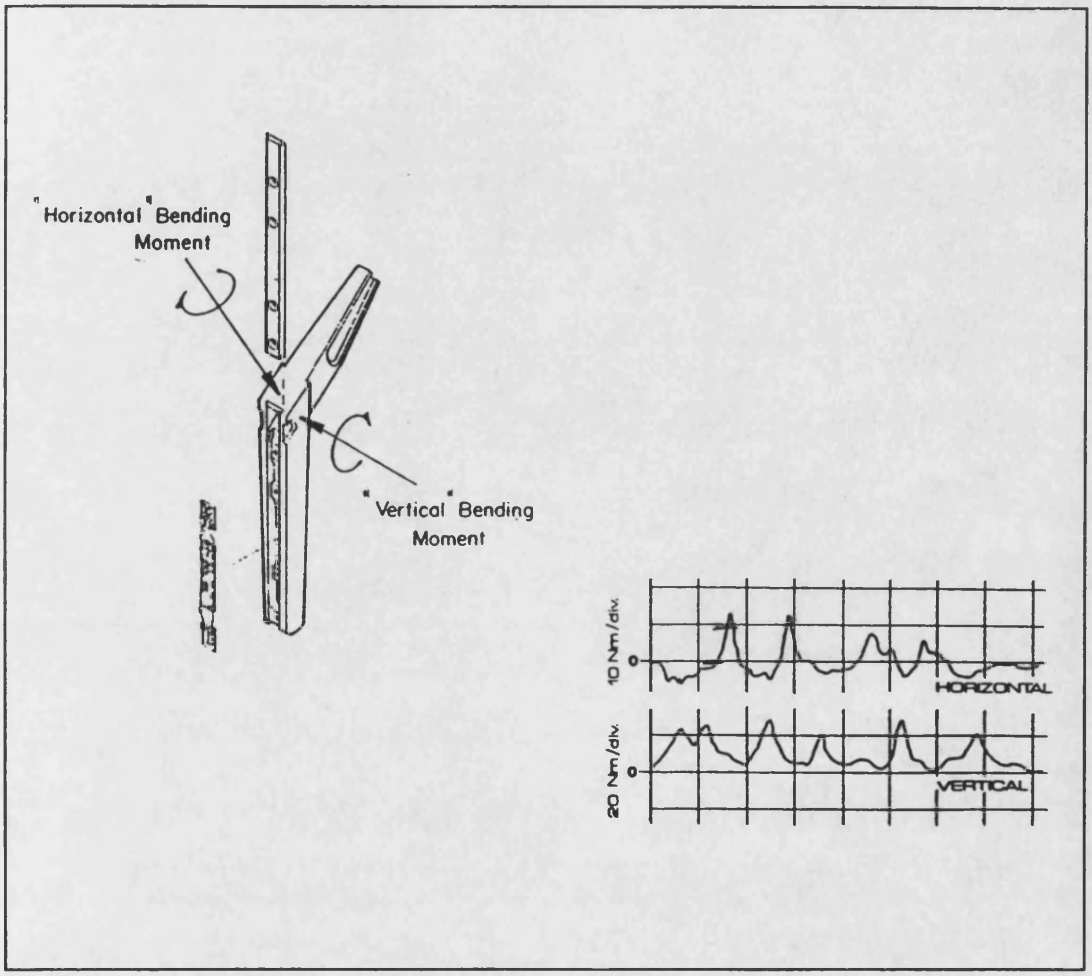

Figure 6-13 The instrumented hip nail of Brown *et al.* (1982) and the load-time output of a patient walking without external support.

	Torsion (Nm)	AP bending (Nm)	ML bending (Nm)
Bone 1	10.4	11.7	-10.4
Bone 2	13.0	18.9	-11.1
Bone 3	10.4	14.3	-13.7
Bergmann *et al.* (1993)	Max=-13	-	Max=-32.5
Schneider *et al.* (1990)	Max=10	Range=2>35	Range=-10>-30
Brown *et al.* (1982)	Peak=-12	-	Peak=-25

Table 6-3 Moments on the femoral shaft when W=65kg during full SLS

CHAPTER 7

HEALING STUDY IN COMBINED LOADING

7.1 INTRODUCTION

The simulated healing study (chapter 5) and the combined loading of a femur during single legged stance (chapter 6) both produced interesting results. The simulated healing process allowed the changing load carrying role of the intramedullary nail to be examined. The reproduction of single legged stance showed that the femur is not only subjected to bending moments but a high degree of torsional loading as well. These two procedures were combined in the next stage of the study. Two nails were tested using the new methodology.

7.2 METHOD

7.2.1 Nail instrumentation

The healing study aimed to measure the proportion of the applied load carried by the nail and fractured femur. During the isolated healing study it was possible to theoretically calculate the load taken by the nail and femur. Due to the complex loading during simulated single legged stance it was not practical to do this. Strain gauges were therefore used to measure the deformation of the nail during the simulated healing process. The strain gauged nails were then calibrated in order to relate the measured deformations with the applied loads.

Two nails were strain gauged, the 12mm Russell-Taylor nail and the 10mm AO unreamed femoral nail (URFN). These two nails were chosen because:

1. They are made from different materials - one is stainless steel, the other titanium alloy
2. In isolated bending and torsional loading modes they have very different rigidities (chapter 4)

3. The manufacturers of unreamed titanium nails suggest that a 9/10mm titanium nail can be used instead of a larger diameter stainless steel nail e.g. 12mm diameter. By comparing these two nails using this methodology the differences, if any, between the two can be identified.
4. The geometry of the two nails allowed the strain gauges to be applied easily. They both had closed cross sections.

The nails were strain gauged in the same manner as the composite femora in chapter 6. However gauges were not applied to record compression due to the problems experienced earlier with this measurement in the composite femora - readings were erratic and calibration was difficult due to the curvature of the bone. Smaller strain gauges were also used because of the size of the nails. The axial gauges used to measure antero-posterior and medio-lateral bending (gauges G2, G4, G6, G8 in figure 6.5) were type WK 06 062AP 350. Two element 90° rosettes were used for torque measurement - type EA 06 062UV 350 (Measurements Group UK Ltd). The strain gauges were positioned at a distance of 220mm from the proximal end of the nail so that they would lie in the fracture gap once it had been created.

Once the strain gauges had been applied the nails were calibrated in isolated antero-posterior bending, medio-lateral bending and torsional loading according to the method used to test the nails in isolation (chapter 4). This allowed the applied moments to be related to the recorded strains.

7.2.2 Testing procedure

Using the standard surgical instrumentation and technique a standard Russell-Taylor nail (12x380mm), without strain gauges, was inserted in to composite bone 1. The femoral canal was reamed to a diameter of 13mm, 1mm greater than the implant, and the nail was locked with one oblique screw proximally and two transverse distal screws. This construct was tested in full single legged stance (SLS) mode, the joint reaction force applied at 21° in the medio-lateral plane and 12° in the antero-posterior plane. The construct was loaded to a maximum of 270N (body weight=10kg) according to the protocol laid down in chapter 6.2.3. The stiffness of the construct and the femoral

strains were recorded. The bone/nail construct was assumed to have the stiffness of a fully healed bone at this stage with the nail still in situ.

The nail was removed and an 80mm mid shaft fracture was created 200mm below the tip of the greater trochanter. This fracture could be grouped as type 32-C3.3 according to the AO fracture classification - an irregular complex fracture of the femoral shaft with extensive shattering greater than 5cm (Appendix A). The strain gauged Russell-Taylor nail was then inserted in to the fractured bone. The nail was inserted in to the distal bone fragment first and locked in position with the two transverse interlocking screws. The proximal nail was then inserted retrograde up in to the proximal bone fragment and locked in place. This prevented the strain gauges from being passed through the medullary canal which may have damaged them. The nail strain gauge wires were passed out through the fracture site and the bone/nail construct was tested in full single legged stance mode again. The stiffness of the construct was determined and strain readings were taken from both the femur and nail. The construct was assumed to have the stiffness of a recently fractured femur before healing begins.

Fracture healing was then simulated by successively layering glass fibre cloth with an epoxy resin across the fracture site. At each stage the stiffness of the construct was measured and strain readings were taken from the femur and the nail.

Only one 10mm AO URFN was available so this was inserted in to a fractured composite bone (bone 2) omitting the fully healed stage and thus avoiding strain gauge damage. The fracture was identical in size and location to that created in composite bone 1. Although in practice the nail should be inserted without reaming, the medullary canal was reamed to a diameter of 10mm to accommodate the nail. This may mean that the unreamed nail had a closer fit with the bone than it would do in practice. The proximal bone fragment was reamed to a diameter of 12mm to allow for the retrograde insertion of the nail. The femur is often reamed proximally in practice to accommodate the larger proximal portion of the unreamed nail. The nail was locked distally with two transverse screws and proximally with one transverse screw in the more distal hole.

The bone/nail construct was then tested in full single legged stance. The stiffness of the construct was found and strain readings from both the femur and nail were taken. Fracture healing was then simulated and readings taken after the application of each layer.

The 12mm AO URFN was inserted in to an intact femur. This was tested in full single legged stance. The stiffness of this construct was used in calculations where a value for the fully healed 10mm construct was required. This was a reasonable assumption as the nails have similar rigidities in isolation.

7.3 RESULTS AND DISCUSSION

7.3.1 Stiffness and strain data

Figure 7.1 shows the load-deflection data recorded when testing the Russell-Taylor nail in a fractured femur during SLS. It is characteristic of all the data recorded in implanted femora during SLS and shows the complex nature of loading a construct. The graph can be divided in to three regions:

1. 0-20N Settling of the construct within the rig.
2. 20-150N Initial elastic loading of the construct
3. >150N A change in the line gradient, although it remains linear, probably as a result of the nail deflecting and changing the area over which it comes in to contact with the bone. The reduction in stiffness implies a decoupling of the nail and bone. It is thought that the gradient will continually change as greater loads are applied and the nail continues to deflect.

It was decided that the slope of the line between 150N and the maximum load should be used to characterise the changing stiffness of the healing construct, thus avoiding the effects of the changing slope at lower loads. As can be seen in figure 7.1, inter test repeatability was always good.

Figures 7.2 and 7.3 show the changing stiffness of each of the constructs with the application of the glass fibre layers. Only one line is shown for each stage but the

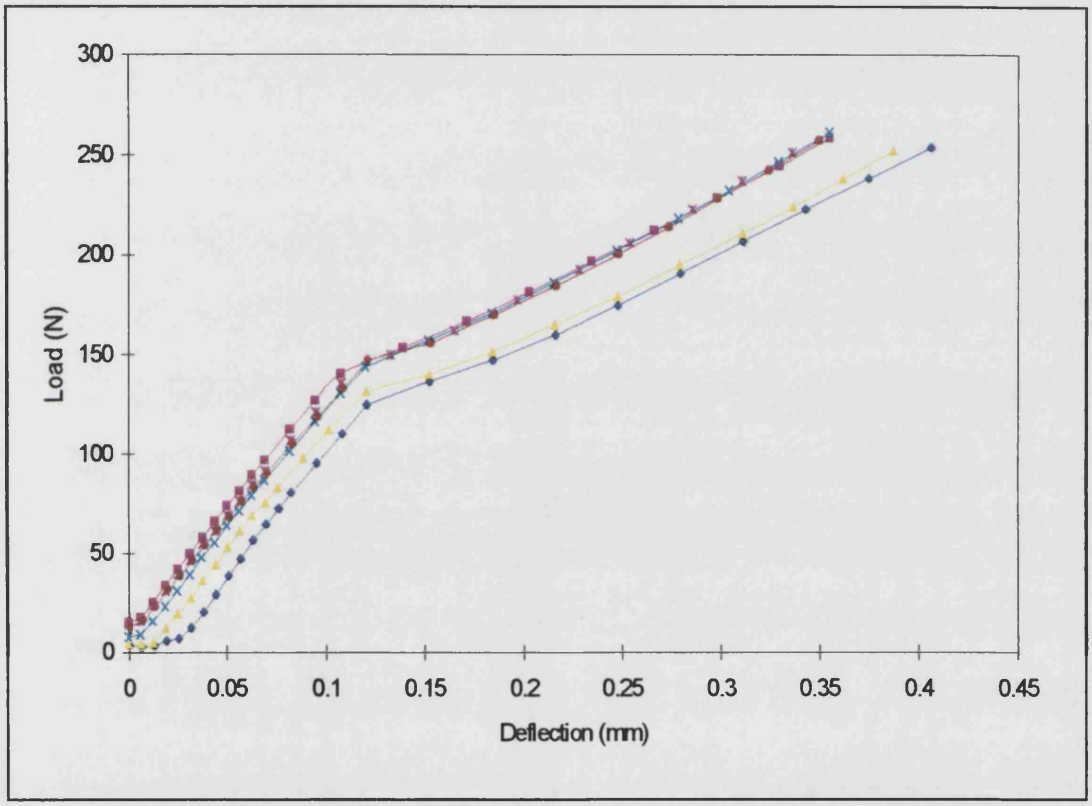

Figure 7-1 Load-deflection data for the Russell-Taylor construct when healing=0%. The results of six tests.

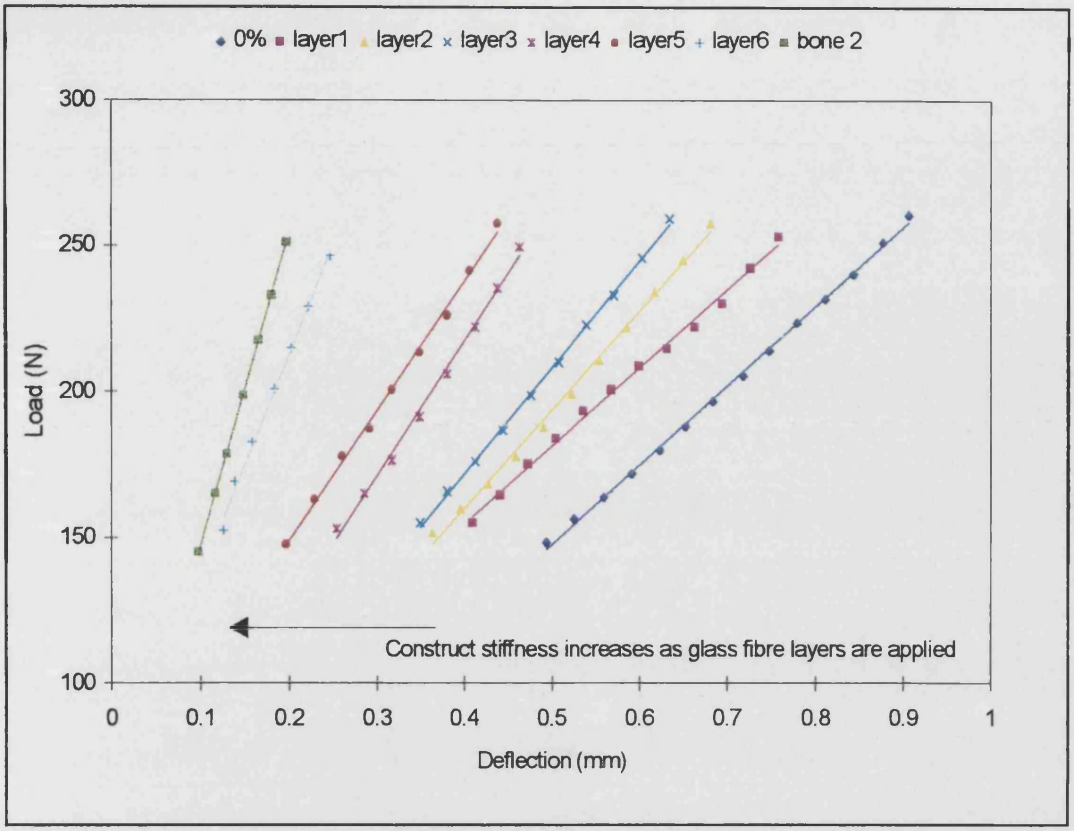

Figure 7-2 The changing stiffness of the 10mm AO URFN construct during the healing simulation N.B. The lines have been offset for clarity

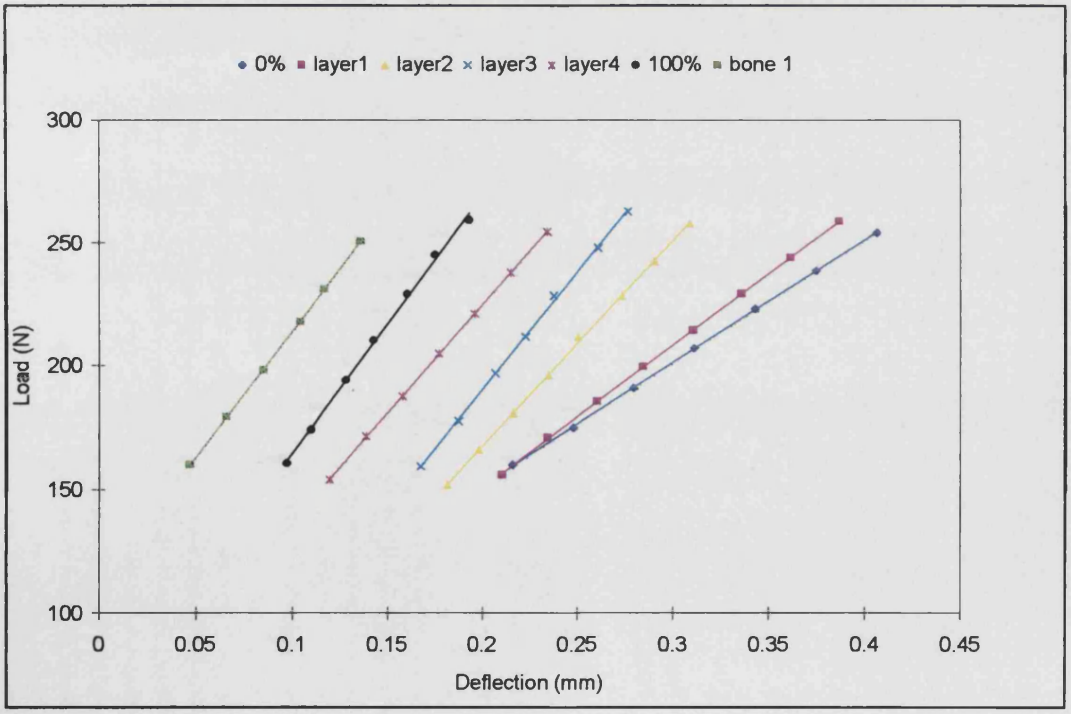

Figure 7-3 The changing stiffness of the 12mm RT construct during healing

	Stiffness ± standard deviation (N/mm)	
	10mm AO URFN	**12mm Russell-Taylor nail**
Bone only	1144.7±65.3	1178.0±89.6
100% healed	1178.6±9.9*	1087.6±37.7
0% healed	234.7±32.1	593.6±40.2

Table 7-1 Summary of the average construct stiffnesses during full SLS. * This is the stiffness of the 12mm AO URFN fully healed construct as the 10mm AO URFN was not tested when fully healed.

repeatability between tests was good. Although the two charts look similar, it must be highlighted that the full scale deflection on the axis of figure 7.2, the 10mm AO unreamed construct is about twice that of figure 7.3.

Table 7.1 compares the rigidity of the two constructs at the non and fully healed stages. At the fully healed stage (100%) it can be seen that the stiffness of the construct is not too different from that of the bone alone. However, on creation of a fracture the stiffness is dramatically reduced. The fractured 12mm Russell-Taylor construct is about half as stiff as the fully healed construct whilst the stiffness of the 10mm AO URFN construct is reduced to a fifth. The difference in the stiffness of the two non-healed constructs is considerable. The 10mm AO URFN construct is about two and a half times less stiff than the Russell-Taylor construct.

The extremely low stiffness of the unreamed nail construct when fractured may have implications for the healing process. Several papers have recently highlighted slow union in fractures treated with unreamed small diameter nails compared to standard reamed nails (Anglen and Blue, 1995; Haddad *et al.*, 1996; Blachut *et al.*, 1997; Giannoudis *et al.*, 1997). The low stiffness of the non-healed construct may lead to excessive displacements at the fracture site thus preventing the formation of cartilaginous tissue (Perren, 1979). Kenwright and Goodship (1989) reported that a 2mm axial displacement (applied cyclically using an actuator attached to an external fixator) was detrimental

in terms of mineralisation and increasing fracture stiffness compared with a 0.5mm displacement and to a rigidly fixed fracture.

Figures 7.4 and 7.5 show the femoral strains measured after the application of each glass fibre layer for the 10mm AO URFN and 12mm Russell-Taylor constructs respectively. Each point represents the average strain measured at 270N from the six tests completed at each stage. The tests were repeatable as shown by the small standard deviations at each point. The same is true of the strains measured in the nails during simulated healing (figures 7.6 and 7.7).

The data shows a distinctive trend. In the non-healed state low strains were measured in both femora. This is because there is no contact between the fractured bone ends and the majority of the load will be transferred via the nail. High strains were measured in the nails at this point.

As the stiffness of the femur was increased during the healing simulation, higher strains were measured in the femora as can be seen in figures 7.4 and 7.5 . This resulted in the strains measured in the nails becoming lower (figure 7.6 and 7.7).

When the constructs reached the fully healed stage the strains measured in the femora were mostly at a maximum and close to the values measured in the bones prior to implantation. In contrast, strains measured in both nails were generally at a minimum.

There are irregularities seen in the trends suggested by these graphs, for example:

1) In both nails the direction of the medio-lateral strain changes during healing. This is the result of the nail deflecting and producing a medial displacement rather than a lateral displacement as occurs naturally in the femur when body weight is applied.

2) When the AO URFN construct stiffness reaches approximately 425N/mm there is a drop in the strain measured in the femur (figure 7.4) and a subsequent increase in the strain measured in the nail (figure 7.6). A similar effect occurs in the Russell-Taylor construct when the construct stiffness reaches 950N/mm.

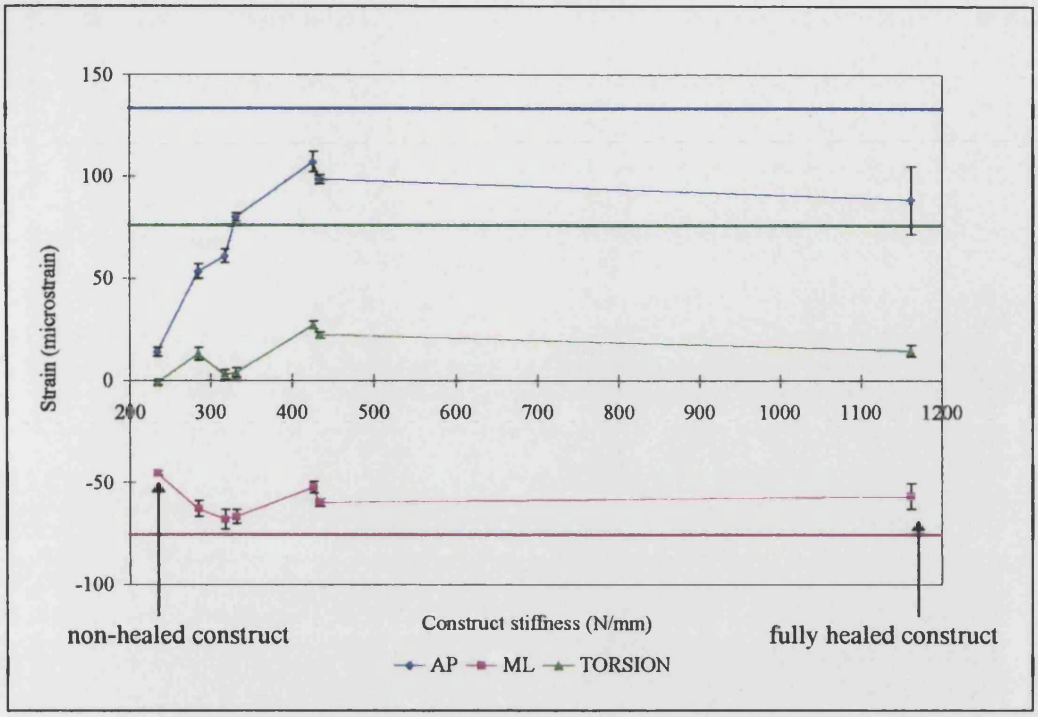

Figure 7-4 Strains measured in the femoral shaft with the 10mm AO URFN at each stage of the healing simulation (± standard deviations). The horizontal lines show the strains measured in the intact femur (bone 2) before implantation.

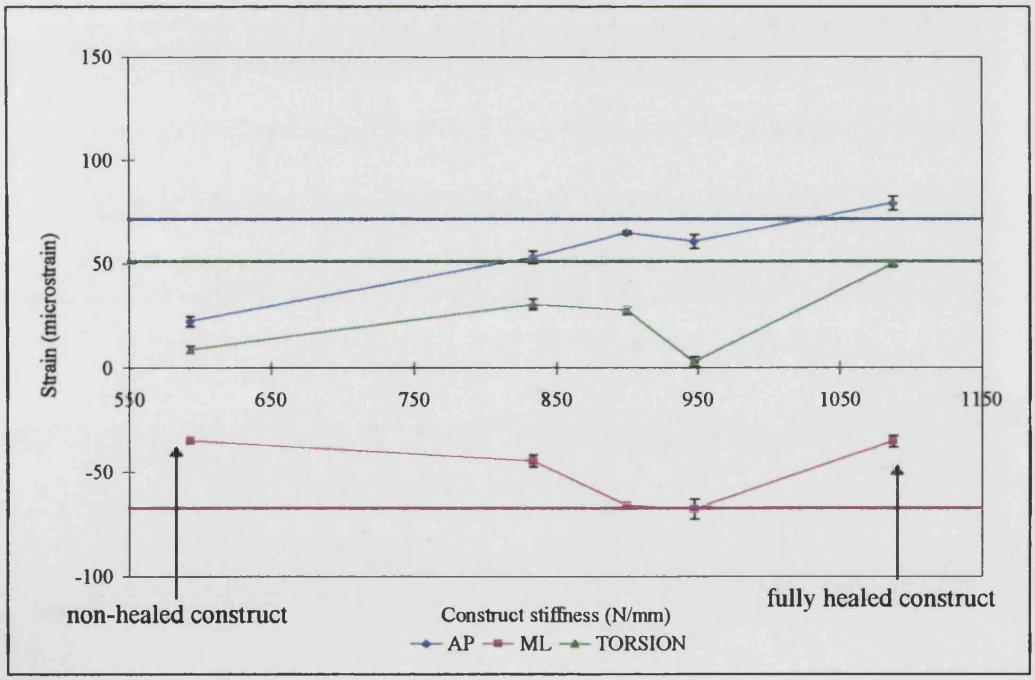

Figure 7-5 Strains measured in the femoral shaft with the 12mm RT at each stage of the healing simulation (± standard deviations). The horizontal lines show the strains measured in the intact femur (bone 1) before implantation.

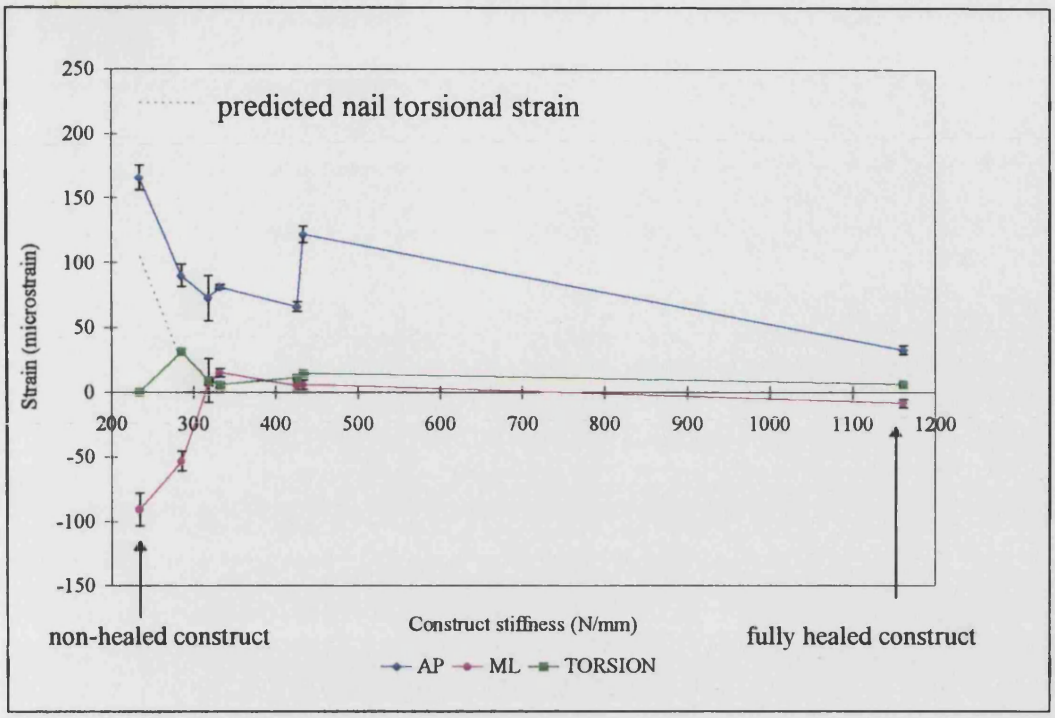

Figure 7-6 The nail strains measured at each stage of the healing simulation (± standard deviations) - 10mm AO URFN

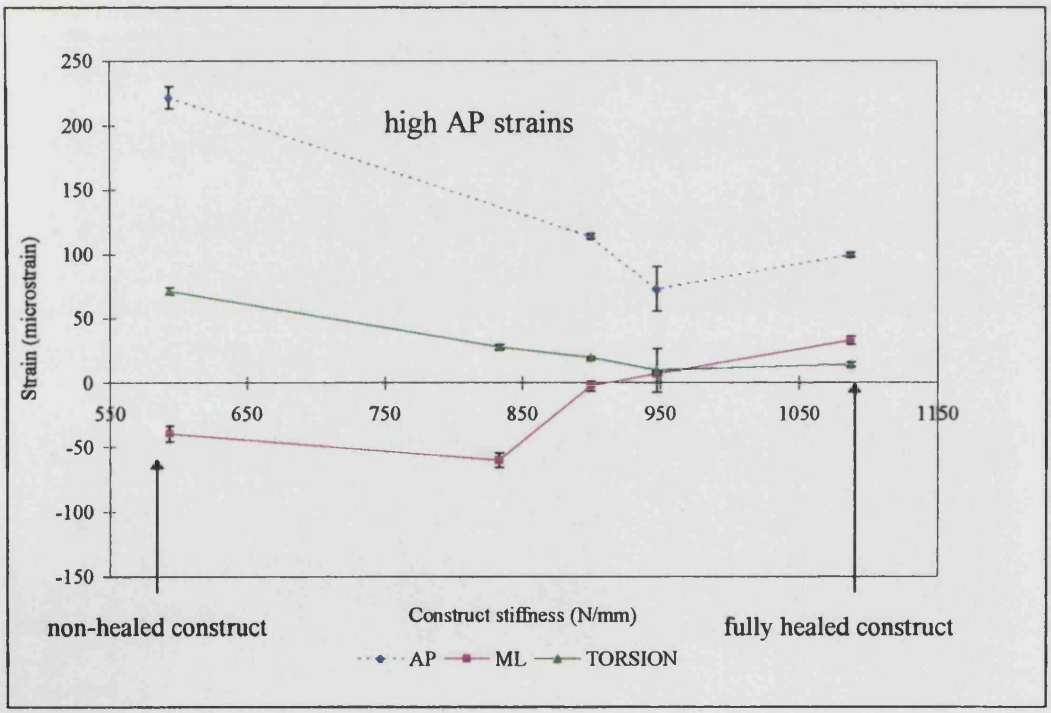

Figure 7-7 The nail strains measured at each stage of the healing simulation (± standard deviations) - 12mm RT

These irregularities are not common to all of the strains measured, they may occur in bending but not in torsion, and are difficult to explain. It is thought that they are the result of the two construct components deflecting relative to each other and changing the points at which they come in to contact. This leads to different loading conditions as the fracture stiffness increases causing localised strains at the fracture gap which may not necessarily be in the same direction as those in the rest of the nail.

It was thought that there may be two instances where the strain readings are misleading. Figure 7.6 shows that when the construct was non-healed there was no torsional strain measured in the 10mm AO URFN. It is assumed that this point is incorrect. If the line is extrapolated back from the second data point, the strain reading would be approximately 100με. This would be more consistent with the fact that the nails should take a large proportion of the load when the bone is fractured. The predicted torsional strain is indicated with a dashed line in figure 7.6 and in subsequent figures.

The antero-posterior strains measured in the Russell-Taylor nail were also higher than those expected. These strains are approximately twice as large as those measured in the intact bones (figure 7.7). However, the antero-posterior strains measured in the nail during the healing simulation were all of a relative magnitude. On inspection, the Russell-Taylor nail was found to impinge on the anterior glass fibre wall of the composite femur. Calculations showed that this contact may have lead to localised bending at the fracture site leading to the high strains measured (Appendix E). The anterior posterior data measured in the Russell-Taylor nail is shown by a dashed line in figure 7.7 and in subsequent figures.

7.3.2 Healing curves

Data from the nail calibration was used to convert the measured strains in to the moments acting on the nail during the healing simulation (table 7.2). The moments acting on the femur during healing were determined in a similar manner using the calibration data given previously in table 6.1. The strains, and therefore the calculated moments, from these tests are representative of those acting on the femur when body weight is 10kg. The calculated moments were scaled up by a factor of 6.5 to show the

magnitude of the moments acting on the nails and femora when body weight=65kg, a more realistic value.

		Torsion	AP bending	ML bending
12mm RT nail	Moment (Nm)	8.56	11.08	11.08
	Strain (με)	344.9±3.7	677.8±11.4	643.2±13.0
10mm AO URFN	Moment (Nm)	3.12	7.92	7.92
	Strain (με)	203.5±1.5	739.9±2.6	742.0±2.2

Table 7-2 Nail calibration data

The 'percentage healing' of the construct was calculated and was used as a measure of the increasing stiffness of the construct as previously calculated in chapter 5.

$$\%\ healing = \frac{current\ construct\ rigidity - rigidity_{0\%}}{rigidity_{100\%} - rigidity_{0\%}}$$

The percentage moment carried by both nails and the femora was calculated as follows:

$$\%\ moment_{\ nail/femur} = \frac{current\ moment_{\ nail/femur}}{total\ moment}$$

where the total moment was taken to be that which the intact femur was subjected to during full single legged stance (shown by the horizontal lines in figures 7.4 and 7.5). Using this data, healing curves were plotted - %moment vs %healing. Figures 7.8 a and b show the healing curves for the 10mm AO URFN and the femur respectively. Figures 7.9 a and b show those of the 12mm Russell-Taylor nail and femur.

Figure 7.8b shows that the less rigid 10mm AO URFN produces a rapid uptake of load in the femur compared with the 12mm Russell-Taylor nail (figure 7.9b). This is the same trend as seen earlier during the healing study using isolated loads (chapter 5).

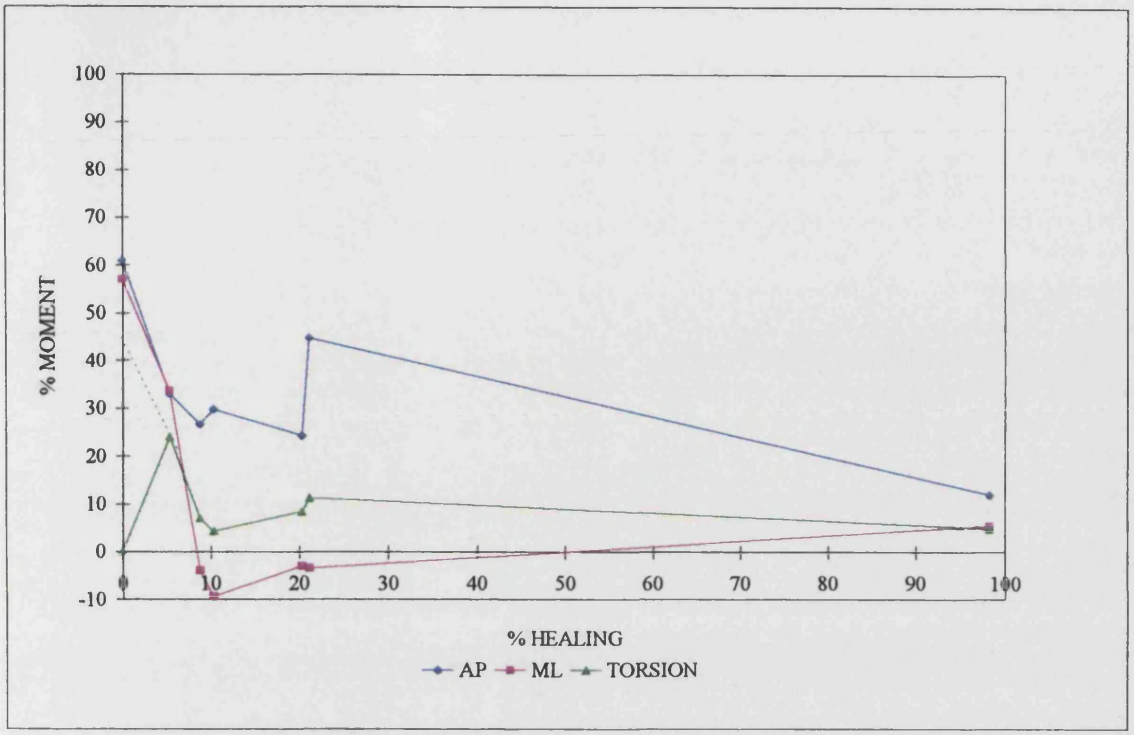

Figure 7-8A Healing curve for the 10mm AO URFN

% moment=100 when AP=18.9Nm; ML=-11.1Nm and TORSION=13.0Nm

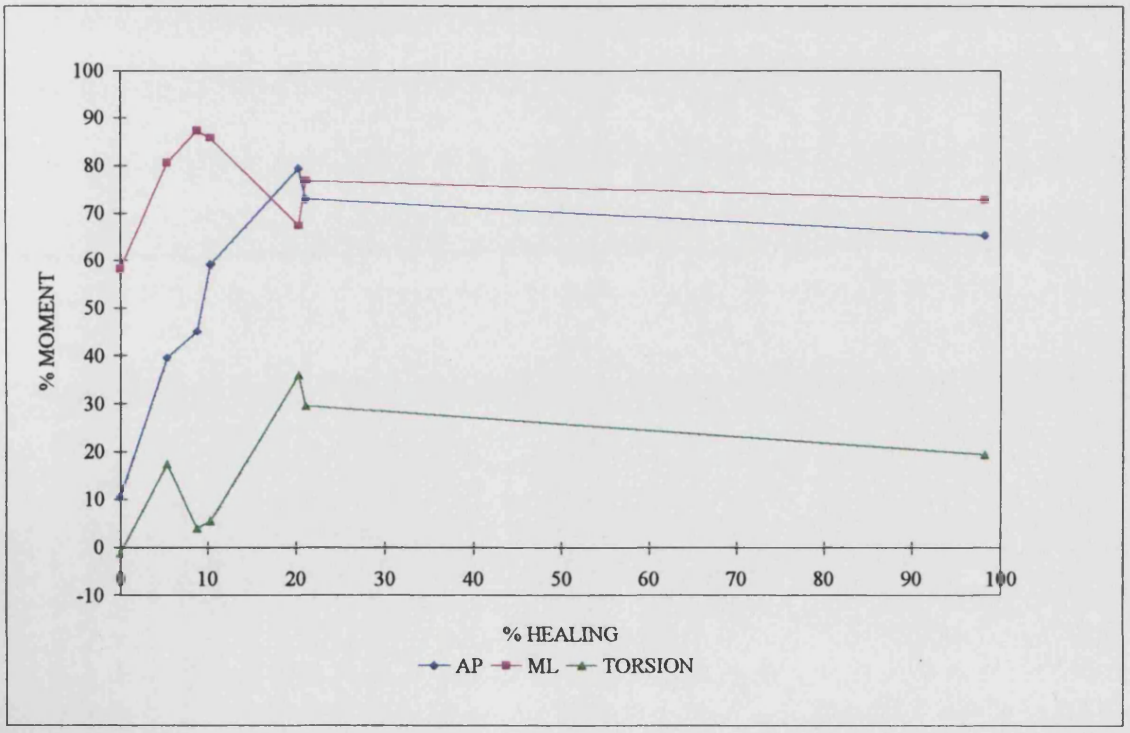

Figure 7-8B Healing curve for the femur implanted with the 10mm AO URFN

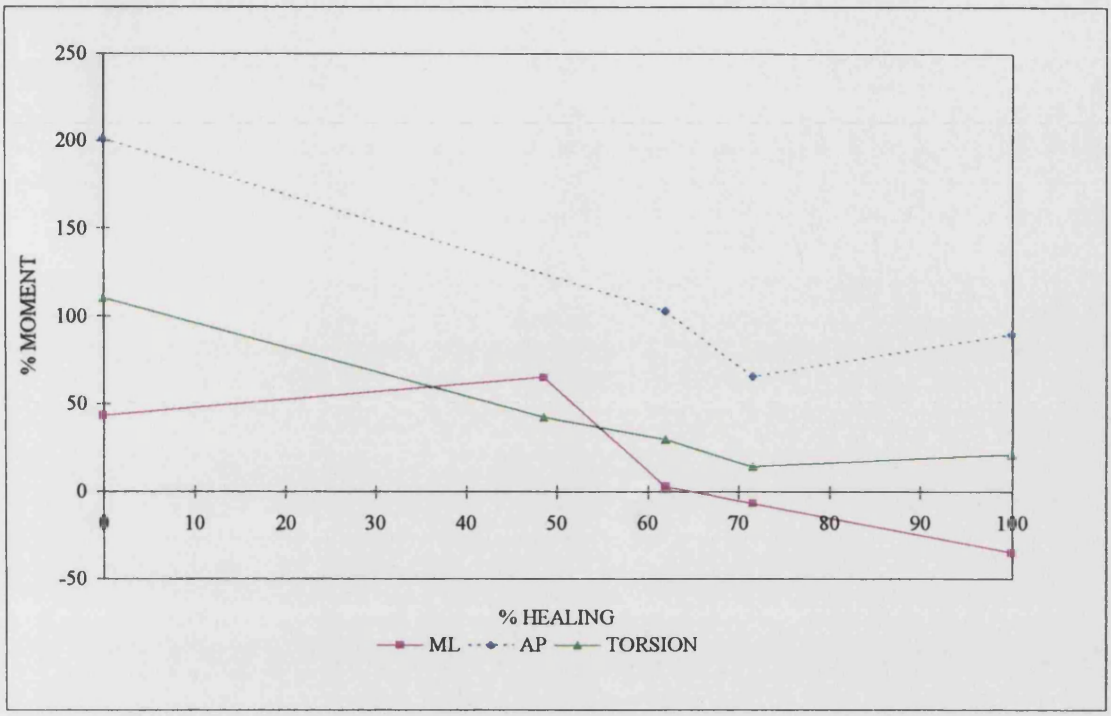

Figure 7-9A Healing curve for the 12mm Russell-Taylor nail

% moment=100 when AP=11.7Nm; ML=-10.4Nm and TORSION=10.4Nm

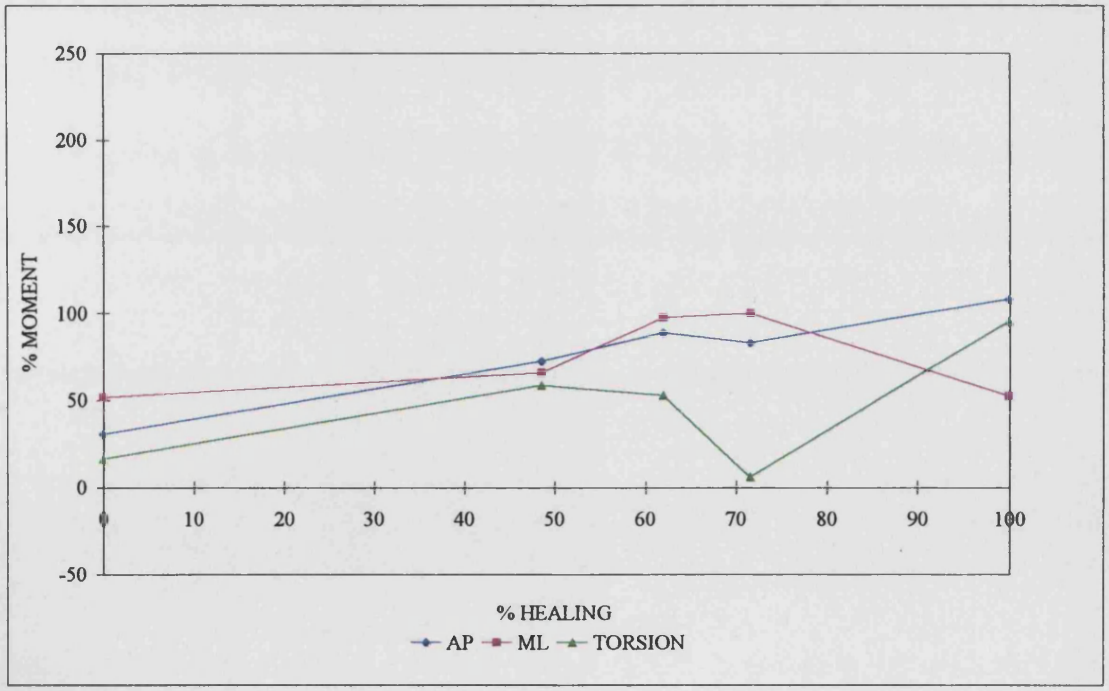

Figure 7-9B Healing curve for the femur implanted with the 12mm Russell-Taylor nail

In the isolated healing study the percentage load taken by the femur in the fractured state was zero but this was not found to be the case when the femoral loads were measured rather than calculated (figures 7.8b and 7.9b). However, it was not unexpected as the nails share load at all stages on account of the interlocking screws and nail/bone friction.

Both femora take approximately 50% of the total medio-lateral bending moment in the fractured state. This is roughly -6Nm in the AO femur and -5Nm in the Russell-Taylor femur. In antero-posterior bending the AO femur takes 10% of the bending moment (2Nm) and the Russell-Taylor femur takes 30% (4Nm). The deflections of the femora resulting from these moments are small (≈0.1mm) and similar regardless of the nail type they are implanted with.

In torsion the Russell-Taylor femur takes 16% (1.7Nm) of the total torsional moment while the AO femur supports no load at all when healing=0%. This would suggest that the 10mm AO unreamed nail is taking a high amount of torsional load at this point (figure 7.8a). This substantiates the claim that the reading from the 10mm AO URFN is incorrect when healing=0%. The predicted value shows the AO URFN to carry 45% of the total moment at this stage (figure 7.8a).

The femoral moments measured resulted in small displacements when healing=0%. However, the rapid load transfer to the femur produced with the AO URFN would lead to an increase in the displacements early during healing. In a stable fracture with contact between bone fragments, the increased loading of the femur seen with the AO unreamed nail early on in healing might lead to a shorter time to union. This was achieved by Kershaw *et al.* (1993) who induced micromovement from one week post-operatively in a group of patients with tibial fractures. However, it seems that the increased loading with the unreamed nail might be detrimental in cases other than the most stable fractures causing excessive micromovement and slow healing. Kenwright and Goodship (1989) showed a 2mm displacement to be detrimental to healing. Hence, the Russell-Taylor nail might be more appropriate for treatment of these less stable fractures.

The femoral strains were only measured on the proximal bone fragment in this study. Strains should be recorded on the distal bone fragment too, in order that the relative displacements of the bone fragments can be measured. It is difficult to determine the effects that nail deflection has on femoral displacement using only one strain measurement.

Using the predicted value for the torsional moment carried by the AO URFN when healing= 0%, the nail is found to support about 45% of the total moment (6Nm). If such a torsional load were exerted on the flexible AO unreamed nail it would lead to a 5° deflection (see table 4.3). The Russell-Taylor nail would deflect only 3° when the bone was completely fractured even though it is subjected to a greater proportion of the total load (100% cf. 45%). This is because it is a more rigid nail.

This torsional deflection is unlikely to cause mid shaft nail failure as failures clinically have been attributed to bending loads (Hutson *et al.*, 1995). It is possible that the torsional deflections could cause interlocking screw breakage due to fatigue (Whittle *et al.*, 1995). A torsional deflection will be applied and then reversed during walking. The AO unreamed nail has locking screws with an outside diameter of 4.9mm and a core diameter of 4.3mm, compared to 6.4mm and 4.9mm in the Russell-Taylor nail. This makes the AO URFN screws more susceptible to failure.

The large torsional deflections may also be responsible for nail fracture at the site of the distal interlocking screw holes. Stress concentration effects around the locking hole, combined with possible 'nicking' of the nail during screw insertion, would increase the probability of the nail fracturing before the screws. Nail fracture around the distal screw holes has been reported in the literature (Franklin *et al.*, 1988; Wu and Shih, 1992).

Both nails support approximately 50% of the total medio-lateral bending moments when the bone is fractured. This is equivalent to a 0.2mm deflection in the Russell-Taylor nail and 0.6mm in the AO unreamed nail. In antero-posterior bending the 10mm AO unreamed nail supports 60% (approximately 1mm deflection) of the total moment whilst

the Russell-Taylor nail supports 200%. These high moments in the Russell-Taylor nail have been attributed to localised bending of the nail at the fracture site.

It is possible that a cyclic displacement of 1mm in the antero-posterior direction could cause fatigue failure of the unreamed AO nail. Implant failures have been reported in the literature, particularly in unreamed nails (Blachut *et al.*, 1997; Krettek *et al.*, 1996). The failures generally occurred in patients who began weight bearing early, often against instruction. Clinically mid shaft nail failures have been attributed to bending loads (Hutson *et al.*, 1995). However, without the Russell-Taylor nail data for comparison, and without fatigue testing the nail at the measured loads, it is difficult to ascertain whether this antero-posterior displacement is the true cause of nail failure.

Throughout healing and at the fully healed stage, the femur implanted with the AO URFN is subjected to larger medio-lateral bending moments than the Russell-Taylor femur. It is possible that after the rapid transfer of load to the femur early in the healing process, the considerable medio-lateral bending of the shaft may produce slow union with the unreamed nail.

At the fully healed stage the femur implanted with the Russell-Taylor nail takes nearly 100% of the antero-posterior and torsional moments (figure 7.9b). Fifty percent of the medio-lateral moment is taken by the femur. There seems to be more stress protection seen with the 10mm unreamed nail (figure 7.8b). In the isolated healing simulation at the fully healed stage, the Russell-Taylor femur carried a lower proportion of the total load compared with the other femora - some 'stress protection' occurred in the femur due to the nails high rigidity. The lack of stress protection seen in the femur in this study might be due to the Russell-Taylor nail having a radius of curvature which is greater than the composite bone (AO=1500mm; RT=2300mm; femur=3400mm). This could improve its ability to share load through more bone/nail contact. Both nails support only a small percentage of the total load when the femur reaches its original stiffness. Nail removal would not appear to be a problem with either nail in this study.

When fully healed the Russell-Taylor nail supports only a small proportion of the total moments in the medio-lateral plane and in torsion. Again, the high antero-posterior moments measured in the Russell-Taylor nail are thought to be localised and specific to this case. If such a large moment were transferred to the femur on nail removal it would lead to refracture of the bone. As refractures with the Russell-Taylor nail are not common in the literature, this figure is assumed to be high.

7.4 SUMMARY

The strains and stiffnesses measured during these tests were of a significant magnitude and were repeatable.

The implanted femora had similar stiffnesses when fully healed, close to the magnitudes measured in the intact bones. When fractured, the 10mm AO unreamed construct was two and a half times less stiff than the Russell-Taylor construct.

The moments acting on the femora were measured using strain gauges, rather than calculated as in the isolated loading study. This showed that the bones did contribute to load carrying when the femur was fractured. The nail is a load sharing device at all times due to the interlocking screws and bone/nail contact along the medullary shaft.

When fractured, both of the femora took similar moments which resulted in small deflections. However, the rapid load uptake with the AO URFN would lead to higher femoral loads and hence deflections early during the healing process. This might lead to slow union with the AO nail unless the fracture was extremely stable preventing a large degree of micromovement. The femur implanted with the Russell-Taylor nail would be subjected to lower moments and smaller deflections.

The results from the healing simulation carried out in single legged stance were in agreement with the general trends seen in the isolated loading study. There was rapid load transfer between the nail and femur with the low rigidity AO URFN. Load transfer was more gradual with the Russell-Taylor nail.

There was a large difference in the moments measured in the nails in torsion. The moments produced about 1.5 times the torsional deflection in the AO unreamed nail as in the Russell-Taylor nail. This might lead to fatigue failure of the interlocking screws, particularly in the unreamed AO nail, or failure of the nails at the site of the locking screw holes.

Throughout healing, the femur implanted with the AO URFN was subjected to larger medio-lateral bending moments than that implanted with the Russell-Taylor nail. The resulting deflections might inhibit fracture healing resulting in slow union.

At the fully healed stage the nails were found to carry a small proportion of the total load while moments in the femora were close to their pre-implantation values (with the exception of the torsional moment in the femur implanted with the 10mm AO URFN). The problems associated with nail removal, and the subsequent transfer of load to the femur, were not thought to be as significant as thought after the isolated loading study.

CHAPTER 8

CLINICAL INTERPRETATION OF RESULTS

8.1 INTRODUCTION

The results obtained during the simulated healing process gave an insight in to the changing role of the nail and femur during the fracture healing process. However, the healing curves can be manipulated to allow a more clinical interpretation of the results. At present, the percentage of the total moment carried by the nails and femora are plotted against the increasing stiffness of the healing bone, %healing. In reality the increasing stiffness of a healing fracture is time dependent and will change from person to person and from case to case. The next chapter reviews the work carried out at the Oxford Orthopaedic Engineering Centre at the end of the 1980's in which the stiffness of tibial fractures treated with external fixation was measured. This is used to relate the load transfer between the nails and femora with time.

8.2 METHOD

8.2.1 Background

At present fracture healing is assessed by a surgeon. This is done with the aid of X-rays and by manipulating the fracture to sense the displacement at the fracture site, effectively determining the fracture stiffness. However, a more accurate method of determining the mechanical integrity of a healing fracture could be useful for deciding when a patient is capable of full weight bearing and when an implant should be removed in addition to assessing clinical union. Such information might also be used to predict cases of delayed or non-union earlier than with conventional methods.

A transducer was designed at the Oxford Orthopaedic Engineering Centre that was used to measure the displacement and hence the stiffness of a healing tibial fracture. The transducer was an isolated unit and could be clamped on to the external fixator of a

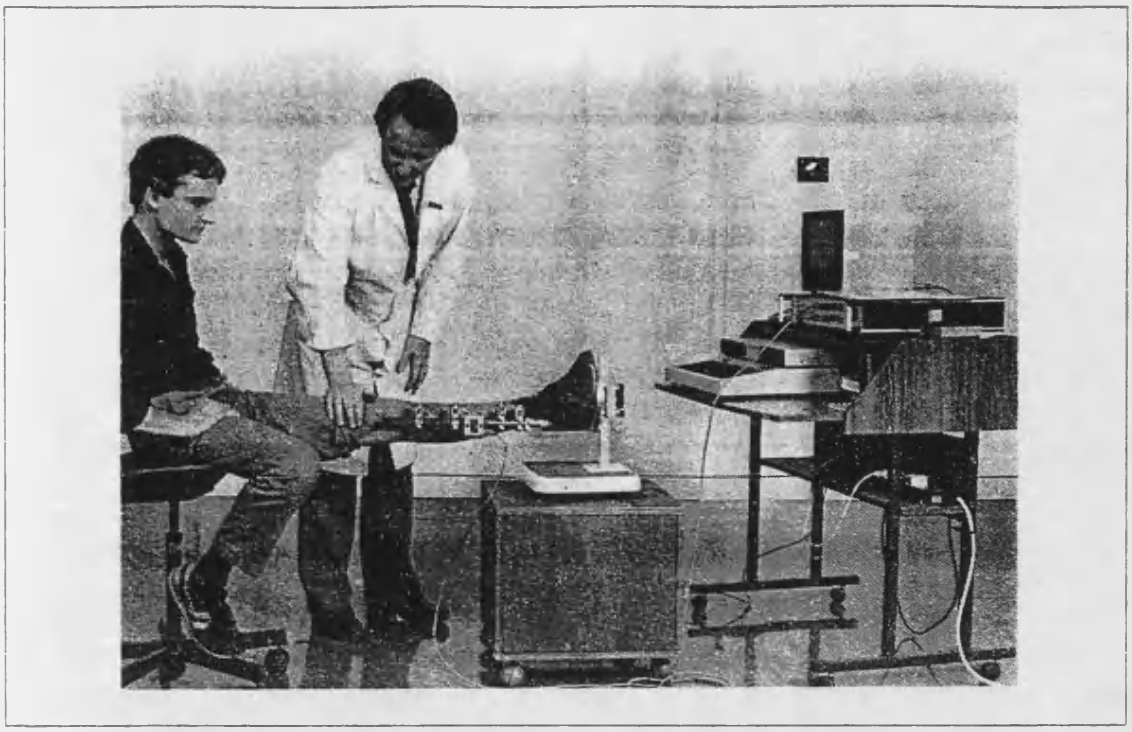

Figure 8-1 Patient undergoing a bending test. From Cunningham *et al.* (1987)

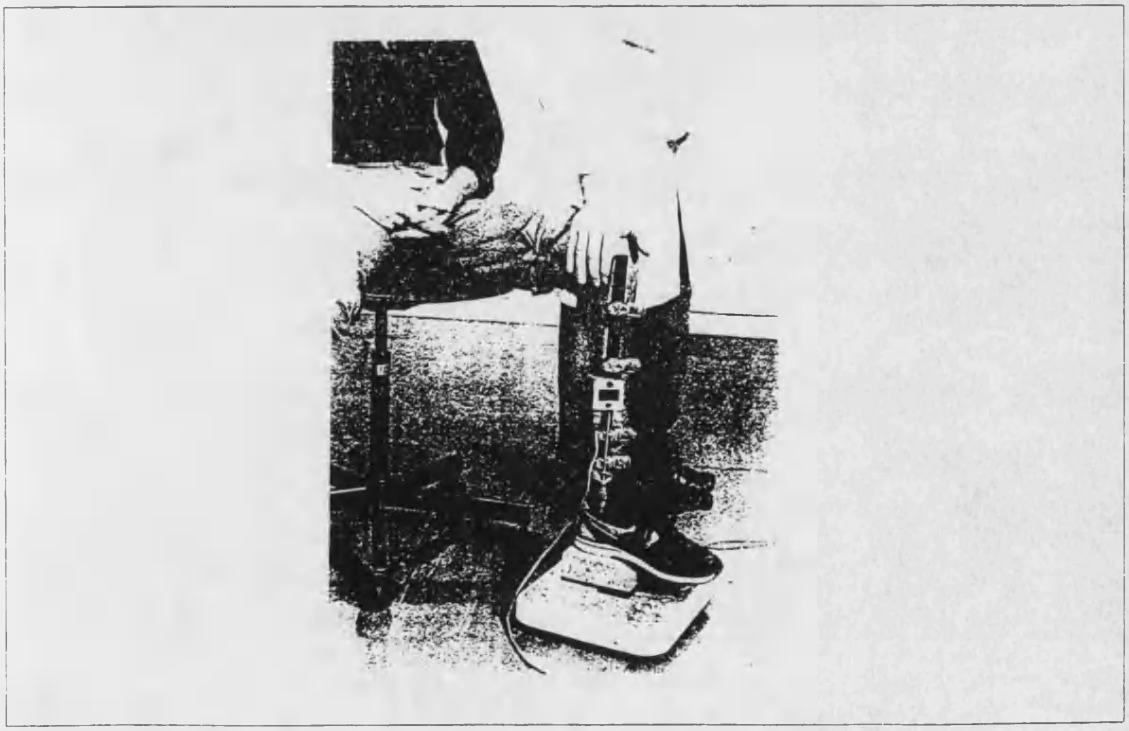

Figure 8-2 Patient undergoing an axial load test. From Cunningham *et al.* (1987)

patient without interfering with treatment. When a patient arrived for post-operative follow-up, the transducer was attached to the external fixator and two tests were carried out.

1. The patients leg was supported horizontally and a downward force exerted on the knee, applying a bending moment to the lower leg (figure 8.1). The heel was placed on a force platform that enabled the applied load to be measured.
2. The patients leg was allowed to rest vertically and a downward force exerted on the knee to compress the lower leg (figure 8.2). The foot was placed on a force platform to measure the applied load.

The transducer measured the overall deflection of the fractured bone and fixator as a whole. However, if the stiffness of the fixator was known, the force-deflection data enabled the axial and bending stiffness of the fracture to be calculated (Cunningham *et al.*, 1987). This methodology was used to monitor the increasing axial and bending stiffness of tibial fractures in a variety of cases (Evans *et al.*, 1988; Cunningham *et al.*, 1990). The measurement of fracture displacement was later refined. At follow-up the fixator column was removed and an electrogoniometer, placed between the fixator pins, was used to measure the fracture angulation in bending and hence the fracture stiffness (figure 2.18). Figures 8.3 and 8.4 show the change in bending stiffness with time for uneventful healing of tibial fractures. The stiffness generally increases with time but there are irregularities in the overall trend. At some points the fracture stiffness dropped below that of the last reading (figure 8.4 when time post injury=6 weeks). The increasing fracture stiffness shows the same erratic pattern as that seen in the combined healing study (chapter 7) - the strains measured in the nails and femora often dropped when they were expected to increase. Figure 8.5 depicts the data measured in a fracture where healing was slow and figure 8.6 for a delayed union.

Richardson *et al.* (1994) hypothesised that clinical union was achieved when the bending stiffness of the fracture in the antero-posterior plane reached 15Nm/degree. In a study of ninety five patients they found no cases of refracture when the fixator was removed after the bending stiffness had reached 15Nm/degree.

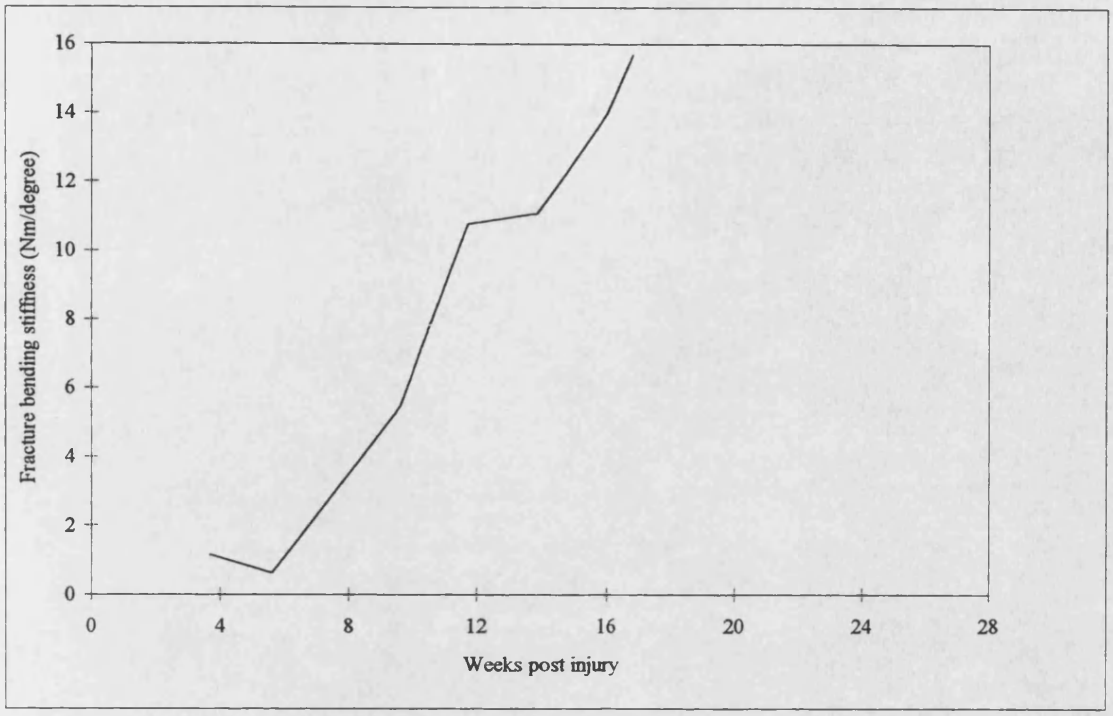

Figure 8-3 Uncomplicated healing of a tibial fracture. From Cunningham *et al.* (1987)

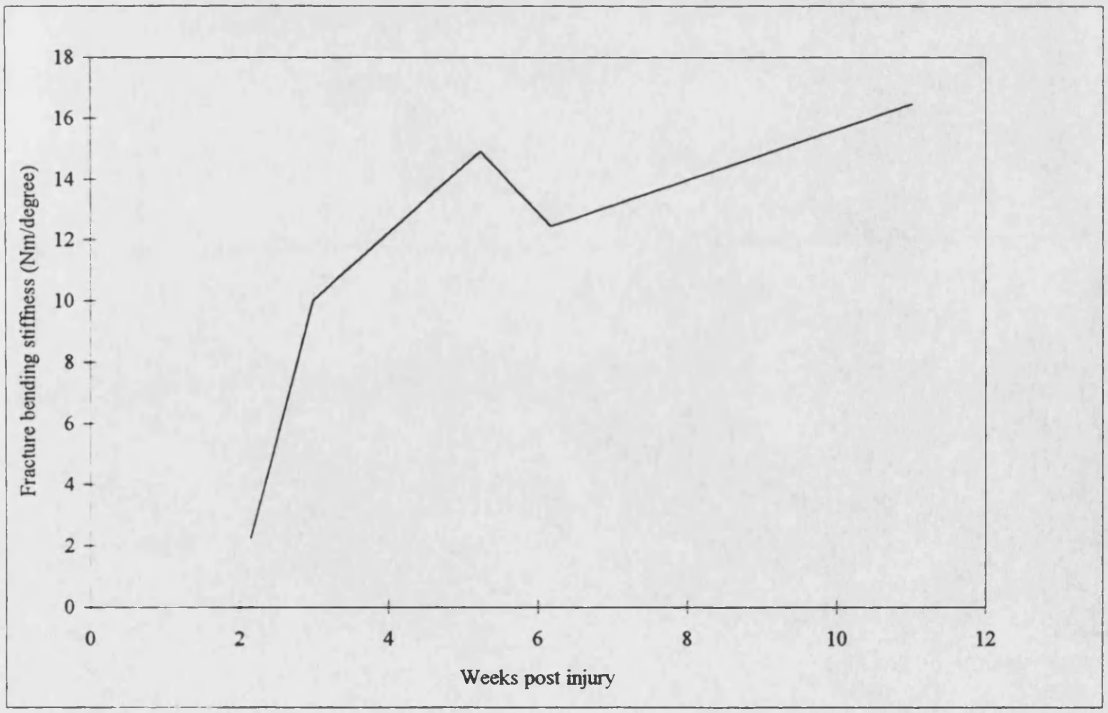

Figure 8-4 Healing of a tibial fracture. From Cunningham *et al.* (1990)

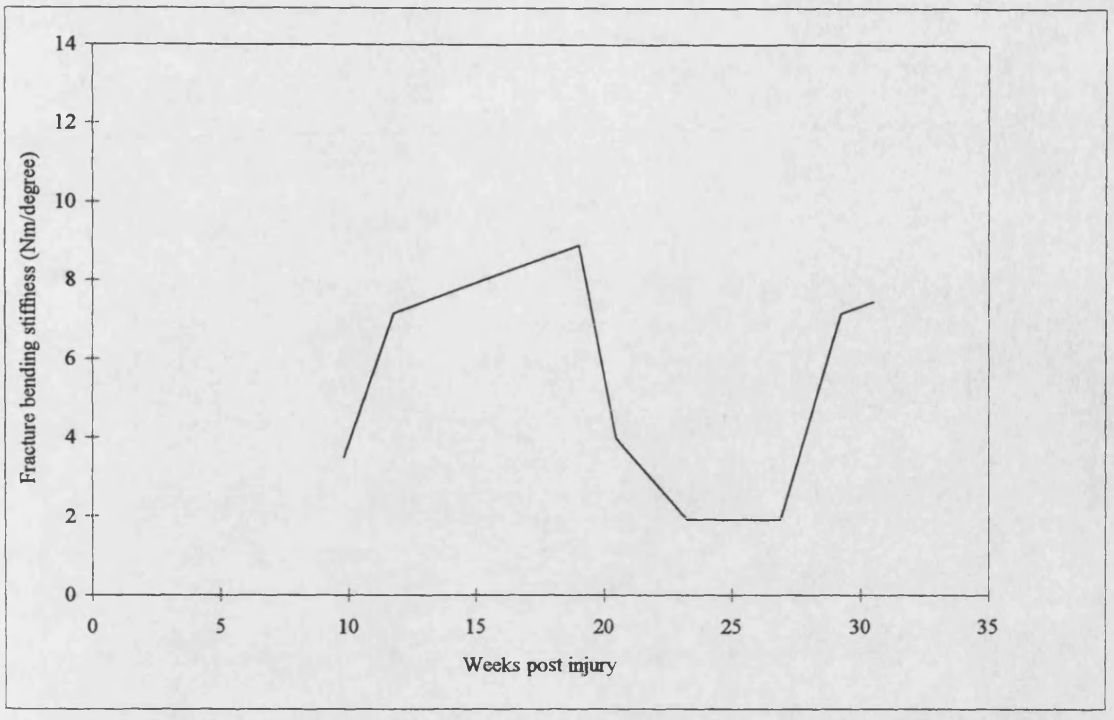

Figure 8-5 Slow healing of a tibial fracture. From Cunningham *et al.* (1987)

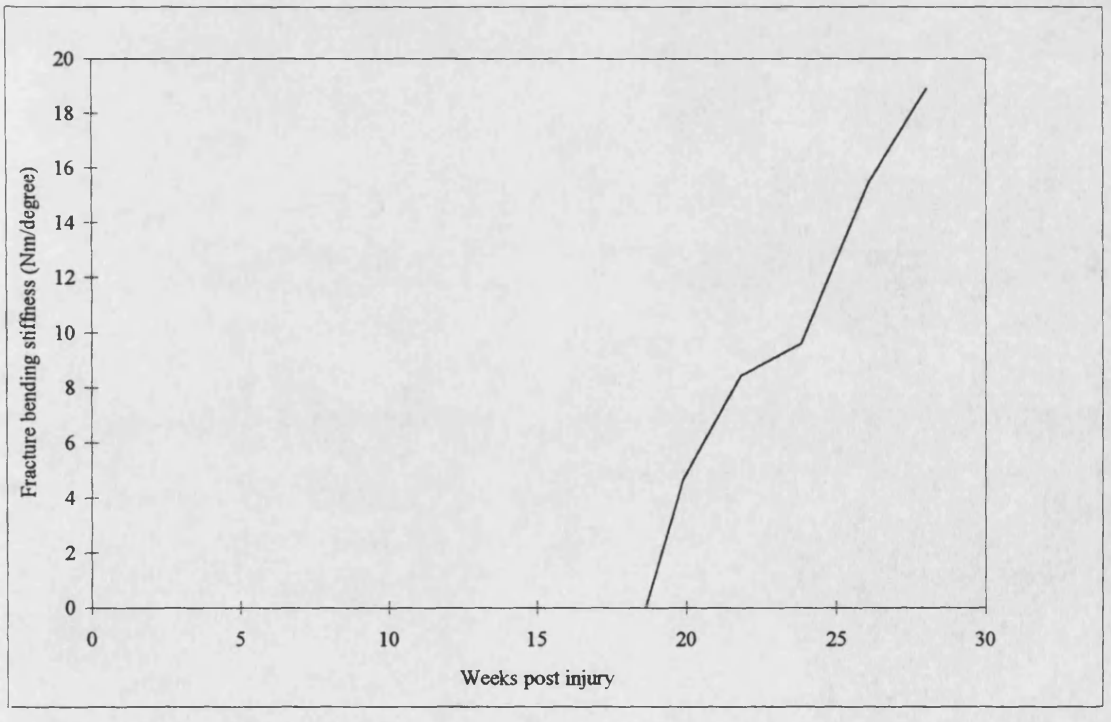

Figure 8-6 Delayed healing in a comminuted tibial fracture. From Cunningham *et al.* (1990)

In order to relate the healing curves of this study (chapter 7) to the stiffness/time data presented in the Oxford studies, the bending stiffness of the constructs needed to be measured during the healing simulation. The clinical bending test (figure 8.1) can be reproduced *in vitro* as a cantilever bending test on the bone/nail constructs with bending occurring in the antero-posterior plane. The fracture stiffness can then be calculated in Nm/degree (figure 2.18), the same units as the Oxford studies.

8.2.2 Cantilever bending tests

The cantilever bending tests were carried out in parallel with the healing study in combined loading (chapter 7). After the constructs had been tested in full single legged stance they were removed from the fixtures and the proximal and distal end of each construct was cast into a rectangular aluminium block using Wood's metal. The distal block was clamped to the work bench and a weight hanger attached to the proximal block in line with the femoral shaft (figure 8.7). The construct was loaded to 30N in 5N increments and the vertical deflection of the construct was measured using the dial gauge. If the distance between the dial gauge and fracture was known (x) then the angular deflection of the fracture could be calculated. The test was repeated three times at each stage of healing until the bending stiffness reached 15Nm/degree.

8.3 RESULTS AND DISCUSSION

For each test, the bending moment (FL) was plotted against the angular deflection of the fracture. A linear regression was performed on each data set and the gradient of this line was found. The correlation coefficient, R^2, was greater than 0.999 in each case. The average gradient, determined from the three tests performed at each stage, gave the bending stiffness of the construct in Nm/degree.

The 12mm Russell-Taylor construct was almost twice as stiff as the 10mm AO URFN construct when the femur was fractured (3.96 cf. 2.25Nm/degree respectively). This large difference between the stiffness of the two constructs when healing=0% was also found during single legged stance. The low stiffness of the AO construct was indicated as a possible cause of the slow union reported in the literature with this nail.

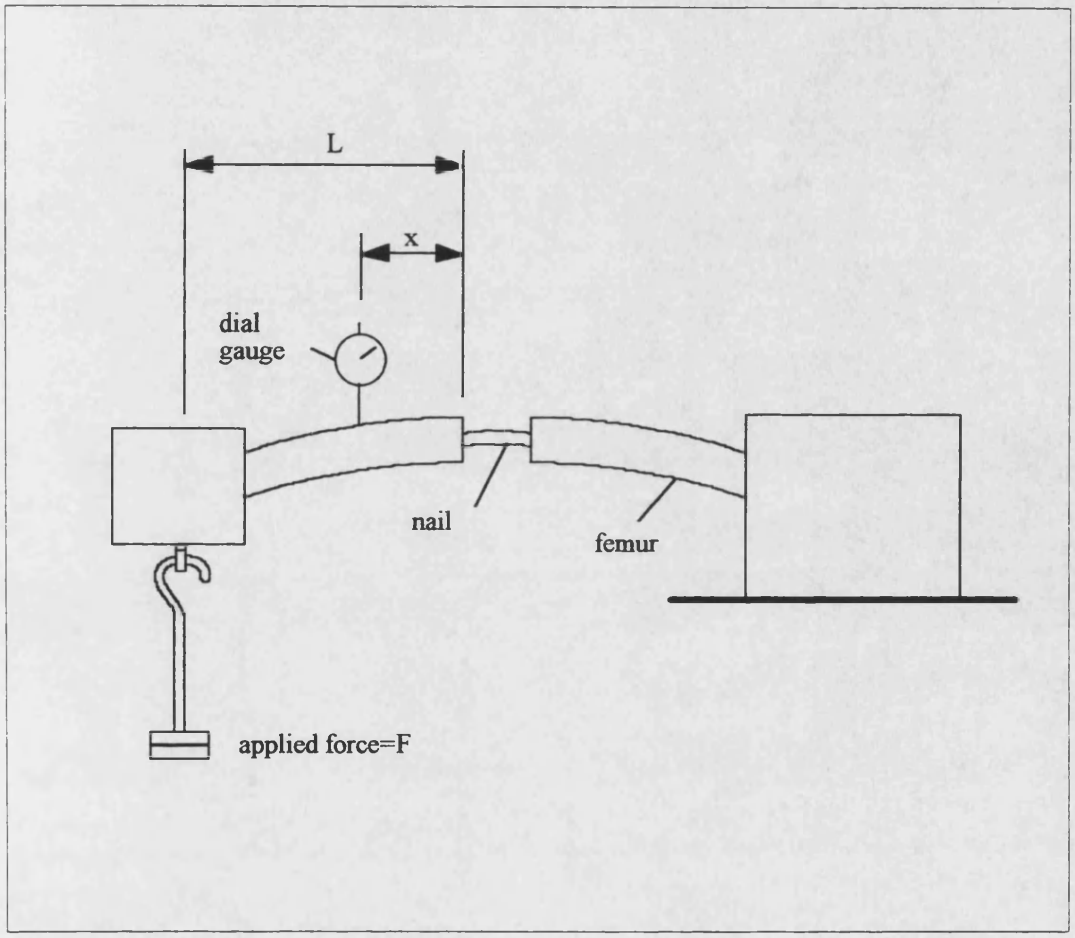

Figure 8-7 Experimental cantilever bending rig where L=bending moment arm and x=distance from the fracture to the dial gauge

Using the experimental results, the fracture stiffness was determined. All the deflections measured were elastic so superposition theory gives:

$$K_{construct}=K_{nail}+K_{fracture}$$

where K is the bending stiffness in Nm/degree and $K_{construct}$ is the construct stiffness measured in the tests. Hence the fracture stiffness $K_{fracture}$ can be determined using:

$$K_{fracture}=K_{construct}-K_{nail}$$

where K_{nail} was assumed to be the bending stiffness of the construct measured when the bone was fractured, when healing=0%. This incorporated the effects of nail/bone friction and the interlocking screws in the stiffness. The fracture bending stiffness was calculated at each stage of the simulated healing process.

The fracture bending stiffnesses were then related to time using the graphs produced by Cunningham *et al.* (1987 and 1990). Although these were obtained by monitoring tibial fracture healing it was assumed that the femoral bending stiffness would increase with time in the same way as the tibial stiffness. Two clinical situations were examined:

1. uncomplicated fracture healing (figure 8.3) where the fracture stiffness increased almost linearly with time from 6 weeks post injury. Union occurred at approximately 16 weeks post injury.
2. slow fracture healing (figure 8.5) where the fracture stiffness fluctuated with time, never exceeding 10Nm/degree. At 30 weeks post injury the fracture stiffness had failed to reach 15Nm/degree, the figure assumed to indicate clinical union.

Delayed union was not examined because the bending stiffness increased in a similar manner to that seen in uncomplicated healing. However, no evidence of healing was seen for the first 18 weeks post injury (figure 8.6).

The percentage of the total moment carried by the nails and the femora during single legged stance (body weight=65kg) was than plotted against time for the above two situations. It was assumed that the fracture would have zero stiffness initially (weeks post injury=0). This was true in this study as there was no contact between the bone fragments when the bone was fractured. The moments carried by the nails and femora when time post injury=0 were therefore assumed to be the same as those when healing=0% (chapter 7).

8.3.1 Uncomplicated fracture healing

Figure 8.8 shows the percentage of the total moment carried by the intramedullary nails, and figure 8.9 the percentage moment carried by the bones during uncomplicated healing. The deflections that the moments produce in the nails and femora are plotted in figures 8.10 and 8.11 respectively. These were calculated using the nail stiffnesses in Appendix C.

Figure 8.9 shows that at 0 weeks post injury the femur implanted with the AO URFN takes a greater proportion of the medio-lateral bending moment while the Russell-Taylor femur takes a greater amount of the torsional and antero-posterior moments. The AO femur takes no torsional moment when the bone is fractured. The deflections that these moments produce are small - less than 0.2mm or 0.2°.

The rapid increase in the moments taken by the AO femur in the healing studies (chapter 5 and 7) is not evident when the percentage moment is related to time (figure 8.9). However, details of the load transfer during the first 4 weeks post injury are only approximated as clinical data is not available for this time period (figure 8.3) - the first data point is joined directly with the second using a straight line. It is possible that a rapid load transfer may occur in the first four weeks after fracture fixation. It would be difficult to show whether this was the case due to the lack of clinical data and because the small changes in bending stiffness during the first 4 weeks are difficult to achieve using the crude application of glass fibre cloth. In general, the rate of moment uptake is similar in both femora during the first four weeks post injury.

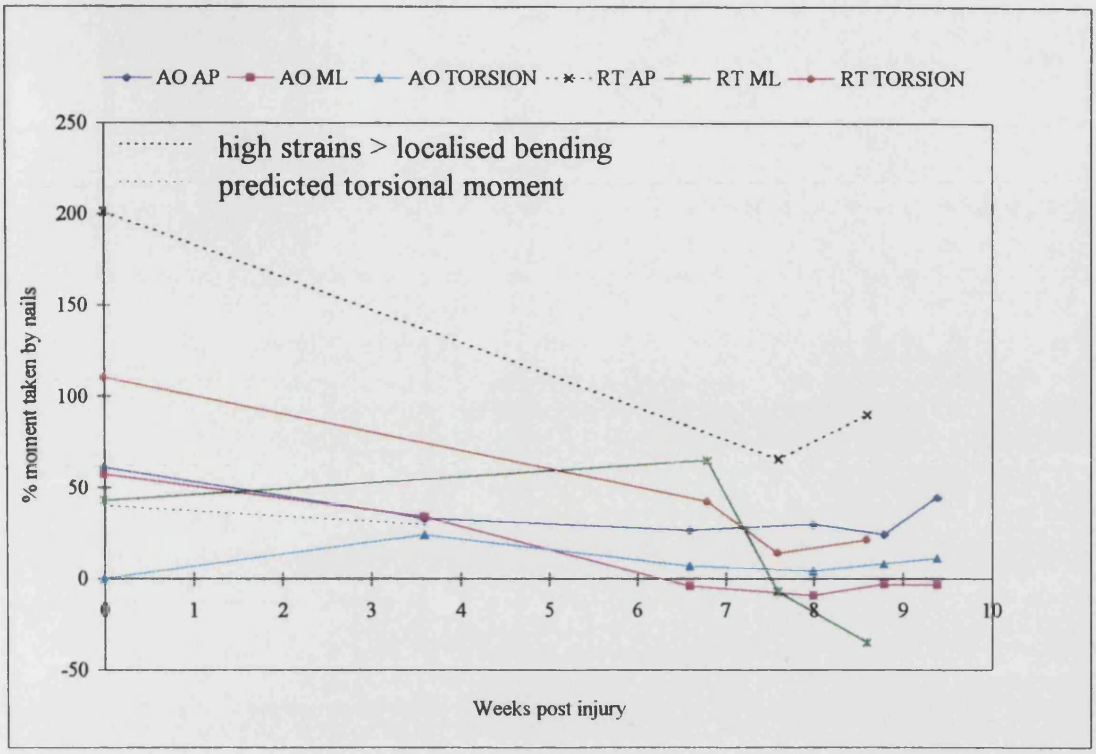

Figure 8.8 Percentage of the total moment carried by the intramedullary nails with time during uncomplicated fracture healing

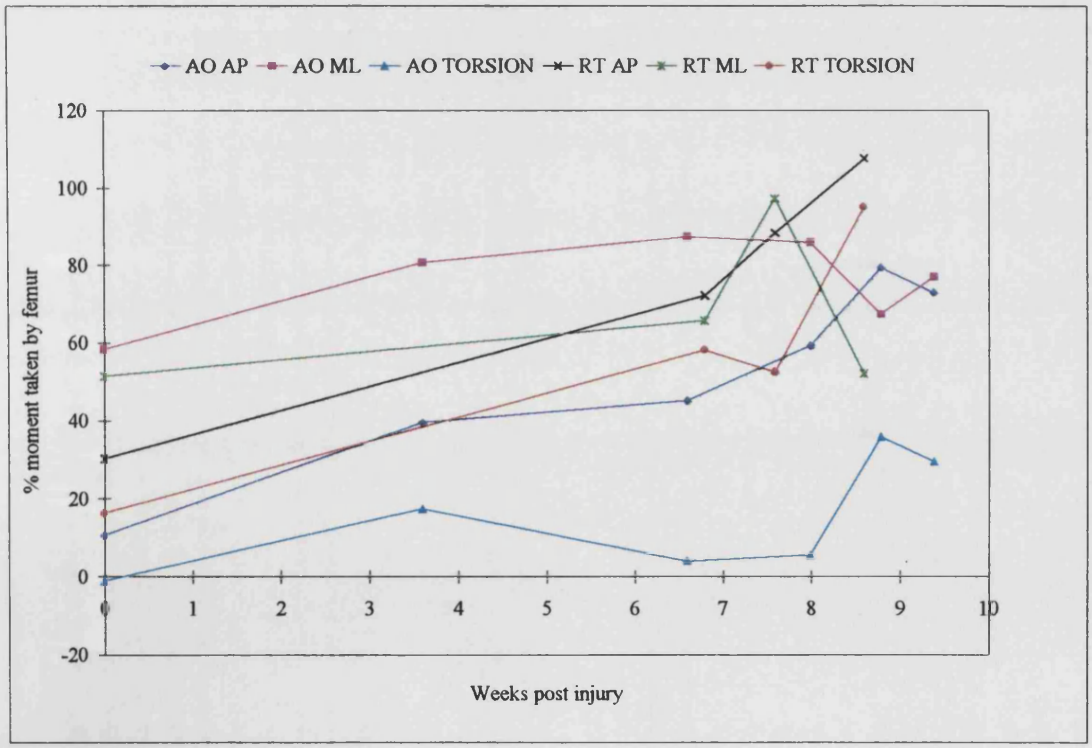

Figure 8.9 Percentage of the total moment carried by the femora with time during uncomplicated fracture healing

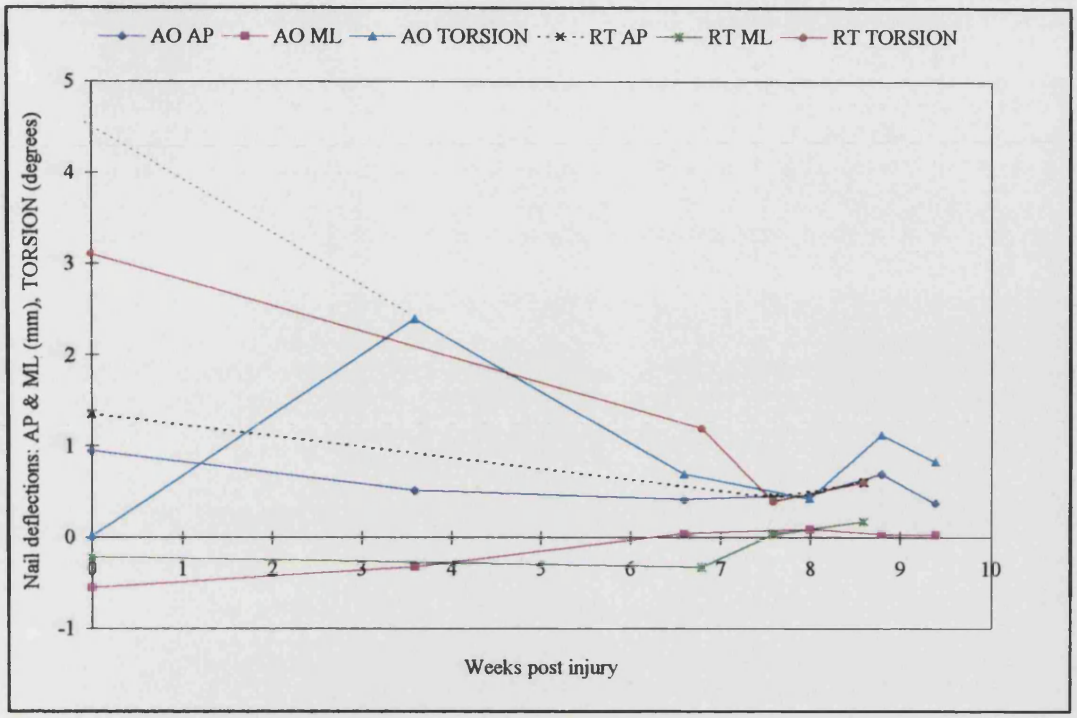

Figure 8.10 The deflections of the intramedullary nails with time during uncomplicated fracture healing.

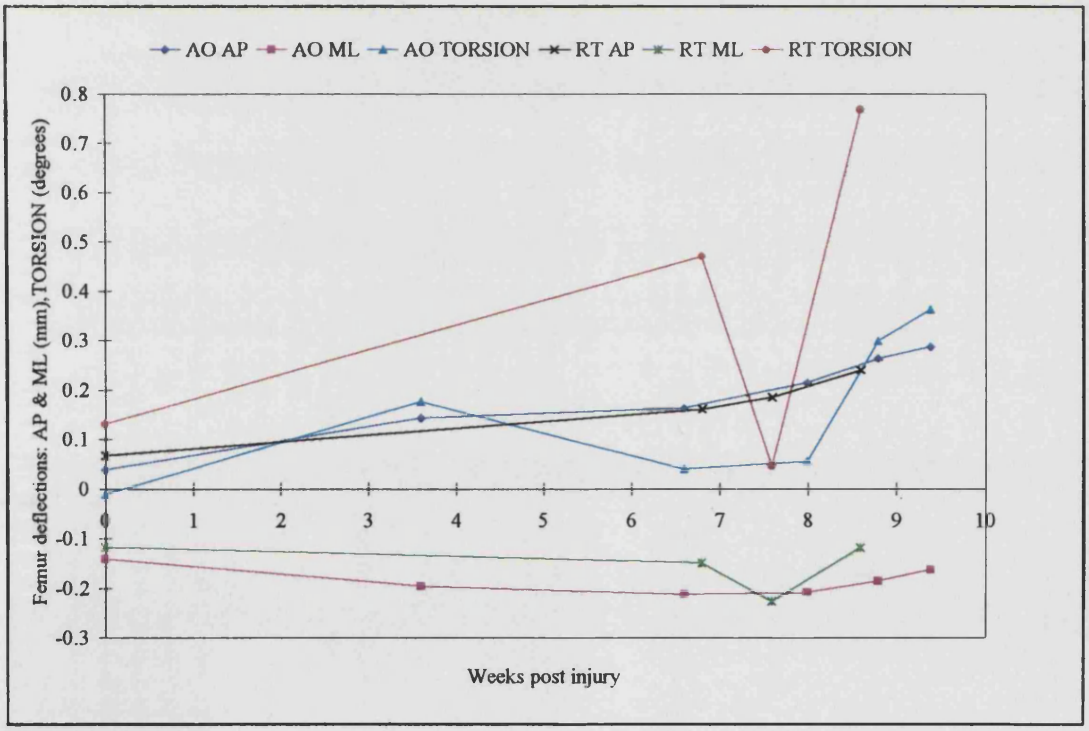

Figure 8.11 The deflections of the femora with time during uncomplicated fracture healing

Figure 8.9 shows that the femur implanted with the AO URFN takes a greater proportion of the total medio-lateral moment than the Russell-Taylor moment until about week 7. The resultant deflections (figure 8.11) are small though and there is only a 0.1mm difference between the deflections of the two nails. However, this is the only parameter that could cause the slow union seen clinically with use of the AO URFN as the Russell-Taylor femur is subjected to greater deflections in both antero-posterior bending and torsion.

With the exception of torsion in the AO femur, over 50% of all moments are carried by the femora at seven weeks post injury (figure 8.9). It is possible that both nails could be removed at this time as loading of the femur does not increase greatly after this. However, it may be that although the fracture stiffness may be sufficient, the strength of the healing femur might not have increased enough to allow the removal of the nail and a return to normal activity. White *et al.* (1977) suggested that there were four biomechanical stages to fracture repair (figure 2.15). It appears that at 7 weeks, the fracture may have reached stage 2 having a high stiffness but any refracture would occur through the original fracture site. Implant removal should occur after stage 3 has been reached, at a time greater than 7 weeks post injury. Although the fracture stiffness remains the same at stage 3 as at stage 2, and loading of the femur will not have increased further, the strength of the bone might have increased sufficiently so that refracture would occur only partially through the original fracture site.

When the bone is fractured both nails take roughly 50% of the total moments. The exception is the Russell-Taylor nail in torsion which takes 110% of the total moment. However, this large moment only produces a torsional deflection of 3° compared to a 5° displacement in the 10mm AO URFN subject to a smaller moment (figure 8.10). This is because the Russell-Taylor nail is more torsionally rigid. Only at week 5 post injury does the torsional displacement of the unreamed AO nail drop below that of the Russell-Taylor nail and the displacement is still as much as 2°. As mentioned in the previous chapter, because clinically nails are seen to fail in bending, it is possible that the high torsional deflections measured could lead to fatigue failure of the AO unreamed nail locking screws (Whittle *et al*, 1995). They would be particularly susceptible due to their

small diameter (4.9mm cf. 6.4mm for the Russell-Taylor nail). In addition, large torsional displacements might lead to nail failure at the site of the interlocking screw holes (Franklin *et al.*, 1988; Wu and Shih, 1992).

At seven weeks post injury, when the femora take over 50% of the total moments, the percentage moments carried by the nails are all less than 50%. However, the torsional displacements of the nails are still high (figure 8.10) and so this, in addition to the fact that bone strength may not be great enough, suggests that nail removal should be left until several weeks later.

8.3.2 Slow fracture healing

Figure 8.12 shows the decrease in the percentage moment taken by the intramedullary nails during slow healing. Figure 8.13 shows the increase in moments taken by the femora if healing is slow. Figure 8.14 shows the nail deflections with time during slow healing calculated using the applied moments and nail stiffnesses (Appendix C). Figure 8.15 shows the femoral deflections during slow healing.

The main difference between the charts showing uncomplicated healing and those showing slow healing are that the percentage moments and deflections fluctuate with time. The magnitudes are the same as those measured initially in uncomplicated healing but they remain at these values for up to 30 weeks, in this case, as the fracture bending stiffness fails to increase (figure 8.5). This accentuates the differences between the two constructs that have already been indicated during uncomplicated healing.

The torsional displacement of the 10mm AO unreamed nail is greater than that measured in the Russell-Taylor nail for approximately 21 weeks (figure 8.14). The cyclic loading of the implant over this period of time caused by patient activity and the flexibility of the nail would increase the likelihood of locking screw failure seen in the unreamed nail and the chance of nail failure at the distal interlocking screw holes.

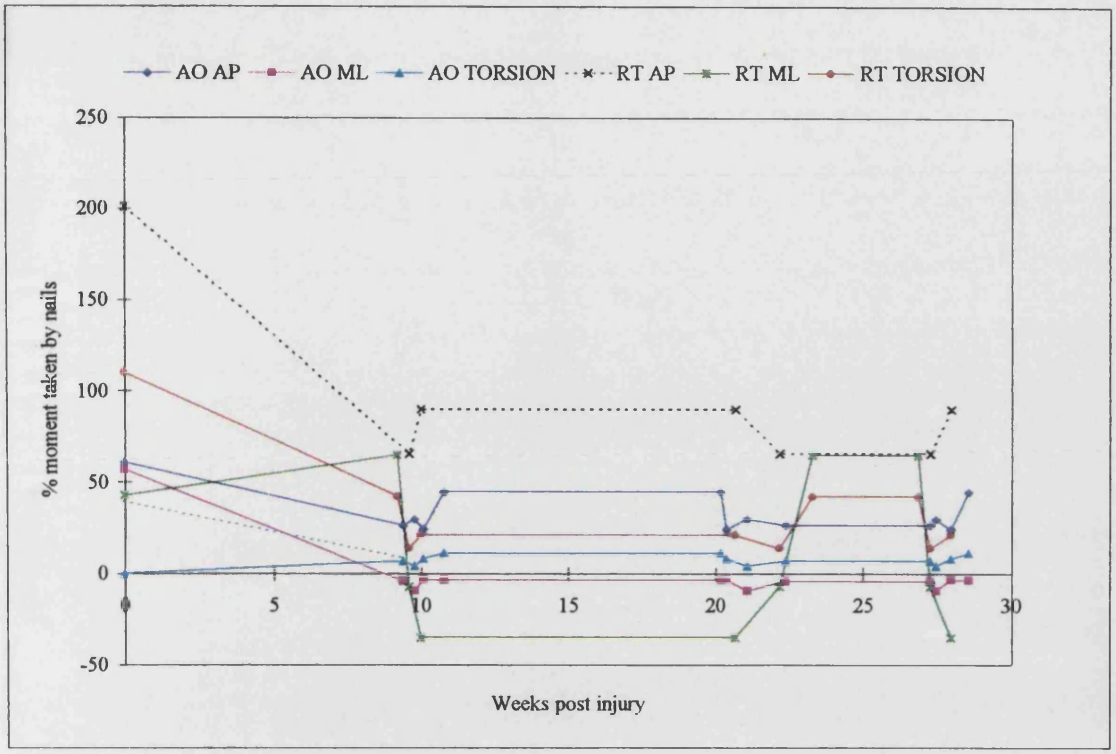

Figure 8.12 Percentage of the total moment carried by the intramedullary nails with time during slow fracture healing

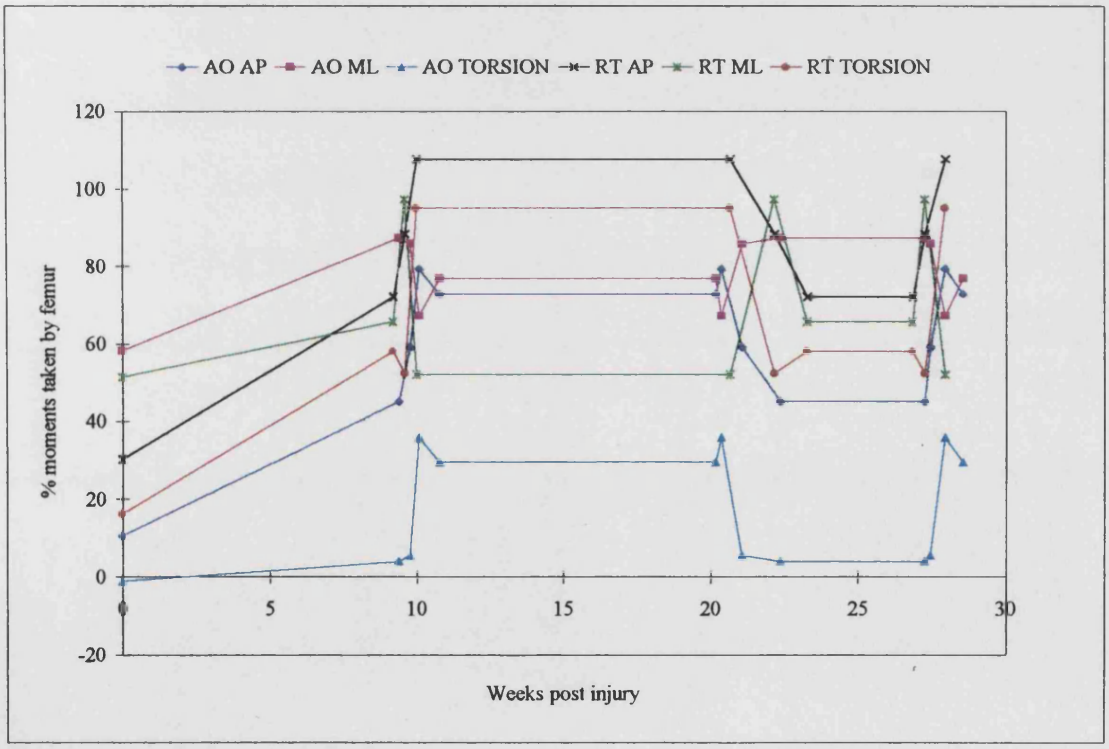

Figure 8.13 Percentage of the total moment carried by the femora with time during slow fracture healing

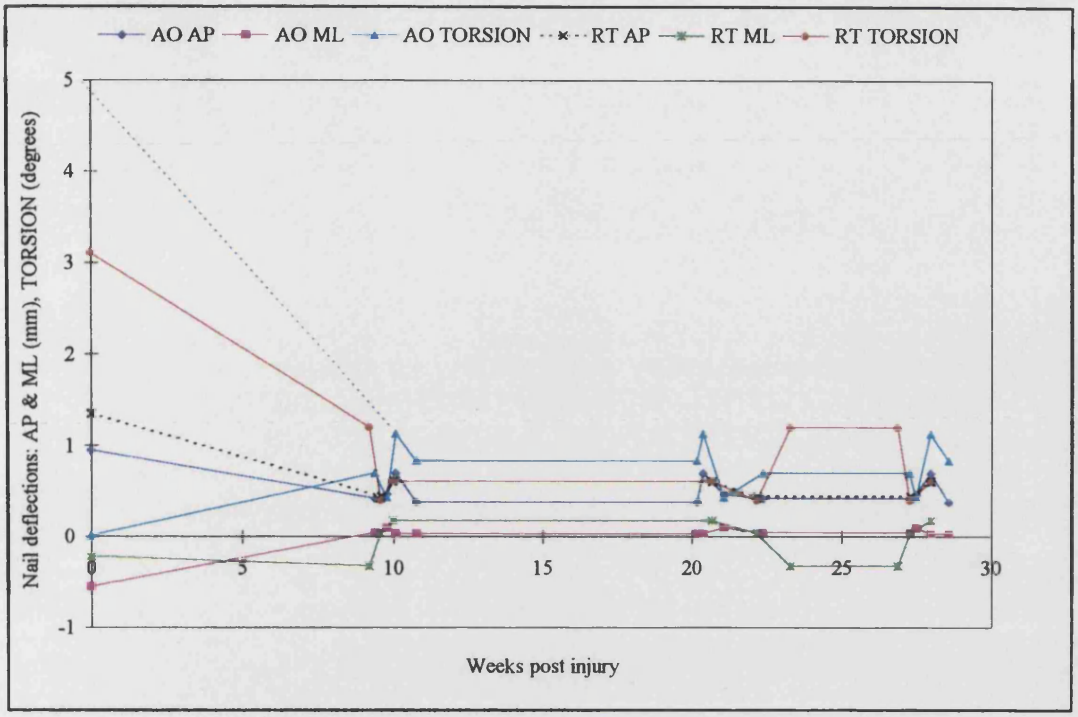

Figure 8.14 The deflections of the intramedullary nails with time during slow fracture healing.

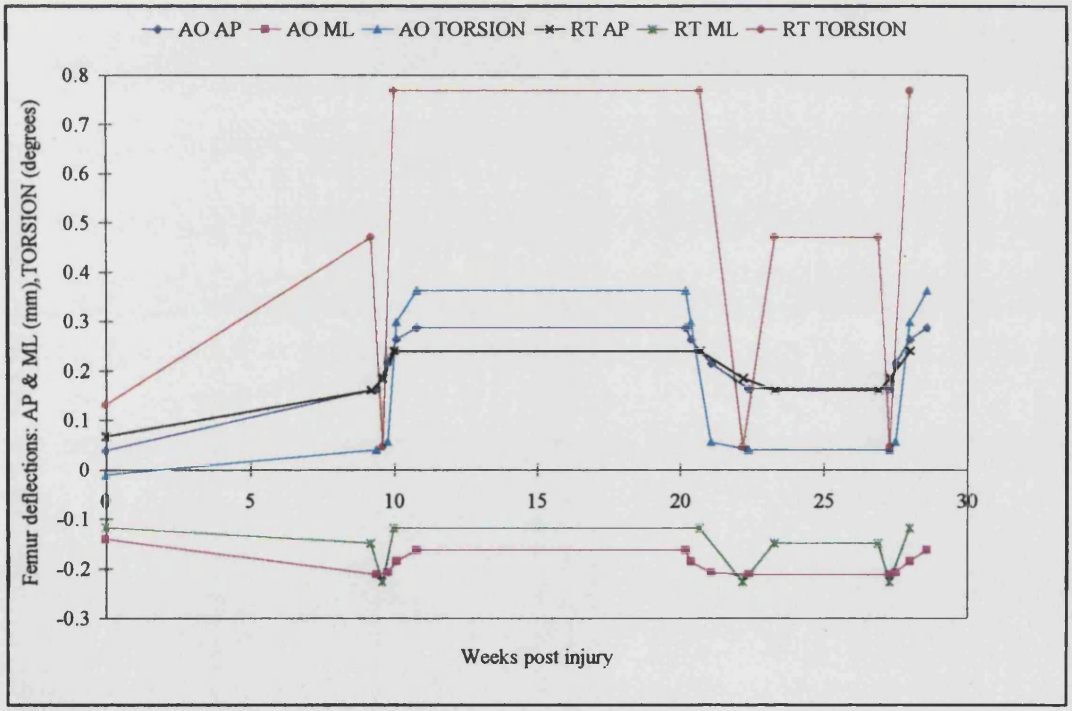

Figure 8.15 The deflections of the femora with time during slow fracture healing

The medio-lateral deflections in the femur implanted with the AO URFN are greater than those in the Russell-Taylor femur for 30 weeks although the magnitude of the deflections are only 0.2mm (figure 8.15). Again, this might cause the slow union seen clinically with the unreamed nail (Anglen and Blue, 1995; Haddad *et al.*, 1996; Blachut *et al.*, 1997; Giannoudis *et al.*, 1997). The femur implanted with the Russell-Taylor nail deflects more in torsion and antero-posterior bending.

It is possible that the slow union documented in the literature is not entirely the result of the medio-lateral bending deflections. A combination of this deflection and the biological effect of not reaming might all contribute. The bony products produced during reaming the medullary canal may be osteogenic (Keating, 1996).

Due to the large percentage moments still carried by the nail at 30 weeks, and the fact that the nail stiffness has not increased, regardless of the strength of the bone, nail removal is not recommended in this case. Cunningham *et al.* (1987) examined this patients X-rays just prior to 30 weeks post injury, and they indicated that the fracture had healed despite the low stiffness. The fixator was removed, but at 31 weeks post injury the bone refractured.

8.3.3 Comparison of the results with Schneider's work

The moments, rather than the percentage moments, carried by the femoral nails during single legged stance were plotted against time in order to compare the magnitudes with those measured *in vivo* by Schneider *et al.* (1990) using an instrumented intramedullary nail. These charts are shown in figures 8.16 and 8.17. The antero-posterior bending moment recorded in the Russell-Taylor nail is probably the result of localised bending, and is indicated by a dotted line. The predicted torsional moment of the AO nail is also shown as a dotted line.

The data recorded by Schneider *et al.* is recorded from approximately 80 days post operatively (figure 2.25) where as the data from this study finishes at this point. If the magnitudes of both are examined at this time then it can be seen that they are similar. Schneider *et al.* recorded approximately 10Nm of medio-lateral bending, a 4Nm torsional moment and a 5Nm antero-posterior bending moment. The moments measured in the

Russell-Taylor nail are closer to the *in vivo* values than those measured in the AO unreamed nail. This is because the instrumented nail had a closed clover leaf cross section similar to the Russell-Taylor nail although it had a 16mm diameter. The bending moments on the Schneider nail increase after 80 days post operatively which is not expected. This trend is not explained in their study.

8.4 SUMMARY

In uncomplicated healing there is a rapid increase in the bending stiffness. In slow healing the bending stiffness remains low and fluctuates.

When plotted against time using data from the Oxford Orthopaedic Engineering Centre, the rapid increase in the moments taken by the AO URFN femur, seen in the earlier healing studies (chapters 5 and 7), was not seen. This is true of the rapid decrease in moments taken by the AO unreamed nail too. The rate of load transfer was similar in both femora.

The AO URFN was subjected to a greater torsional deflection than the Russell-Taylor nail for up to 5 weeks during uncomplicated healing and for 30 weeks during slow healing. The large magnitude of these displacements could lead to the fracture of the interlocking screws in the AO unreamed nail but also to nail failure at the site of the interlocking screw holes.

It was found that in medio-lateral bending the AO femur deflected to a greater extent than the Russell-Taylor femur, although the difference was only about 0.1mm. In slow healing this increased deflection was seen over 30 weeks.

This small medio-lateral deflection might be enough to cause slow union particularly if the deflection extends over a period of 30 weeks. It is also possible that in addition to this deflection, the lack of bone reaming products might also contribute to slow union.

The moments measured in a closed section intramedullary nail *in vivo* and the Russell-Taylor nail moments were found to be of a similar magnitude at 80 days post operatively.

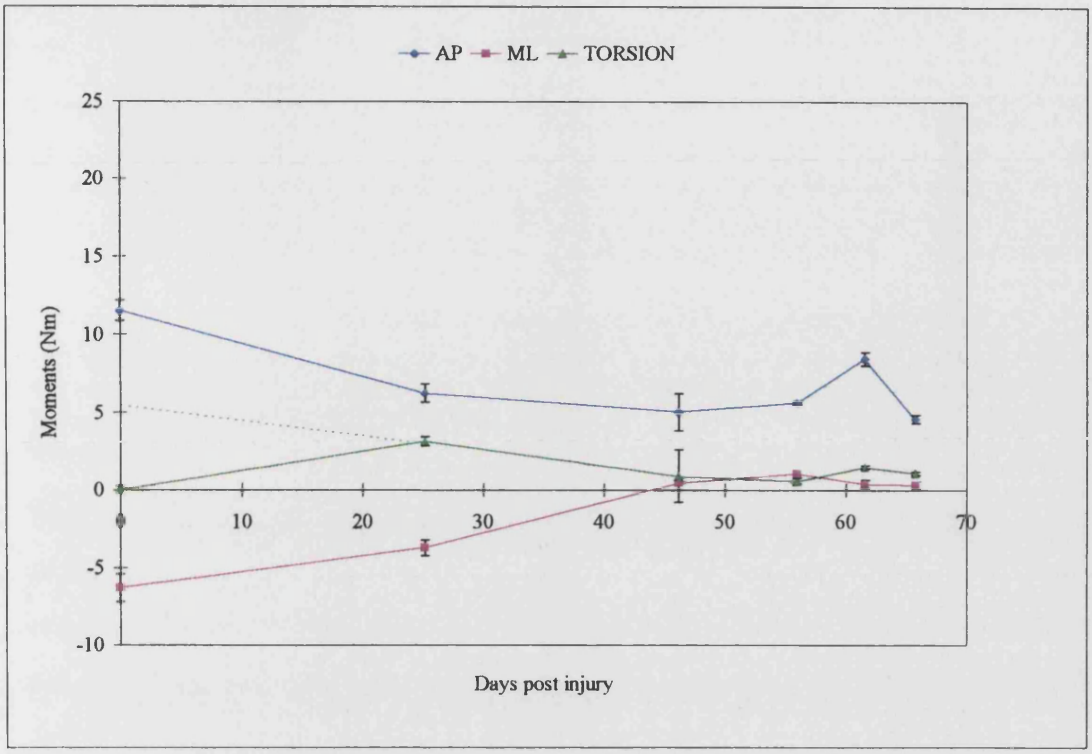

Figure 8-16 Moments taken by the 10mm AO URFN with time

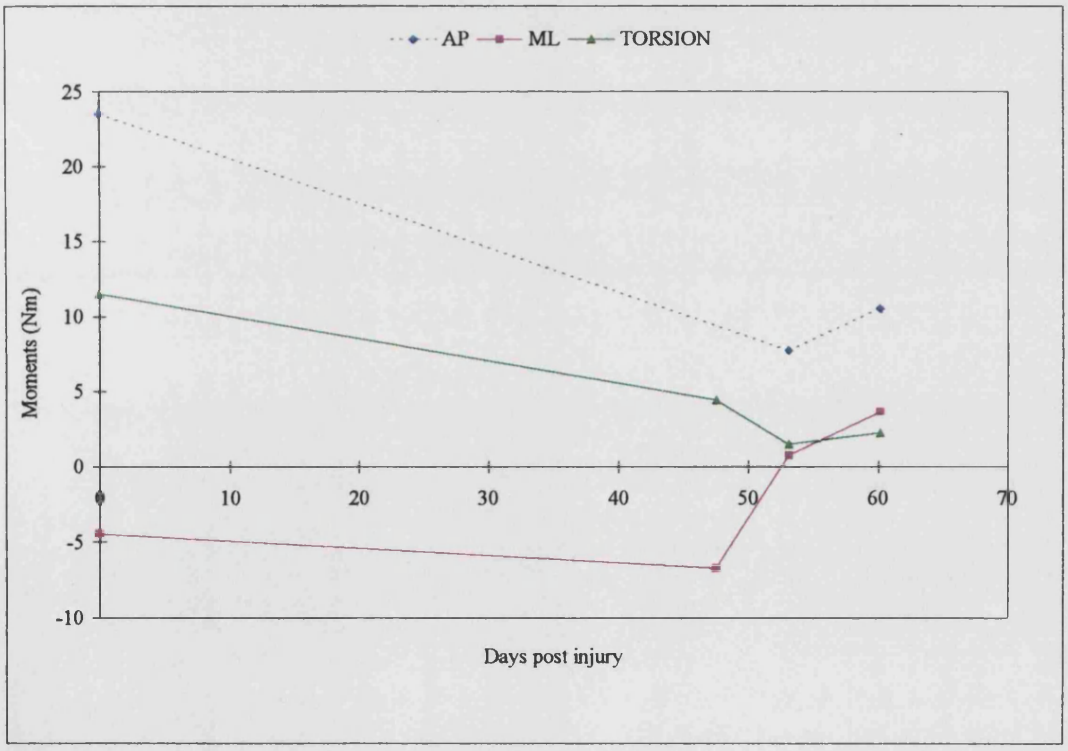

Figure 8-17 Moments taken by the 12mm Russell-Taylor nail with time

CHAPTER 9

CONCLUSIONS AND RECOMMENDATIONS FOR FURTHER WORK

9.1 SUMMARY AND CONCLUSIONS

This study was undertaken to evaluate the pre-clinical mechanical testing of intramedullary nails. A review of the literature showed that there was only one current standard which described a procedure for nail assessment. It was hypothesised that a test protocol which could evaluate the nails under realistic loading conditions would allow a greater insight in to the function of the nail compared with that which is obtained from isolated static testing. This would allow a fair comparison of different implants. If the nail characteristics that provide adequate fixation could be indentified then it would allow the indications and contraindications of a design to be established thereby reducing the *in vivo* complications due to incorrect usage.

The final test protocol involved testing an intramedullary nail during a simulated healing process using a commercially available composite bone model. The nail and femur were strain gauged to allow the antero-posterior and medio-lateral bending moments and the torsional moment taken by each to be measured throughout the study. The nail was inserted in to the femur according to standard surgical techniques and locked both proximally and distally. Subsequently the femur was fractured and then healing was simulated by successively layering glass fibre cloth with an epoxy resin across the fracture site.

To reproduce the loads that the intramedullary nail is subjected to *in vivo,* at each stage of the healing simulation the bone/nail construct was tested under conditions experienced by the femur during single legged stance. The femur was mounted in a shallow tray with the femoral shaft angled at 11° to the vertical in the medio-lateral plane. The effects of the abductor muscles were simulated, force=2x body weight acting at 20° to the vertical

from the greater trochanter. The tension band effect of the iliotibial tract was reproduced acting from the greater trochanter parallel with the femoral shaft with a force equal to body weight. The muscle loads were applied using cables, pulleys and dead weights. Finally the joint reaction was applied, force=2.7x body weight acting at 21° in the medio-lateral plane and 12° in the antero-posterior plane.

The healing constructs were also tested in cantilever bending in order that the changing moments carried by the nails and femur could be related to time post injury.

Two commercially available femoral intramedullary nails were tested using the above procedure. These were:

1. The Russell-Taylor standard femoral nail (12x380mm). This is a stainless steel nail with a hollow clover leaf cross section. It is locked proximally with one oblique screw and distally using two transverse screws. The medullary canal is reamed to 13mm before insertion of the nail.
2. The AO unreamed femoral nail (10x380mm). This nail is made from a titanium alloy and has a solid circular cross section. It is locked proximally with one transverse screw and distally with two transverse screws. The nail is generally inserted without reaming. Minimal reaming might be performed proximally as the proximal end of the nail has a larger diameter.

The results from the tests in combined loading provided the following information.

1. There was a large difference in the stiffness of the two bone/nail constructs in the fractured state. The Russell-Taylor construct was two and a half times more stiff than the AO URFN construct. In contrast, both constructs had a similar stiffness when the bone was 'healed'. The stiffness at this stage was approximately equal to the stiffness of a whole composite bone. The flexibility of the constructs might have implications in the selection of nails for certain types of fracture. The AO unreamed nail might be more appropriate for use in stable fractures. The Russell-Taylor could be used in more severe cases.

2. When the bone is fully fractured, even without contact between bony fragments, the nail and femur share the applied load. This is on account of load transfer through the interlocking screws and due to contact between the nail and bone along the length of the implant. Generally, the intramedullary nails supported a greater proportion of the load at this point.
3. There was a rapid increase in the loads taken by the femur implanted with the AO unreamed nail when plotted against the % healing of the bone. In contrast the load uptake in the Russell-Taylor nail was more gradual. However, when plotted against time, these trends were not apparent. The rate of increase in the loads taken by the bones was similar.
4. The medio-lateral moment measured in the femur implanted with the AO unreamed nail was greater initially and for the first seven weeks during uncomplicated fracture healing than that seen in the Russell-Taylor femur. During slow healing, it was always the greater of the two. Although the measured moment only produced a 0.2mm displacement, it is possible that this could cause the slow union reported in the literature with the unreamed nail.
5. The percentage of the total torsional moment taken by the Russell-Taylor nail was approximately twice that projected in the AO URFN when the bone was fractured. However, due to the high rigidity of the Russell-Taylor nail, the unreamed nail was subjected to greater torsional deflections initially (5° cf. 3°). The AO URFN was subjected to a greater torsional deflection for 5 weeks during uncomplicated healing and for 30 weeks during slow healing. Clinical reports have suggested that intramedullary nails fail in bending. This large torsional deflection might therefore be the cause of the high failure rate of distal interlocking screws reported in the AO unreamed nail. If the intramedullary nail were 'nicked' during screw insertion, it might also cause the failure of the nail in the region of the screw holes.
6. With the exception of the torsional moment measured in the femur implanted with the AO URFN, the femoral moments were close to their pre-implantation values when the fractured bone reached its original stiffness. Stress shielding was small because of the load sharing ability of the implant through bone/nail contact along the length of the medullary canal. If the implants were removed at the fully healed stage, there would be no problem with refracture. If the implant were to be removed before the femur

had reached its original stiffness, it should be checked that the femur is taking the majority and the nail the minority of the load. However, it would be more important to check that the bone has sufficient strength to withstand normal activity.

The test method allowed a comparison of two intramedullary nails under realistic loading conditions. The results were linked to clinical outcomes reported in the literature. It is suggested that a nail with a high torsional rigidity is necessary to reduce screw breakage and nail failure around the interlocking screw holes and adequate support for the healing femur in medio-lateral bending might reduce the incidence of slow union. It is hoped that a greater understanding of the role of existing and new intramedullary nails will be possible by using and developing this test protocol.

9.2 RECOMMENDATIONS FOR FURTHER WORK

The following recommendations are made for further work:

1. A transducer should be developed to allow the accurate recording of nail and femoral loads during the healing simulation instead of using strain gauges attached directly to the nail and bone surfaces. Ideally this should be a separate unit and be adaptable for use with any bone/nail geometry.
2. The transducer should measure the relative displacement of the two bone fragments during healing.
3. The test should be repeated using a large number of each nail type.
4. The fractured bone/nail implants should be fatigue tested using the single legged stance loading conditions to evaluate the failure modes.

Clinical studies are required to determine the following:

1. The change in stiffness and strength of different femoral fractures. Unfortunately the femur is not as accessible as the tibia and such information would be difficult to acquire.
2. The effects of bending and torsional displacements on fracture healing.

In addition, it would be beneficial if a database were set up documenting evidence of damaged nails after implant retrieval. If information on whether a nail failed in bending and torsion and whether the fracture was united at failure were known, it would be extremely useful for the design and development of new implants. This sensitive information may need to be overseen by a third party rather than the implant manufacturers.

CHAPTER 10

REFERENCES

Alho A, Moen O, Husby T, Ronningen H and Skjeldal S, 1992. Slotted versus non-slotted locked intramedullary nailing for femoral shaft fractures. *Arch Orthop Trauma Surg, 111, 91-95.*

Ali A, Sharif I, Kumar A, Scannel T and Kenny F, 1995. Early experience with Marchetti nails. *J Bone Joint Surg, 77B (S3), 340.*

Anglen JO and Blue JM, 1995. A comparison of reamed and unreamed nailing of the tibia. *J Trauma, 39 (2), 351-355.*

Aro HT and Chao EYS, 1993. Bone healing patterns affected by loading, fracture fragment stability, fracture type and fracture site compression. *Clin Orthop, 293, 8-17.*

Azer SN, Krause WR and Salman NN, 1991. *Scientific exhibit, 58th Annual Meeting AAOS, Anaheim, California. U.S. Patent 4,913,137.*

Bankston AB, Keating EM and Saha S, 1992. The biomechanical evaluation of intramedullary nails in distal femoral shaft fractures. *Clin Orthop, 276, 277-282.*

Bankston AB, Keating EM, Saha S and Engelhardt JA, 1986. Biomechanical evaluation of intramedullary rods used in distal femoral shaft fractures. *Orthop Trans, 10, 389-390*

Beals N, 1987. Evaluation of a composite Sawbone femur model. *Research Report ML-87-25, Richards Medical Company, Memphis, Tennessee.*

Beals N, Davidson J and Holbrook J, 1990. Improved fatigue strength of interlocking intramedullary nails. *Second Annual Conference International Society for Fracture Repair, abstract.*

Beals N, DurhamG and Lynch G, 1988. Mechanical characterization of interlocking intramedullary nails. *Research Report, Smith and Nephew Richards Inc, Memphis, Tennessee.*

Bergmann G, Graichen F and Rohlmann A, 1993. Hip joint loading during walking and running measured in two patients. *J Biomech, 26 (8), 969-990.*

Bernirschke SK, Melder I, Henley MB, Routt ML, Smith DH, Chapman JR and Swiontkowski MF, 1993. Closed interlocking nailing of femoral shaft fractures: assessment of technical complications and functional outcomes by comparison of a prospective database with retrospective review. *J Orthop Trauma, 7 (2), 118-122.*

Bertram J, 1989. Standards-generation and dissemination. *Proc I Mech E international conference, The changing role of engineering in orthopaedics, 49-54.*

Bianco PT, Bechtold JE, Kyle RF and Gustilo RB, 1989. Synthetic composite femurs for use in evaluation of torsional stability of cementless femoral prostheses. *Trans ACE/ASME Biomech Symp, San Diego, CA, 297-300.*

Blachut PA, O'Brien PJ, Meek RN and Broekhuyse HM, 1997. Interlocking intramedullary nailing with and without reaming for the treatment of closed fractures of the tibial shaft. *J Bone Joint Surg, 79A (5), 640-646.*

Blumberg KD, Foster WC, Blumberg JF, Adelaar RS, Deblois ME, Hussey RW, Loughran TP and Cardea JA, 1990. A comparison of the Brooker-Wills and Russell-Taylor nails for treatment of patients who have fractures of the femoral shaft. *J Bone Joint Surg, 72A(7), 1019-1024.*

Brand RA, Pederson DR, Davy DT, Kotzar GM, Heiple KG and Goldberg VM, 1994. Comparison of hip force calculations and measurements in the same patient. *J Arthroplasty, 9 (1), 45-51.*

Bråton M, Terjesen T and Rossvoll I, 1993. Torsional deformity after intramedullary nailing of femoral shaft fractures. *J Bone Joint Surg, 75B (5), 799-803.*

Brown RH, Burstein AH and Frankel VH, 1982. Telemetering in vivo loads from nail plate implants. *J Biomech, 15 (11), 815-823.*

Browner BD and Cole JD, 1987. Current status of locked intramedullary nailing: a review. *J Orthop Trauma, 1(2), 183-195.*

Brumback RJ, Reilly JP, Poka A, Lakatos RP, Bathon GH and Burgess AR, 1988a. Intramedullary nailing of femoral shaft fractures, part I: decision making errors with interlocking fixation. *J Bone Joint Surg, 70A (10), 1441-1452.*

Brumback RJ, Uwagie-Ero S, Lakatos RP, Poka A, Bathon GH and Burgess AR, 1988b. Intramedullary nailing of femoral shaft fractures, part II: fracture healing with static interlocking fixation. *J Bone Joint Surg, 70A (10), 1453-1462.*

BS3531: section 14.1, 1990: Specifications for the dimensions of nails of clover leaf and v-shaped cross section and dimensions of extraction hooks.

BS3531: section 23.1, 1991: Bone plates-method for determination of bending strength and stiffness.

BS7251: parts 5-8, 1990: parts 9-10, 1992: part 11, 1993: Orthopaedic joint prostheses.

Bunker TD, 1989. Interlocking medullary nailing. *From 'Frontiers in fracture management' edited by Bunker TD, Colton CL and Webb JK, Dunitz, 139-150.*

Caffinière J-Y de la, Pelisse F and Caffinière M de la, 1994. Locked intramedullary flexible osteosynthesis. *J Bone Joint Surg, 76B (5), 778-788.*

Callaghan JJ, Fulghum CS, Glisson RR and Stranne SK, 1992. The effect of femoral stem geometry on onterface motion in uncemented prous coated total hip prostheses. *J Bone Joint Surg, 74A, 6, 839-848.*

Carlsöö, 1972. How man moves. *William Heinemann Ltd., 117.*

Chao EYS and Aro HT, 1994. Biomechanics of fracture repair and fracture fixation. *From Current practice of fracture treatment: new concepts and common problems, Leung (Ed), Springer Verlag, 33.*

Christensen AB, Ammitzbøll F and Dyrbye C, 1983. Resonance of human tibia-assessment to fracture healing. *From Biomaterials and Biomechanics, Ducheyne P, Van der Perre G and Aubert AE (Eds), Elsevier Science Publishers B.V., 215-220.*

Cornelissen M, Cornelissen P and Van der Perre G, 1982. A dynamic model for a healing fractured tibia. *From Biomechanics: priciples and applications, Huiskes R, Van Campen D and De Wijn J (Eds), Martinus Nijhoff Publishers.*

Cornelissen M, Van der Perre G, Martens M and Mulier JC, 1983. Vibration measurements correlated with mechanical stability characteristics. *From Biomaterials and biomechanics, Ducheyne P, Van der Perre G and Aubert AE (Eds), Elsevier Science Publishers B.V.*

Court-Brown CM, 1991. An atlas of closed nailing of the tibia and femur. *Martin Dunitz, London.*

Coutts RD, Kerina JM, Robins AJ, Hacker SA and Nguyen V-DN, 1994. The mechanical properties of polypropylene fumerate for the temporary fixation of intramedullary rods. *40th Annual meeting ORS, New Orleans, Louisiana, 536.*

Covey DC, Saha S, Lipka JM and Albright JA, 1990. Biomechanical comparison of slotted and nonslotted interlocking nails in distal femoral shaft fractures. *Clin Orthop, 252, 246-251.*

Cristofolini L, Viceconti M, Cappello A and Toni A, 1996. Mechanical validation of whole bone composite femur models. *J Biomech, 29 (4), 525-535.*

Crowninshield RD, Johnston RC, Andrews JG and Brand RA, 1978. A biomechanical investigation of the human hip. *J Biomech, 11, 75-85.*

Cunningham JL, 1997. Personal Communication.

Cunningham JL, Evans M, Harris JD and Kenwright J, 1987. The measurement of stiffness of fractures treated with external fixation. *Eng in Medicine, 16 (4), 229-232.*

Cunningham JL, Kenwright J and Kershaw CJ, 1990. Biomechanical measurment of fracture healing. *J Medical Engineering and Technology, 14 (3), 92-101.*

Curylo LJ and Lindsey RW, 1994. Shaft nonunions: Current etiology and outcome of treatment. *Orthopaedics International Ed, 2 (5), 465-473.*

Davy DT, Kotzar GM, Brown RH, Heiple KG, Goldberg VM, Heiple Jr. KG, Berilla J and Burstein AH. telemetric force measurements across the hip after total arthroplasty. *J Bone Joint Surg, 70A (1), 45-50.*

Deehan MA, Oppenheim W and Aurori B, 1993. Assessment of prognostic indicators in tibia fractures treated with unreamed interlocking intramedullary nails. *J Orthop Trauma, 1993, 7 (2), 162.*

Ebraheim NA and Paley KJ, 1993. Penetration of the distal femur by the distal locking device of Brooker Wills interlocking nail. *Clin Orthop, 297, 218-223.*

Egger EL, Gottsauner-Wolf F, Palmer J, Aro HT and Chao EYS, 1993. Effects of axial dynamisation on bone healing. *J Trauma, 34 (2), 185-192.*

Einhorn TA, Burstein AH and Cowell HR, 1997. Human experimentation. *J Bone Joint Surg, 79A (7), 959-960.*

Engh CA, O'Connor D, Jasty M, McGovern TF, Bobyn JD and Harris WH, 1992. Quantification of implant micromotion, strain shielding, and bone resorption with porous-coated anatomic medullary locking femoral prostheses. *Clin Orthop, 285, 13-29.*

English TA and Kilvington M, 1979. In vivo records of hip loads using a femoral implant with telemetric output. *J Biomed Engrg, 1 (2), 111-115.*

Evans M, Kenwright J and Cunningham JL, 1988. Design and performance of a fracture monitoring transducer. *J Biomed Eng, 10, 64-69.*

Eveleigh RJ, 1995. A review of biomechanical studies of intramedullary nails. *Med Eng Phys, 17 (5), 323-331.*

Fairbank AC, Thomas D, Cunningham B, Curtis M and Jinnah RH, 1995. Stability of reamed and unreamed intramedullary tibial nails: a biomechanical study. *Injury, 26 (7), 483-485.*

Field RE and Rushton N, 1989. Proximal femoral surface strain gauge analysis of a new epiphyseal prosthesis. *J Biomed Eng, 11, 123-129.*

Finlay JB, Chess DG, Hardie WR, Rorabeck CH and Bourne RB, 1991. An evaluation of three loading configurations for the in vitro testing of femoral strains in total hip arthroplasty. *J Orthop Res, 9 (5), 749-759.*

Finlay JB, Rorabeck CH, Bourne RB and Tew WM, 1989. In vitro analysis of proximal femoral strains usinf PCA femoral implants and a hip abductor muscle simulator. *J Arthroplasty, 4 (4), 335-345.*

Fischer KJ, Carter DR and Maloney WJ, 1992. In vitro study of inital stability of a conical collared femoral component. *J Arthroplasty, 7 Supp, 389-395.*

Fish, 1990. Physics and instrumentation of diagnostic medical ultrasound. *John Wiley and Sons Ltd.*

Franklin JL, Winquist RA, Benirschke SK and Hansen ST, 1988. Broken intramedullary nails. *J Bone Joint Surg, 70A (10), 1463-1471.*

Gere JM and Timoshenko SP, 1989. Mechanics of materials, 2nd SI edition. *Published Van Rostrand Reinhold (International) Co. Ltd, London.*

Gerlach UJ and Lierse W, 1990. Functional construction of the superficial and deep fascia system of the lower limb in man. *Acta Anat, 139, 11-25.*

Giannoudis PV, Furlong AJ, Macdonald DA and Smith RM, 1997. Reamed against unreamed nailing of the femoral diaphysis: a retrospective study of healing time. *Injury, 28 (1), 15-18.*

Goodship AE, Watkins PE, Rigby HS and Kenwright J, 1993. The role of fixator frame stiffness in the control of fracture healing. An experimental study. *J Biomech, 26 (9), 1027-1035.*

Green JH and Silver PHS, 1981. The muscles and joints of the lower limb. *From 'An introduction to humna anatomy', Oxford University Press, 128-137.*

Grundnes O and Reikerås O, 1993. Effects of instability on bone healing. *Acta Orthop Scand, 64 (1), 55-58.*

Guichet JM, Casar RS, Alexander H and Frankel VH, 1992. Comparative mechanical testing of intramedullary nails. *38th ORS, Feb 17-20, Washington, D.C.*

Haas N, Krettek C, Schandelmaier P, Frigg R and Tscherne H, 1993. A new solid unreamed tibial nail for shaft fractures with severe soft tissue injury. *Injury, 24 (1), 49-54.*

Haddad FS, Desai K, Sarkar JS and Dorrell JH, 1996. The AO unreamed nail: friend or foe. *Injury, 27 (4), 261-263.*

Hajek PD, Bicknell HR, Bronson WE, Albright JA and Saha S, 1993. The use of one compared with two distal screws in the treatment of femoral shaft fractures with interlocking intramedullary nailing. *J Bone Joint Surg, 75A (4), 519-525.*

Hall, 1987. Russell-Taylor nail surgical technique catalog. *Richards Medical Company, Memphis, Tennessee, 7.*

Hall SJ, 1995. Basic biomechanics. *2nd edition, Mosby.*

Hargreaves DG, Warren PJ, Pereira JA and Hollingdale JP, 1995. Complications following the use of the 'Marchetti' flexible intra-medullary nail. *J Bone Joint Surg, 77B (S1), 4.*

Hazlewood SJ, 1996. A finite element analysis on the importance of abductor muscle forces in comparative femoral strain gage studies. *42nd ORS, Feb 19-22, Atlanta, Georgia.*

Heim D, Schlegel U and Perren SM, 1993. Intramedullary pressure in reamed and unreamed nailing of the femur and tibia-an in vitro study in intact, human bones. *Injury, 24 (S3), S56-S63.*

Hoeltzel DA, Frohrib DA, Fernstrom KA, Hammett R, Gustilo RB and Kyle RF, 1985. The contribution of an implanted intramedullary nail to the load carrying capacity of a fractured femur. *31st ORS, Las Vegas, Nevada, 188.*

Hofmann GO, 1992. Biodegradable implants in orthopaedic surgery - a review on the state-of-the-art. *Clin Materials, 10, 75-80.*

Hutson JJ, Zych GA, Cole JD, Johnson KD, Ostermann PO, Milne EL and Latta L, 1995. Mechanical failures of intramedullary tibial nails applied without reaming. *Clin Orthop, 315, 129-137.*

Johnson KD, Tencer AF and Sherman MC, 1987. Biomechanical factors affecting fracture stability and femoral bursting in closed intramedullary nailing of femoral shaft fractures, with illustrative case presentations. *J Orthop Trauma, 1 (1), 1-11.*

Johnson KD, Tencer AF, Blumenthal S, August A and Johnston DWC, 1986. Biomechanical performance of locked intramedullary nail systems in comminuted femoral shaft fractures. *Clin Orthop, 206, 151-161.*

Kaartinen E, Paavolainen P, Holmstrom T, Slatis P and Happonen RP, 1993. Different healing patterns of experimental osteotomies treated by intramedullary nailing. *Arch Orthop Trauma Surg, 112, 171-174.*

Kapp, W, Lindsey RW, Rudersdorf R, Henry P and LaBlanc A, 1994. Long term effects of retained intramedullary femoral nails on bone mineral density and muscle strength. *Trans OTA, Los Angeles, 174.*

Keating JF, 1996. The osteogenic potential of bone reamings. *Techniques in Orthopaedics, 11 (1), 45-49.*

Kenwright J and Goodship AE, 1989. Controlled mechanical stimulation in the treatment of tibial fractures. *Clin Orthop, 241, 36-47.*

Kershaw CJ, Cunningham JL and Kenwright J, 1993. Tibial external fixation, weight bearing, and fracture movement. *Clin Orthop, 293, 28-36.*

Kinast C, Wyder H, Frigg R and Perren SM, 1987. Biomechanical investigations of the proximal screw of interlocking nails. *Orthop Trans, 11, 295.*

Kneifel T and Buckley R, 1996. A comparison of one versus two distal locking screws in tibial fractures treated with unreamed tibial nails: a prospective randomised clinical trial. *Injury, 27 (4), 271-273.*

Krettek C, Rudolf J, Schandelmaier P, Guy P, Könemann B and Tscherne H, 1996. Unreamed intramedullary nailing of femoral shaft fractures: operative technique and early clinical experience with the standard locking option. *Injury, 27 (4), 233-254.*

Kristiansen B and Borgwardt A, 1992. Fracture healing monitored with strain guages. *Acta Orthop Scand, 63 (6), 612-614.*

Kropfl A, Naglik H, Primavesi C and Hertz H, 1995. Unreamed intramedullary nailing of femoral fractures. *J Trauma, 38 (5), 717-726.*

Küntscher GBG, 1958. The Küntscher method of intramedullary fixation. *J Bone Joint Surg, 40A (1), 17-26.*

Kyle RF, 1985. Biomechanics of intramedullary fracture fixation. *Orthopaedics, 8 (11), 1356-1359.*

Kyle RF, 1994. Fractures of the proximal part of the femur. *J Bone Joint Surg, 76A (6), 924-950.*

Latta LL and Zych GA, 1991. Part II: The mechanics of fracture fixation. *Current Orthop, 5, 92-98.*

Laura PAA, Rossi RE and Maurizi MJ, 1990. Dynamic analysis of a simplified bone model during the proces of fracture healing. *J Biomed Eng, 12, 157-160.*

Lengsfield M, Kaminsky J, Merz B and Franke RP, 1996. Sensitivity of femoral strain pattern analyses to resultant and muscle forces at the hip joint. *Med Eng Phys, 18 (1), 70-78.*

Lewis JL, 1975. A dynamic model of a healing fractured long bone. *J Biomech, 8, 17-25.*

Lin SS, Shah SA, Fitzpatrick MJ and Tuan RS, 1994. Treatment of open fractures with intramedullary rods coated with an antibiotic-impregnated biodegradable drug delivery system. *40th ORS, New Orleans, Louisiana, 292.*

Ling RSM, O'Connor JJ, Lu TW and Lee AJC, 1996. Muscular activity and the biomechanics of the hip. *Hip International, 6 (3), 91-105.*

Lowden IMR, Williamson DM, Nelson IW and Cockin J, 1989. Technical considerations of the AO interlocking nail. *Injury, 20, 222-225.*

Lowet G and Van der Perre G, 1996. Ultrasound velocity measurement in long bones: measurement method and simulation of ultrasound wave propogation. *J Biomch, 29 (10), 1255-1262.*

Lowet G, Van Audekercke R, Van der Perre G, Geusens P, Dequeker J and Lammens J, 1993. The relation between resonant frequencies and torsional stiffness of long bones *in vitro. J Biomech, 26 (6), 689-696.*

Lynch GE and Davidson JA, 1989. Motion at the bone fracture interface with slotted and unslotted intramedullary nails. *Richards Research Report, Smith and Nephew Richards Inc., Memphis, Tennesse.*

Mahaisavariya B and Laupattarakasem W, 1993. Ultrasound or image intensifier for closed femoral nailing. *J Bone Joint Surg, 75B (1), 66-68.*

Marchetti PG, Vicenzi G and Impallomeni C, 1993. An original nail for the intramedullary elastic fixation of metadiaphyseal fractures and pseudoarthroses of femur and tibia. *J Bone Joint Surg, Orthop Proc III, 75B, 286.*

Marchetti PG, Vicenzi G and Impallomeni C, 1994. A new nail for elastic intramedullary fixation in fractures and pseudarthroses of the femur and tibia. *Orthop Int Ed, 2 (5), 403-416.*

Markel and Chao, 1993. Non invasive monitoring techniques for quantitative description of callus mineral content and mechanical properties. *Clin Orthop, 293, 37-45.*

Matthews LS, Kaufer H and Sonstegard DA, 1974. Manual sensing of fracture stability: a biomechanical study. *Acta Orthop Scand, 45, 373-381.*

McDermott AGP, Halifax NS, Russell L, Gross AE and Ready J, 1987. Biomechanical testing of the locking nail principle. *Orthop Trans, 11, 383-384.*

McKibbin B, 1978. The biology of fracture repair. *J Bone Joint Surg, 60B (2), 150-162.*

McLeish RD and Charnley J, 1970. Abduction forces in the one-legged stance. *J Biomech, 3, 191-209.*

McLeod G, 1991. Closed intramedullary locking nails in the management of femoral shaft fractures. *Int J Orthop Trauma, 1 (1), 20-25.*

McNamara BP, Cristofolini L, Toni A and Taylor D, 1994. Evaluation of experimental and finite element models of synthetic and cadaveric femora for pre-clinical design-analysis. *Clin Materials, 17, 131-140.*

Meislin R, Frankel VH and Kummer FJ, 1993. Intramedullary nailing of subtrochanteric fractures: a critical review of device failure and case analysis. *Bulletin Hospital for Joint Diseases, 52 (2), 17-20.*

Melcher GA, Claudi B, Schlegel U, Perren SM, Printzen G and Munzinger J, 1994. Influence of type of medullary nail on the development of local infection; an experimental study of solid and slotted nails in rabbits. *J Bone Joint Surg, 76B (6), 955-959.*

Merchant AC, 1965. Hip Abductor muscle force. *J Bone Joint Surg, 47A (3), 462-476.*

Michel MC, Schneider E, Genge M and Perren SM, 1991. Loading history of an interlocking femoral nail subsequent to fracture treatment. *37th Annual Meeting, ORS, Anaheim, California, 141.*

Miles AW, Eveleigh RJ, Wight BJ and Goodwin MI, 1994. An investigation into the load transfer in interlocking intramedullary nails during simulated healing of a femoral fracture. *Proc Instn Mech Engrs, 208H, 19-26.*

Miller SD, Burkart B, Damson E, Shrive N and Bray RC, 1993. The effect of the entry hole for an intramedullary nail on the strength of the proximal femur. *J Bone Joint Surg, 75B (2), 202-206.*

Moed BR, Watson JT, Goldschmidt P and Van Holsbeeck M, 1995. Ultrasound for the early diagnosis of fracture healing afetr interlocking nailing of the tibia without reaming. *Clin Orthop, 310, 137-144.*

Müller ME, Nazarian S, Koch P and Schatzker J, 1990. Comprehensive classification of fractures of long bones. *Springer-Verlag, Berlin.*

Müller, Mc Iff T, Rahn BA, Pfister U and Weller S, 1993. Intramedullary pessure, strain on the diaphysis and increase in cortical temperature when reaming the femoral medullary canal - a comparison of blunt and sharp reamers. *Injury, 24 (S3), S22-S30.*

Naidu SH, Warner CP and Laird C, 1996. Mechanical stamping. *Clin Orthop, 328, 261-267.*

Nikiforidis G, Bezerianos A, Dimarogonas A and Sutherland C, 1990. Monitoring of fracture healing by lateral and axial vibration analysis. *J Biomech, 23 (4), 323-330.*

Nordin M and Frankel VH, 1989. Basic biomechanics of the musculoskeletal system. *Ed Nordin and Frankel, 2nd edition, Lea and Febiger.*

O'Sullivan ME, Chao EYS and Kelly PJ, 1989. The effects of fixation on fracture healing. *J Bone Joint Surg, 71A (2), 306-310.*

Oh I and Harris WH, 1978. Proximal strain distribution in the loaded femur. *J Bone Joint Surg, 60A (1), 75-85.*

Ordway CB, 1991. AIM titanium femoral nail system catalogue from the ACE Medical Company, Los Angeles, USA.

Otani T, Whiteside LA and White SE, 1993. Strain distribution in the proximal femur with flexible composite and metallic femoral components under axial and torsional loads. *J Biomed Mater Res, 27, 575-585.*

Papagiannopoulos G, Pratt DJ and Rees PH, 1985. Derby intramedullary nail - a biomechanical comparison. *J Biomed Engng, 7, 313-317.*

Paul JP, 1966-67. Forces transmitted by joints in the human body. *Proc Instn Mech Engrs, 181 (3J), 8-15.*

Pennig D, 1994. Current use of the intramedullary nail. *From Current practice of fracture treatment: new concepts and common problems, Leung (Ed), Springer Verlag, 119.*

Perren SM and Beaupre G, 1984. Breakage of AO/ASIF medullary nails: materal related or design tradeoff? *Arch Orthop Trauma Surg, 102, 191-197.*

Perren SM, 1979. Physical and biological aspects of fracture healing with special reference to internal fixation. *Clin Orthop, 138, 175-196.*

Pratt DJ, Papagiannopoulos G and Rees PH, 1987. Derby intramedullary nail: further biomechanical comparison. *J Biomed Engng, 9, 84-87.*

Procter P, 1996. Personal communication dated 03-10-96.

Raiha JE, 1992. Biodegradable implants as intramedullary nails. A survey of recent studies and an introduction to their use. *Clin Materials, 10, 35-39.*

Rees DWA, 1990. Mechanics of solids and structures. *Published McGraw-Hill Book Company, London.*

Reilly DT and Burstein AH, 1975. The elastic and ultimate properties of compact bone tissue. *J Biomech, 8, 393-405.*

Ricciardi L, Perissinotto A and Dabala M, 1993. Mechanical monitoring of fracture healing using ultrasound imaging. *Clin Orthop, 293, 71-76.*

Richardson JB, Cunningham JL, Goodship AE, O'Connor BT and Kenwright J, 1994. Measuring stiffness can define healing of tibial fractures. *J Bone Joint Surg, 76B (3), 389-394.*

Rohlmann A, Mössner U, Bergmann G and Kölbel R, 1982. Finite-element-analysis and experimental investigation of stresses in a femur. *J Biomed Eng, 4, 241-246.*

Russell TA, 1991. Biomechanical concepts of femoral intramedullary nailing. *International J Orthop Trauma, 1 (1), 35-51.*

Russell TA, Taylor JC and LaVelle DG, 1996. The Smith and Nephew femoral interlocking nails catalogue from Smith and Nephew Healthcare Ltd, Cambridge, UK.

Russell TA, Taylor JC, LaVelle DG, Beals NB, Brumfield DL and Durham AG, 1991. Mechanical characterization of femoral interlocking intramedullary nailing systems. *J Orthop Trauma, 5 (3), 332-340.*

Rydell NW, 1966. Forces acting on the femoral head prosthesis. *Acta Orthop Scand, Suppl. 88.*

Ryder SJ, Kyle RF, Campbell SJ, Templeman DC and Orafkovich, 1993. Six year review of all subtrochanteric fractures treated at Hennepin County Medical Centre. *J Orthop Trauma, 7 (2), 160.*

Sanders R, Koval KJ, DiPasquale T, Schmelling G, Stenzler S and Ross E, 1993. Exposure of the orthopaedic surgeon to radiation. *J Bone Joint Surg, 75A (3), 326-330.*

Schemitsch EH, Kowalski M, Senft DC and Swiontkowski MF, 1993. Acute effects of reamed versus unreamed locked nailing on blood flow in a fractured sheep tibia model. *J Orthop Trauma, 7 (2), 161-162.*

Schmotzer H, Tchejeyan G and Song J, 1992. A comparison of various loading configurations of the proximal femur for the evaluation of reconstructive surgical procedures. *Proc Instn Mech Engrs, 206H, 29-36.*

Schneider E, Michel MC, Genge M and Perren SM, 1990. Loads acting on an intramedullary femoral nail. *From Implantable telemetry in Orthopaedics, Bergmann, Graichen, Rohlmann (Eds), Forschungsvermittlung der FU, Berlin, 221-227.*

Sedel L, Christel P, Dewas J, de Charentenay FX and Leray J, 1980. Comparison of the effects of intramedullary nailing or plating on the mechanical properties of fracture callus. *J Biomed Engng, 2, 89-92.*

Shah KM, Nicol AC and Hamblen DL, 1995. Fracture stiffness measurement in tibial shaft fractures: a non-invasive method. *Clin Biomech, 10 (8), 395-400.*

Simonian PT, Chapman JR, Selznick HS, Benirschke SK, Claudi BF and Swiontkowski MF, 1994. Iatrogenic fractures of the femoral neck during closed nailing of the femoral shaft. *J Bone Joint Surg, 76B (2), 293-296.*

Singh M, Nagrath AR and Maini PS, 1970. Changes in the trabecular pattern of the upper end of the femur as an index of osteoporosis. *J Bone Joint Surg, 52A, 457.*

Smith JT, Goodman SB and Tischenko, 1991. Treatment of comminuted femoral subtrochanteric fractures using the Russell-Taylor reconstruction intramedullary nail. *Orthopaedics, 14 (2), 125-129.*

Star AM, Whittaker RP, Shuster HM, Duda J and Menkowitz E, 1989. Difficulties during removal of fluted femoral intramedullary rods. *J Bone Joint Surg, 71A (3), 341-344.*

Stürmer, 1993. Measurement of intramedullary pressure in an animal experiment and propositions to reduce the pressure increase. *Injury, 24 (S3), S7-S21.*

Szivek JA and Gealer RL, 1991. Comparison of the deformation response of synthetic and cadaveric femora during simulated one-legged stance. *J Appl Biomat, 2, 277-280.*

Szivek JA, Weng M and Karpman R, 1990. Variability in the torsional and bending response of a commercially available composite 'femur'. *J Appl Biomat, 1, 183-186.*

Tarr RR and Wiss DA, 1986. The mechanics and biology of intramedullary fracture fixation. *Clin Orthop, 212, 10-17.*

Tencer AF and Johnson KD, 1994. Biomechanics in orthopaedic trauma. *Martin Dunitz.*

Tencer AF, Johnson KD and Sherman MC, 1988. Biomechanical considerations in intramedullary nailing of femoral shaft fractures. *Techniques Orthop, 3(3), 1-5.*

Tencer AF, Johnson KD, Johnston WC and Gill K, 1984. A biomechanical comparison of various methods of stabilization of subtrochanteric fractures of the femur. *J Orthop Research, 2, 297-305.*

Terjesen T and Svenningsen S, 1988. The effects of function and fixation stiffness on experimental bone healing. *Acta Orthop Scand, 59 (6), 712-715.*

Tower SS, Beals RK and Duwelius PJ, 1993. Resonant frequency analysis of the tibia as a measure of fracture healing. *J Orthop Trauma, 7 (2), 179.*

Traisnel M, le Maguer D, Hildebrand HF and Iost A, 1990. Corrosion of surgical implants. *Clin Materials, 5, 309-318.*

UCLA, 1953. The pattern of of muscular activity in the lower extremity during walking. *University of California Report, Berkeley.*

Whittle AP, Russell TA, Taylor JC and Lavelle DG, 1992. Treatment of open fractures of the tibial shaft with the use of interlocking nailing without reaming. *J Bone Joint Surg, 74A (8), 1162-1171.*

Whittle AP, Wester W and Russell TA, 1995. Fatigue failure in small diameter tibial nails. *Clin Orthop, 315, 119-128.*

Woodard PL, Self J, Calhoun J, Tencer AF and Evans EB, 1988. The effect of implant axial and torsional stiffness on fracture healing. *J Orthop Trauma, 1 (4), 331-340.*

Wu C-C and Shih C-H, 1992. Biomechanical analysis of the mechanism of interlocking nail failure. *Arch Orthop Trauma Surg, 111, 268-272.*

Wu J-J, Shyr HS, Chao EYS and Kelly PJ, 1984. Comparison of osteotomy healing under external fixation devices with different stiffness characteristics. *J Bone Joint Surg, 66A (8), 1258-1264.*

Zimmerman KW and Klasen HJ, 1983. Mechanical failure of intramedullary nails after fracture union. *J Bone Joint Surg, 65B (3), 274-275.*

APPENDIX A

AO FRACTURE CLASSIFICATION SYSTEM

(From Müller *et al.*, 1990)

Humerus (12) Radius/ulna (22) Femur (32) Tibia/fibula (42)

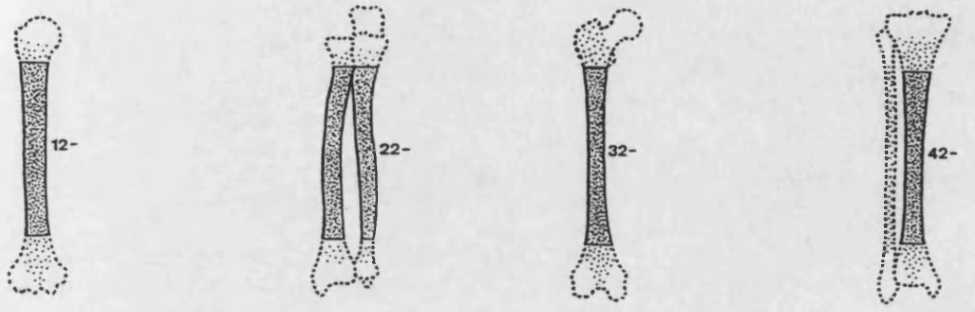

12
32
42

A simple	A1 spiral	
	A2 oblique	
	A3 transverse	
B wedge	B1 spiral	
	B2 bending wedge	
	B3 fragmented wedge	
C complex	C1 spiral	
	C2 segmental	
	C3 irregular	

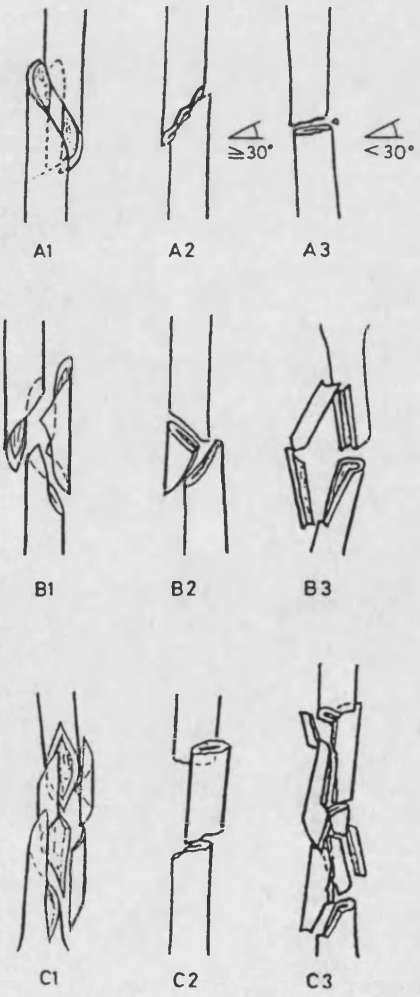

APPENDIX B

THE AREA PROPERTIES AND RIGIDITIES OF THE SIX INTRAMEDULLARY NAILS TESTED

	Theory				Autocad				Experimental			
	I_x mm^4	EI_x Nm^2	I_y mm^4	EI_y Nm^2	I_x mm^4	EI_x Nm^2	I_y mm^4	EI_y Nm^2	EI_x Nm^2	St dev Nm^2	EI_y Nm^2	St dev Nm^2
10mm ACE	291.60	32.08	455.10	50.06	281.3	30.94	318.7	35.06	35.05	0.18	39.02	0.08
10mm URFN	490.87	54.00	490.87	54.00	490.9	54.00	490.9	54.00	47.50	0.43	44.70	0.72
12mm AO	389.10	77.82	447.48	89.50	231.1	46.22	298.8	59.76	59.35	1.92	32.30	0.53
12mm URFN	698.84	76.87	698.84	76.87	697.7	76.75	697.6	76.74	67.40	0.27	65.20	0.46
12mm ACE	674.20	74.16	976.90	107.46	671.8	73.90	768.0	84.48	76.55	0.75	69.38	0.08
12mm RT	600.95	120.19	600.95	120.19	606.1	121.22	606.1	121.22	79.12	4.25	80.62	1.19

Table B-1 Table of intramedullary nail bending rigidities

	Theory		Autocad		Experimental	
	J mm^4	GJ Nm^2	J mm^4	GJ Nm^2	GJ Nm^2	St dev Nm^2
12mm AO	21.14	1.69			2.22	0.06
10mm ACE	73.24	2.93			2.93	0.05
12mm ACE	303.75	12.15			8.11	0.24
10mm URFN	981.75	39.27	981.8	39.27	24.60	0.30
12mm URFN	1704.60	68.19	1395.3	55.81	27.31	1.70
12mm RT	1201.00	96.08	1212.2	96.98	68.77	4.10

Table B-2 Table of intramedullary nail torsional rigidities

APPENDIX C

NAIL AND FEMORA STIFFNESS DATA

	AP bending stiffness (Nm/mm)	ML bending stiffness (Nm/mm)	Torsional stiffness (Nm/degree)
12mm RT	17.39	20.65	3.69
12mm AO URFN	17.47	16.68	1.42
10mm AO URFN	12.14	11.37	1.31
12mm ACE	19.80	18.05	0.50
10mm ACE	9.08	10.14	0.18
12mm AO	11.26	8.47	0.13
Composite femur	52.45	45.56	12.85

APPENDIX D

THEORETICAL CALCULATION OF THE CONSTRUCT RIGIDITY IN TORSION DURING HEALING

HEALING=0%

When the bone is fractured, the nail twists between the proximal and distal sets of screws. The femur contributes little to the rigidity of the construct. Hence at this stage:

$$GJ_{construct}=GJ_{nail}$$

HEALING=100%

When fully healed, both the nail and femur contribute to the rigidity of the construct. The standard equation for torsion of a cylinder gives:

$$GJ=\frac{T}{\theta}\cdot L$$

where G=shear modulus of elasticity, J=polar moment of area, T=applied torque, θ=angle of twist and L=working length.

Considering this equation for each component of the construct gives:

$$GJ_{nail}=\frac{T_{nail}}{\theta_{nail}}\cdot L_{nail} \quad \text{.....1}$$

$$GJ_{bone}=\frac{T_{bone}}{\theta_{bone}}\cdot L_{bone} \quad \text{.....2}$$

$$GJ_{construct}=\frac{T_{construct}}{\theta_{construct}}\cdot L_{construct} \quad \text{.....3}$$

And assuming there is no slippage between the nail and bone, the total torque, $T_{construct}$ is given by:

$$T_{construct}=T_{bone}+T_{nail} \quad \text{.....4}$$

Substituting equations 1, 2 and 3 in to equation 4 and assuming the angle of twist and length are the same for all components gives:

$$GJ_{construct}=GJ_{bone}+GJ_{nail} \quad \text{.....5}$$

Table D.1 compares the experimental torsional rigidities for the Russell-Taylor and 10mm AO URFN constructs with those calculated theoretically using the above equations. The theoretical nail rigidities have been calculated previously and are shown in Appendix B. The theoretical Sawbone rigidity was calculated as $221Nm^2$ on page 105. There is good agreement between values.

	Theoretical GJ (Nm^2)	**Experimental GJ (Nm^2)**
Russell-Taylor - 0%	96	81
Russell-Taylor - 100%	317 (221+96)	350
AO URFN - 0%	39	36
AO URFN - 100%	260 (221+39)	237

Table D-1 Theoretical and experimental torsional rigidities for two constructs.

N.B. The composite femur has theoretical GJ=$221Nm^2$ (see page 105).

HEALING=50%

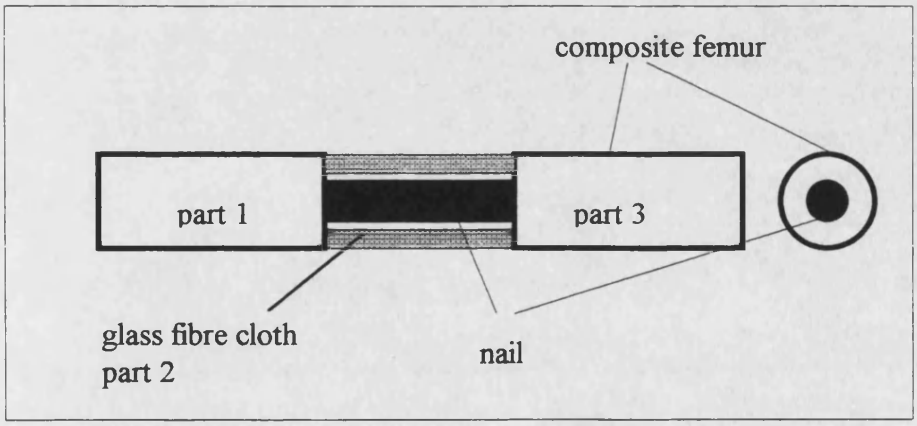

Figure D-1 Schematic of the composite femur and nail during the healing process

Considering the construct shown in figure D.1 and applying equation 5 gives:

$$GJ_{construct} = GJ_{bone} + GJ_{nail}$$

However, the rigidity of the bone is derived from the rigidity of its three components; the composite bone, parts 1 and 3, and the glass fibre cloth, part 2. Analysing the bone as a stepped shaft where the total twist, θ_{bone}, is given by:

$$\theta_{bone} = \theta_1 + \theta_2 + \theta_3 \quad \text{.....6}$$

Substituting the standard torsion equation for each component in to equation 6 gives:

$$\theta_{bone} = \frac{T_{bone}L_{bone}}{GJ_{bone}} = \frac{T_1L_1}{GJ_1} + \frac{T_2L_2}{GJ_2} + \frac{T_3L_3}{GJ_3} \quad \text{.....7}$$

But for a stepped shaft;

$$T_{bone} = T_1 = T_2 = T_3$$

And;

$$L_{bone} = L_1 + L_2 + L_3$$

Dividing equation 7 by T_{bone} and L_{bone}, and given that $L_1=L_3$ and $GJ_1=GJ_3$ gives:

$$\frac{1}{GJ_{bone}} = \frac{2}{GJ_1\left(2+\frac{L_2}{L_1}\right)} + \frac{1}{GJ_2\left(1+\frac{2L_1}{L_2}\right)} \quad \text{.....8}$$

For the Russell-Taylor construct, when healing=50%, the experimental torsional construct rigidity=214Nm^2. The torsional rigidity of the Russell-Taylor nail=69 Nm^2 (Appendix B). Substituting these values in to equation 5 gives:

$$GJ_{bone} = GJ_{construct} - GJ_{nail} = 214 - 69 = 145\text{Nm}^2$$

Substituting this value of GJ_{bone} in to equation 8 and assuming GJ_1=221.4 Nm^2 (page 105), L_1=0.11m and L_2=0.03m gives:

$$\frac{1}{145} = \frac{2}{503} + \frac{1}{8.3GJ_2}$$

This gives the rigidity of the glass fibre cloth, GJ_2=41Nm^2. Assuming G_2=4GPa for glass fibre cloth gives the polar moment of area, J=10 309mm^4. If the fibre cloth is attached to the outside of the bone, hence R_i=13.5mm, the cloth thickness can be found using:

$$J = \frac{\pi}{2}\left(R_o^4 - R_i^4\right)$$

This gives R_o=14.1mm. This shows that when healing=50% the thickness of glass fibre cloth around the bone measured (14.1-13.5)=0.6mm. It is estimated that each layer of cloth is approximately 0.2mm in thickness which means that when healing=50%, three layers of cloth had been applied to the construct. This is of the right order of magnitude.

APPENDIX E

CALCULATION OF THE AP BENDING STRAINS IN COMBINED LOADING

The high AP strain measured in the Russell-Taylor (RT) nail can be explained by considering the contact between the nail and femur in this plane. When the fractured RT construct was inspected the nail was found to impinge severely on the anterior aspect of the glass fibre bone wall on either side of the fracture. This might lead to localised bending of the nail across the fracture gap and hence the high strains measured.

Theoretically, this situation can be compared to four point bending of the nail where the contact between the bone and nail at the fracture site is represented by the two forces, P, in figure E.1.

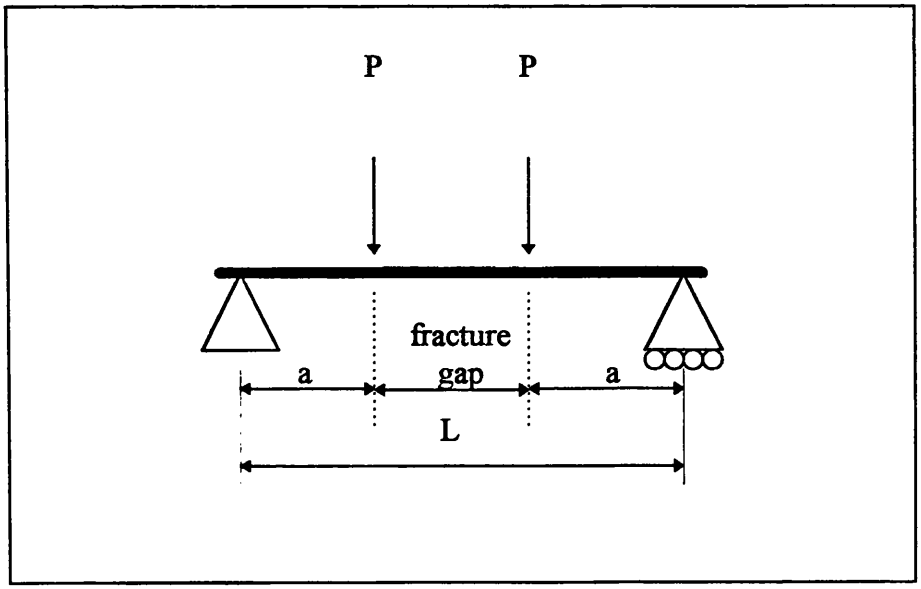

Figure E-1 Four point loading of the Russell-Taylor nail in AP bending

The central deflection, δ, of the nail is given by:

$$\delta = \frac{Pa}{24EI}\left(3L^2 - 4a^2\right) \quad \text{.....1}$$

where EI=bending rigidity of the nail.

Considering the deformation of a beam in bending, we find that:

$$R = \frac{y}{\varepsilon_x} \quad \text{.....2}$$

$$\delta = \frac{L^2}{8R} \quad \text{.....3}$$

where R=radius of curvature of the beam due to bending, ε_x=the longitudinal strain at a distance=y from the neutral axis and L=length of the beam (Gere and Timoshenko, 1989). Substituting equations 2 and 3 into equation 1 gives:

$$\frac{L^2\varepsilon_x}{8y} = \frac{Pa}{24EI}\left(3L^2 - 4a^2\right)$$

Rearranging gives:

$$\varepsilon_x = \frac{Pay}{3L^2EI}\left(3L^2 - 4a^2\right)$$

Figure E.2 shows the effect of varying the length of the fracture gap (L-2a) on the strain. For this calculation L=0.25m, y=6mm and EI=79Nm^2 for the RT nail in AP bending. It was assumed that P=35N.

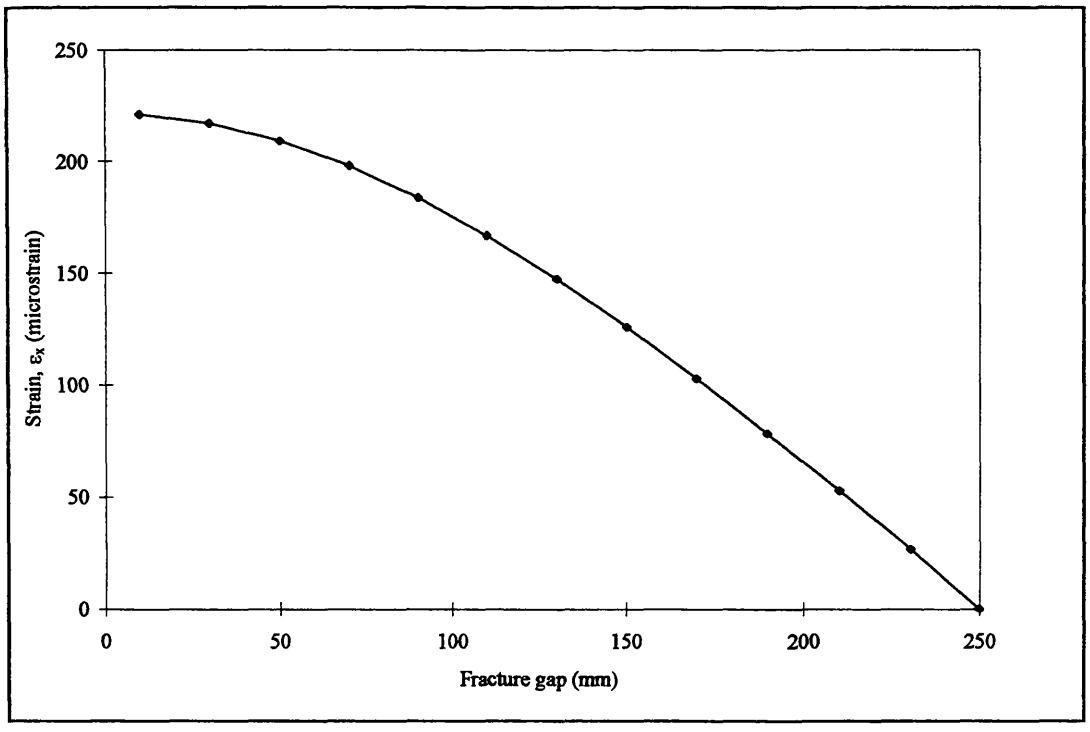

Figure E-2 The effect of the fracture gap length on the longitudinal strain

This chart shows that when the nail bends across a small fracture gap (e.g. 30mm), large strains are measured due to localised bending (≈200με). If the length over which the nail is loaded increases (e.g. 200mm), the strain is reduced dramatically (≈50με).

This may explain the high AP strains recorded in the Russell-Taylor nail during combined loading. The nail was not in contact with the bone in the medio-lateral plane and so the strains in this plane were of a lower magnitude.

APPENDIX F

GLOSSARY OF TERMS

abductor muscles	muscles of the hip that allow the lower limb to moved away from the midline of the body, or abducted
anterior	describing the front portion of a body
cadaveric	corpse like
cancellous	spongy, lattice like bone
cartilage	dense connective tissue e.g. found at the end of movable bones
comminuted fractures	fractures with more than two fragments
cortex, cortices	the hard outer part of the bone
diaphysis	the shaft of a long bone
distal	situated furthest from the central body
endosteum	membrane that lines the marrow cavity of a bone
epiphyses	bone growth plates that produce new bone as part of the normal growth procedure. The plates close during early adulthood.
fat embolism	fat clot that is carried by the blood through the circulation and may become lodged at some point
femur	the thigh bone between the hip and knee joints
fluoroscope	an instrument on which X-ray images may be viewed directly without taking and developing photographs
gluteus	3 muscles of the buttock responsible for thigh movement
humerus	bone of the upper arm between the shoulder and elbow joints

image intensifier	(see fluoroscope)
in vitro	out of the body e.g. in a laboratory
in vivo	in the body
isthmus	a constricted or narrowed part of an organ
lateral	relating to the side of a body situated furthest from the midline
ligament	a connective tissue that links two bones together at a joint
linea aspera	rough ridge found on the posterior surface of the femur
malunion	bone deformity resulting from healing of a fracture in which the bone ends are poorly aligned
medial	relating to the side of a body nearest the midline
maxillofacial	relating to the face, jaws and related structures
medullary canal	the inner region of a bone
muscle	a tissue whose cells have the ability to contact, producing movement or force
non-union	failure of a bone to heal
orthopaedics	the science and practice concerned with the bones and joints of the skeleton
osteoarthritis	a disease of the joint which may result from overuse and is common in the elderly
osteogenesis	the formation of bone
osteoporosis	loss of bony tissue resulting in brittle bones
osteotomy	surgical operation to cut bone in two parts
periosteum	layer of connective tissue that covers the outside of a bone
physiological	referring to the body
posterior	situated at the back of a body
prosthesis	any artificial device that is attached to the body as an aid

proximal	situated nearest to the central body
retrograde	going backwards, in the opposite direction to the normal
tendon	connects muscle to bone and transmits muscle forces to a bone facilitating movement
tibia	the shin bone and largest bone of the lower leg between the knee and ankle joints
trabecula	thin bars of bony tissue in cancellous bone

APPENDIX G

LIST OF CONFERENCE PUBLICATIONS

Eveleigh RJ, Wight BJ, Miles AW and Goodwin MI, 1994. The load transfer in intramedullary nails during healing. *Second World Congress of Biomechanics, July 10-15, Amsterdam, Netherlands, II-335b.*

Goodwin MI, Miles AW, Eveleigh RJ and Wight BJ, 1995. An experimental study into the load sharing characteristics of intramedullary nails during simulated healing of a femoral fracture. *Minimal-Invasive Traumatology Synposium, February 2-3, Salzburg, Austria, 72.*

Eveleigh RJ, Miles AW, Goodwin MI and Bishay M, 1996. A biomechanical study of the ACE Medical Company femoral intramedullary nail during a simulated healing process. *Minimal-Invasive Traumatology Synposium, February 8-9, Salzburg, Austria, 63.*

Al-Sayaad C, Goodwin MI, Eveleigh RJ and Miles AW, 1997. An experimental study into the mechanical properties of intramedullary nails in the treatment of subtrochanteric fractures. *Minimal-Invasive Traumatology Synposium, February, Salzburg, Austria.*

Eveleigh RJ, Miles AW and Weston RB, 1997. Simulating combined loading in the proximal femur for evaluation of fracture fixation systems. *European Orthopaedic Research Society, April 22-23, Barcelona, Spain.*

Eveleigh RJ and Miles AW, 1997. Simulating combined loading in the femur in vitro: a comparison of five configurations. *British Orthopaedic Research Society, Autumn Meeting, Cardiff, UK.*

APPENDIX H

JOURNAL PUBLICATIONS

Miles AW, Eveleigh RJ, Wight BJ and Goodwin BJ, 1994. An investigation into the load transfer in interlocking intramedullary nails during simulated healing of a femoral fracture. *Proc Instn Mech Engrs, 208H, 19-26.*

Eveleigh RJ, 1995. A review of biomechanical studies of intramedullary nails. *Med Eng Phys, 17 (5), 323-331.*